12-1994

The Kinetics of Volatile Lead Compound Formation During Simulated Hazardous Waste Incineration

Joel Thomas Shor
University of Tennessee, Knoxville

To the Graduate Council:

I am submitting herewith a dissertation written by Joel Thomas Shor entitled "The Kinetics of Volatile Lead Compound Formation During Simulated Hazardous Waste Incineration." I have examined the final electronic copy of this dissertation for form and content and recommend that it be accepted in partial fulfillment of the requirements for the degree of Doctor of Philosophy, with a major in Chemical Engineering.

George C. Frazier, Major Professor

We have read this dissertation and recommend its acceptance:

James Adcock, Wayne Davis, Robert Counce, B. Oliver, J. Watson

Accepted for the Council:
Carolyn R. Hodges

Vice Provost and Dean of the Graduate School

(Original signatures are on file with official student records.)

To the Graduate Council:

I am submitting herewith a dissertation written by Joel Thomas Shor entitled, "The Kinetics of Volatile Lead Compound Formation During Simulated Hazardous Waste Incineration." I have examined the final copy of this dissertation for form and content and recommend that it be accepted in partial fulfillment of the requirements for the degree of Doctor of Philosophy, with a major in Chemical Engineering.

George C. Frazier

George C. Frazier, Major Professor

We have read this dissertation and recommend its acceptance:

James L. Adcock

Wayne T. Davis

Robert M. Counce

Jack Watson

Ken T. Allen

Accepted for the Council:

Lee Minkel

Vice Provost
and Dean of the Graduate School

THE KINETICS OF VOLATILE LEAD COMPOUND FORMATION DURING SIMULATED HAZARDOUS WASTE INCINERATION

A Dissertation

Presented for the

Doctor of Philosophy

Degree

The University of Tennessee

Joel T. Shor

December 1994

DEDICATION

I dedicate this work to my family.

ACKNOWLEDGEMENTS

I would like to thank many people who have contributed much to this effort: Don Carpenter, Lynn Glover, Jim Mabon, Ralph McGill, Doug Fielden and his crew, Ted Long, Paul Hatmaker, Frank Holliway, W. D. Bostick, L. V. Gibson, John Begovich, and Jonathan Plummer. This work was supported by the Office of Technology Development of the U.S. Department of Energy, and special thanks are made to A. Malinauskas and J. Moore. I would especially like to recognize my supervisor, Suman Singh, for his never-wavering support and the members of my committee, Drs. J. Adcock, R. Counce, W. Davis, B. Oliver, and J. Watson, for their generous aid. To my advisor, Dr. George Frazier, from whom I have learned more than from anyone else, I am most grateful. Special recognition is accorded to Nancy Smith, Constance Powell, Johnnie Hatmaker, Lori Gorman, and Jerry King for their graphics skills and work.

ABSTRACT

Air pollution from fine metal-containing particles (and vapors) formed during hazardous waste incineration has attracted less attention than other incinerator emissions. Recently, however, metal pollution has become subject to more stringent regulations. The U.S. Environmental Protection Agency has announced limitations on the emissions of ten toxic metals. Pollution control systems that will effectively remove fine (submicron) metal-containing particles from flue gases are difficult to construct. Incinerators have not been designed or operated to minimize the formation of such particles. Industrial-scale incineration testing has produced anomalous results for air emissions of lead and other metals.

To gain a better fundamental understanding of the generation of metal emissions, the kinetics of the formation of volatile pollutants in simulated incinerator kilns were experimentally examined as a function of temperature and acid gas concentration. The chemical reactions between lead oxide, a common toxic metal found in hazardous waste streams, and hydrogen chloride, commonly produced in hazardous waste incineration are the specific focus. Descriptive models were constructed of the kinetics and mass transport of the lead dichloride and oxychloride intermediate compounds that were found to be generated.

Fine particulate matter composed of lead dichloride was produced.

At temperatures between 260 and 310°C, the hydrochloridation reaction kinetics were measured, and an apparent activation energy of 22 kcal/mol was obtained. At 300°C an apparent reaction rate of 10-7 mol/(cm^2·s) was found at 2000 ppm of HCl. At higher temperatures, the formation of lead dichloride was diffusionally controlled, principally in the liquid or solid ash phases, and, until 600°C was reached, changed little from the 10-7 mol/(cm^2· s) rate in approximately 30- to 60-min batch hydrochloridation experiments. An interesting phenomenon was found in that at temperatures greater than 590°C, a glassy surface ash phase was formed while at temperatures between 450 and 590°C, a distinctly liquid ash phase was formed. The glassy ash phase grew rapidly in thickness and exhibited a lower volatility of lead dichloride than did the liquid phase formed at lower temperatures. This has interesting implications for incineration because this research has revealed a situation in which a higher volatility product is formed at lower temperature, contrary to most expectations and to purely equilibrium considerations.

TABLE OF CONTENTS

LIST OF TABLES

LIST OF FIGURES

LIST OF SYMBOLS

A, area of particle, or distance in angstroms

a, lattice cell parameter

C, concentration, mol/cm^3, usually pertains to HCl

c, lattice cell parameter

D, diffusivity, cm^2/s, or characteristic diameter

D_p, particle diameter

H_k, Henry's law constant, $atm \cdot\cdot mol^{-1} \cdot cm^{-3}$

I_1, concentration of intermediate 1, mol/cm^3

I_2, concentration of intermediate 2, mol/cm^3

J_i, diffusive flux of species i, $mol/(cm^2 \cdot s)$

k, overall reaction rate constant, $(moles/cm^3)^{-1}\ s^{-1}$

k_{mt}, mass transfer coefficient, cm/s

k_1, reaction rate constant, reaction of intermediate I1

k_2, reaction rate constant, reaction of intermediate I2

M, metal species

N, also diffusive flux, mol/(cm2 · s

N_{sh}, Sherwood number

N_{sc}, Schmidt number

N_{re}, Reynolds number

n, stoichiometric coefficient

R_p, reaction rate, Lee model, $mol \cdot cm^{-3} \cdot s^{-1}$

R_{po}, initial reaction rate, Lee model

R, particle initial radius, general reaction rate

r, particle radius

s, position of moving boundary

S_g, specific surface area of particle

t, time

V, volume, cm^3, or vaporization rate [(Eq. (2.5.17)]

v, fluid velocity

x, vapor mole fraction

Subscripts

a, pertaining to species a

b, pertaining to species b

c, pertaining to species c

s, with respect to surface area or with respect to solid phase

e, effective, applied to diffusivity

0, initial as applied to boundary conditions or reaction rate

2, pertaining to second stage of reaction

Greek Letters

α, correction factor to account for Stefan Maxwell flow

η, effectiveness factor, Lee model

τ_p, characteristic pore plugging time

τ_{sf}, derived parameter [(Eq. (4.3.5)], Lee model

μ, fluid viscosity

ρ, fluid density

γ, activity coefficient

1. INTRODUCTION

Incineration has grown in the United States during the last decade in response to regulations governing the land disposal of wastes, especially hazardous wastes. Of particular difficulty and interest is the disposal of chlorinated organic wastes, including polychlorinated biphenyls, which represent a long-term danger to groundwater if the material is landfilled, because of their relative inertness to biodegradation. The other presently developed alternatives to landfill and incineration are deep well injection and ocean disposal, which have met with much political and scientific uncertainty (Theodore and Reynolds, 1987). Incineration offers the opportunity to destroy forever and quantitatively these hazardous materials, converting them to less noxious materials such as sodium chloride, carbon dioxide, and water. Unfortunately, hazardous organics are frequently found with contamination from other materials, such as metals, which obviously cannot be destroyed in an incinerator and which may be volatilized.

Toxic and hazardous waste incineration has generally been optimized to destroy hazardous organic materials. Operating conditions of temperature and residence time in the combustion chamber are strictly specified to ensure the destruction of the organics (Brunner, 1989). Little attention has been directed to the conditions under which

metals volatilize and are released as air pollutants. Only in recent years has the U.S. Environmental Protection Agency (EPA) advanced regulations governing such emissions. Formerly standards existed only for gross particulate concentrations (0.08 grains per dry standard cubic foot), though state regulations occasionally governed specific metals (Theodore and Reynolds, 1987). In Europe and Japan, controls on metal emissions are often tighter and more specific than those in the United States (Millot, 1992). Incinerator operators are often faced with limiting their feed materials to very low concentrations of metals since regulations require that they make the worst-case assumption that all metals in the feed are emitted from the stack. It would be prudent to anticipate tightened federal regulations in the United States in the future.

It would be useful if the air emissions occurring for given feed conditions could be better understood. Much is known about the efficiency of most air pollution control devices (Perry and Chilton, 1973). Particulates between 0.1 and 1 μm in diameter are difficult to remove except with sophisticated and expensive equipment such as ionizing wet and dry electrostatic scrubbers or bag filters (Perry and Chilton, 1973). Operational problems often exist with these types of equipment. Even with state-of-the-art air pollution control equipment, advances in incinerator combustion chamber design and operation could reduce the

load to this equipment and the generation of secondary wastes (often liquids) therefrom. Our attention will be directed to the formation of particulates less than 1 μm in aerodynamic diameter.

Particulate pollutants may conceivably form in many ways during incineration. They may result from the volatilization and subsequent condensation of metals or metal compounds which have appreciable vapor pressures at kiln gas temperatures, an average of about 1250 K (Bennett and Knapp, 1982). (Kiln bed temperatures may actually be much lower.) These pollutants may be entrained from solid wastes fed to the kiln. They may be formed during the combustion of organometallic compounds or during the highly exothermic oxidation of elemental metals (even metals with high boiling points may thus be volatilized) where particles reach local temperatures much higher than that of the kiln bed. They may be formed during the evaporation, decomposition, and bursting of inorganic metal salt melts in the waste feed (Mulholland and Sarofim, 1990). They may be formed during incineration of carbonaceous sludges containing metal inclusions. And they may be formed during the reaction between metal oxides and chlorine compounds in the feed, as was examined in this project.

Although industrial incinerators accept a wide range of feeds consisting of organic and aqueous liquids, hazardous sludges and solids typically contain the highest

concentrations of metals and organics (Theodore and Reynolds, 1987) and are an appropriate focus of research. Hazardous and toxic wastes furthermore contain large quantities of chlorinated organics which generally form hydrogen chloride during combustion and provide the reactant for the proposed mechanism evaluated in this project. In general, as will be discussed, chloride compounds of metals exhibit comparatively high volatilities.

1.1 OBJECTIVE

The objective of this study is to determine the mechanisms of metal volatilization from the reaction of metal oxide, specifically lead oxide (PbO) and hydrogen chloride (HCl) under feed conditions similar to those found in waste incinerators. Attempts will be made to correlate the rate of production of volatile lead compounds with the properties of the system (e.g., metal oxide and chloride properties, temperature, and operating conditions such as gas composition.) It is hoped that such knowledge can be used to guide the design and operation of waste incinerators for minimum production of fume, i.e. submicron particulate, of toxic metals.

A second experimental approach that was briefly tried is the investigation of the reduction of metal oxide particles in a carbonaceous matrix to their more volatile (in general) suboxide and metallic forms. In coal research

this process has been found to result in the production of fine metal oxide fume when the reduced species are reoxidized. This subject is discussed in more detail in the literature review and theory sections.

1.2 METHODOLOGY

An experimental program, the details of which are provided in the Sect. 3, was implemented to obtain data from a specially designed laboratory reactor. The data from this device are interpreted in terms of descriptive models of condensed phase-gas reactions in which both reaction rate and diffusional kinetics may be significant.

2. LITERATURE REVIEW

This review considers the history of particulate air emissions research, which began primarily with investigations of coal combustion in which certain basic principles were established. More recent research relevant to incineration is then reviewed and the specific focus of this present work, metal hydrochloridation, is established. Finally, related studies of the formation of metal chloride species in other fields are discussed.

2.1 PARTICULATE MATTER FROM COAL COMBUSTION

Current literature on metal air pollutant formation is not highly specific to incineration problems; however, particulate emissions from coal combustion have been extensively investigated and studied. Davison et al. (1974) found that the particulates from coal combustion were enriched in volatile elements in inverse proportion to their size. He hypothesized the existence of a volatilization/condensation mechanism to explain this phenomenon. Smith et al. (1979), studying coal combustion, believed that the enrichment in volatile elements observed by Davison did not extend to submicron particles. Smith hypothesized that submicron particles were formed as a result of the bursting of ash particles because of the rapid evolution of volatile vapors during combustion. Davison's

hypothesis has attracted much wider acceptance, however. Davison reasoned that the relatively large surface-to-volume ratio of the finer particles results in their surface enrichment in the more volatile metals by condensation.

There are several seminal papers on the thermodynamics and transport of fume particles authored separately and jointly by Neville and Quann under the tutelage of A. Sarofim (Neville et al., 1981; Quann and Sarofim, 1982). Neville found that the temperature of a burning coal particle was much higher than the furnace temperature and that the temperature the particle attained was strongly correlated with the quantity of submicron ash generated. For this reason, Neville hypothesized that this submicron ash is produced from volatilization and later condensation of the mineral matter. He was able to vary the particle combustion temperature by altering the concentration of oxygen in a laminar-flow drop- tube furnace. He found that if coal ash (minus the carbon) was injected into the same furnace, the rates of submicron fume generation were much lower. Neville reasoned that the enhanced quantities of fume generated during the coal combustion were caused to some extent by the reduction of the metallic oxides to more volatile suboxide or elemental form. To what extent the lower generation rates are due to the absence of carbon (meaning that the reduction no longer could occur) or to the lower char particle temperature or other reasons is unclear. Neville

found that calcium and magnesium were strongly volatilized from lignite coals while silicon, though predicted to volatilize, did not. He searched for an explanation.

Quann (Quann and Sarofim, 1982) provided a possible explanation with his model of coal char mineral inclusion volatilization. As discussed later in the theory section, he solved the diffusion equation with source terms arising from the variably sized mineral inclusions. Quann found that if inclusions were of molecular scale, as in the case of organically bound metals in lignite coals, diffusive resistance from the particle to the bulk gas was controlling in the production of volatiles. If the inclusions were approximately 50 angstroms in diameter, then pore diffusive resistance became controlling. Many questions remained unanswered: for example, why the concentration of magnesium oxide varied in the fume from two different lignites of similar chemical and physical composition and why calcium was found in the fumes from certain lignites and not others.

Neville (Neville and Sarofim 1982) in a second paper constructed a model to predict the concentration of metal in the gas phase with respect to distance from the surface of the charring particle, assuming a source of reduced metals inside the particles. He found that iron and magnesium nucleated first in the boundary layer of the char particles and were consequently found in the interiors of the ash fume particles. More volatile metals such as sodium and

antimony, condensing later, were found on the particle surfaces. Silica was also found on the surface, and Neville attributed this phenomenon to the slower oxidation of the reduced silicon when it encountered the higher oxygen potential in the boundary layer.

Helble and Sarofim (1983), studying different coal feeds, identified micron-sized fume that resulted from fragmentation and centrifugal slinging of bits of porous feed particles. Our focus here, however, is principally on submicron particle formation, and Helble did not address this subject extensively.

Based on the work of Quann, Neville, and Sarofim, it may be stated that unanswered questions exist concerning fume formation, the high-temperature kinetics of the metal reduction mechanisms, and the validity of the mechanisms at the lower temperatures characteristic of incineration.

Coal combustion such as in central power stations, the subject of the previously discussed work, can be distinguished from incineration. The temperature, carbon content, ash composition, and combustion geometry are all different. In coal combustion, particles are suspended in the gas stream. When feeding combustible solids to incinerators, the combustion typically takes place in a bed that tumbles along the walls of a rotary kiln. When feeding combustible liquids to an incinerator, burning takes place in gases at the periphery of droplets, the interior

temperature of which may be quite low. Incinerator feeds are not generally rich in carbon, incinerators operate at lower temperatures (1200°C is a practical maximum), and the ash may take many different forms.

2.2 INCINERATION RESEARCH

Most incineration research has been performed in semiindustrial-scale incinerators, where control and repeatability are serious problems. An experimental small-scale (2.0×10^6 Btu/h) incinerator, built by the EPA in Arkansas, has been used more extensively (Carroll et al., 1990) than most other incinerators to determine the emissions of metal pollutants from simulated waste feeds. The number of variables in commercial-scale incineration experiments is large: the efficiency of the scrubbers, the variation in a solid feed composition (possibly even more variable than in coal combustion), the variation in the residence time of metals in the kiln and secondary combustion chamber, the variation in sample representativeness, and other factors. Mass balances are almost always elusive, and often trends are difficult to establish.

Kaiser and Tolciss (1963) studied air pollution resulting from the burning of polyvinylchloride (PVC)-insulated copper wire in an incinerator equipped with a primitive (by today's standards) scrubber of approximately

94% total collection efficiency. A full 10% of the incinerator feed material was discharged in the raw flue gas particulate and fume before it entered the scrubber. Most of this particulate matter was soluble, and copper and zinc were significant components. Kaiser and Tolciss concluded that metal chlorides form in large quantities when PVC is incinerated in the presence of metals.

Waterland et al.(1991), working at the Arkansas Environmental Protection Agency research incinerator, found that certain metals (e.g., cadmium and bismuth) with volatile oxide or chloride forms were not often found in kiln ash; Waterland defined such metals as "volatile." Arsenic was not "volatile" in his experiments even though the elemental, oxide, and chloride forms have low boiling points. Anomalies with arsenic have been noted in other studies and are hypothesized to result from the reaction of the acidic arsenic oxides with basic metal oxides present in the feed. The small amount of arsenic that was found in the flue gas, however, consisted of very fine fume, which may mean that at some point a fraction of the arsenic was vaporized during the incineration.

Waterland found that increasing the chlorine to a concentration of 8 wt % of the organic feed led to a greater concentration of fine particles in the flue gases particularly those containing Pb, Cr, and Cd. Increases beyond 8% had no further effect. Though the particle size

distributions shifted toward the submicron range (for nearly all metals studied (i.e., As, Cd, Bi, Pb, Ba, Cu, Sr, and Mg, though not Cr) as the kiln temperature was raised, the shift was greatest for the most volatile metals. Interpretation of the results of Waterland's study is complicated by the fact that mass balances were not achieved. Lead was found to be very volatile; it was found in low concentrations in the kiln ash in one series of tests and not found in a second series of tests under the same conditions. No clear explanation of these discrepant results can be found. They may be caused by a change in burner orientation resulting in a slight difference in kiln bed temperature. This small change in bed temperature and significant change in air emissions partly motivate our focus on lead.

Waterland summed the quantities of a metal collected from all sources (bottom ash, stack gas, and scrubber liquors) and normalized the partition coefficient based on that sum rather than on the total input. The total input never matched the output. His data are therefore subject to the vagaries of poorly representative sample collection.

In one of the few instances of laboratory-scale incineration research, Mulholland and Sarofim (1991) introduced, individually, cadmium, lead, and nickel nitrate solution droplets of purportedly controlled size distributions into a high-temperature furnace and studied

the morphology of the resulting distribution of particles. They found a trimodal distribution that resulted, they reasoned, from some particles bursting during nitrate decomposition while others remained intact. They were not able to explain the origin of the intermediate-size mode, however. One difficulty they encountered was maintaining a narrow size distribution of precursor droplets. Once formed, the droplets tended to agglomerate before entering the combustion zone. They theorized that the bursting occurred when the nitrate decomposition took place at a rate similar to that of viscous relaxation of the melt. The viscosity of the melt was, in their view, a critical parameter in the final particle structure. No chemical analysis of the particles was performed. Another plausible explanation of their results, however, is that the bursting particles resulted from the formation of a dry salt on the outside of the sphere while the internal liquid volatilized. This phenomenon is frequently observed in spray drying, and it may not be necessary to refer to the more complex mechanism described by Mulholland to explain these results.

Kistler and Widner (1987) pyrolyzed sewage sludge in a laboratory-scale furnace at different temperatures for 1 h and found that cadmium and mercury were quantitatively volatilized at temperatures of 600 and 350°C respectively. They demonstrated that cadmium oxide would not volatilize at these conditions in the absence of the carbonaceous char.

No difference was observed, however, between the amounts of zinc and copper volatilized, despite the large difference in their boiling points. This finding suggests that their technique was not particularly sensitive. They did demonstrate, however, that incinerator feed materials can create the same reducing conditions as coals.

2.3 LEAD AND METAL OXIDE HYDROCHLORIDATION

Chaleroux (1960) studied the kinetics of the reaction between pure HCl and a large number of metal oxides as a function of temperature, sample geometry, and sample size. His work most closely resembles the present experimental investigation. Chaleroux, however, experimented only with pure HCl gas that was subjected to atmospheric pressure for a fixed duration of 6 h in each test. He placed samples of the metal oxide powders in sample boats and flowed the HCl gas over them; consequently, his technique was subject to complex diffusional resistances. Chaleroux's investigation was, by his own admission, only a beginning in the complex study of heterogeneous gas/solid reactions; nevertheless, he was able to uncover some interesting relationships.

Calcium, magnesium, manganese, cobalt, nickel, and chromium oxide reacted only very slightly at 298°C, and their reaction rates increased monotonically with temperature to near completion at 600°C. Copper, lead, mercury, silver, zinc, and tin oxides presented relative

minima in the curve representing extent of reaction versus temperature. Calcium oxide seemed to exhibit this behavior on occasion as well. Chaleroux attributed this relative minimum to a catalytic effect from the water produced from the hydrochloridation reaction. As the temperature was increased, the water eventually evaporated so quickly that it was not able to exert much catalytic effect. As the temperature advanced still further, the effect of the rising kinetic constants eventually raised the reaction rates again. Lead oxide exhibited a minimum reaction rate at a very low temperature (i.e., 70°C). The less thermodynamically stable allotropic form of lead oxide, massicot, reacted slightly more rapidly at the low temperatures at which Chaleroux was able to resolve the effect of chemical reactivity. At temperatures above 300°C, all samples reacted to completion after 6 h. No activation energies were provided.

Srinivasachar et al. (1992) investigated the reaction between lead metal and 400 to 1000 ppm of HCl, performing tests both with and without 200 ppm SO_2 at temperatures between 900 and 1000°C. His work is difficult to interpret for several reasons. Oxygen was not excluded from the system, making it difficult to assess the extent to which PbO was forming. No control was made of the surface area available for reaction, since lead and lead oxide may be liquid at the temperatures considered. The extent of

reaction was determined as the extent of volatilization of lead dichloride only, and no record of a material balance was provided. Srirvasachar et al. were, however, able to determine that sulfur dioxide had no effect on the production of lead dichloride particulate matter and that the volatilization and reaction were augmented with increasing temperature. A proprietary sorbent was used to scrub the lead chloride vapor with some success. Ball and Casson (1978) investigated the reactions between HCl at pressures of 0.2 to 1 atm and $PbCO_3$ and white lead [$PbCO_3Pb(OH)_2$] at temperatures of 150 and 200°C. They were curious whether any reaction intermediates might be found; however, they were only able to identify $PbCl_2$ as the reaction product at the high HCl concentrations they used. The hydrochloridation of lead carbonate displayed a bilinear reaction rate on a semilog plot against inverse temperature, which suggests a change in mechanism at a temperature near 100°C. Ball and Casson analyzed their data in terms of a diffusion-controlled reaction; however, they ambiguously discuss the reaction in terms of varying frequency factors and activation energies characteristic of chemical reaction kinetic control.

Michell (1973) investigated the mechanisms by which PbO stabilizes polyvinylchloride polymers. Gaseous HCl was fed to a polymer melt containing white lead and lead carbonate at 182°C, and samples of the reaction product were

periodically removed from the melt for analysis. Although the presence of organolead compounds complicates this system and distinguishes it from the system that is the object of our investigation, it is interesting to note that Michell believed that he found a lead oxychloride intermediate. The intermediate was analyzed using x-ray diffraction but was not definitely identified.

Zilberman et al. (1969), again investigating the mechanisms of lead compound stabilization of PVC polymers, reacted HCl gas with lead oxides and sulfates. Data on specific reaction conditions were not provided. Lead sulfate alone was not too reactive; however, $PbO\text{-}PbSO_4$ reacted more energetically than free PbO. Only mechanical mixtures of $PbCl_2$ and PbO were found in reaction products; no evidence of lead oxychlorides was found.

Uberoi and Shadman (1990) found that metakaolinite effectively removed approximately 80% of the $PbCl_2$ fume that they volatilized from a powder inside a high-temperature furnace. They believed that the following reaction took place:

$$Al_2O_3{\cdot}2SiO_2 + PbCl_2 + H_2O \text{ -->} PbO + Al_2O_3{\cdot}2SiO_2 + 2HCl \quad (2.3.1)$$

However, Uberoi and Shadman were not certain whether their lead was sorbed as lead chloride, as lead oxide, or perhaps as neither. Chloride was found in an Auger analysis of

their sorbent particles but not in any crystalline form of lead dichloride. Uberoi and Shadman's process assumes that $PbCl_2$ is formed quantitatively and that there is no diffusional or kinetic resistance to its formation. They expressed an interest in the results of our research. Eddings and Lighty (1991) experimented with silica adsorbents for $PbCl_2$, also making the assumption that the $PbCl_2$ in an incinerator is formed without kinetic impediments.

Like Uberoi and Shadman, Ho et al. (1992) assumed that lead chloride is formed inside an incinerator kiln and volatilized. Under optimal conditions Ho was able to capture 90% of the lead in his charge using a fluidized-bed incinerator with limestone as the sorbent. Although Ho noted that lead oxychlorides may also form, he did not offer any analytical data to indicate that this occurred in his investigations.

2.4 OTHER METAL OXIDE HYDROCHLORIDATION INVESTIGATIONS

Heertjes and Jessurun (1973) reacted cobalt, iron, and nickel (in the mineral laterite) with gaseous HCl and steam to find the optimum conditions with which to preferentially chlorinate cobalt and nickel and win them from their ores. He found, like Chaleroux, that the water in both the cobalt and nickel hydrous oxides, bound water, appeared to promote the reaction with HCl. Reaction with nickel was never more

than 80% complete, which Heertjes hypothesized to be because of the existence of an unreactive compound of nickel. This was not true of cobalt; the extent of recovery could be increased, for example, by leaching the product and resubmitting it to a second HCl treatment. To better correlate his data, he developed a reaction kinetic model that considered bound water. The size of the granule was significant also.

O'Mara (1971) studied the reaction of calcium and potassium carbonates (and other metal compounds) with the HCl gas generated during the pyrolysis and combustion of polyvinyl chloride. He found that the same percentage of the calcium and potassium compounds reacted in pyrolysis or combustion at 600°C regardless of their concentration in the resins. Metal chloride compounds were believed to have formed. No explanation was offered.

Jacobson et al. (1990) studied the high-temperature reactions between metals oxides and metals with chlorine. In the case of cobalt, they found evidence that chlorine vapors penetrate a thin cobalt(II) oxide layer to react with underlying cobalt metal to yield the volatile chloride. Oxygen was less able to penetrate the oxide layer. Jacobson found that the presence of chlorine drastically increases the corrosion of nickel because of penetration of the nickel oxide layer by chlorine, its reaction with nickel, and the vaporization of nickel chloride.

In a most recent development (Wyslouzil et al., 1992) investigated the reaction between lead metal and HCl as a function of temperature and HCl concentration and other parameters such as CO and SO_2 concentrations. Wyslouzil identified $PbCl_2$ as the volatile species and measured volatilization rates but was unable to generate any quantitative reaction rate data, because of uncontrolled surface areas of the samples, among other problems.

2.5 THEORETICAL BACKGROUND

Theory will be considered for two different experimental approaches: (1) reactions between metal oxides and HCl and (2) reduction of metal oxides in a carbonaceous matrix, such as may exist in certain incinerator sludge feeds.

2.5.1 Reaction Between Metal Oxide and Hydrogen Chloride

The reaction between metal oxides and HCl (lead oxide will be the particular focus of this inquiry) is a heterogeneous gas/solid reaction, assumed here to be noncatalytic. It is represented in Eq. (2.5.1):

$$PbO+2HCl=PbCl_2+H_2O \qquad (2.5.1)$$

The reaction is studied as feasible primarily in the range of temperatures such that the product $PbCl_2$ is solid or liquid. This reaction may be analyzed kinetically in terms of frequency factors, apparent activation energy, and adsorption equilibrium constants; for design purposes, however, the rate of reaction may be represented as follows (Wen, 1968):

$$R_a = -k_s C_a^m C_b^n, \qquad (2.5.1a)$$

where R_a represents the rate of reaction; k_s, the rate constant; C_a and C_b the concentrations of reactants; and m and n the orders of reaction. Wen notes, too, that most noncatalytic solid gas reactions are not reversible since the solid structure of the product is usually quite different from that of the reactant.

Diffusion and/or reaction kinetics may represent the rate controlling resistance to the disappearance of reactant. Three basic models may be used: (1) the unreacted shrinking core, (2) the homogeneous model, or (3) combinations of the first two models. In the unreacted shrinking core model, it is assumed that the reaction takes place at an interface, initially at the surface of the particle and gradually moving inward. In the homogeneous model, the reaction takes place simultaneously throughout the particle in which the effective diffusivity of gaseous

reactant is large. In general, in this analysis the diffusive resistance in the bulk gas is assumed to be small.

Wen considered the most general model (the third, or combination model), accounting for both the shrinking core and homogeneous cases in terms of a two-stage reaction. In the first stage, the reaction takes place at a surface layer of the particle and an ash layer has not yet formed. In the second stage, an ash layer has formed at the surface of the particle and the reaction zone is now in the particle interior. The effective diffusivities in the two zones, the ash and the reaction layers, are generally different. For stage 1, we have a material balance [Eq. (2.5.2)]:

$$D_{ea}\partial^2 C_a/\partial x^2 - \partial C/\partial t - kC_a n C_{so} \qquad (2.5.2)$$

where C_a is the concentration of the gaseous reactant, C_{so}, is the initial solid concentration, k is a reaction rate constant, D_{ea} is the effective diffusivity in the reacting solid, and n is a stoichiometric coefficient. We have a reaction rate term:

$$\partial C_s/\partial t = -kC_{s0}C_a n \qquad (2.5.3)$$

where C_s is the solid concentration, with the boundary conditions

$$D_{ea}\partial C_a/\partial r = k_m(C_{a0}-C_a) \text{ at } r=R \tag{2.5.4}$$

$$dC_a/dr = 0 \text{ at } r=0 \text{ also } C_s=C_{s0} \text{ at } t=0 \tag{2.5.5}$$

where k_m is a mass transfer coefficient in the gas phase and R is the radius of the particle. For the second stage of reaction, we have

$$0 = D_{ea2}\partial^2 C_{a2}/\partial x^2 \tag{2.5.6}$$

with the boundary conditions

$$D_{ea2}dC_{a2}/dr = k_m(C_{A0}-C_{a2}) \text{ at } r=R \tag{2.5.7}$$

$$C_s = 0 \text{ for } r_m<r<R \tag{2.5.8}$$

$$C_a = C_{a2} \text{ at } r=r_m \tag{2.5.9}$$

$$D_{ea2}dC_{a2}/dr = D_{ea}dC_a/dr \text{ at } r=r_m \tag{2.5.10}$$

$$C_s = C_{s0} \cdot f(C_{a0}, D_{ea}, k, a) \text{ at } r = r_m \text{ , } t = t_c \qquad (2.5.11)$$

where r_m is the radius of the reacting core zone, the subscript *2* refers to variables within the reacted ash zone, t_c refers to the time required for the solid to react completely to the radius r_m, and *f* is a function representing the solution to the stage 1 problem. The material balance in the reacting core zone is the same as in stage 1. These equations may then be solved to obtain the concentration profile.

Many hypotheses underlie this development. It assumes that the solid state structures of the reactant and ash zones are both homogeneous and that the diffusion of the gas in each zone can be described by effective diffusivities. It assumes equimolar counterdiffusion, which may not be a good postulate in the case of the lead oxide reaction. Isothermal conditions are assumed. The reaction takes place at pseudo-steady state, as noted, and viscous flow through the pores is neglected.

2.5.2 Metal Reduction Mechanism

Quann and Sarofim (1982) studied in detail the mechanisms of metal reduction inside the carbonaceous char of coal. Raask and Wilkins (1965), who originated the theory that metals are reduced locally during coal

combustion, studied gasification in which hydrogen and carbon monoxide were present in significant concentrations. The question of how the metals are actually reduced inside a char remains.

Quann believed that the oxygen potential at the char particle surface is too great to permit reduction and that it must occur inside a particle by a process outlined as follows.

Oxygen must first diffuse from the bulk gas to the particle surface. It will react initially in a thin layer at the particle surface to form carbon monoxide. The carbon monoxide formed at the surface diffuses into the particle and reacts with metal oxides to form volatile elemental or suboxide metal as follows:

$$MO_n(s) + CO \rightarrow MO_{n-1}(g) + CO_2 \qquad (2.5.12)$$

where M represents the metal species.

Quann assumes that the reaction shown in Eq. (2.5.12) is in equilibrium at the metal oxide inclusion surface and that the process is diffusion controlled. The reduced metal, or partially reduced metal oxide, of relatively high vapor pressure, diffuses through the porous char matrix to the char particle surface and through the fluid boundary layer around the particle, where it encounters high oxygen potential, oxidizes, and precipitates to form a fine fume. Quann believes that as the particle temperature drops,

oxygen penetrates farther into the particle and the potential of carbon monoxide drops, shifting the reduction equilibrium.

Quann mentions in passing the Boudouard reaction:

$$C + CO_2 = 2CO \qquad (2.5.13)$$

The carbon dioxide formed inside the particle by the reaction shown in Eq. (2.5.12) can react to generate additional carbon monoxide to resupply the reactants of Eq. (2.5.12). The reaction shown in Eq. (2.5.13) may or may not be in equilibrium. Quann takes no position on this point; however it should not be ignored. The kinetics of the reaction may be significant, and data are available (Yang and Steinberg, 1977).

Quann formulates a theory taking into account the radii of the metal inclusions (all assumed to be equal), their concentrations, and the Knudsen diffusion of the metal vapor through the particles. The principal question to be resolved is whether or not diffusion is the controlling resistance to mass transfer in the external gas film or inside the porous particle. We will encounter a similar question in connection with the kinetics of the PbO hydrochloridation reaction. In the latter case, the situation is much more complex since the metal inclusions

can interact. It is this interaction that is one focus of the theory.

Quann drew on an earlier theory of Felderhof (Felderhof and Deutch (1976) which considered vaporization of metals as occurring from numerous metal inclusions, of small size relative to the coal particles, and of low volume fraction. These are called sources. At the sources the gas/solid reaction was assumed instantaneous. Since Quann assumed that the metal reduction reaction was in equilibrium, his theory would be consistent in this respect. Consider a heterogeneous reaction at steady state between particles and sources. (Quann could consider a quasi steady state since the time required to burn a char particle in its entirety is much greater than the time required for the internal diffusive process.) He assumed an isothermal particle and spherical symmetry. For this symmetry, the diffusive flux, J_a, is taken as

$$J_a = -D_e dn_a/dr \qquad (2.5.14)$$

where n_a is the concentration in this case of CO and r is the radial distance from the source (i.e., the inclusion, not the particle). For a constant D_e, effective diffusivity, the mass balance on reactant *a* is therefore written as

$$\frac{1}{r^2}\frac{d}{dr}\left(r^2\frac{dn_a}{dr}\right)=0 \qquad (2.5.15)$$

for boundary condition (1) $n_a = n_o$ as r approaches infinity and boundary condition (2) $n_a = 0$ at $r = R$, where R is the inclusion radius. The solution of Eq. (2.5.15) is as follows:

$$n(r)=n_o-n_o\frac{R}{r} \qquad (2.5.16)$$

Taking the derivative of $n(r)$ we may obtain the flux that can be integrated over the surface area of the inclusion to yield the vaporization rate, V_i, from a single inclusion:

$$V_I=4\pi D_e R n_o \qquad (2.5.17)$$

Returning to the macroscopic scale, Quann and Felderhof introduce a material balance over a spherical shell, this time of the char particle:

$$cD_e\nabla^2 x_m+\rho_I V_I(r)=0 \qquad (2.5.18)$$

where V_i is given by Eq. (2.5.17), ρ_i is the number density of inclusions, C is the total molar vapor concentration, x_m is the metal mole fraction in the vapor, and D_e is the effective diffusivity in the porous char. In applying this effective diffusivity, Quann assumes that the pore radius is small in relation to the inclusion radius. The rate of combustion of the total char particle is slow in comparison with the previously described diffusive process, which is considered to occur in a quasi steady state. The inclusions are assumed not to change appreciably in diameter during the burning. Quann also assumes that the rate of burning is proportional to the radius of the char as has been empirically demonstrated in combustion technology. The boundary conditions are

$$\frac{dx_m}{dr}\Big|_{r=o}=0 \qquad (2.5.19)$$

$$-4\pi r_i^2 c D_e \frac{dx_m}{dr}\Big|_{r=r_i}=4\pi R D_o \alpha x_{ms} \qquad (2.5.20)$$

where α is a correction for Stefan Maxwell flow (multicomponent diffusion), x_{ms} is the metal concentration

at the particle surface, r_i is the radius of the char particle, and D_o is the diffusivity of oxygen.

Equation (2.5.20) is solved to yield an expression for the concentration of metal vapor with respect to the radius of the particle, from which can be deduced the vapor mole fraction at the particle surface. Quann introduces an "effectiveness factor," the ratio of the vaporization rate of metal from the particle to the product of the vaporization rate from a single inclusion and the total number of inclusions within the particle. This is an analogy to the effectiveness factor used in characterizing the efficiency of a porous catalyst, where the factor is the ratio of the average concentration inside the pores to that at the surface of the catalyst for first-order reactions.

Quann's theory has explained qualitatively the differences in the amounts of metal volatilized from bituminous and lignite coals, which have macroscopic and molecular size distributions of metal inclusions respectively. The theory predicted, for example, that the fractional vaporization rate from a particle of bituminous coal was inversely proportional to the diameter. Data bear this out. In the case of the lignite coals, the fractional vaporization rate is proportional to the inverse second power of the radius. This theory is also supported by data. These relationships would not hold for a kinetically

controlled reaction or in a model without interactions between inclusions, Quann maintains.

Difficulties with Quann's theory are several: the pores are assumed to be all the same diameter and the effective diffusivity is assumed to be constant, both of which are unlikely. The effect of the Boudouard reaction which may be important, is ignored. The drop in accuracy of the correlation, large at lower temperatures, is not explained, and the behavior at such temperatures may be of special interest to incineration. Quann notes that the correlation between the total metal volatilized in low-rank coals (where the metal is dispersed on the molecular scale) and its concentration does not agree with the theory. The potential effects of multicomponent oxides such as those found in many minerals are neglected, and such effects may be significant, particularly in incinerator feeds.

Quann's theory is therefore a starting point for an analysis that addresses the varying geometry of an incinerator char and that may provide enhanced sophistication.

2.5.3 Metals of Interest

A range of metals are of interest because of their toxicity or suitability as surrogates for hazardous metals found in incinerator feeds. The U.S. EPA list of ten hazardous metals: Pb, Cr, Cd, Tl, As, Sb, Cr, Hg, Ag, and

Ni. Incinerator gas temperatures range between 600 and 1000°C (Bonner et al., 1981), temperatures at which many of these metals and their compounds can be expected to have appreciable vapor pressures.

Vapor pressures for PbO and $PbCl_2$ are shown in Figure 2.5.1. Kiln bed temperatures vary widely between 200 and 1000°C and may be much lower than the gas temperatures (Cundy et al., 1989).

As seen in Table 2.5.1, certain elements (e.g., uranium) are more volatile than their oxides and that the chlorides (though sometimes unstable) are generally more volatile than the elements. There are exceptions. Arsenic and lead, among others, have oxides that are more volatile than their elemental forms, and their chloride compounds are potentially of greater concern to incinerator operation. Chromium metal is believed to have volatile complex oxychlorides. Magnesium and calcium, of low toxicity and not of direct interest in incineration, may be interesting because of the availability of data from previous research in coal combustion. Metals such as beryllium and uranium, because of their high toxicity, usually require surrogates. Cadmium and bismuth are important metals to examine. Because their elemental forms are more volatile than their oxides, they are on the EPA regulated list of hazardous or controlled metals, and they have been found in incinerator stack gases. Antimony is of interest because of its

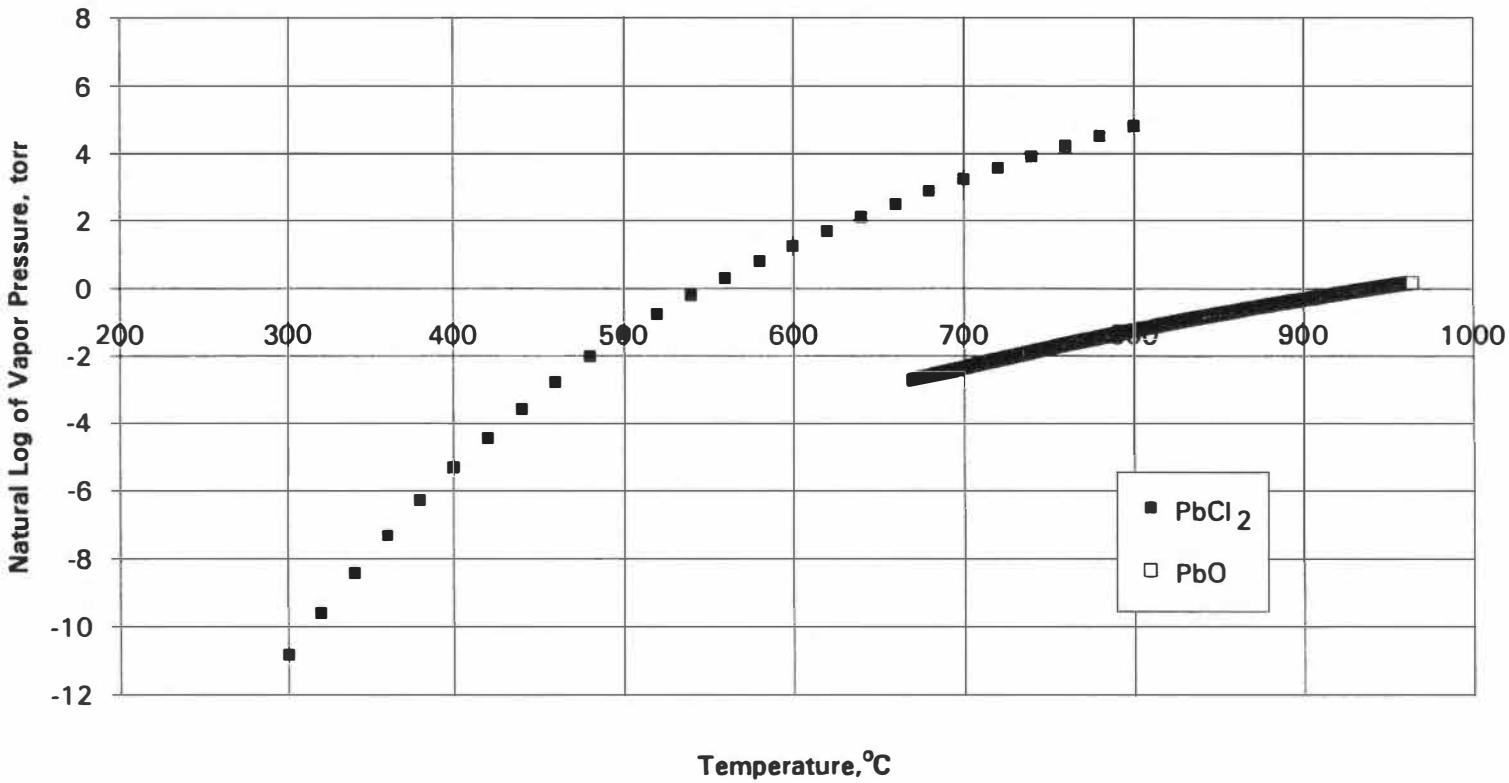

Figure 2.5.1. Comparison of vapor pressures of lead oxide and lead chloride.

Table 2.5.1. Melting and boiling points of selected metals, oxides, and chlorides at one atmosphere pressure

Species	Melting Point, °C	Boiling Point, °C
As	327	613[b]
As_2O_3		315[a]
AsCl3	-18	130
Ag	961	2210
AgCl	445	1550
Ag_2O	16	300b
Be	1280	2770
BeO	2550	3900
$BeCl_2$	440	520
Bi	276	1560
Bi_2O_3	820	1890
$BiCl_3$	227	300d
Mg	650	1107
MgO	2852	3600
$MgCl_2$	708	412
Ca	838	1440
CaO	2570	2850
$CaCl_2$	430	1490
Cd	321	767
CdO		900b
$CdCl_2$	568	960
Cr	1875	2665
Cr_2O_3	1900	---
$CrCl_2$	993	1490
Zn	420	907
ZnO	1800	--b
$ZnCl_2$	283	732
Pb	327	1740
PbO	886	--
$PbCl_2$	501	950
Sb	631	1910
Sb_2O_3	656	1550
$SbCl_3$	73	283
U	1132	3818
UO_2	2500	--
Ucl4	540	792

[a]decomposes.
[b]sublimes.

Source: CRC Handbook of Chemistry and Physics, 1972.

extremely volatile chloride and its presence on the EPA list.

The basic working hypothesis is that if metal chlorides are volatilized, they will nucleate as fine fume. It is important nonetheless to verify this hypothesis in some experiments and to attempt to establish the conditions such as temperature and gassing rate under which fuming occurs.

3. EXPERIMENTAL PROCEDURE, APPARATUS, AND TECHNIQUES

Experimentation was divided into two efforts: (1) attempts to narrow the field of focus (the problem of metal emissions) and (2) the specific investigation of the kinetics of the lead oxide hydrochloridation. Several possible avenues of research were examined before this particular focus was selected.

3.1 EARLY INVESTIGATIONS OF METAL REDUCTION MECHANISMS

As discussed in Sect. 2.1, fine particulate can be generated through the volatilization of metals in their suboxide and elemental forms. This reduction is usually caused by action of CO or elemental carbon during combustion and is dependent on the presence of solid carbonaceous material at high temperature in the proximity of the metal species. In a separate mechanism, evidence has been offered that fine particulate can be formed through the fracturing or explosion of aggregates containing or producing gases during the evaporation or combustion processes.

3.1.1 Early Background Investigations

In order to assess the reduction/volatilization mechanism, oxide powders of zinc, magnesium, and other metals were mixed with heavy oils such as diesel fuel number 2 and lubricating oils (slightly heavier than number

2 oil) and suspended from a fine quartz fiber, and platinum and tungsten wires inside a vertical tube furnace. To assess the fracturing mechanism, nitrate solutions of 1 to 10 wt % zinc and calcium were prepared and also suspended from the various rods. The latter mixtures wetted the suspension rod but would not form a pendent drop. In both cases the techniques were generally unsuccessful in producing volatiles or particles. The residence time of the droplet in the furnace was on the order of a second, and the droplet remained in liquid form until it exited the high-temperature zone. While some liquid remained, the temperature of the droplet would have remained low. A solid carbonaceous material was not formed in the time frame of these experiments, and the droplet probably remained relatively cool, below the vaporization point of the heaviest fraction of the number 2 fuel oil. In one case, the $Zn(NO_3)_2$ solution seemed to enlarge and explode to produce particles, but the technique was too irreproducible to provide quantifiable data.

A sample of carbon powder, mixed with MgO at a mole ratio of 1:1.5, was placed inside a thermogravimetric analyzer under an inert gas in an attempt to evaluate the reduction/volatilization hypothesis under more-controlled conditions. The sample was ramped at 3°C/min to 1200°C and held for 1 h at temperature. This temperature and time represent a maximum hazardous waste incinerator temperature

and a maximum kiln residence time. The results from these experiments were of particular interest. No reduction or volatilization of the MgO took place, but the carbon powder disappeared completely even in an atmosphere of nitrogen. Air or water contamination could not be identified. A special gas chromatographic filter specific for oxygen was installed, and helium was used as an inert blanketing gas; however, but the carbon portion of the sample again volatilized. Since carbon has a very high boiling point (4839°C) in its elemental form, it is likely that some compound, possibly CO, formed from reaction with adsorbed water and oxygen. Since the carbon was of the activated form with a high surface area, this hypothesis seems reasonable. However, as a result of the difficulty excluding oxygen from the reaction, this avenue of investigation was dropped by the experimentalists and judged to be an unrealistic simulation of an incinerator. In an actual incinerator environment, it appears unlikely that oxygen would ever be excluded to the extent to which it was excluded in the laboratory and even in the laboratory, volatilization of the metal was not observed.

3.1.2 Preliminary Scoping Experiments with PbO Hydrochloridation

As noted earlier, metal chlorides have, in general, higher vapor pressures than metal suboxide or elemental forms. For this reason and the infrequent success in producing particles from carbonaceous mixtures of metal oxides, hydrochloridation reactions were investigated. As shown in Figure 3.1, a simple apparatus was assembled to examine the progress of the reaction of HCl with PbO powder placed in a horizontal quartz boat within a horizontal tube furnace. The HCl gas flowed over the bed of PbO powder at concentrations between 500 and 2000 ppm in either air or mixtures of nitrogen. The temperature was varied from 50 to 500°C. The sample and boat were removed after each experiment and weighed to determine the extent of reaction. Although there was evidence of a reaction between HCl and PbO at temperatures above 300°C, the data were highly scattered and the procedure was extremely cumbersome. The weight gains were small and were easily obscured if any sample was lost by volatilization or in the transportation and weighing processes. A grey-white coloring of the surface of the PbO powder contained in the boat was also evidence of reaction. Occasionally a bright orange color was observed, which may have been the result of a

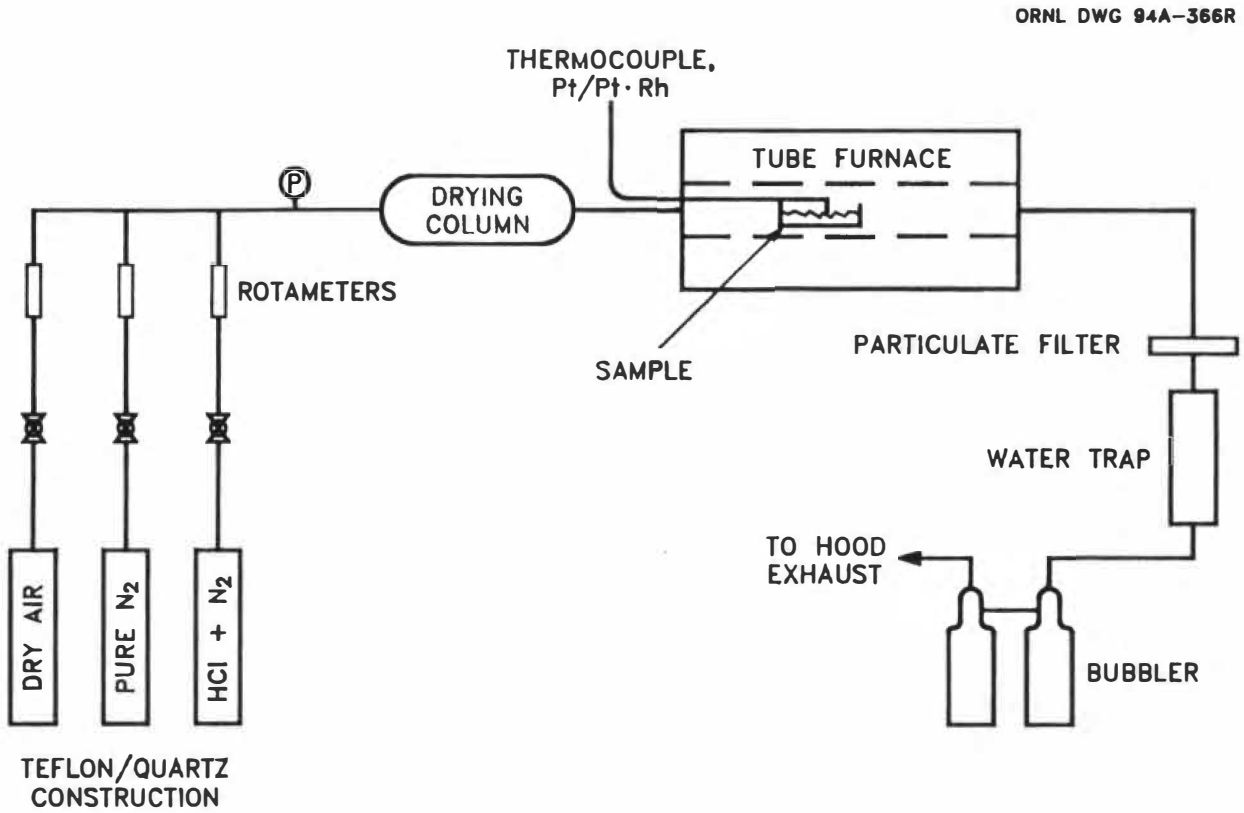

Figure 3.1. Horizontal furnace experimental apparatus.

polymorphic alteration in the PbO crystal. The results were encouraging in that reaction was clearly observable and measurable; however, the technique required modifications to improve reproducibility and practicality.

3.2 PRINCIPAL EXPERIMENTAL APPARATUS AND PROCEDURE

3.2.1 Introduction

This apparatus consists of a vertically mounted high-temperature furnace with a single heating zone. A quartz tube was mounted inside the furnace to serve as a reaction chamber. A sintered pellet of PbO was hung from a platinum wire, which connected to a nylon monofilament line that was hung from the bottom hook of a Mettler model AE100 bottom-weighing balance of a mass resolution of 0.001 g. The overall schematic is shown in Figure 3.2. The appartus is similar to that of Figure 3.1 but has on-line mass measurement capability and other modifications. A photograph of the apparatus is shown in Figure 3.3.

Cylinders of nitrogen, argon, dry air, and HCl were used to provide inert and reactive atmospheres to the system. The gas flow rates were measured using rotameters and then mixed in "tees" before being fed in upflow to the reaction tube, which contained a 3-in. section of 0.25-in. diam quartz pellet packing. After reacting, the gases exited a side arm of the quartz reaction tube and were met and

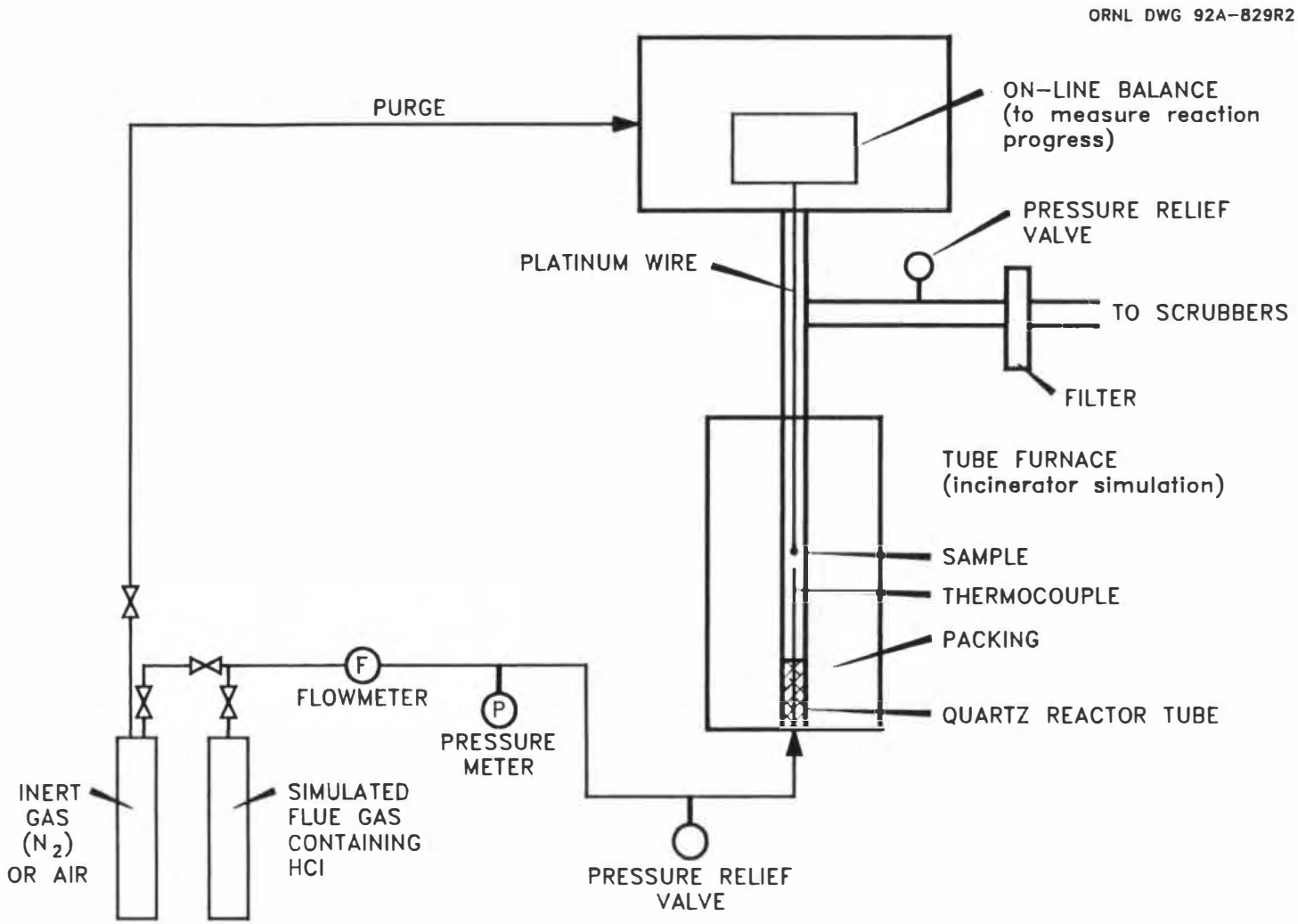

Figure 3.2. Vertical furnace experimental apparatus with on-line data collection.

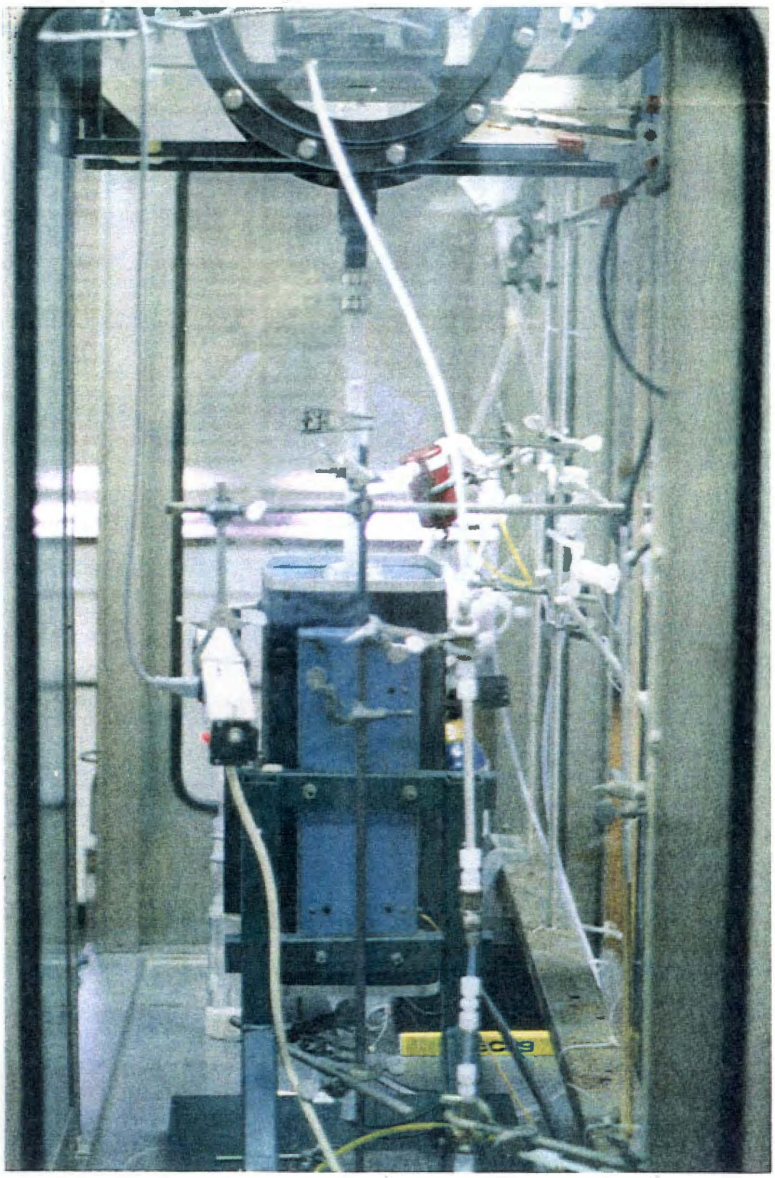

Figure 3.3. Photograph of vertical furnace experimental apparatus.

mixed with the purge gas that was fed to the balance chamber to prevent any residual HCl or particulate from entering the balance chamber and damaging the balance.

3.2.2 Materials

Hydrogen chloride, a certified 5% mixture in N_2, from Air Products and Chemicals provided the reactive gas. Two cylinders were used in the course of approximately 250 runs. Reagent-grade lead oxide powder was used to prepare the sintered sample pellets. Their preparation is described later in the procedure section. The surface area of the powder was measured using the BET (Brunauer, Emmett, Teller) technique, and the surface area, pore size distribution, and pore volume of the sintered pellets were measured using mercury porosimetry. The results are given in Table 3.1. Plant air filtered through a $CaSO_4$ dehydrator was used, principally along with bottled air, N_2, and argon (used in the preparation of sample pellets) of high purity. Texaco Havoline 10W/40 lubricating oil was used in the manometer to minimize reaction with the HCl gas and provide acceptable pressure resolution. Sodium hydroxide solution was used in the two-stage bubblers to scrub residual HCl from the exiting gases. A sodium hydroxide pellet bed was used as a final scrubber.

Table 3.1. Lead oxide powder and pellet physical characteristics

BET surface area of powder	
Sample 1	0.0515 m^2/g
Sample 1	0.0538 m^2/g
Sample 3	0.0642 m^2/g
Pellets	
Pore diameter	2.03 μm
Density	7.65 g/cm^3
Pore area	0.84 m^2/g
Skeletal density	9.38 g/cm^3
Porosity	0.18

3.2.3 Apparatus Construction

The description of the apparatus will in general proceed from the gas cylinders to the final scrubber stage in the direction of reacting gas flow.

A 33-scf cylinder size 7 with CGA 330 fitting was equipped with a two-stage stainless steel regulator, bonnet vent adaptor, and "Chromnut" mounting nuts, all from Air Products and Chemicals. Regulators in metals more noble than stainless steel were not available, and it was decided that the anhydrous HCl mixture was sufficiently compatible

with stainless steel. In practice, no corrosion was noted over the course of 2 years of experimentation.

All construction materials which came into contact with the HCl were of stainless steel, Teflon, quartz, platinum, or polyethylene. Initially, Teflon pipe fittings were used to provide connections to the HCl metering rotameter; however, they were found to be too prone to cross-threading and were dropped in favor of stainless steel. The stainless steel fittings lasted a number of months before corrosion became severe; it was difficult to exclude all moisture from the assembly. The HCl rotameter, Cole Parmer model L-03217-60 tube N062-01S, was of Teflon and glass construction with a sapphire float and a Teflon needle valve. This rotameter was replaced with a meter of identical design when a piece of dust became attached to the sapphire float and hindered its rotation. The sapphire ball was actually later removed and cleaned, and the first rotameter was kept as a spare. The inert gas rotameter was a Cole Parmer model L-03269-19 tube number NO82-03ST with a stainless steel float.

Initially, all tubing, valves, and fittings were of Teflon PFA (perfluoroalkoxytetrafluoroethylene) in a 0.25-in. standard size. As noted in Figure 3.2, the lines from the two rotameters met in a mixing tee shortly past the meter exits. One line proceeded thence to the bottom of the tube furnace, and a second dead-ended to the manometer. The detailed design of the quartz reaction tube is shown in

Figure 3.4. Ball and socket or taper quartz joints were used at the ends of the tube to permit connection and disconnection. The taper joints were found to be slightly easier to seal. Through the bottom joint a fitting was provided to accommodate a closed-ended quartz tube, 0.25 in. in diameter, inside of which a 24 AWG Type R Pt-13% Rh versus platinum and later a Type K NiCr versus NiAl thermocouple was placed. Alumina sleeve spacers were used to prevent the thermocouple wires from crossing. The Type R thermocouple proved to be very easily broken during installation and removal because of its brittleness, its high temperature capability proved unnecessary, and its corrosion resistance was obviated because of its encapsulation in the quartz rod. It was replaced by the much less expensive Type K thermocouple. The thermocouple junction itself extended beyond the alumina spacers and was placed as near as possible to the pendent sample without actually touching it. The bottom 3 in. of the reaction tube was filled with 0.125-in.-diam quartz pellets made from sliced sections of quartz rod 0.375 in. in length. Although quartz spheres would have been preferable as packing, they could not be located.

The tube furnace was a high-temperature Lindberg Model 54081-A, 800 W, 115/230 V, with a 20-in. heating zone, equipped with silicon carbide heating elements. Initially no controller other than a Variac variable-voltage

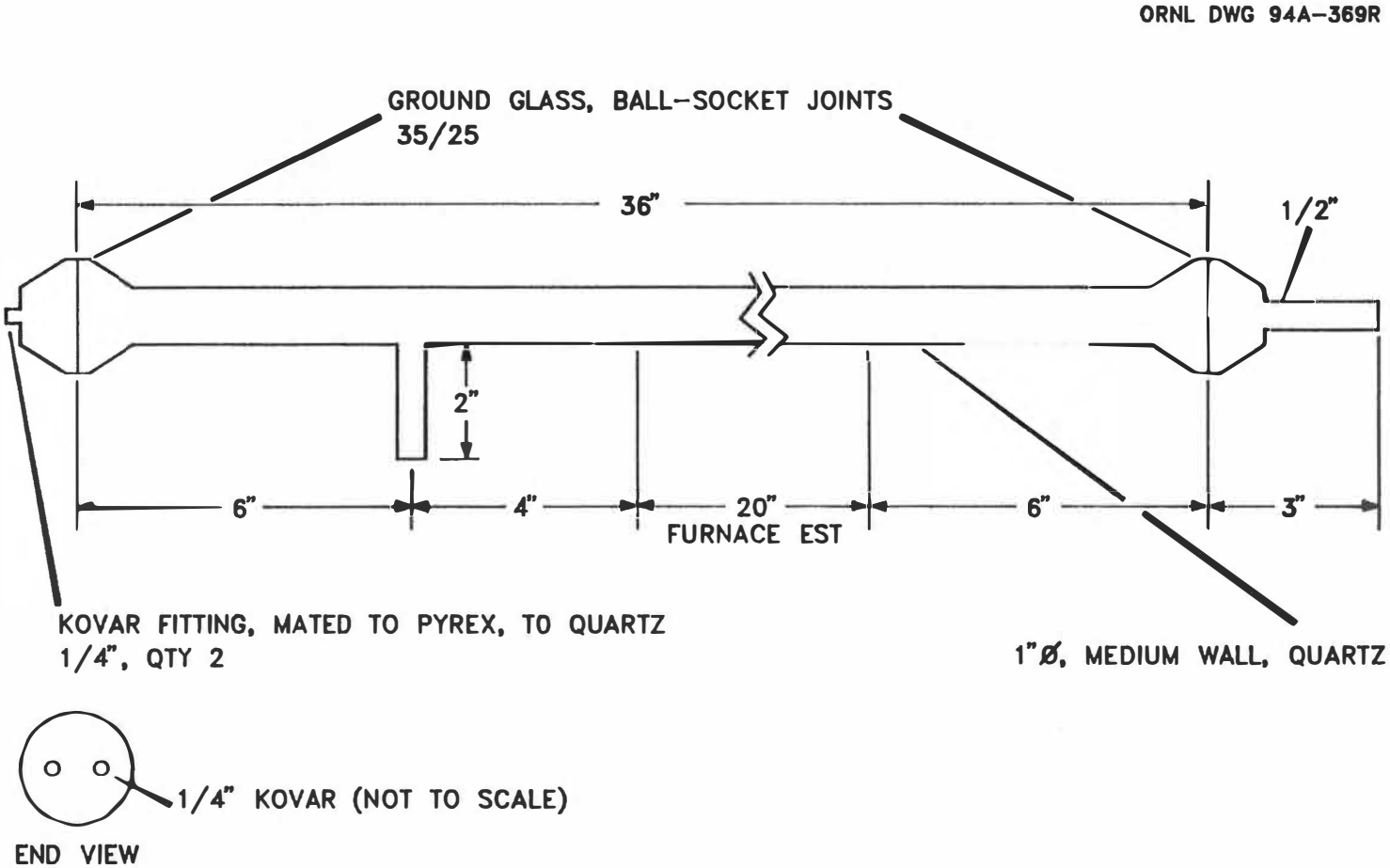

Figure 3.4. Quartz reaction tube.

transformer, which was used to adjust the temperature. This proved inadequate as the temperature of operation was raised, and an Omega model CN310KF temperature controller with self-tuning capability was installed. Initially the control point was inside the furnace near the coils; however, this location provided poor control because of the distance between the sample and the heating coils and the consequent lag in response time. The internal tube thermocouple, used to measure the sample temperature, was then instituted as the controlled temperature. All temperatures were recorded on a Johnson Yokogawa model microR 100T strip-chart recorder, which accommodated all varieties of thermocouples.

The reacting gases and particulate fume exiting the tube furnace met the outgoing purge gas from the balance chamber. The sample itself was hung from a platinum wire that was arranged in links of about 1.5 in. each. This was quite important to provide the wire some flexibility and at the same time permit the sample to hang reasonably plumb. A gold plated link chain was attempted but the plating was too porous to prevent corrosion. Platinum and platinum/rhodium wire from broken Type R thermocouples proved very useful in this capacity and did not corrode excessively. The platinum link wire did not extend the entire way to the balance but met a brass fishing line connector that was attached to a

nylon monofilament line that was then tied to the bottom hook of the Mettler balance.

A Mettler model AE50 microprocessor-based bottom-loading balance with 0.001-g mass resolution was used. It was sufficiently compact to fit inside the pressurized purge chamber, maximum pressure 20-in. water column, and could be interfaced to an IBM 8088 basic PC, which recorded mass data at variable time intervals. A software package called Mettler Balance Talk from Labtronics, Inc., Guelph, Ontario, designed specifically for the Mettler instruments, was used to record data and control the balance. The balance could be turned on, tared, and adjusted remotely. Since the balance was inside a purge chamber at all times and the chamber was not easily opened and closed, it was desirable to have this remote operability.

The purge chamber was a schedule 80 PVC flanged pipe, 12 in. in diameter with two transparent Plexiglas bolted plates. The design is shown in Figure 3.5. Holes were drilled in the Plexiglas sheet to accommodate the RS232 parallel interface connector, the power supply, and purge gas fitting. The purge gas was controlled with a dedicated rotameter and flowed at all times. No evidence of fume or HCl penetration to the balance chamber was ever detected. A distance of approximately 2 ft separated the exit of the tube furnace from the balance, and the balance remained sufficiently cool.

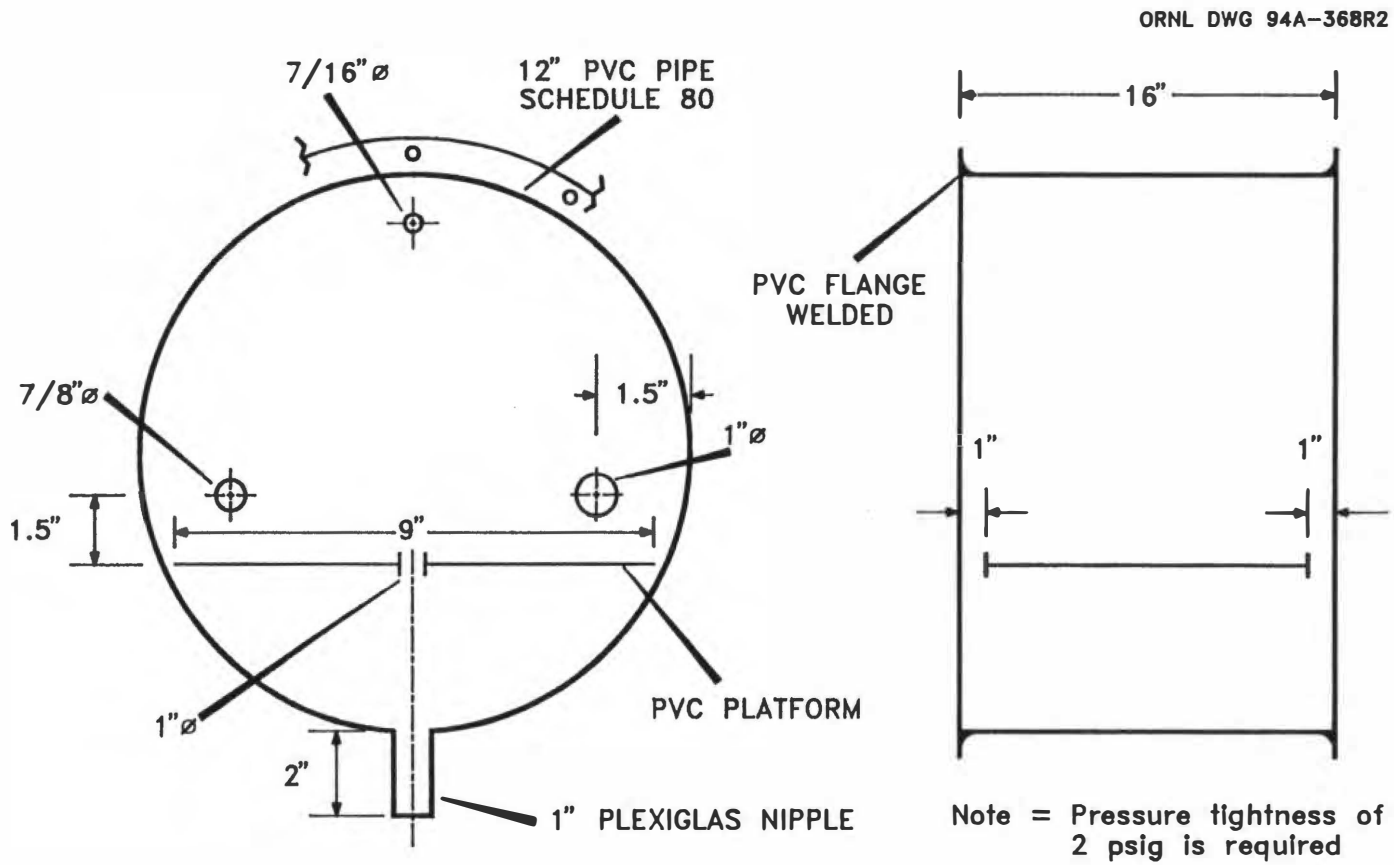

Figure 3.5. Balance pressure chamber.

The purge gas and reacting gas streams were combined in a 0.5-in. corrugated Teflon tube (used to facilitate connecting skewed fittings) and entered a 0.1-μm Headline cartridge filter with a stated 99.9% particle collection efficiency at 0.1 μm. The gas exited this filter without a significant pressure loss until the filter became heavily loaded, at which time it was replaced. The gas proceeded to two parallel 12-in. glass bubbler columns filled to a 2 in. depth with alumina 0.125-in-Berl saddle packing. As a final guard, a 4-in-diam plastic funnel was filled with sodium hydroxide beads, and the gas passed through it before finally exiting to the California hood exhaust. A pH indicator was used in the tubing from the bubblers to the funnel to detect any acid gas breakthrough. None was ever observed.

Some of the Teflon tubing and fittings which were placed downstream of the tube furnace were replaced with polyethylene in the course of the experimentation because of the poor workability and bendability of the Teflon tubing. No degradation of the tubing was found after 6 months of service. In particular, fittings and tubing which were located downstream of the experimental apparatus were not critical. Teflon fittings and tubing may have been more prone than other plastics to compression set and after a certain time in service they assumed the position and shape in which it was installed.

3.2.4 Sample Preparation Procedure

Our objective was to produce PbO samples of an easily modeled geometry and of reproducible chemistry and porosity. Several techniques were tried before settling on a two-stage sintering procedure, which was adopted largely by trial and error. A short cylindrical pellet or a sphere could be easily modeled. However, a sphere, in particular, is hard to produce because the mold is difficult to machine. A cylinder was chosen as a more tractable solution.

An additional complication was the need to hang the pellet from an inert wire in the center of the tube furnace. Thin (1-mil) platinum wire was chosen for this purpose.

Initially the technique was to take a finely ground sample of lead oxide powder, dumped, not tamped, into an inert mold and sintered until it was strong enough to remove from the mold but not so strong as to have bonded to the mold. Graphitic carbon was chosen as a first iteration for the mold material because it was not expected to adhere strongly to the PbO, it was easily machined to the proper shape, and it could withstand high temperatures. This choice was quickly abandoned because the graphitic carbon oxidized rapidly enough to reduce the lead oxide quantitatively. Lead metal was the result. Noble metals were considered for a period but abandoned for reasons of practicality and procurement time. Next, ceramic materials known as Macor and Lavite were attempted. Both

disintegrated rapidly at 900°C within 30 min, probably from reaction with the PbO (itself a good fluxing agent), and could not be recovered after a sintering experiment. The result was the same with steel.

Inconel and nickel molds were then machined as shown in Figure 3.6 from 0.5-in. rod stock. The molds were drilled 0.5 in. deep, 0.25 in. in diameter. Inconel suffered the same fate as the steel and Lavite, but nickel worked well and displayed very little deterioration. Samples became increasingly difficult to remove from the molds with use, however, and several different cleaning techniques were tried, including sand blasting and scrubbing, to remove a scale that appeared to be a greenish-colored NiO. All eventually proved inadequate. Also, problems persisted in the degree of sintering and consequently in the porosity of the pellet and the available reaction surface area. Hydrochloridation data were not reproducible.

Two developments overcame these problems: an inert gas furnace and a two-stage sintering process. The inert gas technique greatly reduced the degradation of the molds and facilitated sample removal through slow cooling of the assemblies in the inert atmosphere. The staged sintering technique was even more significant. One of the difficulties, as noted, was finding a sintering temperature and time that produced samples of sufficient integrity to

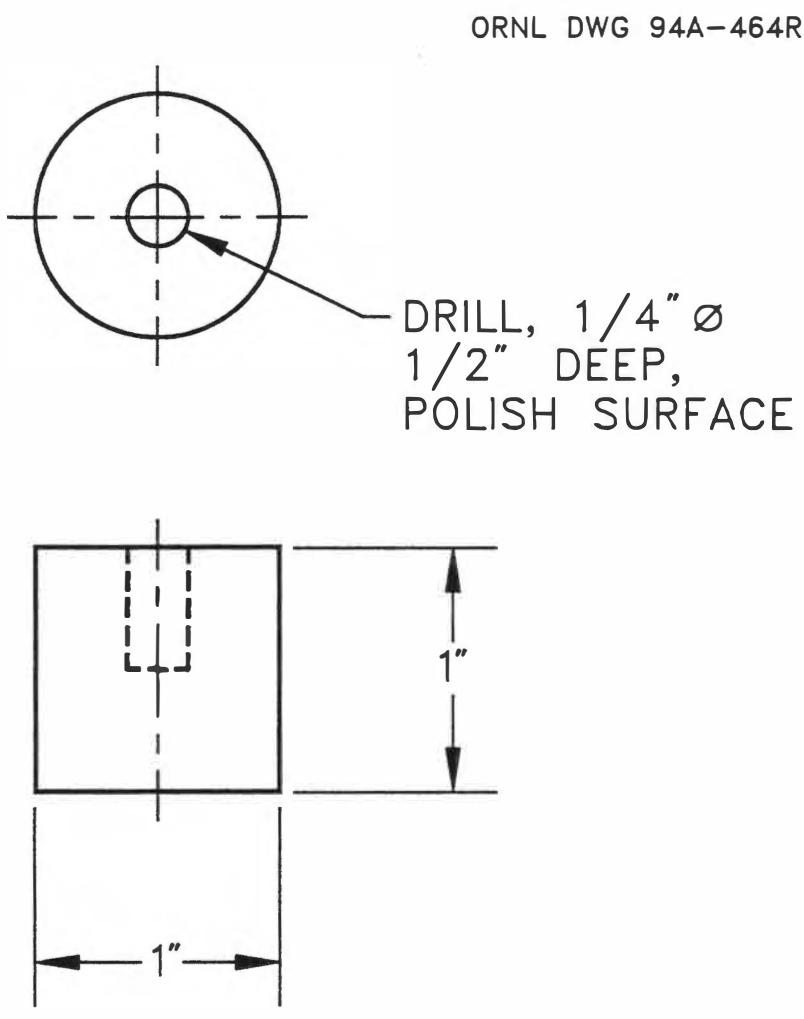

Figure 3.6. Sample pellet molds.

permit their removal from the molds without falling apart, at the same time avoiding conditions that could melt the samples to the side walls of the mold. This difficulty was solved by sintering the samples at 860°C for 10 min, cooling them, removing them from the molds, and then sintering them again outside their molds at 800°C for 1 h, all in nitrogen. After the first sintering, the samples were easily removed from their molds but were quite porous and friable; however, the samples were sturdy following the 1-h sintering.

Other techniques were tried. A plunger was machined of stainless steel to attempt to press pellets as others had done (Uberoi and Shadman, 1992), but the pellets could not be removed without disintegrating, similar to the early sintering technical problem. A MgO mold release was used with the nickel molds, but it contaminated the pellets excessively and offered no clear benefit.

Small improvements were made to the two-stage, inert gas sintering technique during the course of the experimentation. Sieving the PbO powder, which tended to cake with time, improved the quality and reproducibility of the pellets and helped prevent fissures. A slow cooling period after the high-temperature sintering also reduced cracking of the samples.

3.2.5 Hydrochloridation Experimental Procedure

First, a fresh PbO sintered pellet was hung inside the tube furnace from the air-purged bottom-weighing balance. The recording of the sample weight was begun with the computer. The taper or ball joint was reclamped and tightened to seal the reaction tube. The purge gas and the carrier gas flow were then begun and the furnace brought to temperature. When the measured temperature of the sample had stabilized at the set point as established by the straight line printed by the chart recorder, the hydrochloridation experiment was ready to start.

The official beginning of the experiment was at the moment the HCl/N_2 flow valve was opened. This moment was noted in the experimental log and on the computer that recorded the weight on the balance. Since the HCl/N_2 flow was only approximately 5% of the total flow through the reaction tube, it did not seem to affect the temperature noticeably when the flow was started. The temperature was monitored and recorded in the laboratory notebook at several times during the course of the experiment. After the temperature controller was installed, the temperature varied by no more than 1°C, even during the course of a high-temperature experiment. When the experiment was terminated, the HCl/N_2 valve was closed and the flow was allowed to decay, a process that required about 1 min. With experience, the rotameter needle valve could be preset and the HCl

regulator block valve opened to begin an experiment at a given flow rate. At the end of the experiment, the block valve was simply closed.

After the HCl had been purged, the apparatus was opened and the reacted pellet removed and typically quenched rapidly to room temperature. Following certain runs, the sample was allowed to remain at temperature for a period of time while weight data continued to be collected every minute. In a few instances, this data collection was continued at temperature for a week to bring the sample to a constant final weight and to volatilize all volatile reaction products. In other cases, the temperature of the sample was raised following the run in order to hasten volatilization or to observe the effect it produced. In rare instances, the temperature of the furnace was lowered to some intermediate value following the run. However, all data collected during an individual hydrochloridation were isothermal.

3.2.6 Analytical Methods

A wide variety of instrumental techniques was used to analyze pellets following the hydrochloridation experiments. The workhorse of techniques, however, was x-ray fluorescence, wavelength and energy dispersive analysis. X-ray powder diffraction patterns were obtained on the PbO powders, the entire reacted pellets, and the films of

reaction products. Electron spectra were also made of the surfaces of reacted pellets with and without sputtering to inspect elemental profiles. Reflective Fourier transform infrared (FTIR) spectra were made of sample surfaces. Scanning electron micrographs were made of the particulate and of cross-sectioned pellets that were cast in epoxy resins and polished with 1 μm diamond grit. The PbO powder was analyzed using an Oak Ridge K-25 Site in-house designed nitrogen BET surface area analyzer and a Micromeritics model 9305 mercury porosimeter. Petrographic examination of the samples was considered. However, sample preparation techniques in which samples are cast in epoxy resin, sliced, and polished were not possible with samples of the friability encountered here. Periodically, samples of the particulate were collected for physical and chemical analysis.

3.2.7 Experimental Difficulties

The hanging wire required cleaning and repair after several runs. The sample not infrequently fell from its hanging wire, creating a large number of difficulties. The PbO is a good solvent, even with quartz, and PbO pellets that had fallen tended to fuse the quartz packing together and make it impossible to remove the thermocouple tube without breaking it. Once, the reaction tube itself developed a pinhole from the corrosive effects of the PbO.

4. RESULTS AND DISCUSSION

4.1 DATA TREATMENT

Data were acquired on the progress of the hydrochloridation reaction of PbO using various thermogravimetric techniques depending on the temperature. X-ray fluorescence and diffraction and other analytical methods were used to supplement thermogravimetric results. Data were acquired over a range of temperatures from 260°C, where chemical reaction was first observed, to 690°C, at which point the thermogravimetric technique could no longer produce reproducible data. Based on the thermogravimetric data and the morphology of the hydrochloridated specimens, four distinct temperature regimes of reaction were identified. This discussion focuses on these four regimes. Global reaction rates (the average reaction rates throughout the course of the reaction) are shown in Figures 4.1.1 and 4.1.2 at 2000 and 4000 ppm HCl respectively. These graphs would suggest at least three distinct behaviors: a rapid rise in reaction rate at temperatures below 310°C, which we call Regime 1; a plateau region extending to around 600°C, which encompasses Regimes 2 and 3; and a region of rising reaction rate between 600 and 690°C (with more data scatter), which we designate Regime 4. The plateau region is divided into two regimes based on the morphology of the

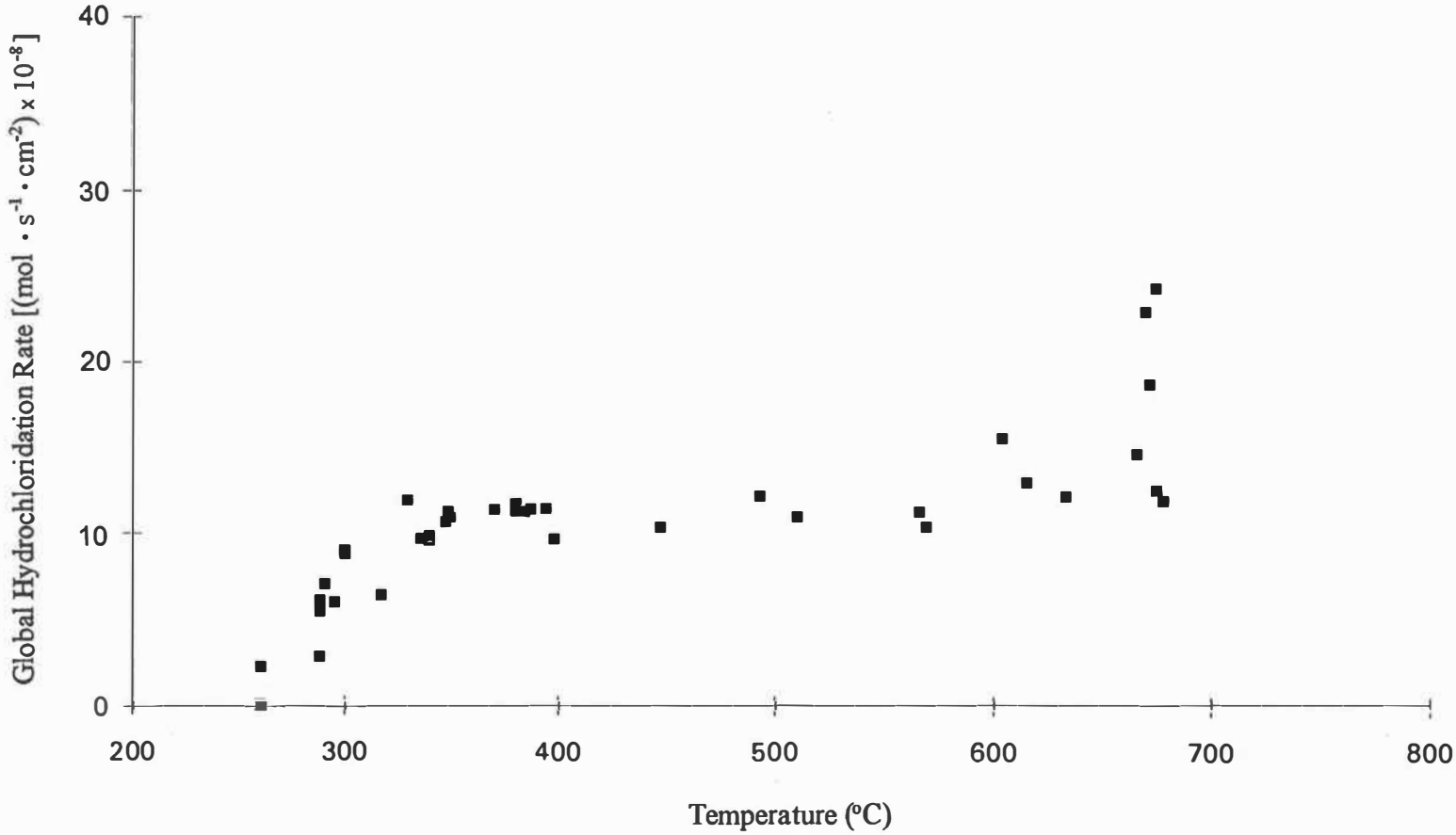

Figure 4.1.1. Global hydrochloridation reaction rates versus temperature, 2000 ppm HCl.

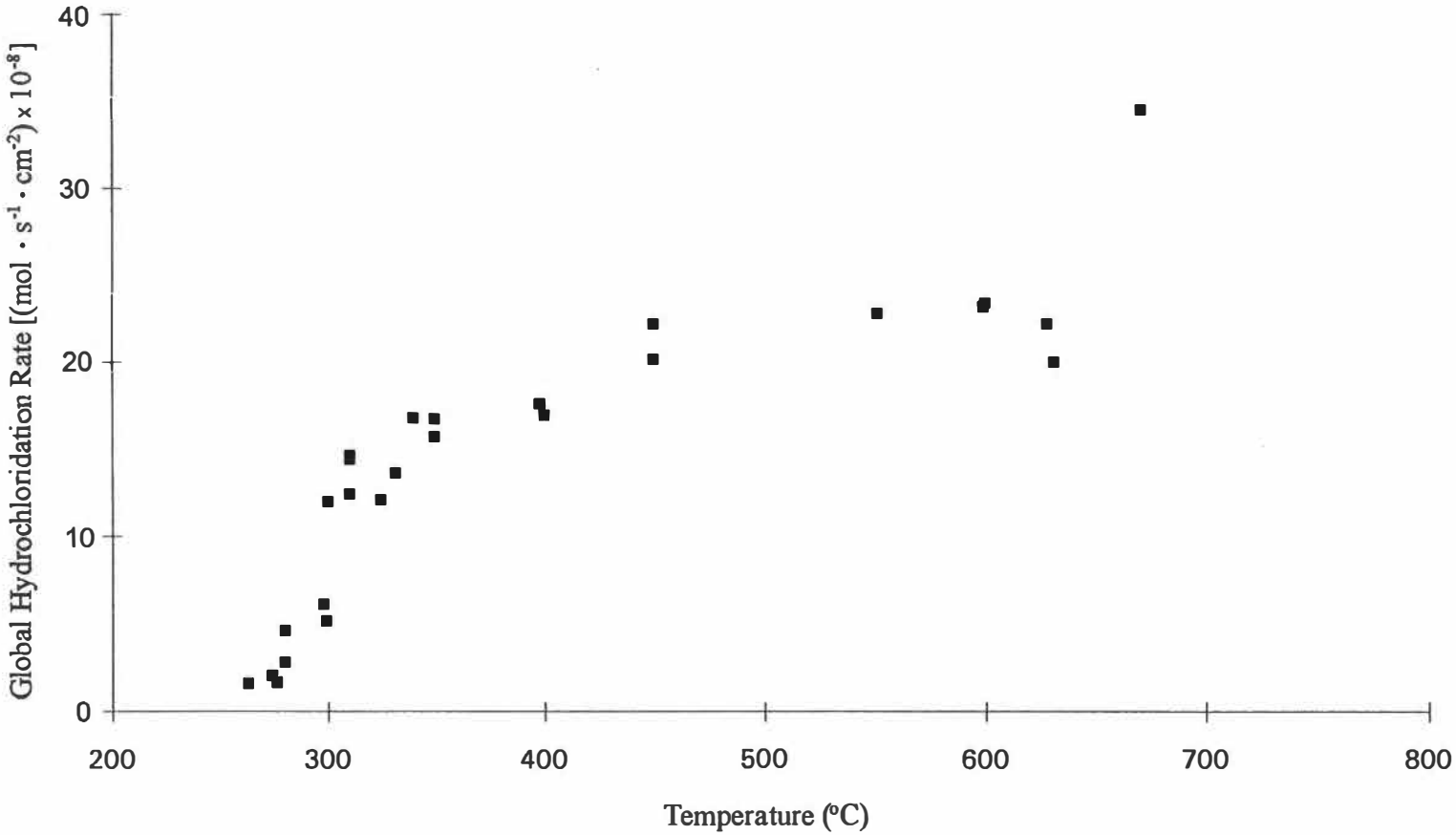

Figure 4.1.2. Global hydrochloridation reaction rates versus temperature, 4000 ppm HCl.

particles and differences in the thermograms, even though the global reaction rates are quite similar. Between 310 and 450°C, a solid porous ash phase is formed, and from 450 to 590°C, near the PbO-$PbCl_2$ eutectic temperature, a liquid ash phase of gradually increasing volatility (as observed in the thermograms) is formed.

At temperatures between 250 and 310°C (Regime 1), the gain in mass of the PbO pellet could be determined as a function of time, and global and local reaction rates may be calculated. Assuming a volatile gaseous HCl reactant and H_2O product and a nonvolatile $PbCl_2$ product, the reaction

$$PbO(s)+2HCl(g)=PbCl_2(l,s,g)+H_2O(g) \qquad (4.1.1)$$

if taken to completion, would yield an increase in mass of 24.7%. Since the initial and final masses of the pellet are determined, the extent of conversion can be calculated. In Regime 1, models of chemical kinetic and diffusional control will be applied.

In Regime 2, between 310 and approximately 450°C, at which point volatilization begins to become important in the time frame of our experiments, a model primarily of solid-phase diffusional resistance will be provided. The reaction rate can be still calculated as in Regime 1 from the weight gain.

In Regime 3, at temperatures between 450 and 590°C, a modification to the above thermogravimetric technique is necessary since the volatilization of $PbCl_2$ becomes measurable and interferes with the simple weight gain technique of Regimes 1 and 2. In Regime 3, as will be shown, the volatilization of $PbCl_2$ eventually becomes so great that only a weight loss is observed. There is a temperature near 500°C at which the weight loss and gain nearly match and no change in the mass of the sample is observed although morphological evidence of reaction can be found.

The progress of the reaction cannot be followed as readily with respect to time because of these interacting influences in Regime 3; however, global reaction data can still be extracted. This is done by allowing the reaction to proceed with simultaneous hydrochloridation and $PbCl_2$ weight loss to a quasi steady state. In practice, this required only a few minutes. Then the steady state reaction is conducted for a comparatively long period of time, 30 to 90 min, after which the HCl flow ceases and the system is purged of reactant gas. Next the sample is allowed to remain at temperature, or the temperature is even raised. The lead dichloride is then allowed to volatilize over a long period of time, 24 h or more, until the sample has reached a constant weight. The total mass of lead dichloride formed can be then determined based on the assumption

(supported by the absence of lead oxychlorides in the fume from the reaction) that all volatilization occurred in the form of lead dichloride, not as an oxychloride. Since the total reaction time and the total mass of lead dichloride formed were known, the global reaction rate could be calculated.

In Regime 4, between 590 and 680°C, the range at which most of the remainder of experiments were conducted, combinations of the two techniques, initial weight gain and total weight loss, were effective. As will be seen in this regime, the initial reaction rate was quite high and a weight gain was again observed as at low temperatures. The initial reaction rate could again be calculated based on the weight gain at 2000 ppm HCl. At 4000 ppm the volatilization rate was too great to permit this calculation. The reaction could be ended by purging the system, increasing the temperature, and allowing the lead chloride to volatilize over a period of days. The total lead chloride formed, and consequently the global reaction rate, could be then calculated. If the reaction was allowed to proceed for approximately 30 min or more, the volatilization rate became approximately equal to the reaction rate and there was a period of time at which the sample mass changed little. However, the global reaction rate was not constant, and the system was not at steady state.

4.2 THERMODYNAMIC TREATMENT

As a preface to the work in chemical reaction kinetics, the thermodynamics of the reaction between PbO and HCl were considered to determine to what extent, if any, the reaction is possible. Although the Gibbs free energy of reaction could be calculated directly as a function of temperature from data in the JANAF tables (Stull and Prophet, 1971), it was more convenient to use a computer database and code to determine these and other parameters of the PbO-HCl-$PbCl_2$ system whenever they were available. Values for the Gibbs free energies as a function of temperature for the hydrochloridation of lead oxide are given in Table 4.1.

Table 4.1. Thermodynamic data of the PbO hydrochloridation reaction to form $PbCl_2$ with respect to temperature

T (°C)	Δ H (kcal/mol)	Δ G (kcal/mol)	K
100.00	-47.393	-37.299	7.039E+021
150.00	-47.323	-35.951	3.712E+018
200.00	-47.234	-34.612	9.745E+015
250.00	-47.127	-33.284	8.047E+013
300.00	-47.000	-31.966	1.549E+012
350.00	-46.856	-30.661	5.677E+010
400.00	-46.693	-29.368	3.431E+009
450.00	-46.513	-28.087	3.084E+008
500.00	-41.006	-26.852	3.900E+007
550.00	-40.718	-25.946	7.751E+006
600.00	-40.437	-25.057	1.872E+006
650.00	-40.163	-24.184	5.320E+005
700.00	-39.897	-23.326	1.734E+005
750.00	-39.638	-22.481	6.345E+004
800.00	-39.386	-21.649	2.565E+004
850.00	-39.142	-20.828	1.130E+004
900.00	-45.477	-19.931	5.168E+003
950.00[a]	-45.246	-18.847	2.333E+003
1000.00	-45.014	-17.773	1.125E+003

[a] Melting Point PbO = 890°C.
Source: HSC Outokompu, Pori, Finland.

As can be observed in Table 4.1, the reaction between PbO and HCl is highly thermodynamically favorable over the entire range of temperatures from 100 to 1000°C, which covers all four of our reaction regimes. Since the reaction is exothermic and the products are increasingly gaseous and of increasing entropy, the free energy becomes less negative with rising temperature, although it is still quite pronounced at 1000°C. Other researchers (Eddings and Lighty, 1991) have explored the formation of $PbCl_4$ and found it to be the preferred reaction in a multireaction equilibria. Unfortunately, they do not specify a reaction pathway, and we were unable to confirm their results assuming a PbO starting compound as shown in Table 4.2. However, if PbO_2 is assumed, as seen in Table 4.3, then the thermodynamics at least indicate $PbCl_4$ formation, is in preference to $PbCl_2$ but not strongly. No mention of PbO_2 was made in Eddings paper, and the discrepancy remains unexplained. Eddings, among others, believes that the reason $PbCl_4$ is not observed is kinetic. This would not be surprising in view of the increased complexity of the reaction; however, it does not seem necessary to resort to this hypothesis in the light of the present thermodynamic data.

Table 4.2. Thermodynamic data of the PbO hydrochloridation Reaction to form $PbCl_4$ with respect to temperature for the reaction $PbO+4HCl(g)=PbCl_4(g)+H_2O(g)$

T (° C)	Δ H (kcal/mol)	ΔG (kcal/mol)	K
50.00	-2.395	4.890	8.487E-011
150.00	-1.313	20.089	4.204E-011
250.00	-0.117	25.018	3.528E-011
350.00	1.298	29.700	3.827E-011
450.00	3.009	34.131	4.830E-011
550.00	4.621	38.337	6.616E-011
650.00	6.994	42.298	9.667E-011
750.00	9.826	45.979	1.506E-010
850.00	13.162	49.359	2.481E-010
950.00[a]	10.481	52.788	3.691E-010
1000.00	12.659	54.474	4.448E-010

[a]Melting Point PbO - 890°C.
Source: HSC Outokompu, Pori, Finland.

Table 4.3. Thermodynamic data of the PbO hydrochloridation reaction to form $PbCl_4$ with respect to temperature for the reaction $PbO_2+4HCl(g)=PbCl_4(g)+2H_2O(g)$

T (°C)	Δ H kcal/mol	Δ G kcal/mol	K
50.00	-36.802	-32.357	7.677E+021
150.00	-37.063	-30.946	9.647E+015
250.00	-37.364	-29.468	2.049E+012
350.00	-37.689	-27.930	6.256E+009
450.00	-38.033	-26.338	9.129E+007
550.00	-38.387	-24.697	3.612E+006
650.00	-38.741	-23.013	2.810E+005
750.00	-39.087	-21.291	3.534E+004
850.00	-39.421	-19.536	6.335E+003
950.00[a]	-39.738	-17.752	1.486E+003
1000.00	-39.889	-16.850	7.811E+002

[a] Melting Point PbO - 890°C.
Source: HSC Outokompu, Pori, Finland.

4.3 REGIME 1, T = 260 to 310°C

4.3.1 Introduction

At temperatures below 310°C, a rapidly increasing rate of reaction is observed as a function of temperature at HCl concentrations of 2000 and 4000 ppm. Figures 4.3.1 through 4.3.4 provide representative thermograms of Runs 326, 328, 331, and 323 at temperatures of 260, 280, 290, and 300°C respectively. At the lowest temperatures, the thermograms begin to exhibit curvature and asymptotic behavior at reaction times of 60 min. In these figures the mass gains were normalized with respect to the external surface area of the particle. The sample porosities were approximately equal. Figures 4.3.5 and 4.3.6, for Run 299 at 260°C and Run 306 at 328°C, illustrate that the behavior at 4000 ppm HCl is qualitatively similar. In general as the temperature is raised, the rate of weight gain rises and becomes more nearly linear. The initial rate of reaction at low temperature may be quite rapid and is characteristic of the chemical reaction kinetics. Binocular microscope photographs are shown in Figures 4.3.7 through 4.3.10 for representative Runs 324 at 260°C, 329 at 280°C, 330 at 290°C, and 335 at 310°C. The photographs indicate a gradually thickening ash layer as the temperature is raised. At 260°C the surface may be less than fully covered during the reaction time of 90 min. At this temperature, we also observed, though it is not clearly indicated here, that a layer of grey ash was

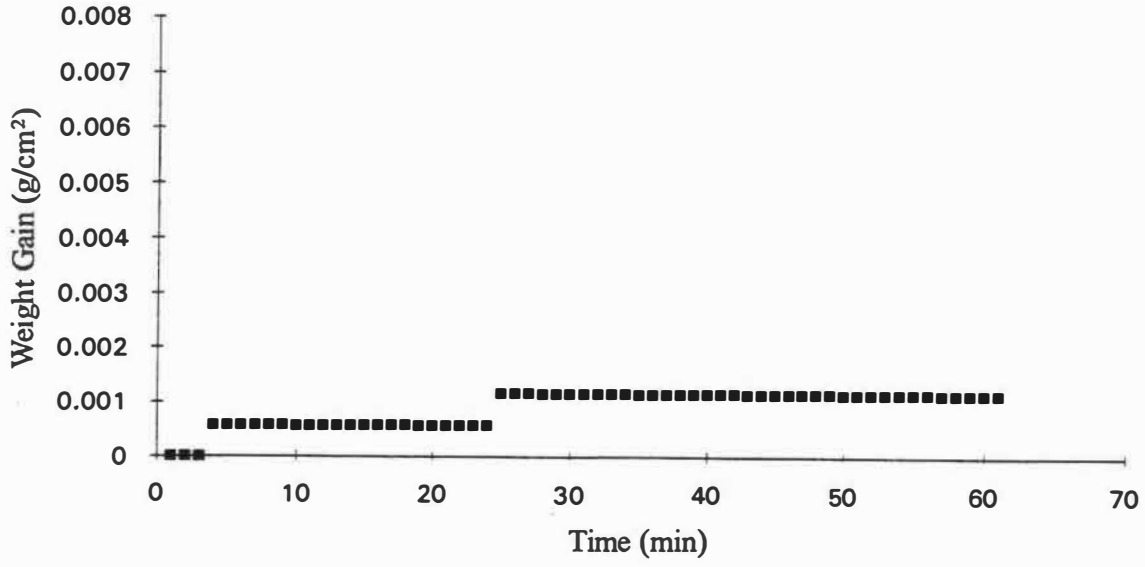

Figure 4.3.1. Thermogram of Run 326, T = 260°C, 2000 ppm HCl.

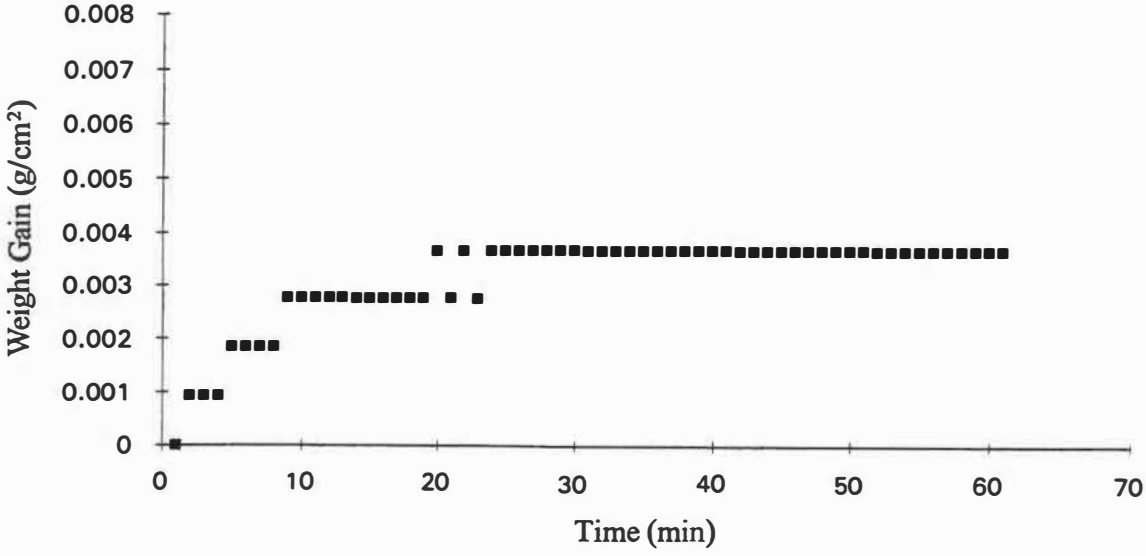

Figure 4.3.2. Thermogram of Run 328, T = 280°C, 2000 ppm HCl.

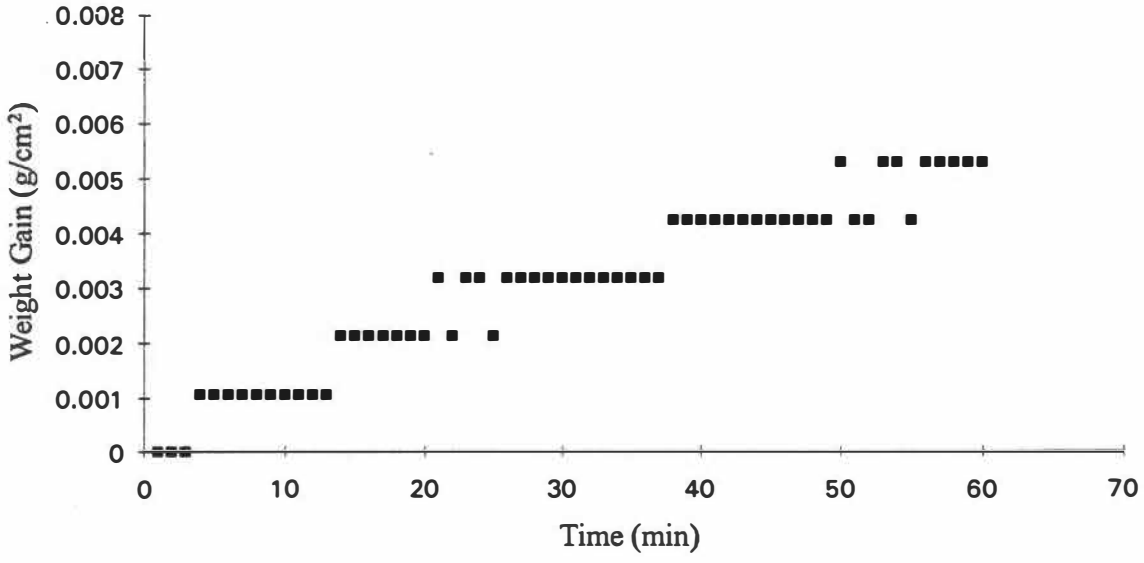

Figure 4.3.3. Thermogram of Run 331, T = 290°C, 2000 ppm HCl.

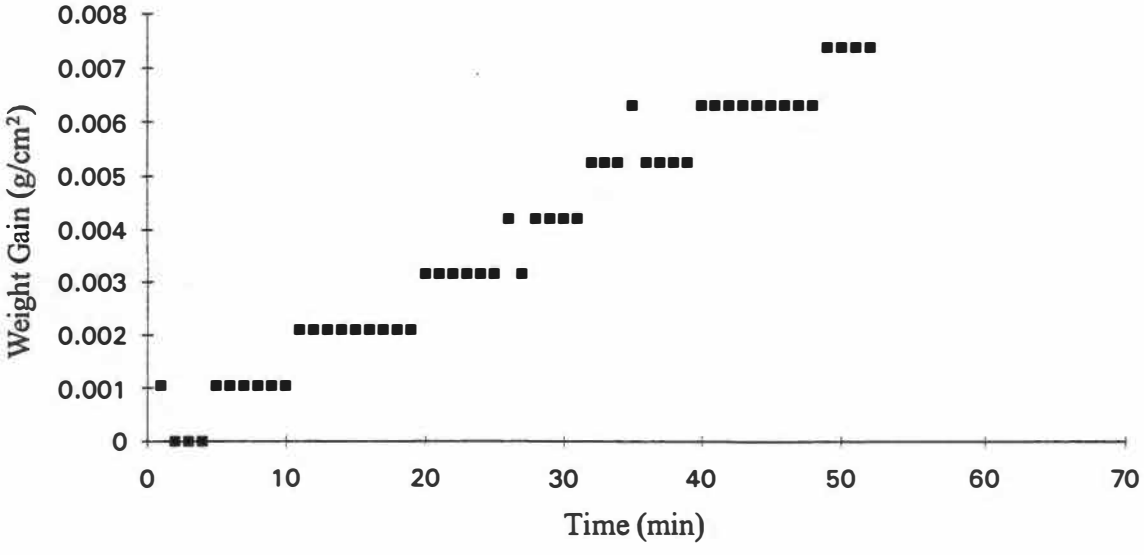

Figure 4.3.4. Thermogram of Run 323, T = 300°C, 2000 ppm HCl.

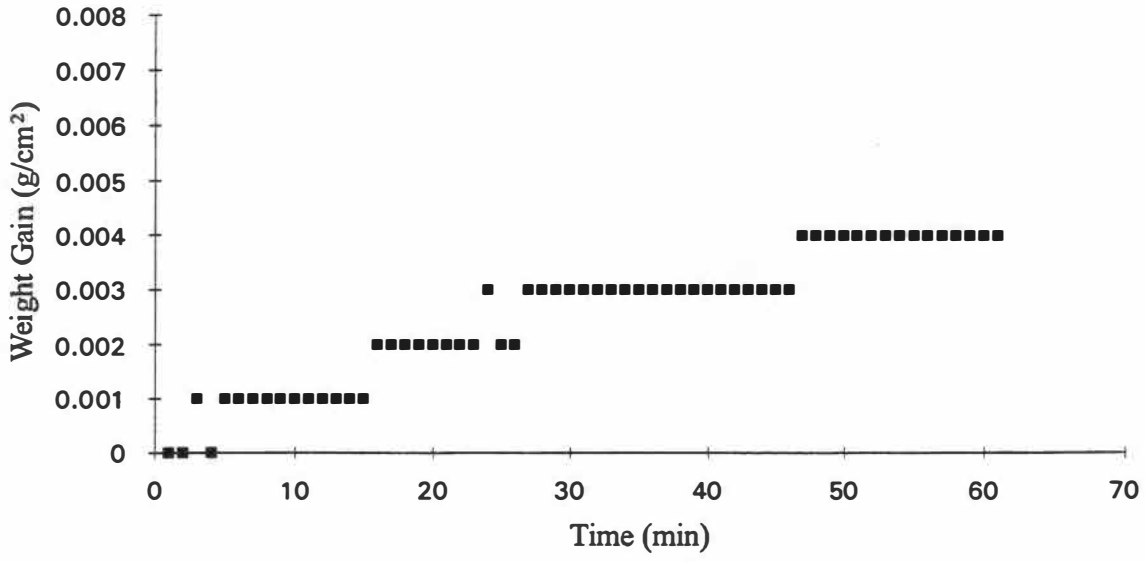

Figure 4.3.5. Thermogram of Run 299, T = 260°C, 4000 ppm HCl.

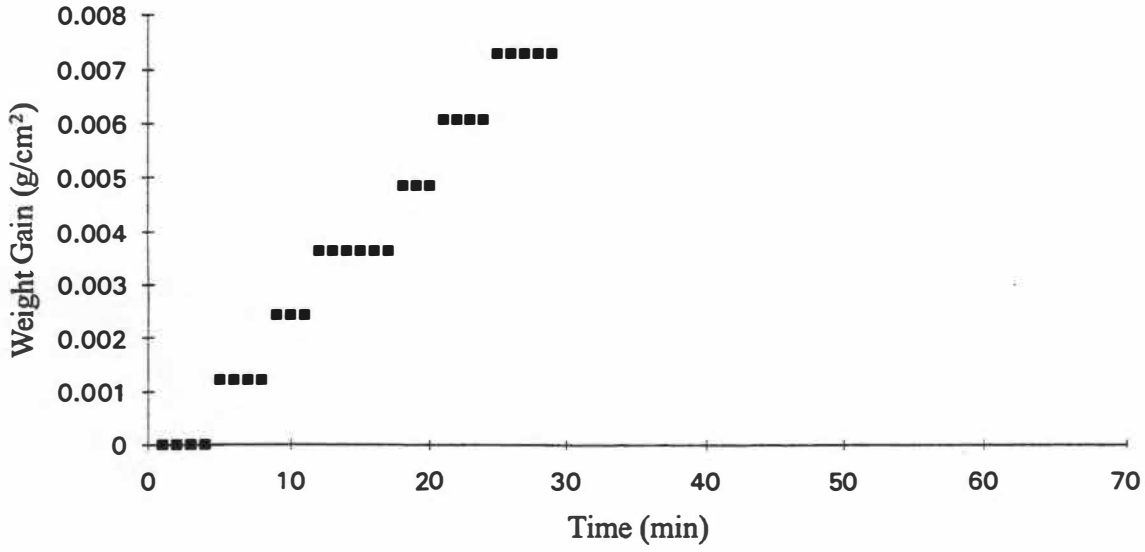

Figure 4.3.6. Thermogram of Run 306, T = 328°C, 4000 ppm HCl.

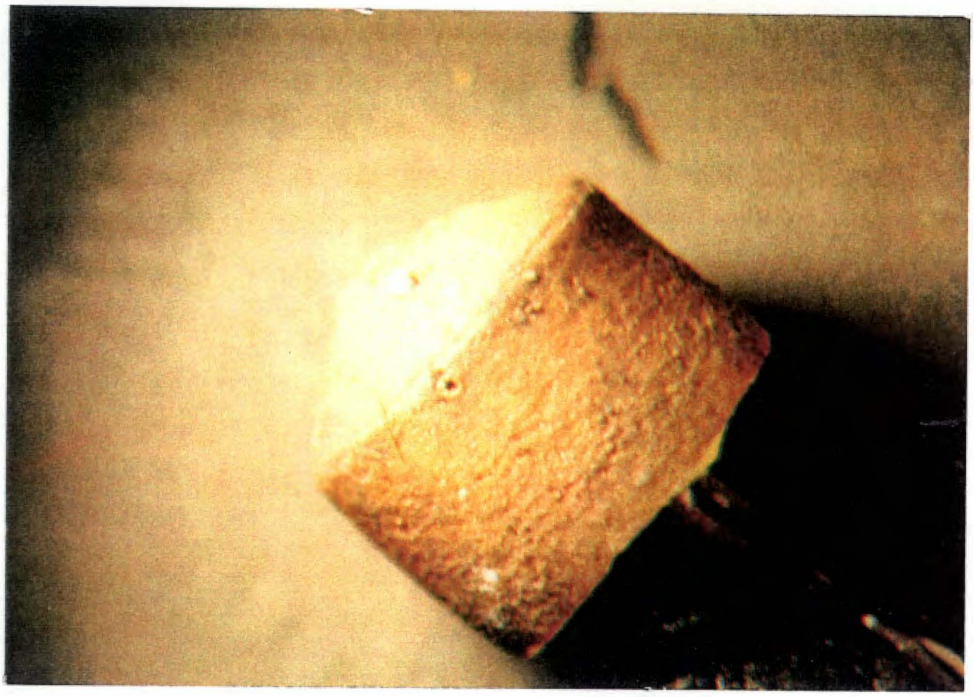

Figure 4.3.7. Photograph of pellet from Run 324, prepared at 260°C, 90 min, 2000 ppm HCl.

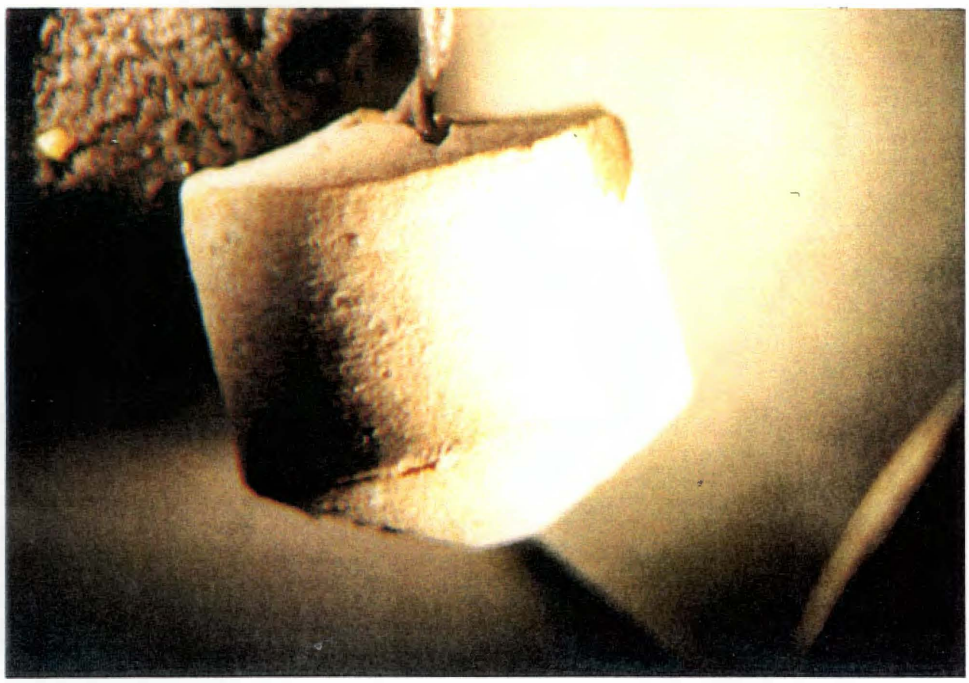

Figure 4.3.8. Photograph of pellet from Run 329, prepared at 280°C, 65 min, 2000 ppm HCl.

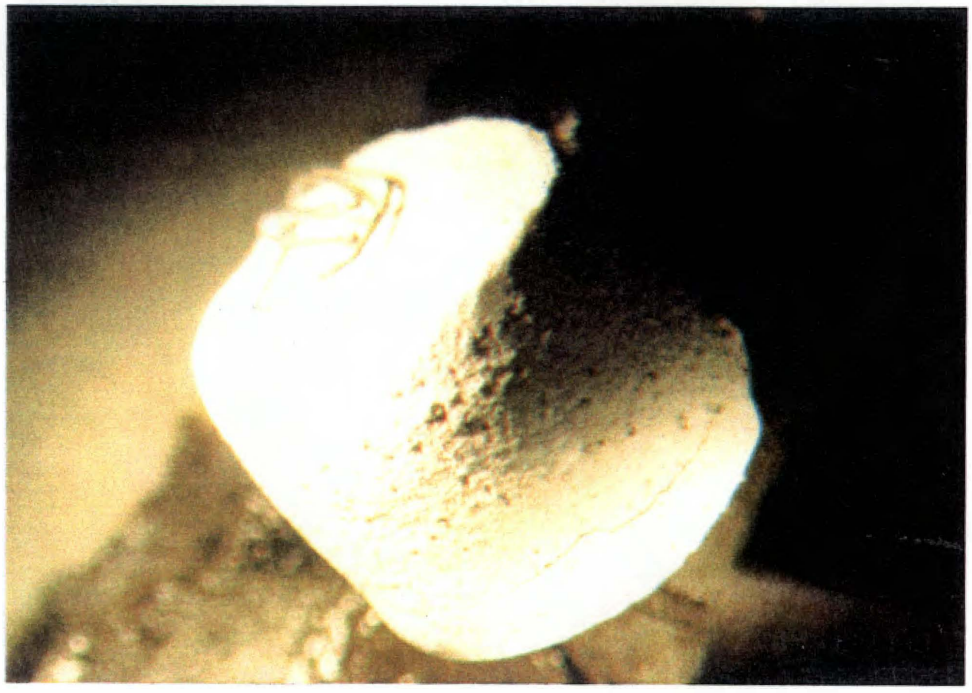

Figure 4.3.9. Photograph of pellet from Run 330, prepared at 290°C, 90 min, 2000 ppm HCl.

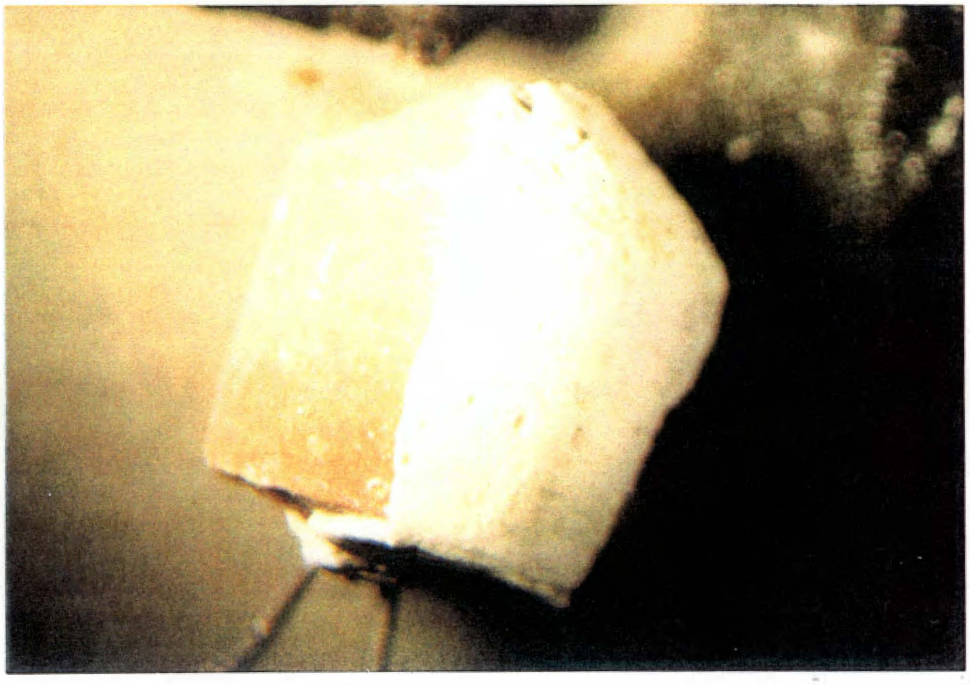

Figure 4.3.10. Photograph of pellet from Run 335, prepared at 310°C, 60 min, 2000 ppm HCl, ash layer chipped off.

formed under a dusting of white ash. At 310°C, after hydrochloridation, a section of the white $PbCl_2$ ash was chipped from the pellet prepared in Run 335 and an underlying grey layer was again observed; this layer seemed to be less friable than the $PbCl_2$ covering. Below 260°C, no increase in mass of the sample is found, and no morphological changes are apparent during the 1- to 2-h time frame at the reactant concentrations of HCl that are typical of those of incineration. Chaleroux (1960) observed, however, that reaction was complete within 6 h at these temperatures in pure HCl gas at 1 atm. Our use of the less-concentrated HCl has enabled us to resolve some of the reaction kinetics that were blurred in Chaleroux's work.

Figures 4.1.1 and 4.1.2, displaying global hydrochloridation rates versus temperature at 2000 and 4000 ppm of HCl, respectively, show that the rate of hydrochloridation rises rapidly between approximately 260 and 310°C. An Arrhenius plot of these data (natural logarithm of reaction rate versus inverse absolute temperature), shown as Figure 4.3.11, reveals an activation energy of 22.2 kcal/mol, (R^2=0.84) which is a reasonable indication of chemical kinetic control. Table 4.3.1 contains the raw data that were used to produce Figure 4.1.1, and Table 4.3.2, those that were used to produce Figure 4.1.2.

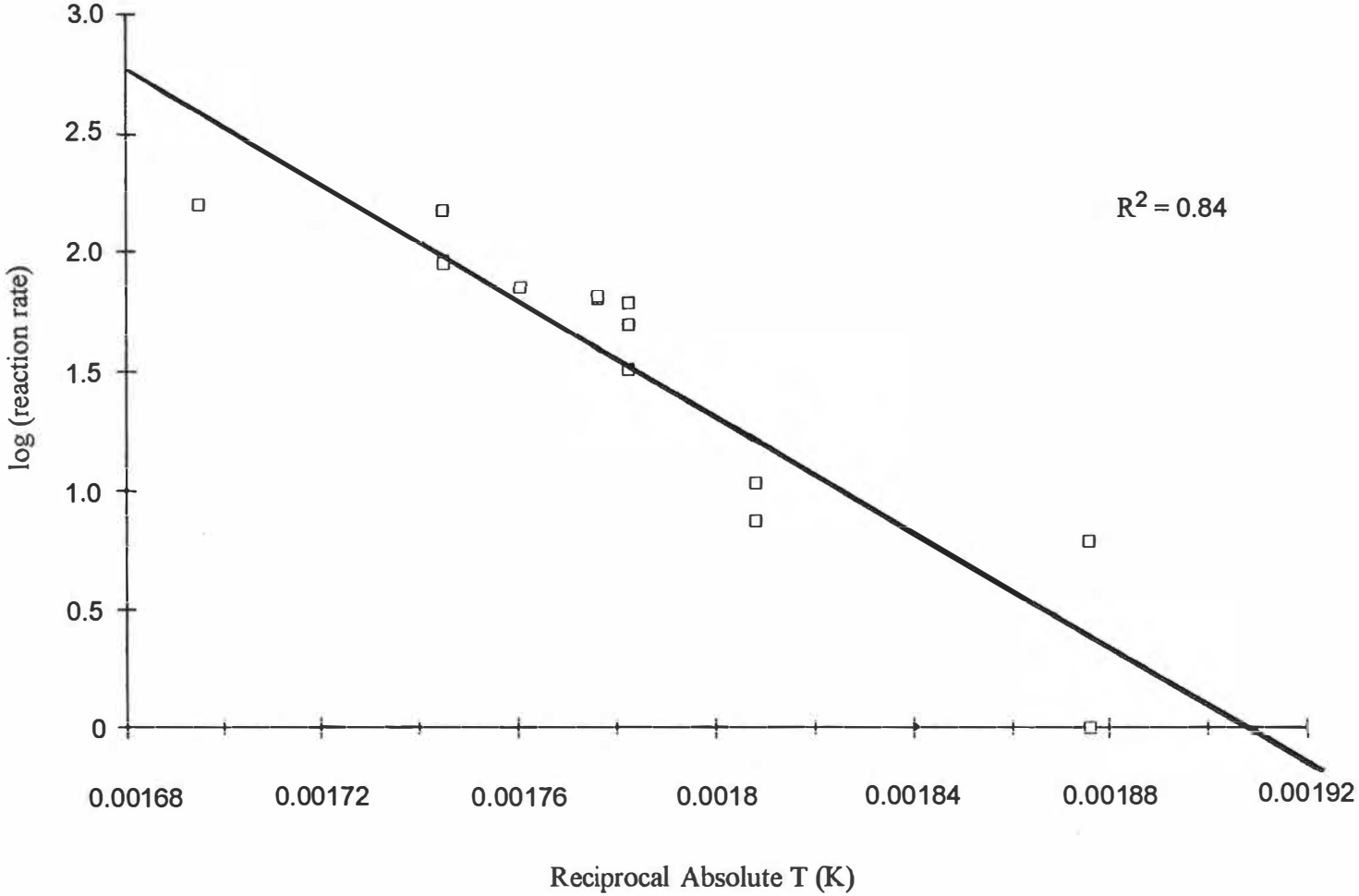

Figure 4.3.11. Arrhenius plot of the natural logarithm of hydrochloridation reaction rate versus reciprocal absolute temperature, 2000 ppm HCl.

Table 4.3.1. Global hydrochloridation reaction rates, 2000 ppm HCl

Run	Reaction Rate [10^{-8} x mol/(cm^2 · s)]	T (°C)
145	566	11.3
146	493	12.2
147	288	2.8
149	675	12.54
151	678	11.94
152	510	10.94
153	288	6.06
153	350	10.92
154	349	11.24
155	398	9.68
156	447	10.34
157	370	11.36
159	317	6.36
165	666	14.7
165	569	10.4
167	288	5.44
167	290	7.02
168	295	5.96
168	340	9.56
171	340	9.8
173	336	9.68
174	340	9.84
183	349	11.12
187	348	10.68
195	394	11.42
198	380	11.72
199	380	11.3
207	384	11.24
210	387	11.4
219	300	9
226	633	12.2
234	670	23
236	672	18.8
237	604	15.6
241	675	24.4
248	615	13
250	300	8.78
254	260	0
258	330	11.92
259	260	2.2
266	280	4.5
267	280	2.8
268	280	2.4
270	625	11.2
271	500	9.46
272	290	6.12
273	552	11.4
274	448	11.04
275	450	10.22
293	700	14.84
294	500	10.4

Table 4.3.2. Global hydrochloridation reaction rates, 4000 ppm HCl

Run	T (°C)	Reaction Rate [10^{-8} × mol/(cm^2 · s)]
266	276	1.65
267	274	2.04
268	298	6.1
269	299	5.14
270	350	16.76
271	350	15.7
272	400	16.98
273	398	17.6
274	450	20.2
275	450	22.2
259	671	34.6
296	551	22.8
297	600	23.4
293	599	23.2
294	628	22.2
295	631	20
296	551	22.8
299	263	1.584
303	280	2.8
304	340	16.8
305	325	12.08
306	332	13.64
335	310	14.4
336	310	12.4
337	300	12
342	310	14.6
343	280	4.6
344	297	6.6

4.3.2 Descriptive Model, Regime 1

Evidence of chemical reaction first appears upon hydrochloridation at 260°C as the appearance of a grey and white ash and in a weight gain of the PbO specimen during the course of an approximately 60-min run time. As will be discussed further, x-ray fluorescence analysis reveals that the reacted pellets contain chlorine, which was not present in the original pellets. The reaction rate, as measured by weight gain, becomes slower as time advances. No loss of weight could be observed if the sample was allowed to remain at temperature after hydrochloridation was ended in this regime. This observation suggests that the ash had very little volatility (i.e., a level beneath our ability to measure). Two descriptive models are implemented to explain these results. The first is a progressive conversion model similar to a concept of Levenspiel (1972). In this model chemical reaction and diffusional resistance are both significant and a distinct boundary between ash and substrate is not found. The second model, the work of Lee and Georgakis (1981), posits that a gas/solid reaction occurs on the walls of the pores, which are gradually filled with an ash of lower density than the substrate that effectively chokes further reaction after a certain time. In the first model, as a starting point, Eq. (4.3.1) is applied:

$$D_e \partial^2 C/\partial x^2 - \partial C/\partial t + k_r C \qquad (4.3.1)$$

where C is the concentration of HCl, D_e is the effective diffusivity, and k_r is the reaction rate coefficient. This is an equation of unsteady state diffusion and chemical reaction. This model assumes that the reaction is first order and homogeneous with respect to the HCl concentration and that an effective diffusivity can be defined based on a constant porosity and tortuosity of the particle and particle ash. Although the specimens are cylindrical, it assumes that the reaction can be modeled in one- dimensional rectilinear coordinates because the reaction zone is very thin, on the order of 20 μm compared with a particle radius of 5000 μm. It further assumes that there is only one product of the reaction and that there is no difference in the porosity of the ash and unreacted core. The concentration of HCl in the ash at the surface of the particle is assumed to be constant and to reflect saturation of the surface. This assumption is supported by the similarity in global reaction rates at 2000 and 4000 ppm HCl. The concentration of HCl in the solid phase is assumed to be low; therefore, convective flux is neglected. The vaporization of $PbCl_2$ reaction product is negligible in this regime (i. e., vapor pressure of 1E-10 torr at 310°C). No

solid state diffusion of reaction products is stipulated. It is believed that, because of the general thinness of the grey layer, the reaction to form the final $PbCl_2$ product proceeds only slightly slower than that to form the grey intermediate ash layer. The chemical reaction effectively raises the rate of mass transfer to the interior of the pellet. Boundary conditions are

$$C|_{x=0} = 0.02 \ , \quad \left.\frac{\partial C}{\partial x}=0\right|_{x=\infty} \ , \quad C|_{t=0}=0 \qquad (4.3.2)$$

where C is the concentration of HCl and x is the distance from the particle surface.

Results of this model are shown as a solid line in Figure 4.3.12 alongside data of Run 300, performed at 300°C. Partial differential equations [Eqs. (4.3.1 and 4.3.2)] were solved using an explicit finite difference technique as shown in Appendix A1. The numerical results are shown in Appendix A2. A schematic representation of the concentration profiles with respect to distance in the ash layer is shown in Figure 4.3.13. This model has three significant adjustable parameters C_o, k_r, and D_e of HCl and although it has the advantage of being more fundamentally based than the Lee and Georgakis technique as we shall see, it does not produce a better fit. The sum of the squares of the error between the model-predicted values and the data for Run 300 is 1.06E-4 mg^2.

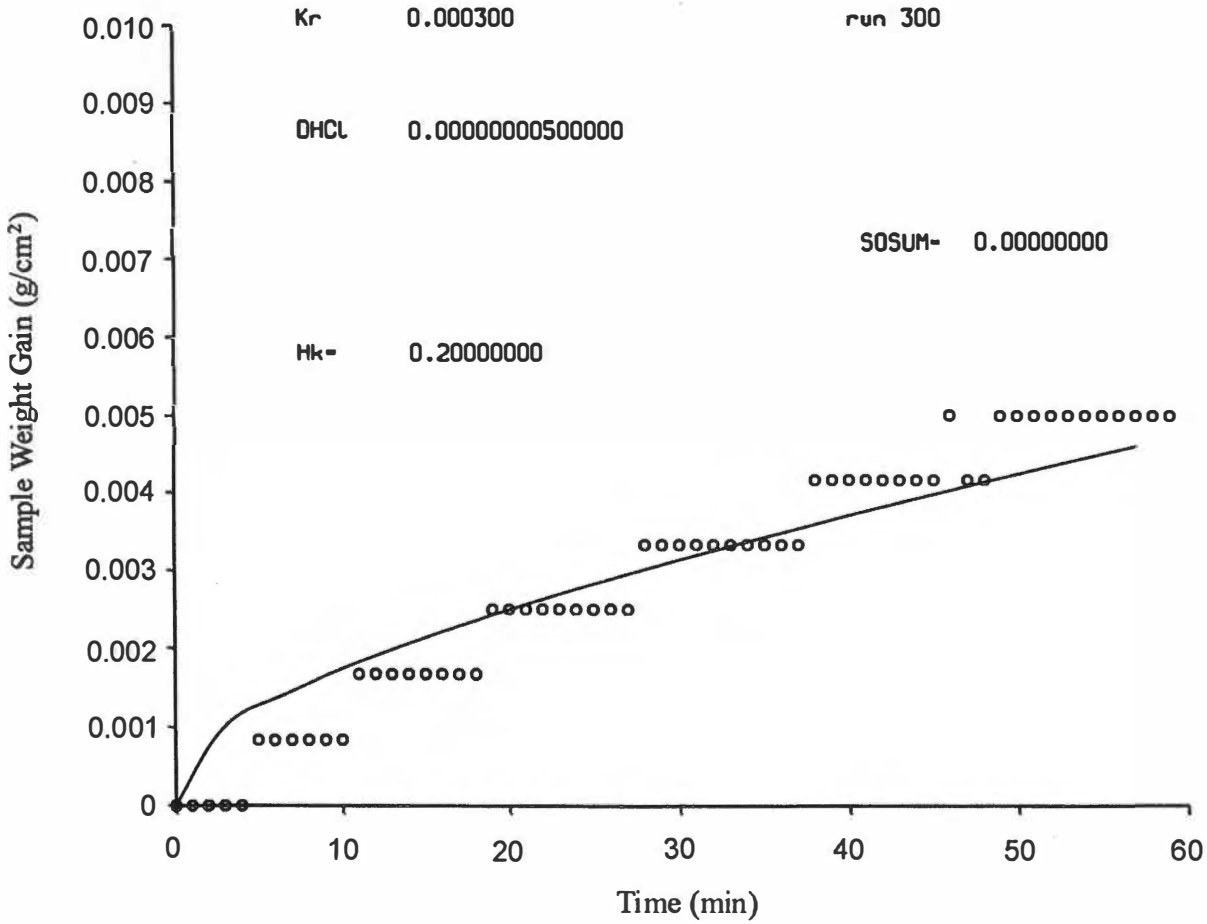

Figure 4.3.12. Comparison of progressive conversion (fixed boundary conditions) model (solid line) and experimental data (circles) of thermogram of Run 300 at 300°C.

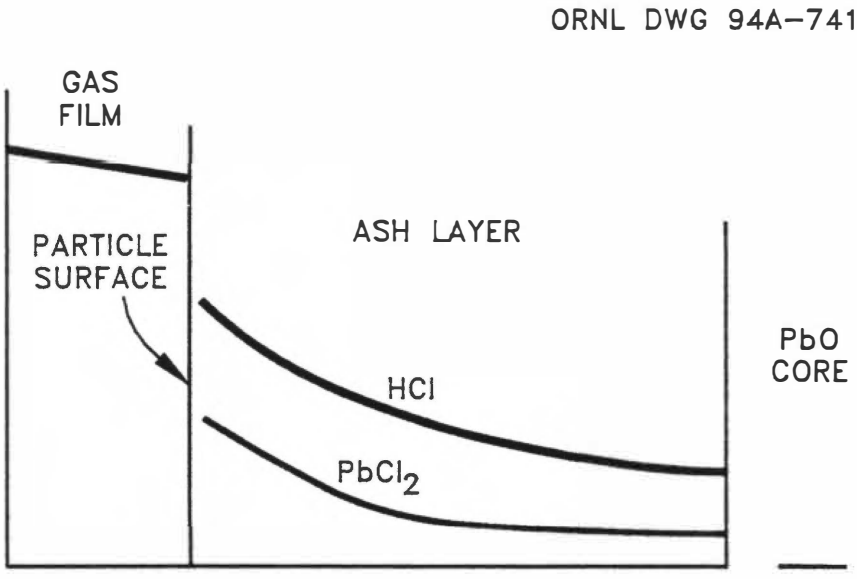

Figure 4.3.13. Approximate profile of ash and fluid composition, Regime 1.

Wen, using a more sophisticated treatment of the diffusion equation [Eq. (4.3.1)] with different boundary conditions, considered the reaction to progress in two separate stages, both at pseudo steady state as discussed in Sect. 2.5.1. During the first stage of reaction, Eq.(4.3.1) is solved with a diffusivity characteristic of the unreacted particle. During the second stage, two ash layers, one of fully reacted material having a characteristic diffusion coefficient and another of partially reacted material of a different diffusivity are assumed to have built up. This scheme does not seem to have the utility now that it might have had 30 years ago since computer algorithms can readily accommodate variations in such properties. In the current modeling, no data on effective diffusivities in the ash or unreacted particles are available.

Lee and Georgakis worked specifically with limestone and SO_2, but the nature of our system, in which the particles are porous and the $PbCl_2$ reaction product is less dense than the PbO substrate, is similar. As the reaction progresses, the pores become gradually smaller and smaller until an asymptotic regime is reached. Lee defines two parameters, the first characteristic of the chemical reaction kinetics based on the initial reaction rate and the second based on the time required to effect total plugging of the pores. The global reaction rate is described in the following equation:

$$R_p(t) = R_{po}\, e^{-t/\tau_p} \qquad (4.3.3)$$

where the initial reaction rate is expressed:

K = reaction rate constant
C = concentration of reactant
ρ_a = density of particle
S_g = specific surface area of particle
η = effectiveness factor of particle
τ_p = characteristic pore plugging time

$$R_{po} = \frac{4}{3}\pi r^3\, \rho_a\, K S_g C \eta \qquad (4.3.4)$$

Equation (4.3.4) indicates a flux balance at the surface of the particle. A parameter τ_{sf} is defined as follows:

$$\tau_{sf} = \frac{1}{K S_g \rho_\alpha \eta} \qquad (4.3.5a)$$

$$R_p(t) = (4/3\pi r^3)\, C/\tau_{sf} e^{-t/\tau_p} \qquad (4.3.5b)$$

Figure 4.3.14 shows the results for Run 326 at 260°C, and Figure 4.3.15, those for Run 328 at 280°C. The activation energy of reaction calculated based on this model was approximately 17 kcal/mol. The sum of the squares of the error is 1.29E-6 $(gm/cm^3)^2$ for Run 326 and 5.43E-6 for Run 328.

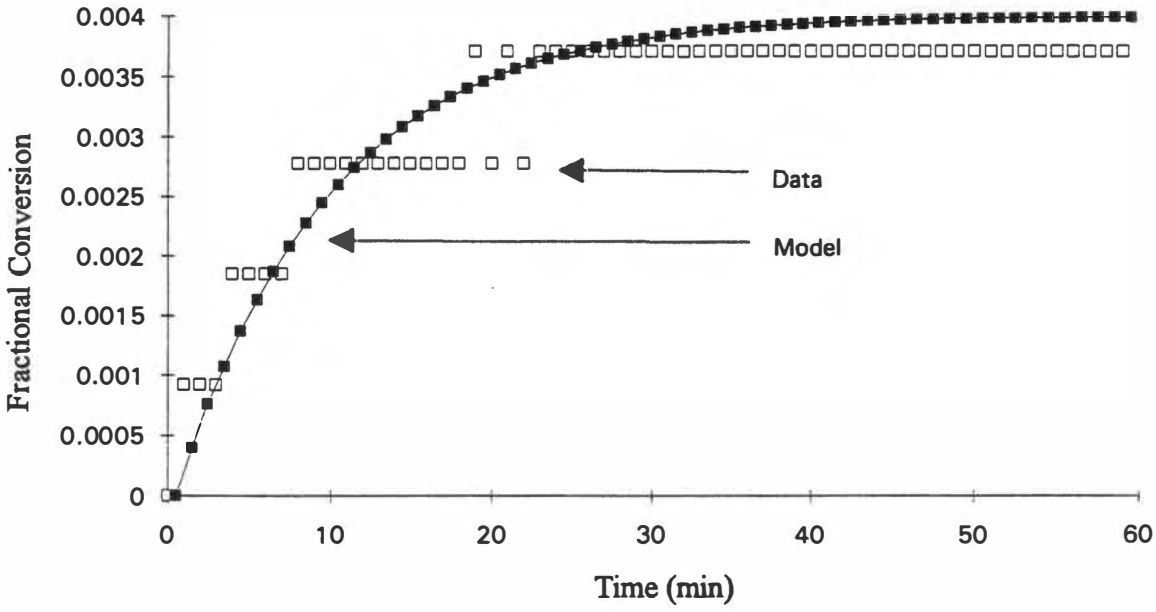

Figure 4.3.14. Thermogram of Run 328, T = 280°C, 2000 ppm HCl.

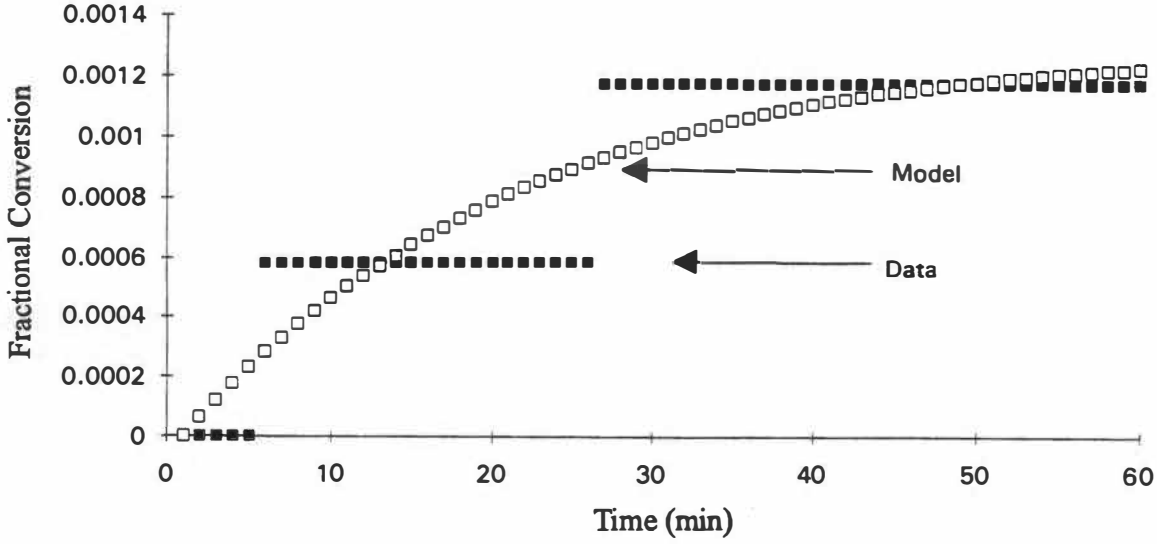

Figure 4.3.15. Thermogram of Run 326, T = 260°C, 2000 ppm HCl.

In conclusion, Regime 1 is a range of temperatures between 260 and 310°C at which the PbO hydrochloridation reaction appears to be under combined chemical kinetic and solid state diffusive control, exhibiting an average of 22 kcal/mol activation energy. An apparent reaction rate of 10.E-8 moles/sec/cm^2 was found at 2000 ppm HCl at 300°C. Models of progressive conversion (in which diffusion and chemical reaction are both significant rate terms) and models of pore plugging (in which chemical reaction slows to the halting point because of increases in solid state diffusive resistance) are both reasonable descriptors of thermogravimetric data. Effective diffusivities were in the range of 5E-9 cm^2/s as revealed by the progressive conversion model.

4.4 REGIME 2, T = 325 to 450°C

4.4.1 Introduction

The thermogravimetric behavior of the PbO pellets when reacted with HCl at 2000 or 4000 ppm in this temperature regime is notable for the absence of change as the temperature is raised from 325 to 450°C. The thermograms are generally fairly straight and rise throughout this regime. As noted in Figures 4.1.1 and 4.1.2 (Sect. 4.1), global reaction rate does not seem to rise with respect to temperature at 2000 ppm HCl and rises only slightly, perhaps 25% at 4000 ppm.

Differences among the thermograms at a given temperature are probably more readily attributable to variations in the surface areas of the samples (which were difficult to control because of minor differences in the surface finish of molds and in the packing characteristics of the samples) and errors in the normalization of areas. Occasionally, a break will be seen in the thermogram, as suggested in Figure 4.4.1 of Run 191 at 420°C, which produces a bilinear relationship. Note that the time scale in this figure extends to 200 min, greater than that in previous thermograms. This break may be due to a cracking of the product ash layer. If the reaction is allowed to proceed to very long periods of time, we eventually begin to observe a slight bending in the thermogram, which may be attributed to $PbCl_2$ ash diffusional resistance, as seen at 183 min, in Run 187, 370°C, as shown in Figure 4.4.2.

Photographs of samples reacted in this temperature regime indicate a uniform covering of white crystals, which have been further identified as containing chiefly lead and chlorine. Generally observed underneath this white covering is a second layer of ash of a distinctly grey color and much less friable character as noted also in Regime 1 and seen in Figure 4.4.3, showing Run 306 at 328°C.

This grey sublayer of ash is the object of some further investigation. A series of x-ray photoelectron spectra (also known as electron spectroscopy for chemical analysis, ESCA)

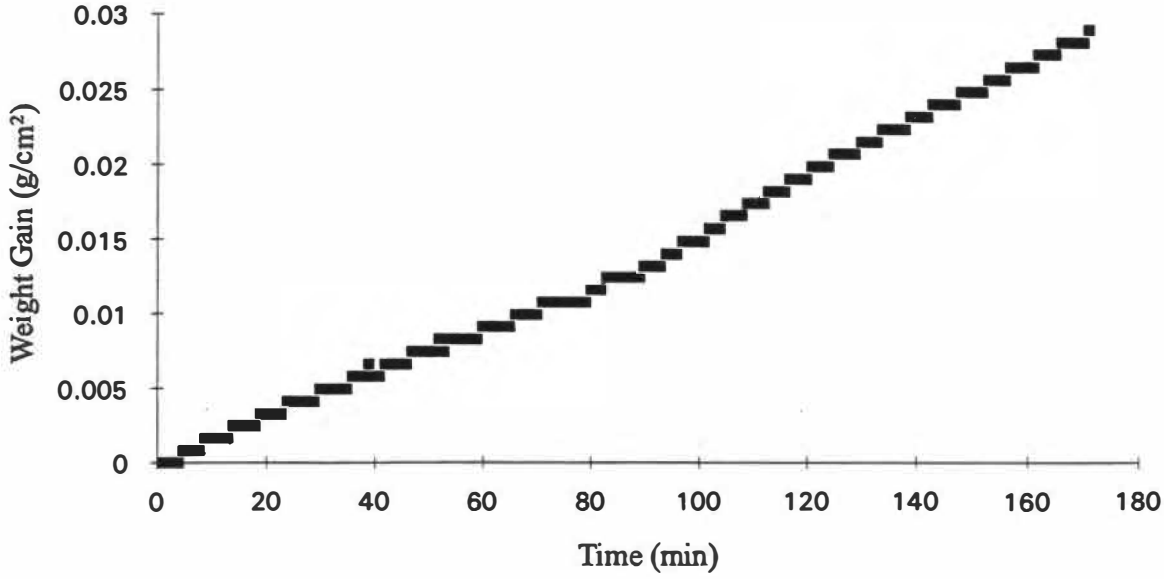

Figure 4.4.1. Thermogram of Run 191, T = 420°C, 2000 ppm HCl.

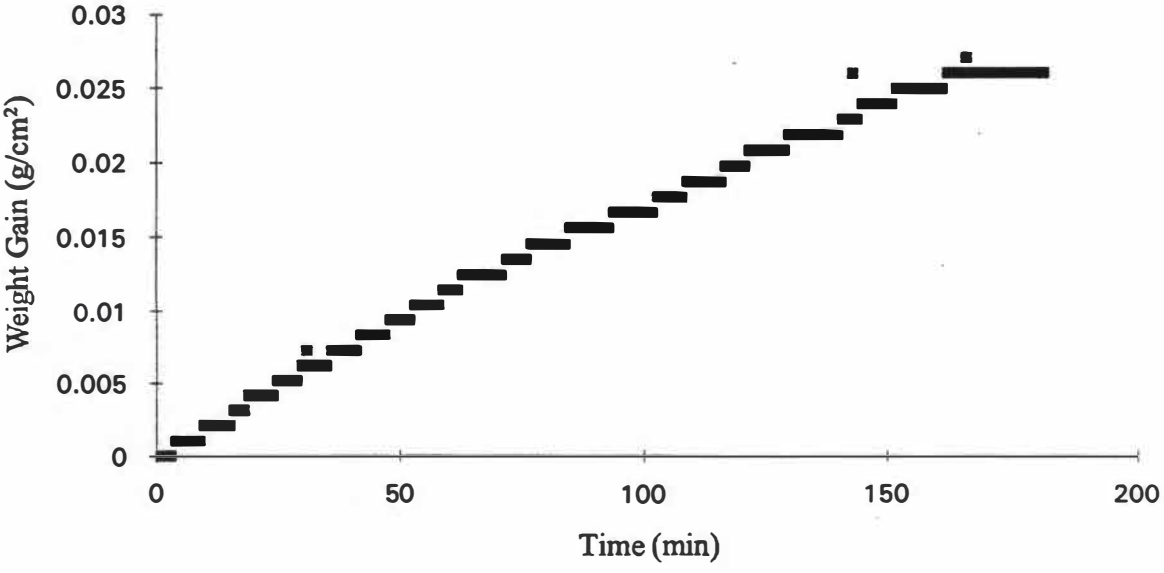

Figure 4.4.2. Thermogram of Run 187, T = 370°C, 2000 ppm HCl.

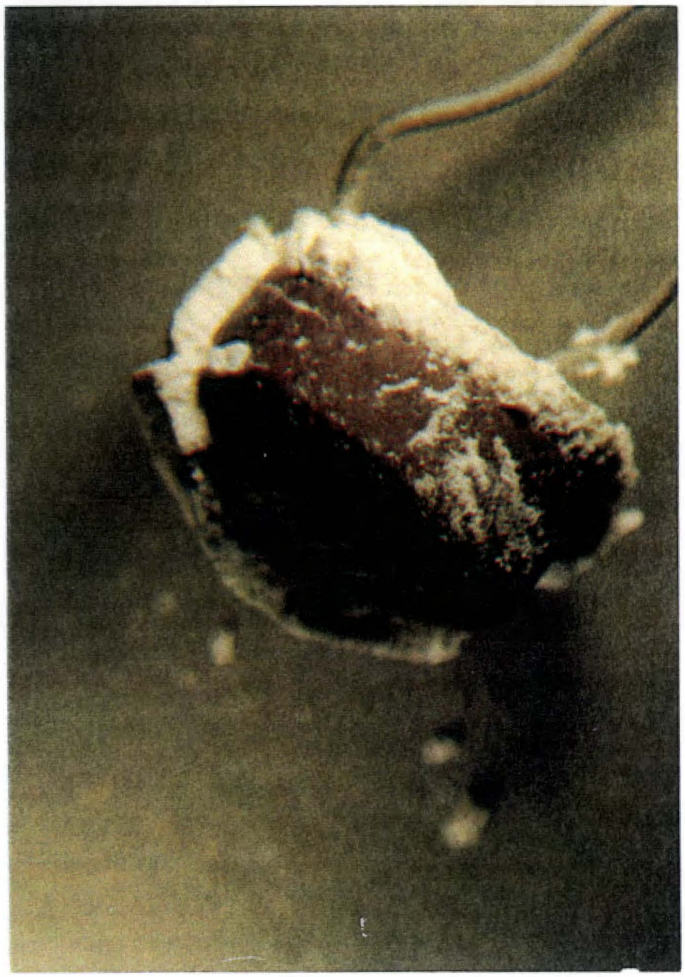

Figure 4.4.3. Photograph of pellet from Run 306, prepared at 328°C, 115 min, 4000 pm HCl.

was made of a sample from Run 271 that was generated at 350°C and was typical of this temperature regime. The white layer had been scraped off, with the hope of establishing a stoichiometry of lead, oxygen, and chlorine. ESCA, however, is only a semiquantitative technique, and from the first the samples exhibited carbon contamination, probably from carboncoating, which exceeded any lead, oxygen, or chlorine signal. Argon ion sputtering was performed to remove the surface contaminations and also to determine if there was a compositional variation with depth. A spectrum of the photoelectron energies is shown in Figure 4.4.4 of Run 271 prepared at 350°C. Several lead peaks are evident, as well as one of oxygen and several of chlorine. A plot of the elemental composition versus sputtering time is shown in Figure 4.4.5. No compositional variations with respect to sputtering depth were identified. The elemental composition of the sample as revealed after sputtering is shown in Table 4.4.1. The carbon may also arise from a earlier carbon coating of the sample to improve the electron microscopic imaging.

The closest match to a known compound would probably be PbOHCl, and this is hard to confirm since hydrogen is invisible with this analytical technique. However, this may be an important clue as we will see when other analytical techniques are applied.

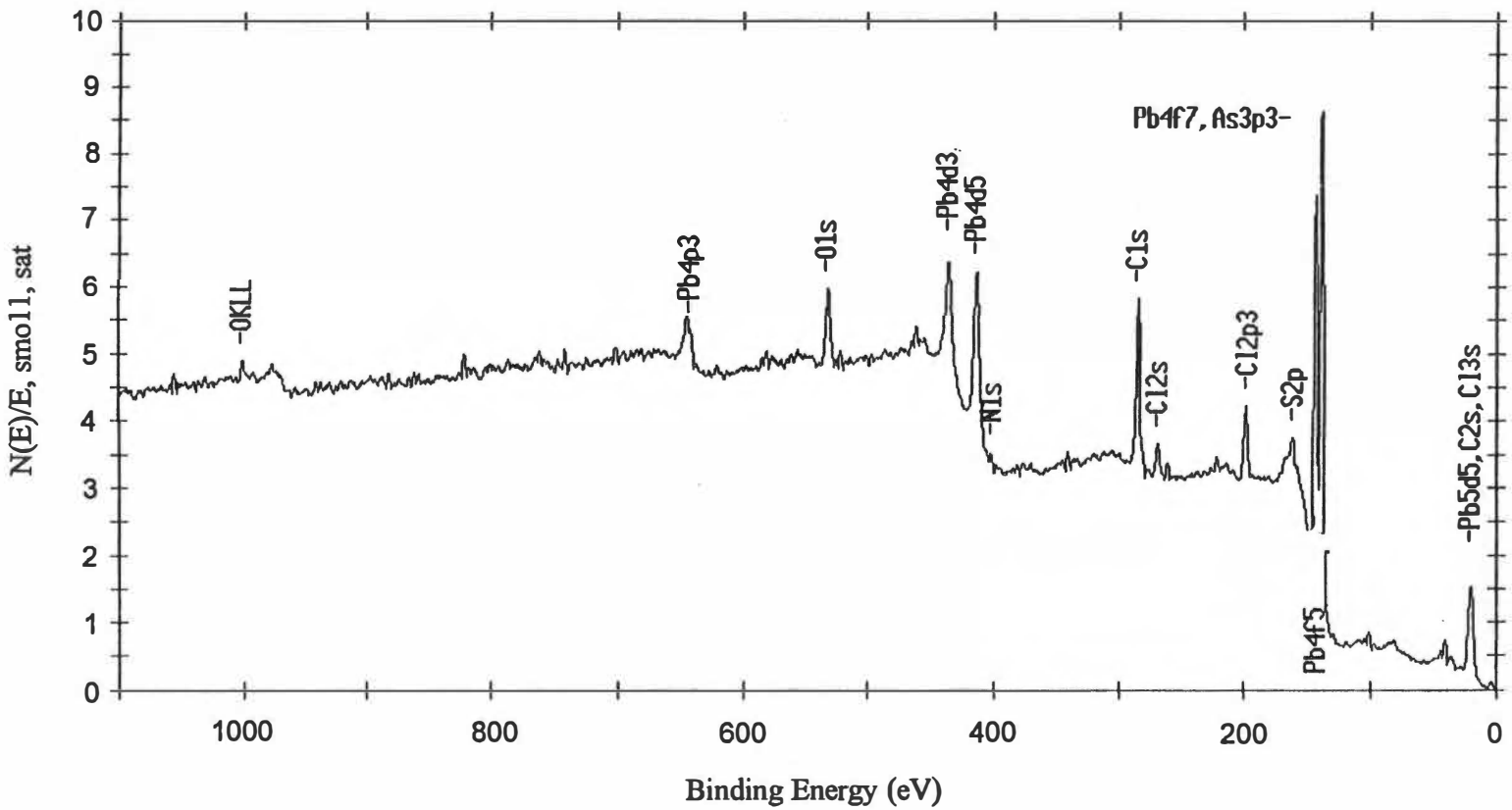

Figure 4.4.4. Elemental analysis of extreme surface layer of grey ash from Run 271.

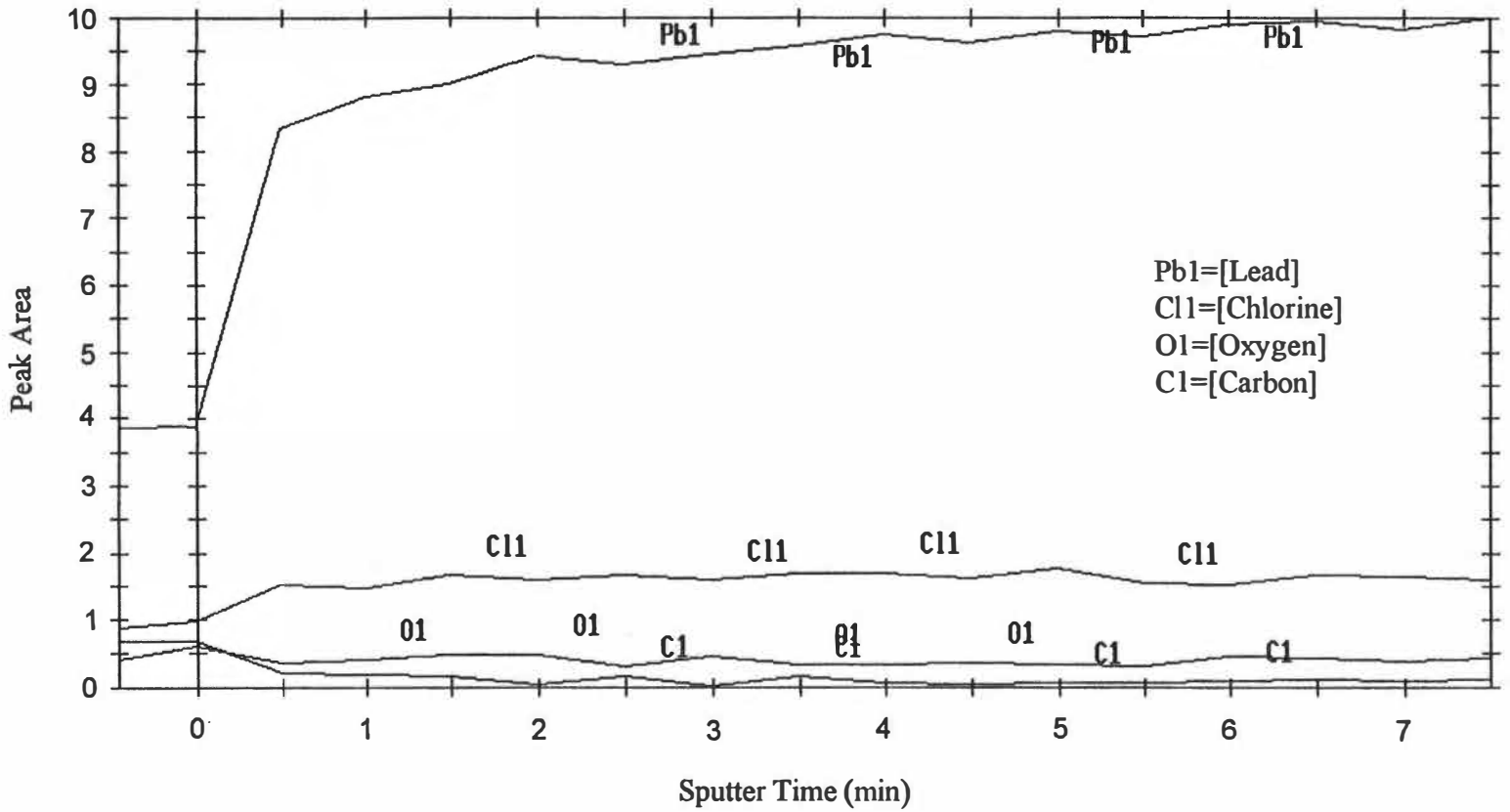

Figure 4.4.5. ESCA elemental profile of grey layer of ash from Run 271, prepared at 350°C, 93 min, 2000 ppm HCl.

Table 4.4.1. Elemental analysis of surface of pellet from Run 271

Element	Sensitivity factor	Concentration (mol %)
Lead	8.329	10.62
Chlorine	0.891	10.41
Oxygen	0.711	14.81
Carbon	0.296	64.43

4.4.2 Descriptive Model, Regime 2

Regime 2 displayed the fewest changes (morphological or thermogravimetric) with temperature, and the simplest model is applied to explain the results. The Frossling equation, also known as the Ranz Marshall correlation of fluid phase mass transfer (or heat transfer) in turbulent or laminar flow to a sphere, is applied (McCabe and Smith):

$$k_{mt}D_p/D\text{-}N_{sh}\text{-}2.0\text{+}0.6N_{Re}^{0.5}N_{Sc}^{0.33} \qquad (4.3.6)$$

where N_{sh} is the Sherwood number, N_{re} is the Reynolds number, N_{sc} is the Schmidt number, k_{mt} is the mass transfer coefficient, D_p is the particle diameter, and D is the fluid

phase diffusivity. The Schmidt and Reynolds numbers are defined as follows:

$$N_{Sc} = \frac{\mu}{\rho D} \qquad (4.3.7)$$

$$N_{Re} = V\rho D_p/\mu \qquad (4.3.8)$$

where V is the fluid velocity, D_p is the effective particle diameter, μ is the viscosity, and P is the density of the gas phase.

The observed global reaction rates for a few representative experiments in this temperature regime and the predicted rates per the Frossling equation are shown in Table 4.4.2.

Table 4.4.2. Comparison of calculated and measured mass transfer rates

Temp (°C)	Run	Measured rate [10^{-8} × mol/(cm^2 · s)]	k (cm/s)	Calculated rate [10^{-8} mol/(cm^2 · s)]	N_{Re}
288	153	6.73	3	14.948	5.6
348	167	10.6	3.5	15.8	5.3
398	168	9.68	4.1	16.6	4.98

In Regime 2, we note that fluid phase mass transfer is not yet likely to be controlling. There is only a small change

in the predicted mass transfer rate with temperature, which is consistent with the relative insensitivity of the diffusion coefficient to temperature. As can be observed in Figure 4.4.2 of Run 187 at 370°C, the mass transfer control is not purely fluid phase because, under such conditions, the thermogram would not bend with increasing reaction time, providing the particles were not changing greatly in size. There was a slight enlargement in a particle as a result of reaction, but attempts to correlate the change in particle diameter with changes in the reaction rate showed that this effect was negligible. A schematic representation of the qualitative appearance of the concentrations of $PbCl_2$ and HCl that the model predicts are shown in Figure 4.4.6. The HCl concentration profile is similar to, but slightly thicker than, that of Regime 1, with the beginning of a slight appearance of $PbCl_2$ in the gas phase.

In summary, Regime 2 is characterized by a major diffusional resistance in an underlying solid ash phase, which is a grey oxychloride intermediate compound. On the surface is a second layer of ash composed of $PbCl_2$, which also begins to exhibit an influence on the hydrochloridation rate after long reaction times. Global hydrochloridation rates are approximately 10-7 mol/sec/cm^2 at 2000 ppm of HCl. Increasing the HCl concentration to 4000 ppm very nearly doubles this hydrochloridation rate. Two advancing reaction fronts can be observed in this regime, but it is difficult

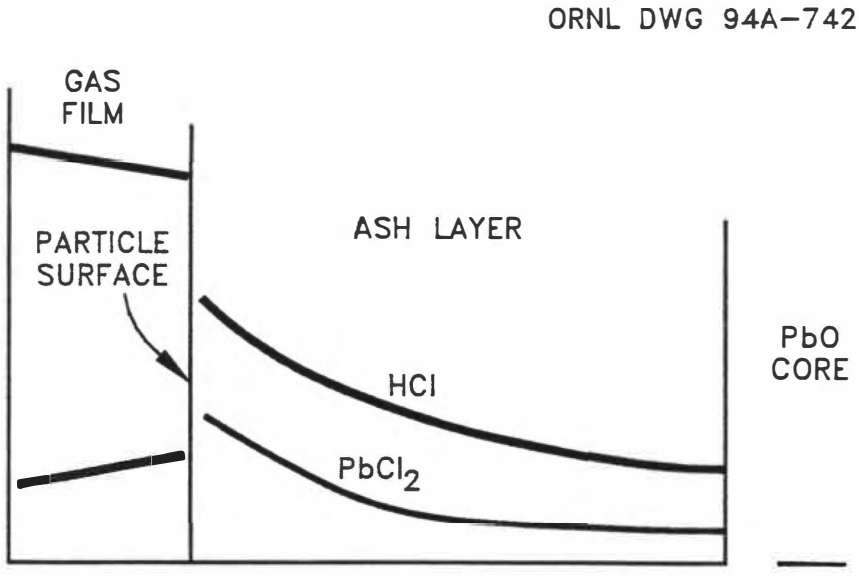

Figure 4.4.6. Schematic of approximate concentration profiles of HCl and $PbCl_2$, Regime 2.

to collect data on their motion because of their thinness and variable porosity.

4.5 REGIME 3, T = 450 to 590°C

4.5.1 Introduction

In this temperature range, a liquid reaction product is formed, but the global reaction rate is largely unchanged (within experimental uncertainty) from that in Regime 2. A low-melting eutectic is formed in the PbO-$PbCl_2$ system at 450°C, which is approximately the temperature at which we first observed a distinctly liquid reaction product. One should consider that the phase diagram represents a system that does not include water or HCl, both of which may be present. As in Regime 2, a greater reaction rate is observed at 4000 ppm than at 2000 ppm HCl. At the higher concentrations of HCl, the data were easier to acquire and are less scattered.

As seen in Figures 4.5.1 through 4.5.3, which are thermograms of Runs 274, 285, and 228 at 448, 505, and 550°C, respectively, the apparent lack of change in the global reaction rate does not mean that large changes do not appear in the reaction thermograms. At 448°C, Run 274, we see a sharp rise in the reaction thermogram; as the volatility of the reaction product rises, however, the thermograms flatten to the point (around 510°C at which little change in mass occurs despite an obvious reaction.

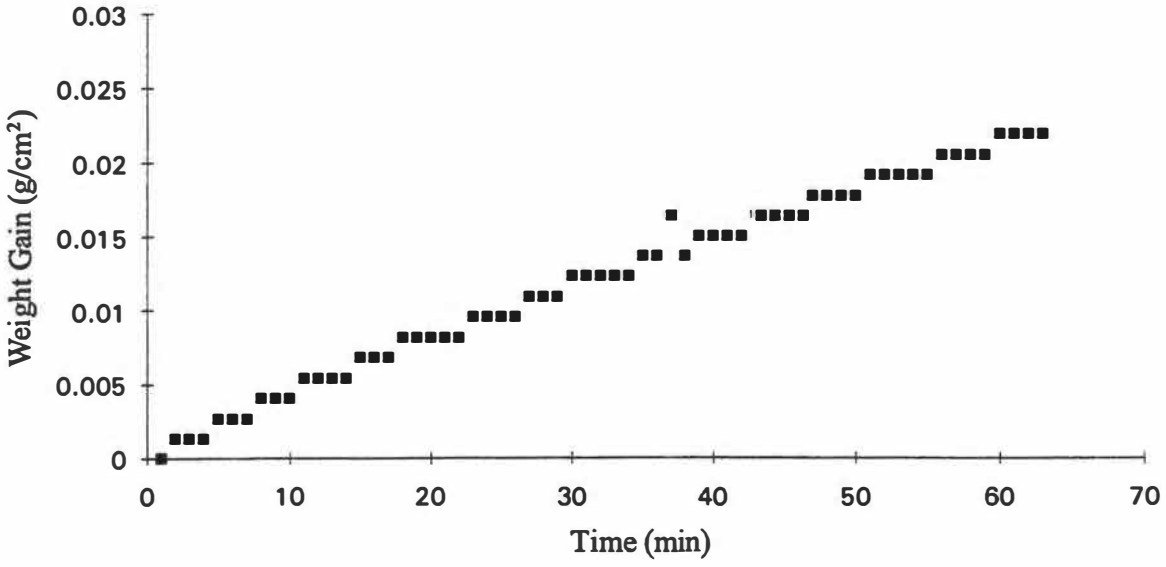

Figure 4.5.1. Thermogram of Run 274, T = 448°C, 4000 ppm HCl.

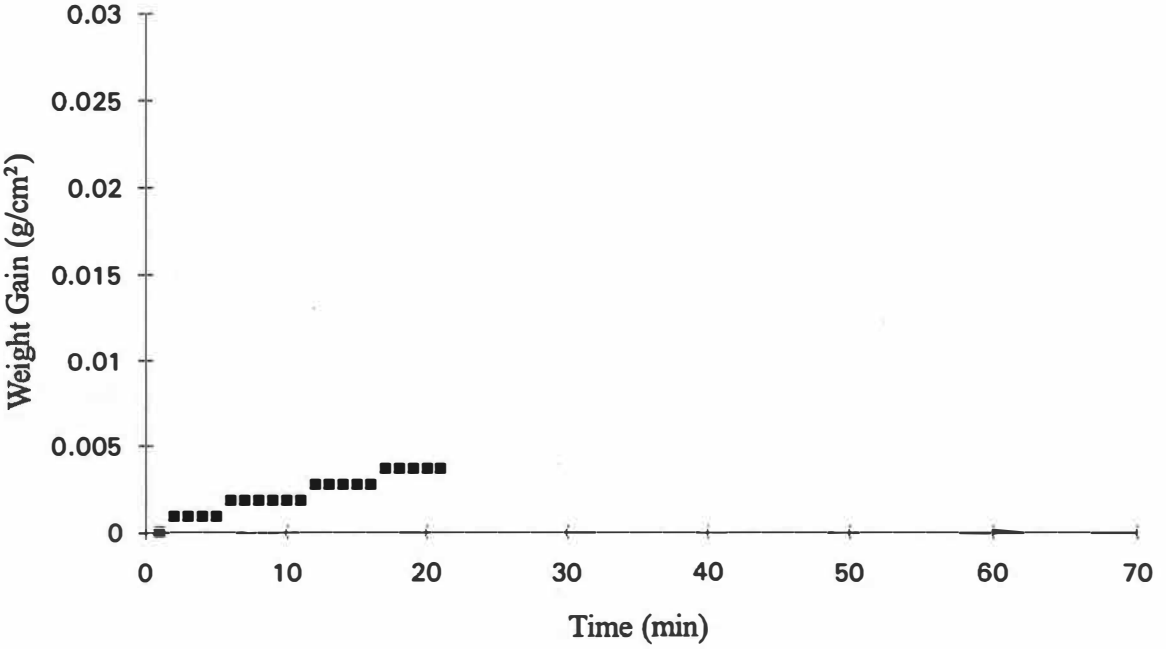

Figure 4.5.2. Thermogram of Run 285, T = 505°C, 4000 ppm HCl.

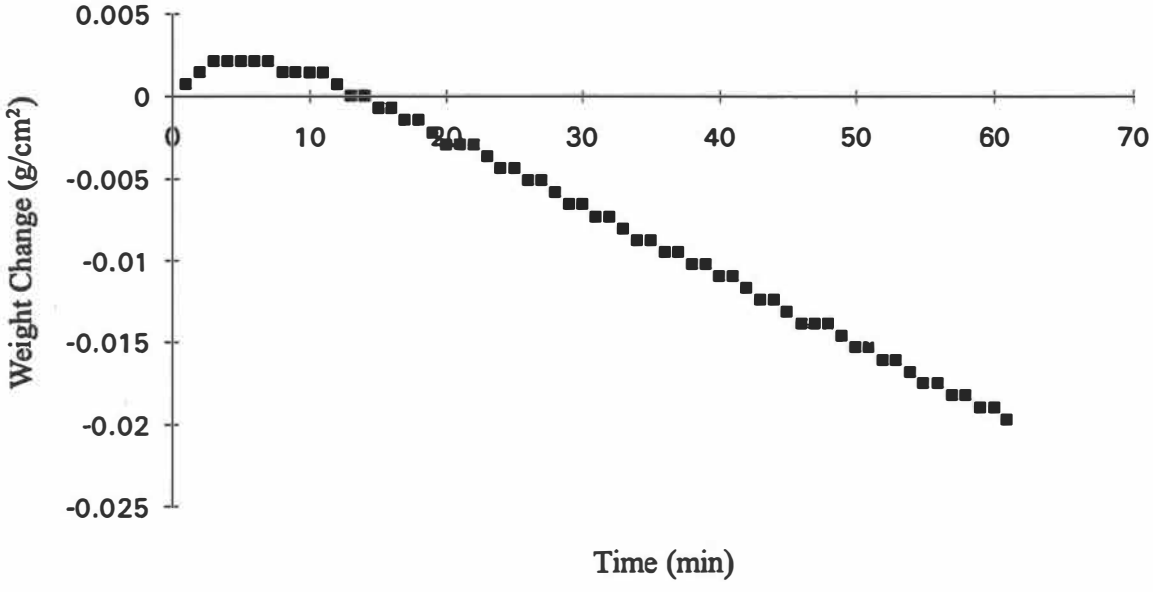

Figure 4.5.3. Thermogram of Run 228, T = 550°C, 2000 ppm HCl.

At this temperature, near the melting point of $PbCl_2$, evidently the rate of hydrochloridation just matches the mass rate of $PbCl_2$ volatilization.

In Figure 4.5.3, Run 228 at 550°C, we see that the rate of weight loss from volatilization has overcome the rate of weight gain from hydrochloridation. The reaction product appears to be liquid at this point, and drips were a problem. Figure 4.5.4, a photograph of a reacted sample of Run 227 at 550°C, suggests that crystals, probably of $PbCl_2$, formed at the surface during quenching. The eutectic temperature of the $PbCl_2$-PbO system, shown in the phase diagram Figure 4.5.5, is near 450°C, and that is the approximate temperature at which we see the beginnings of a dark ash in the quenched pellet. (Observe Figure 4.5.6 of Run 159 at 446°C.)

One interesting question which arises in connection with the observation of a liquid reaction product at the surfaces of the pellets is whether this liquid film is an inhibiting influence on the diffusion of HCl to the reactive core of the particle. As we will see, at slightly higher temperatures, the liquid film becomes increasingly more volatile and finally disappears during the first phase of reactions in Regime 4. The disappearance of the liquid film is accompanied by an increase in the reaction rate as will be noted.

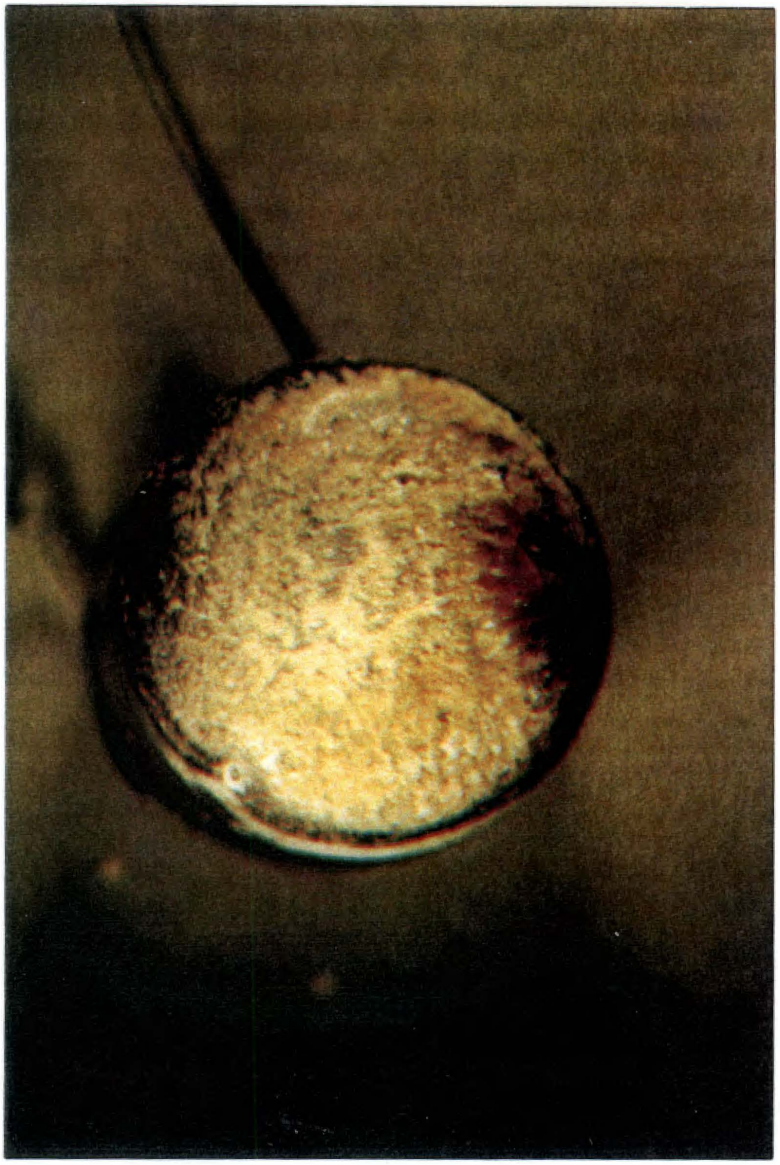

Figure 4.5.4. Photograph of reacted pellet from Run 227, prepared at 550°C, 30 min, 2000 pm HCl.

Figure 4.5.5. Phase diagram PbO-$PbCl_2$ system (adapted from Renaud, *Can. J. Chem.*, *48*, 2061, 1970).

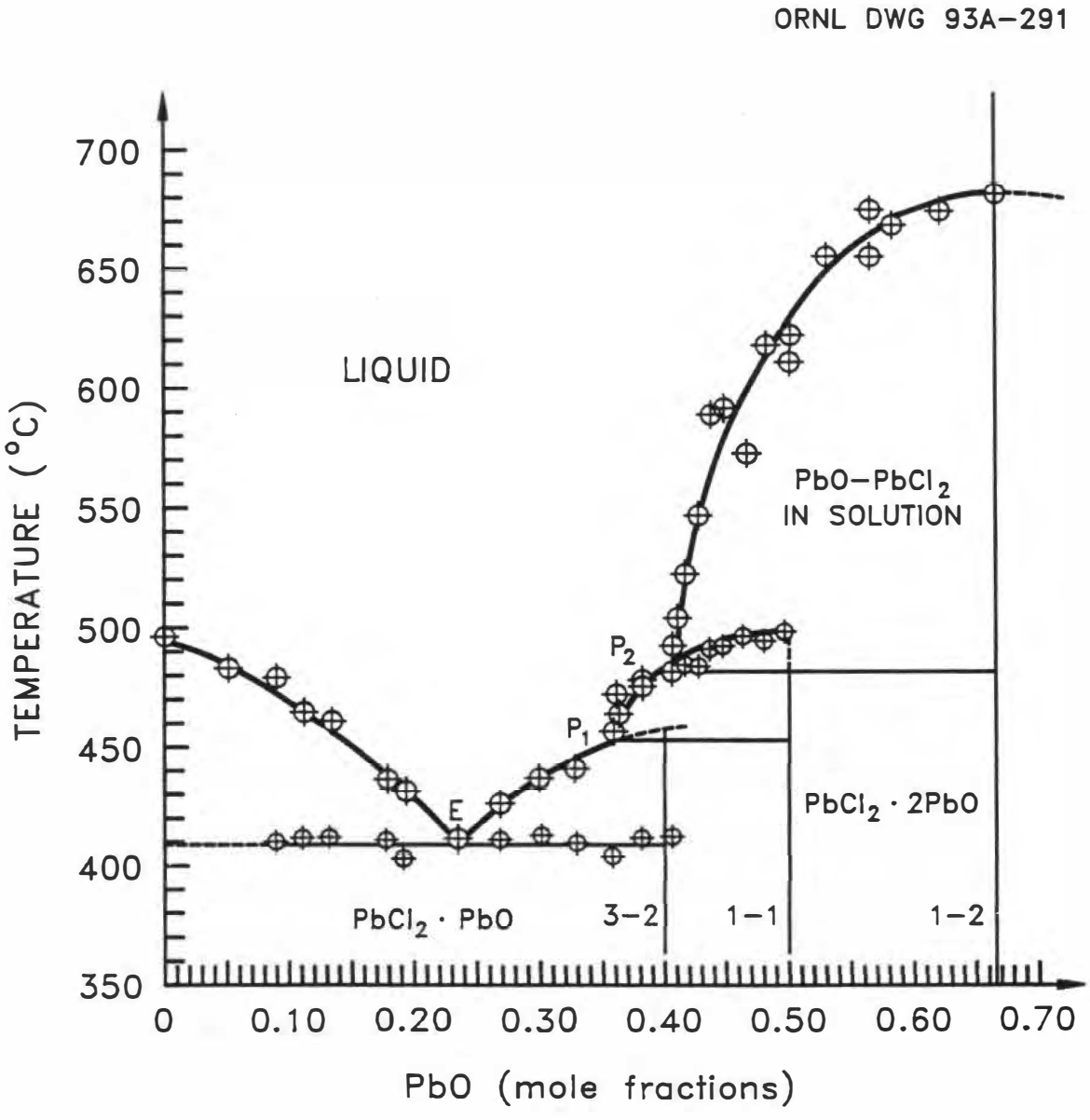

Figure 4.5.6. Photograph of pellet from Run 227, prepared at 450°C, 75 min, 2000 pm HCl.

Several interesting observations can be made based on the results in this temperature regime. Increasing temperature between 510 and 590°C yields gradually increasingly steep thermograms of weight loss versus time (i.e., the product vaporizes more rapidly, as one would expect, as its vapor pressure rises). Secondly, a short interval exists, perhaps 5 min at most, after the HCl flow has started in which there is typically little weight change or perhaps even a small increase. Thirdly, and this is most readily observable at an HCl concentration of 4000 ppm, the volatilization will continue after the HCl flow has been stopped for several minutes as in Run 282, Figure 4.5.7. This suggests that a layer rich in $PbCl_2$ was formed at the particle surface. Fourthly, as seen in an extension of the thermogram of Run 282, Run 282b, shown in Figure 4.5.8, the particle can be brought to a point at which the weight no longer changes with time. Fifthly, the constant weight loss that the specimens exhibit during reaction in this regime appears to continue to reaction periods of 90 min. Occasionally, at a long reaction time, a drop would drip from the specimen, additional evidence that the product is fairly liquid at temperature. A measurement of the particle diameters after reaction reveals that they have shrunk several microns. Consequently, there are actually two moving boundaries in this regime, that of the ash-core interface and that of the particle surface.

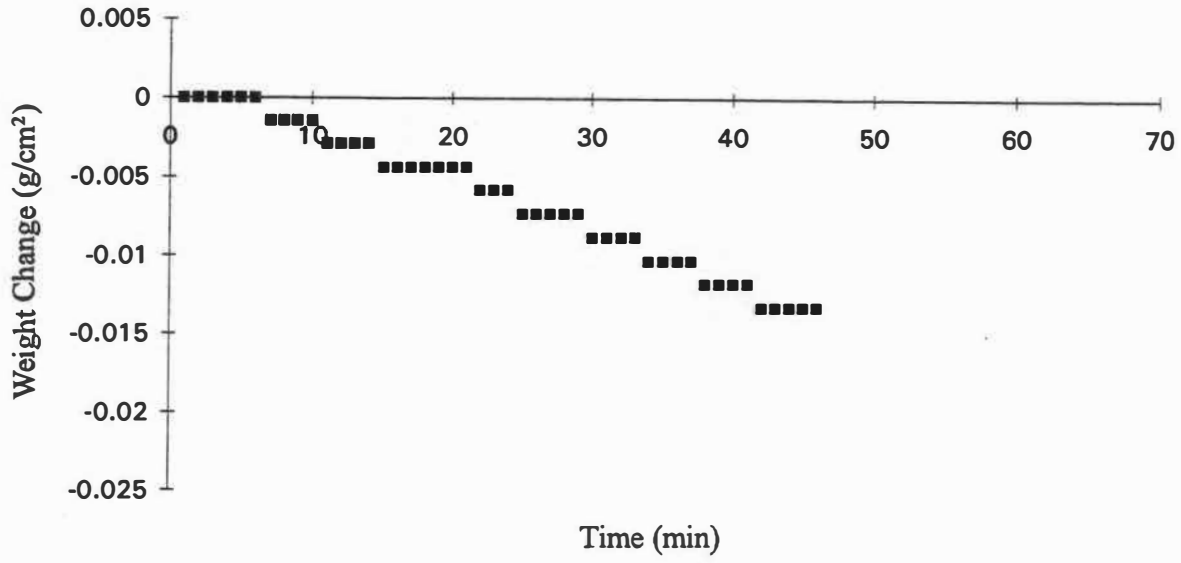

Figure 4.5.7. Thermogram of Run 282, T = 553°C, 4000 ppm HCl.

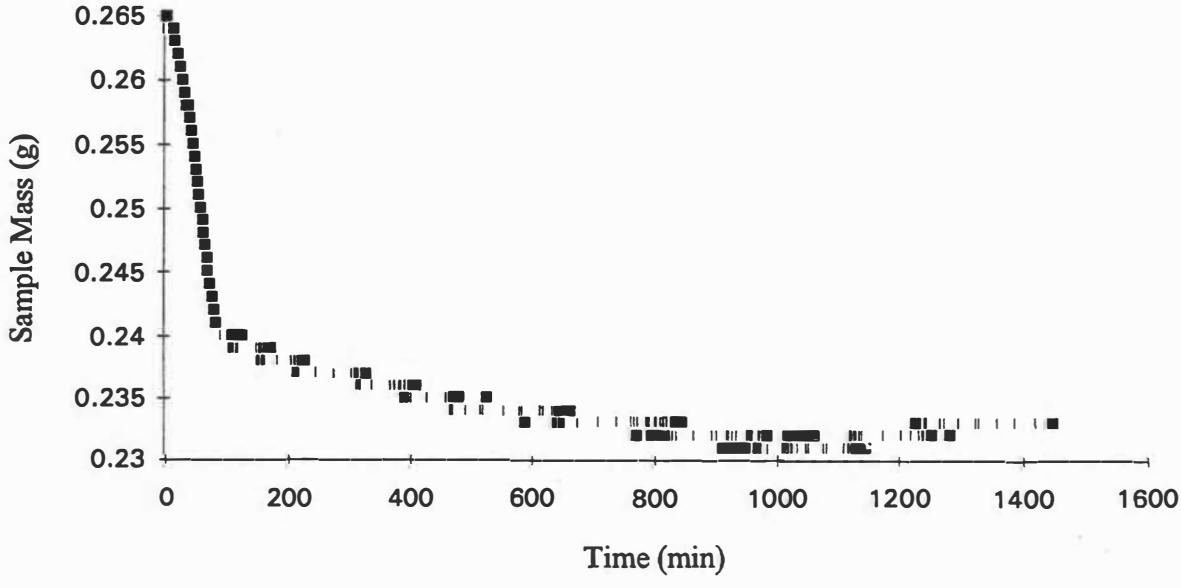

Figure 4.5.8. Thermogram of Run 282b, T = 553°C, 4000 ppm HCl.

Electron and optical micrographs were made of cross sections of specimens from Regime 3. Pellets were encapsulated in epoxy and polished with 1-μm diamond grit to facilitate the making of micrographs and to permit the analysis of the elemental concentration versus distance by wavelength dispersive, electron-induced x-ray fluorescence. An optical micrograph is shown in Figure 4.5.9 at 12× and an electron micrographic enlargement of the ash film is shown in Figure 4.5.10 at 1000×. As can be seen in both micrographs but more readily in the electron micrograph, there are actually two phases within the ash. An outer phase extends about one-third of the thickness of the total ash. This may be a relatively pure phase of $PbCl_2$ in equilibrium with another liquid phase of lead oxychloride as can be observed on the phase diagram, Figure 4.5.5.

A graph of the wavelength dispersive x-ray fluorescence elemental analysis of the ash layer (normalized weight percent) from Run 228 is shown in Figure 4.5.11. This technique is good for establishing the relative, but not the absolute, concentrations of the elements based on lead, oxygen, and chlorine standards. Unfortunately no exact standards are available; PbS, ThO_2, and $TlCl_3$ were used, and consequently matrix corrections were approximate. Contamination from the epoxy binder was in evidence as bubbling occurred during the analysis. The sample was not

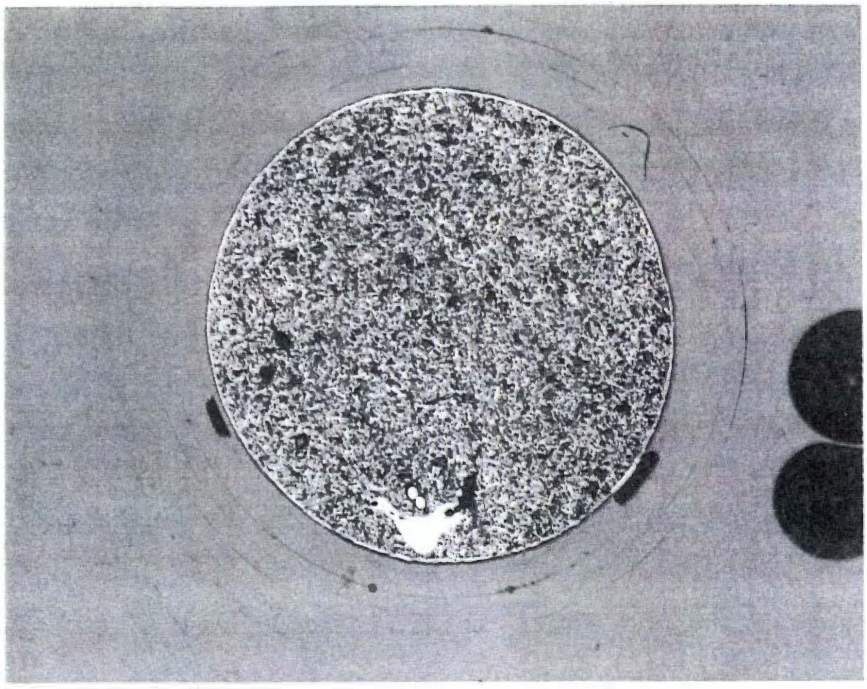

Figure 4.5.9. Light micrograph at 12× of cross section of pellet from Run 228, prepared at 555°C, 66 min, 2000 ppm HCl.

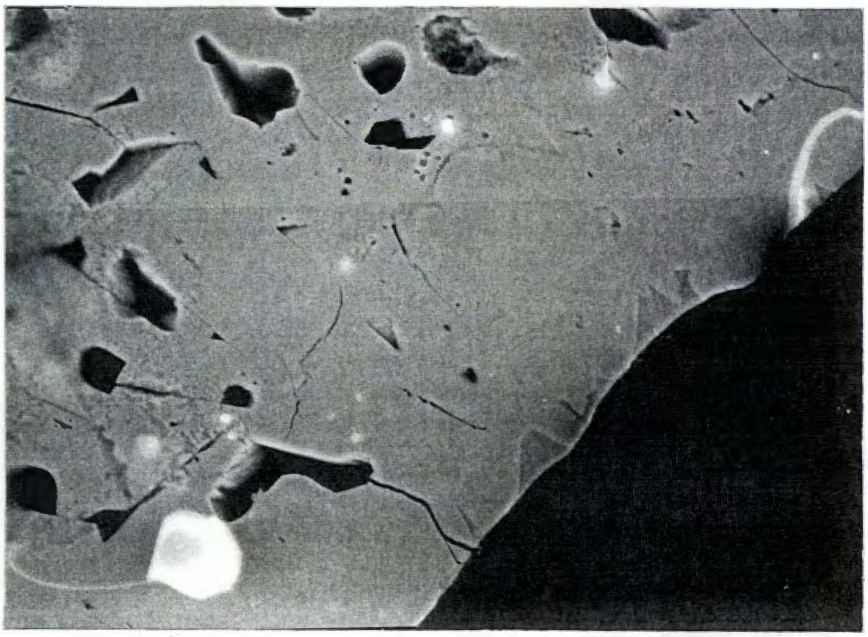

Figure 4.5.10. Electron micrograph at 1000× of outermost surface of ash, from Run 228, prepared at 555°C, 66 min, 2000 ppm HCl.

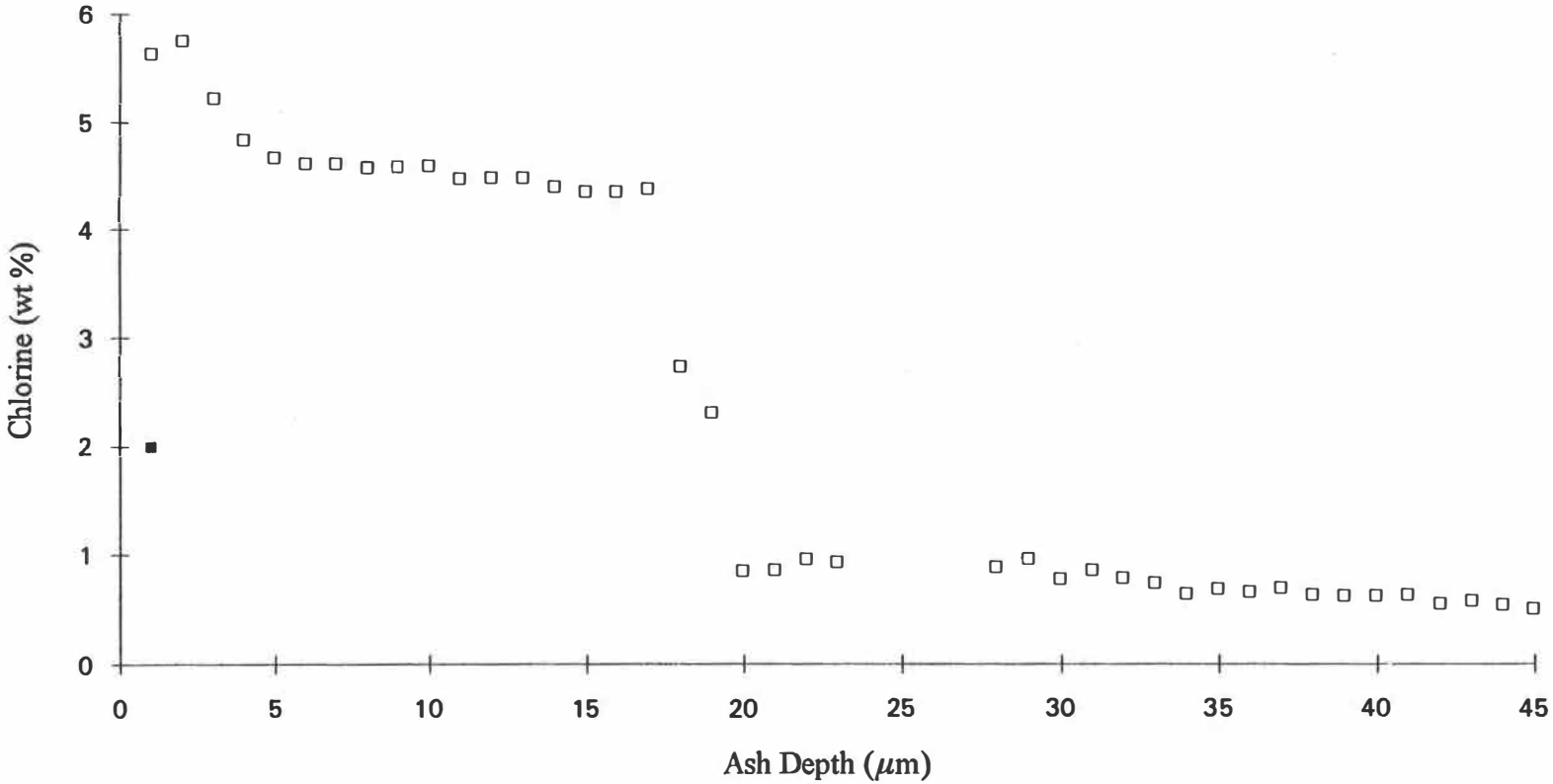

Figure 4.5.11. Profile of chlorine elemental concentration versus distance from pellet surface, wavelength dispersive x-ray fluorescence analysis, Run 228, time = 20 min.

conductive, charging was a problem, and the graphite coating may have reduced the x-ray count. Nevertheless, the data indicate that the chlorine-containing ash is about 20 μm in thickness, which is consistent with the optical micrographs and similar to the thickness in the electron micrographs, although electron micrographs were taken at only one radius.

The small residue of chlorine observed up to a distance of perhaps 100 μm may be an artifact of the polishing operation, or it may be a small quantity of chlorine that has diffused further into the specimen matrix. It is unfortunately near the noise level of the fluorescent analysis. The small rise in chlorine concentration near the surface of the particle may be due to the beginnings of a barrier to the diffusion of $PbCl_2$ at the surface where it volatilizes, or it may be due to an artifactual strengthening of the x-ray signal owing to a decline in absorption near the particle surface. A schematic of the qualitative concentrations of HCl, intermediate 1, and $PbCl_2$ are shown in Figure 4.5.12. The intermediate concentration is fairly flat as it first forms in the interior of the particle and then drops near the surface, where $PbCl_2$ forms in high concentration.

4.5.2 Descriptive Model, Regime 3

In this regime we have chosen a model of chemical reaction and liquid and gas phase diffusion with a single

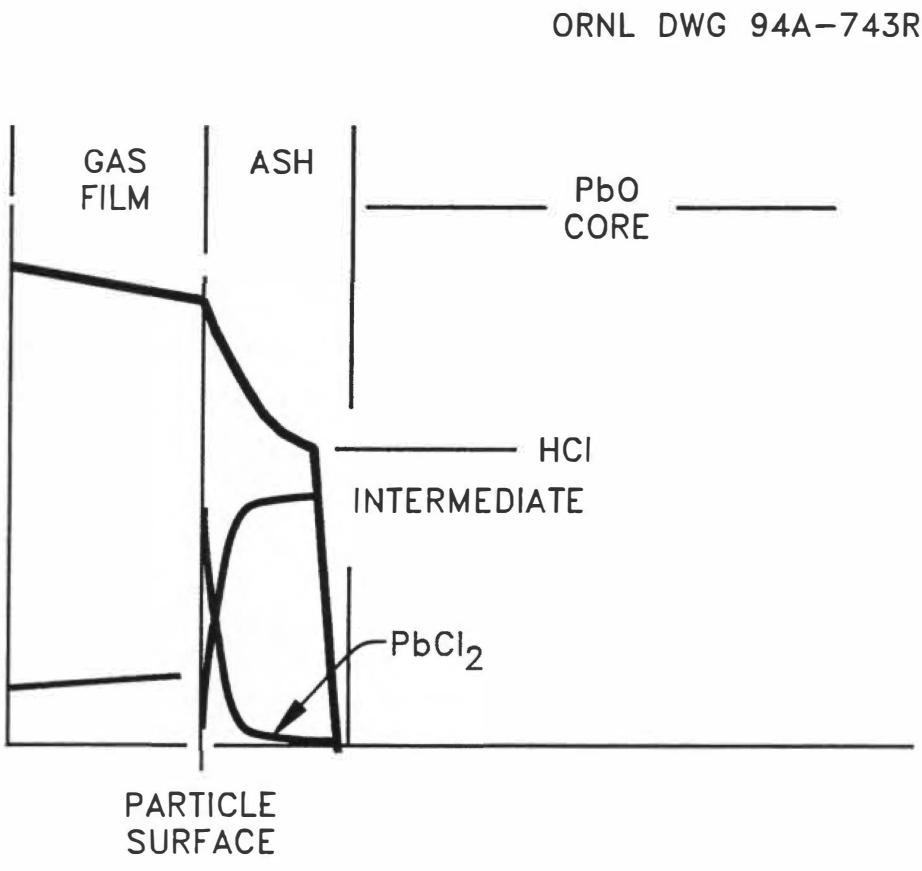

Figure 4.5.12. Schematic of approximate concentration profile of HCl and $PbCl_2$, Regime 3.

moving boundary. Although it would be more realistic to include two moving boundaries, the mathematics becomes more complex. The assumptions of this model are as follows. (1) Only the movement of the boundary between the unreacted PbO core and the ash is moving. (2) Shrinkage of the particle is negligible. (3) An intermediate oxychloride compound is formed that is a solid of low diffusivity. (4) The intermediate is formed very rapidly as an interfacial reaction of HCl and PbO. (5) HCl reacts homogeneously in the intermediate ash to form $PbCl_2$ in a second reaction, which is relatively slow. (6) Reaction proceeds through an intermediate I1 as illustrated in the following equations:

$$2HCl+3PbO \rightarrow (PbO)_2PbCl_2(I1) + H_2O \qquad (4.5.1)$$

$$4HCl + I1 \rightarrow 3PbCl_2 \qquad (4.5.2)$$

Mass balances on infinitesimal cross sections with consideration of chemical reaction yield the following equations and boundary conditions:

$$D\partial^2 C/\partial x^2 = \partial C/\partial t + k_{r1} C_{HCl} C_{PbO} n_c \qquad (4.5.3)$$

where C=[HCl] unless identified as [PbO] and k_{r1} is the

$$-D\partial C/\partial x=Cds/dt \qquad (4.5.4)$$

reaction constant to produce I1

where s is the position of the advancing boundary,

$$N_c|_{x=0}=-D\partial C/\partial x|_{x=0} \qquad (4.5.5)$$

where N_c is the flux of HCl at the particle surface,

$$C|_{t=0}=0 \qquad (4.5.6)$$

which is the initial condition. Also, simultaneously, intermediate is formed and diffuses as

$$D_{I1}\partial^2 I1/\partial x^2= \partial I1/\partial t \qquad (4.5.7)$$

where I1 = [Intermediate I1] and D_{i1}= diffusivity of I1 (artifactual), with the boundary conditions

$$I1|_{t=0}=0 \qquad (4.5.8)$$

$$I1=0,\ x<s \text{ and } I=I_o,\ x=s \qquad (4.5.9)$$

A similar relationship and boundary conditions hold for $PbCl_2$. A sharp boundary is observed between the ash and a unreacted core, so we use a finite difference technique involving a moving boundary at the ash-core interface. The $PbCl_2$ is assumed to diffuse slowly; otherwise, in this

model, the $PbCl_2$ concentration would fall rapidly at the interface and the volatilization rate would then decline. This assumption is somewhat similar to asserting that the $PbCl_2$ (liquid) on the surface remains at the surface element. The high concentration of $PbCl_2$ at the surface also impedes the diffusion of HCl into the particle because the Henry's law constant of HCl in $PbCl_2$ is lower than in the chemisorptive PbO. The intermediate, I1, is modeled as diffusing only rapidly enough to account for shrinkage of the particle during reaction. Since the volatility of $PbCl_2$ is much less at this temperature than at 670°C, as we will see in Regime 4, its concentration and activity must be great in Regime 3. Data of the activity of $PbCl_2$ in a melt of $PbCl_2$-PbO were available (Hacetoglu and Flengas, 1990), and these data were inputted to the computer model. The listing and numerical results of this model are shown in Appendices B1 and B2 respectively. Because of this model's similarity to the Regime 4 model, its algorithmic development is discussed in the section pertaining to the model of Regime 4. Graphical results of the Regime 3 model are shown in the curves of Figures 4.5.13 and 4.5.14 for Run 228, at 550°C, and Run 310, at 580°C. The shape of the curves was found to depend strongly on the reaction rate constant and the value of the artifactual diffusion of the intermediate but not strongly on the value of the Henry's law constant. The value of the HCl diffusivity

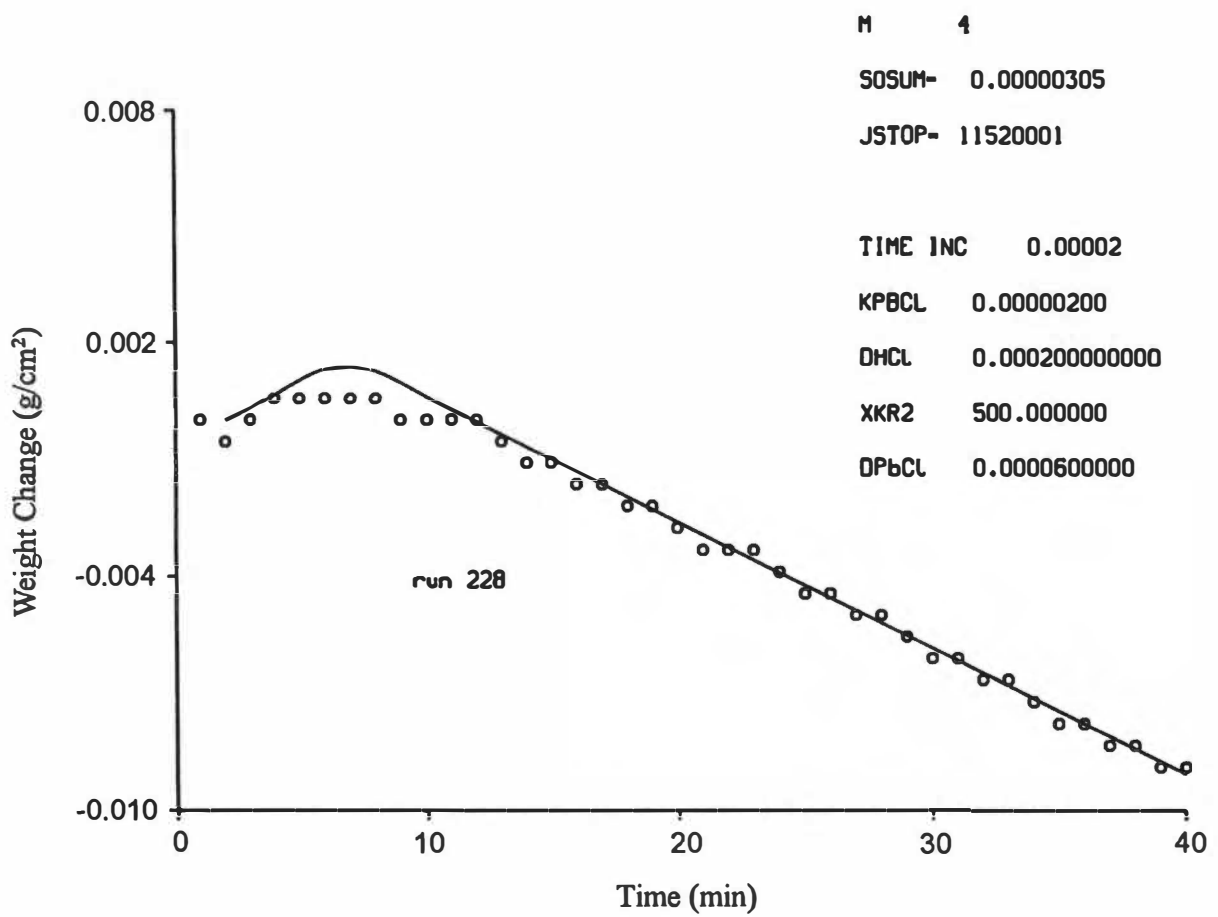

Figure 4.5.13. Thermogravimetric results of Run 228 at 555°C, data shown as squares, model results as solid line.

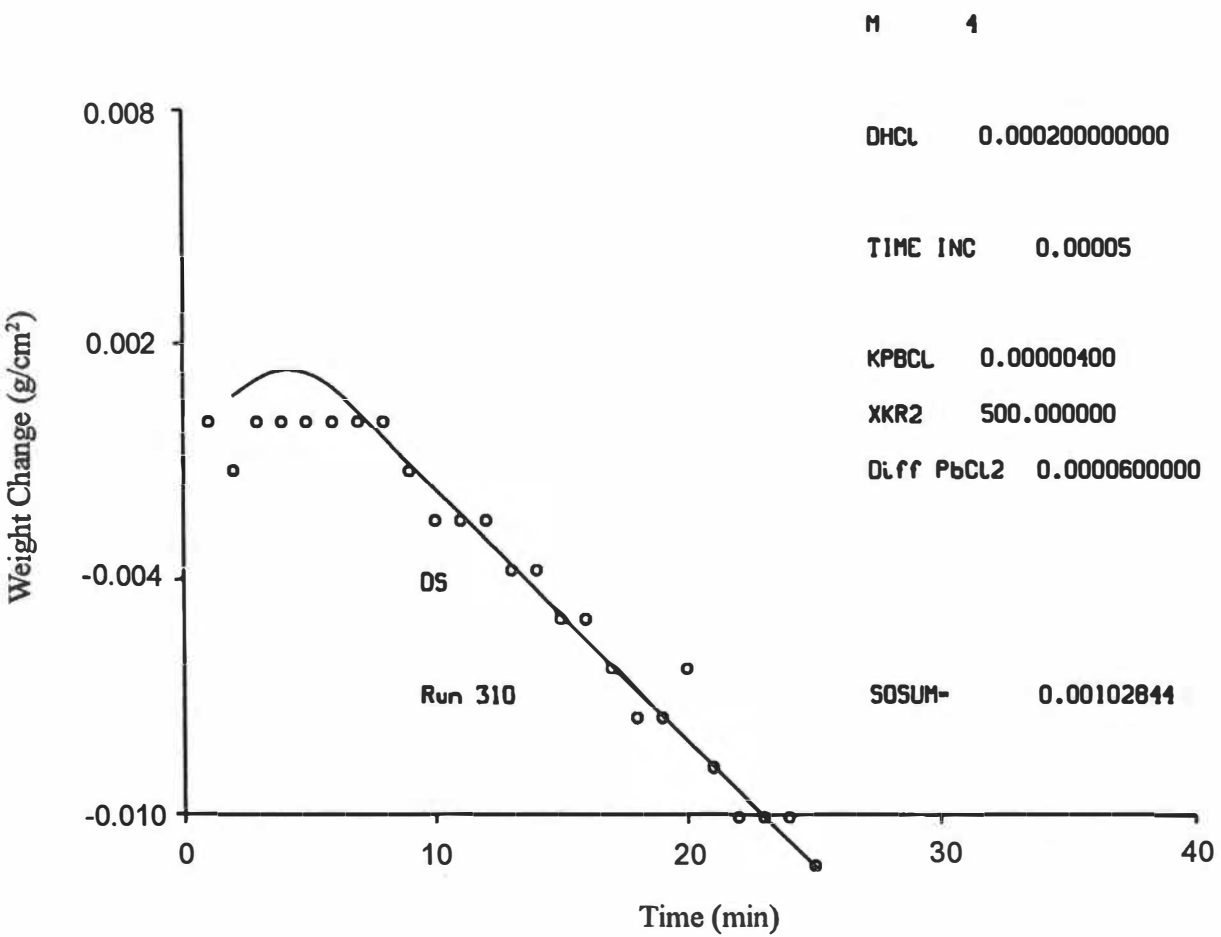

Figure 4.5.14. Thermogravimetric results of Run 310 at 580°C, data shown as squares, model results as solid line.

is 2E-4 cm^2/s, which is not an unrealistic value of a liquid phase coefficient at these elevated temperatures. (A diffusivity of 1E-4 cm^2/s is considered typical of water at 25°C, and the molten $PbCl_2$, like other molten salts, has a waterlike consistency.) The diffusivity of $PbCl_2$ is set at 5E-5 cm^2/s, very nearly one-fourth that of HCl, on the assumption that the diffusivity varies inversely with the molecular radius. Radii were determined from the Table of Interatomic Distances and Configuration in Molecules and Ions. The vapor pressure of $PbCl_2$ and its activity are inputted directly from experimental data, as noted. The Henry's law coefficient, 0.20 mole fraction/(mole•cm^3) is hard to compare since there are no data on similar systems. These particular values are comparatively high, but this is also a chemisorptive system.

In summary, Regime 3 is characterized primarily by diffusional resistance in the condensed phase; however, in this case, we can more easily measure the rate of advancement of a moving boundary and apply a model of chemical reaction and diffusion using the advancing front as a boundary condition. Though the global reaction rates are virtually unchanged from those in Regime 2, significant differences in the physical chemical behavior are observed. A lead dichloride rich phase forms at the particle surface over a solid phase intermediate, probably a lead oxychloride layer. The thickness of the moving boundary can be

described approximately by using a model of chemical reaction and diffusion with a moving boundary value condition. Chemical reaction is modeled as occurring homogeneously in the solid ash phase, and artifactual diffusivities of $PbCl_2$ and intermediate are inserted into the model to account for the particle shrinkage during reaction. Otherwise, the model becomes mathematically very complicated because of the existence of two moving boundary value conditions.

4.6 REGIME 4, T = 590 to 670°C

4.6.1 Introduction

This is the most interesting temperature regime and exhibits the most unexpected results. As indicated briefly in Sect. 4.5, at temperatures around 550°C at HCl concentrations of 4000 ppm, we see an initial rise of perhaps 1 mg in the thermogram for several minutes followed by a rapid and steady drop. At temperatures above 590°C, a significant initial rise in the thermograms is seen in every case at concentrations of 2000 and 4000 ppm. Moreover, this rise may be several percent of the sample mass and 30 min or more in duration. This can be seen in Figures 4.6.1 and 4.6.2, thermograms of Run 245, produced at 672°C, and Run 284, at 670°C, both conducted at 2000 ppm HCl. Run 284 was quenched before the thermogram begin to exhibit a weight loss. Extensive electron and optical micrographs were taken

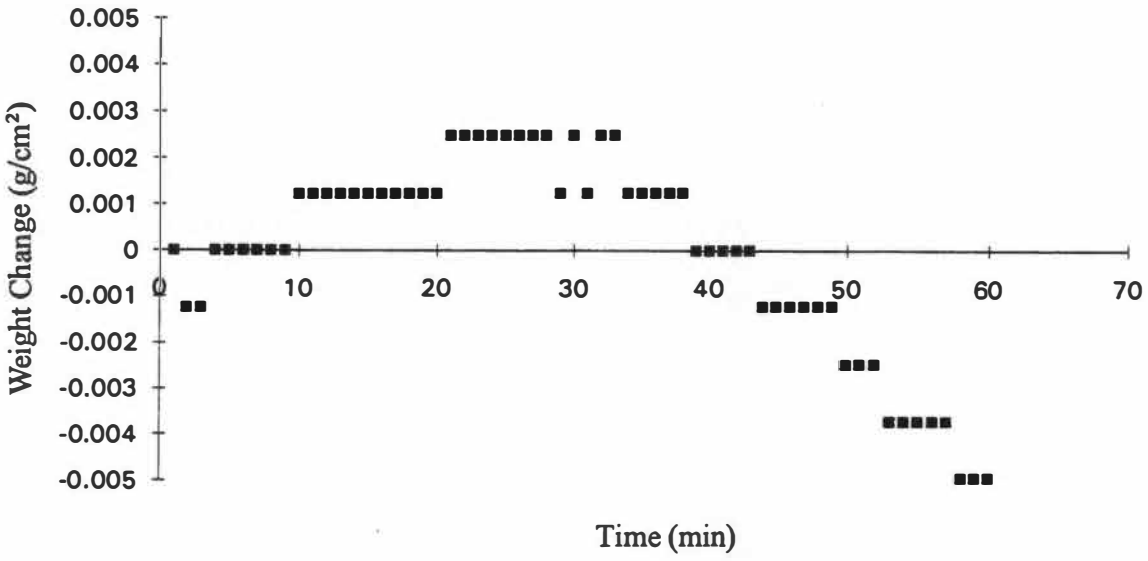

Figure 4.6.1. Thermogram of Run 245, T = 672°C, 2000 ppm HCl.

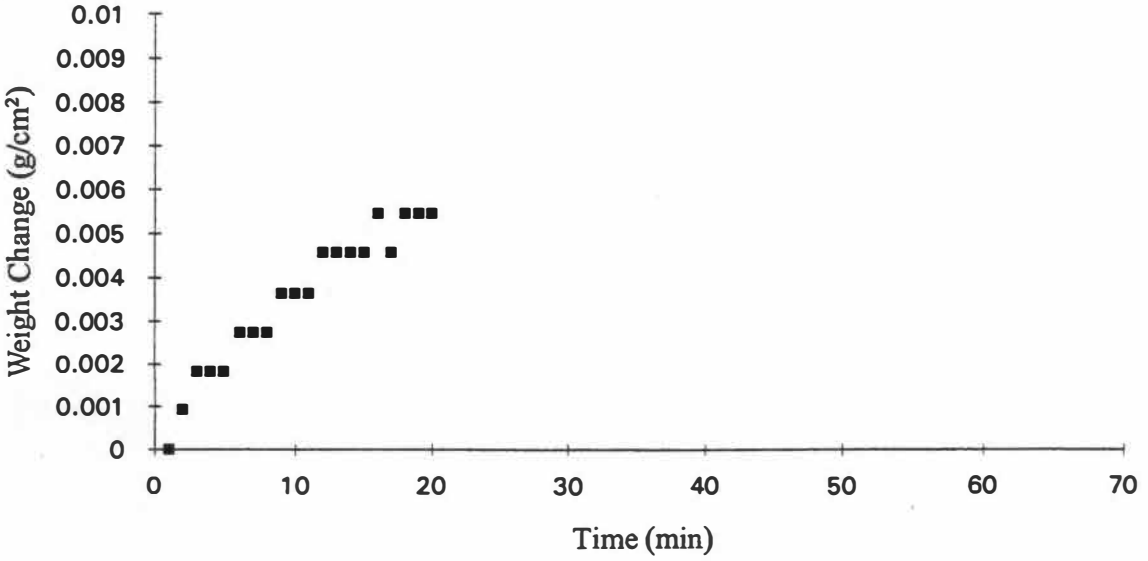

Figure 4.6.2. Thermogram of Run 284, T = 674°C, 2000 ppm HCl.

of these two runs in particular. Figure 4.6.3 of Run 174 at 670°C illustrates the behavior of the reacted sample during the 153 min of hydrochloridation. The pellet was then allowed to remain at 670°C for about 2000 min; the temperature was then raised to 692°C and the thermogravimetric data collection continued another 1000 min. At approximately 700°C the weight loss was not further observable over a period of days. Simple unreacted PbO pellets were also held at this temperature for a period of days and exhibited no weight loss within the vagaries of our data collection. We were then able to determine the full extent of the $PbCl_2$ losses and therefore a global reaction rate. Figure 4.6.4 is an extended view of Run 174 and might be compared with Figure 4.5.8 of Run 282 at 553°C to make the point that the quantity of chlorine remaining after reaction at 670°C was much more substantial.

A very interesting phenomenon was noticed in examining the global reaction rates of samples treated in this temperature regime when they were compared with results from Regime 3. Table 4.6.1 provides data on the volatilization rates of $PbCl_2$, measured by difference as previously described, of runs in Regimes 3 and 4 treated at a range of temperatures and times. It will be seen that at short reaction times the molal loss of $PbCl_2$ is undetectably small at a temperature near 630°C and rises at 670°C to approximately 2E-8 moles/(sec $\cdot cm^2$). At 670°C the rate is

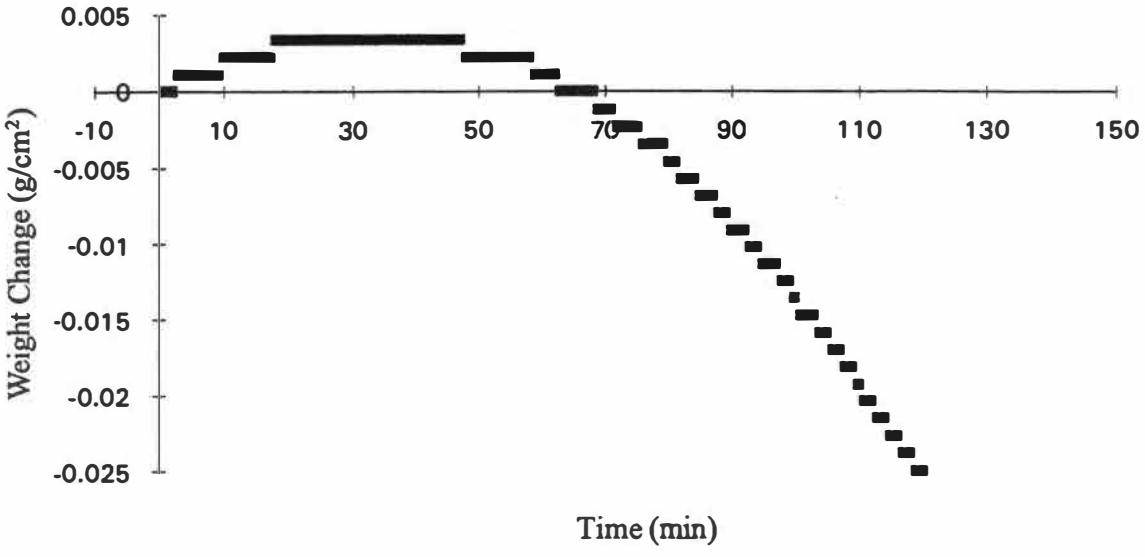

Figure 4.6.3. Thermogram of Run 174, T = 670°C, 2000 ppm HCl.

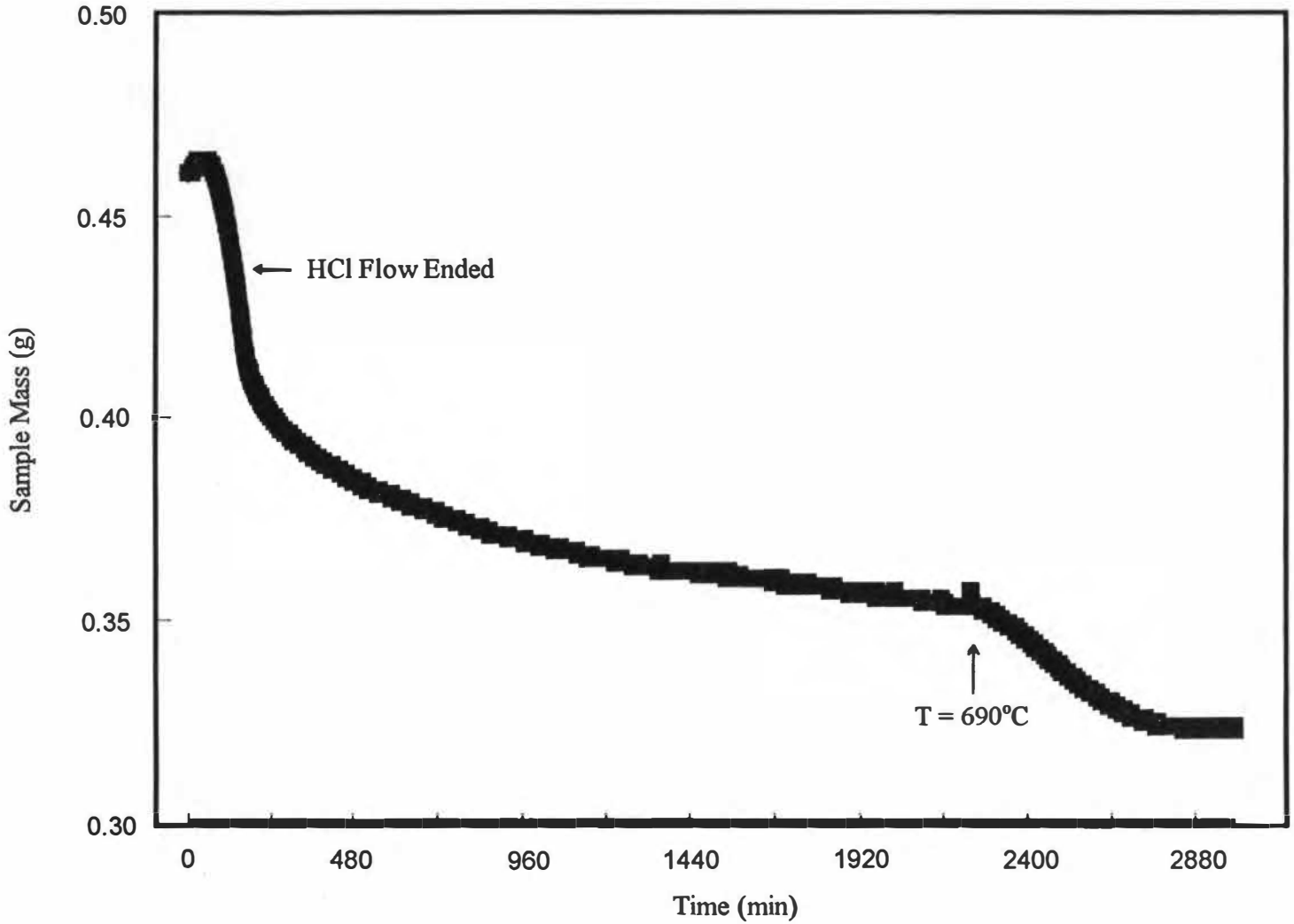

Figure 4.6.4. Extended thermogram of Run 174, T = 672 to 690°C, demonstrating extensive weight loss after end of HCl flow.

still only about half the volatilization rate of most samples in Regime 3, where the volatilization rates are about 4E-8 moles/(sec • cm^2).

Table 4.6.1. $PbCl_2$ volatilization rates during hydrochloridation reaction, determined by difference

Run	T (°C)	Volatilization rate [10^{-8} × mol/(cm^2 · s)]		Reaction time (min)
		Data	Model	
173	563	3.95		55
174	670	3.96		153
183	570	4.06		107
198	670	2.15		120
199	670	2.25		120
208	630		0.26	30
210	494	1.99		124
217	639	nil		62
219	630	nil		61
228	555		2.0	66
245	670		1.9	60
245	670		3.6	120

As seen in Figures 4.6.5 of Run 307 at 603°C and 4.6.6 of Run 208 at 630°C, there is a rise in the extent of the "hump" or plateau period with temperature, but the differences between specific runs at 630 or 670°C are less clear and can be obscured in variations, we believe, in the initial surface areas of the lead oxide specimens. Variations are usually seen in the extent of the weight gain period and its relative size, but its occurrence is predictable. Not a single experiment at these temperatures failed to exhibit a plateau. At HCl concentrations of 4000

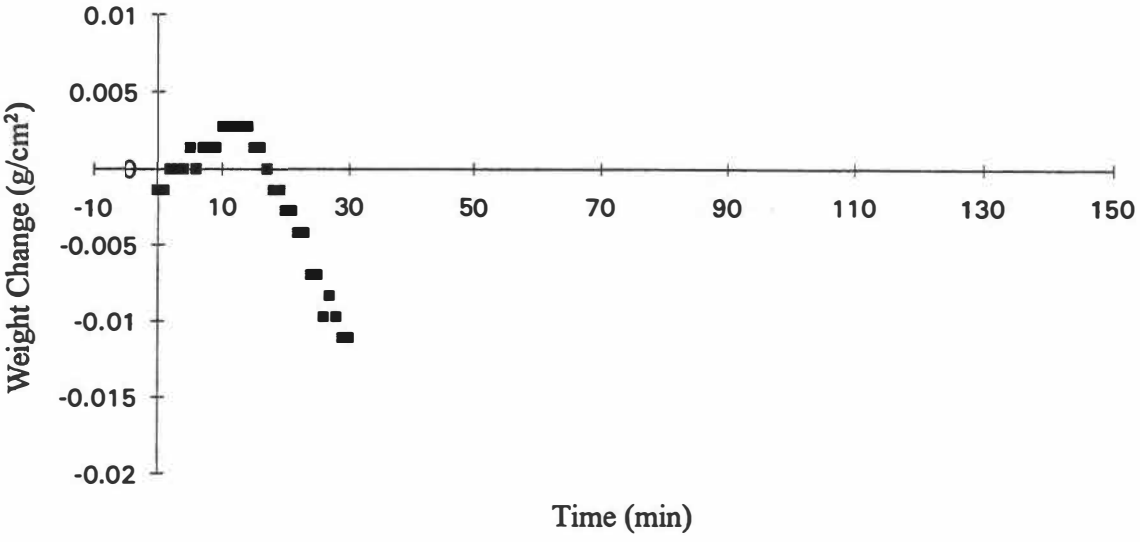

Figure 4.6.5. Thermogram of Run 307, T = 603°C, 2000 ppm HCl.

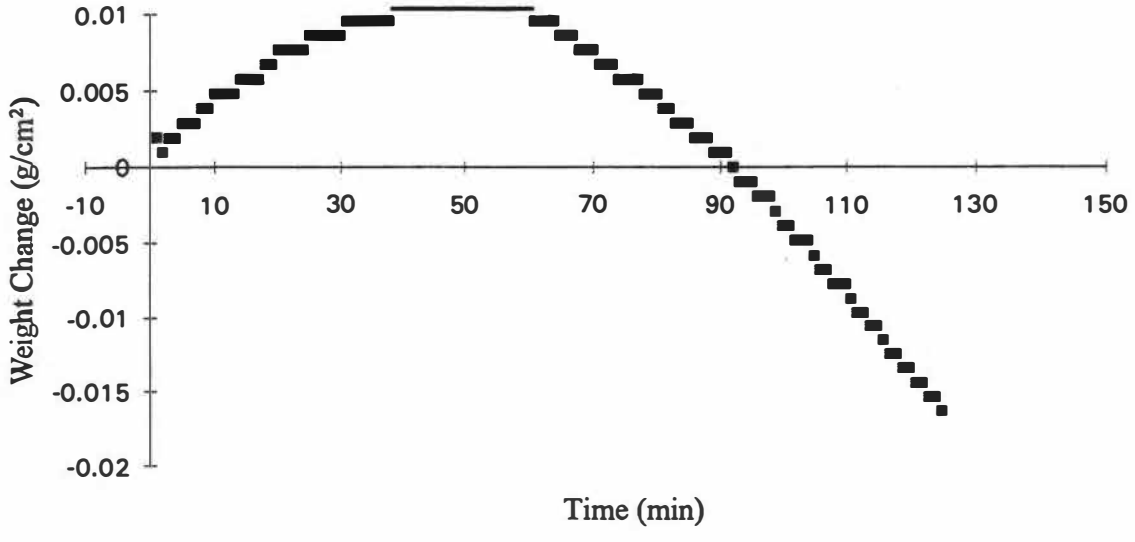

Figure 4.6.6. Thermogram of Run 208, T = 630°C, 2000 ppm HCl.

ppm, as seen in Figure 4.6.7 for Run 246, the behavior was very similar, except that difficulty was encountered with small amounts of the sample dripping after reaction times in excess of about 20 min, a period of time in which an appreciable amount of liquid product developed. This had been observed occasionally at 2000 ppm, at much longer reaction times (i.e., 2 h). Examination of the quenched samples at these conditions generally suggested that a fairly liquid layer had formed and collected as the beginnings of a droplet at the bottom of the specimen. Figure 4.6.8 is the thermogram of such a particle from Run 314, reacted for 134 min at 660°C. Figure 4.6.9 shows a low-magnification color picture of an unpolished cross section of Run 314 (on the right) and a similar cross section from Run 313 (on the left) prepared under the same conditions. Notice the evidence of fusion at the particle surfaces and the formation of a darker inhomogeneous layer. A few experiments were conducted at 740°C and even at 790°C; however, the reaction product was volatile, very inviscid, and quickly dropped off. The initial weight gain period, however, was still present.

4.6.2 Ash Characterization

Figures 4.6.10 and 4.6.11 display the cross sections in visible light at low magnification of specimens generated at 672°C for 20 and 60 min from Runs 284 and 245 respectively.

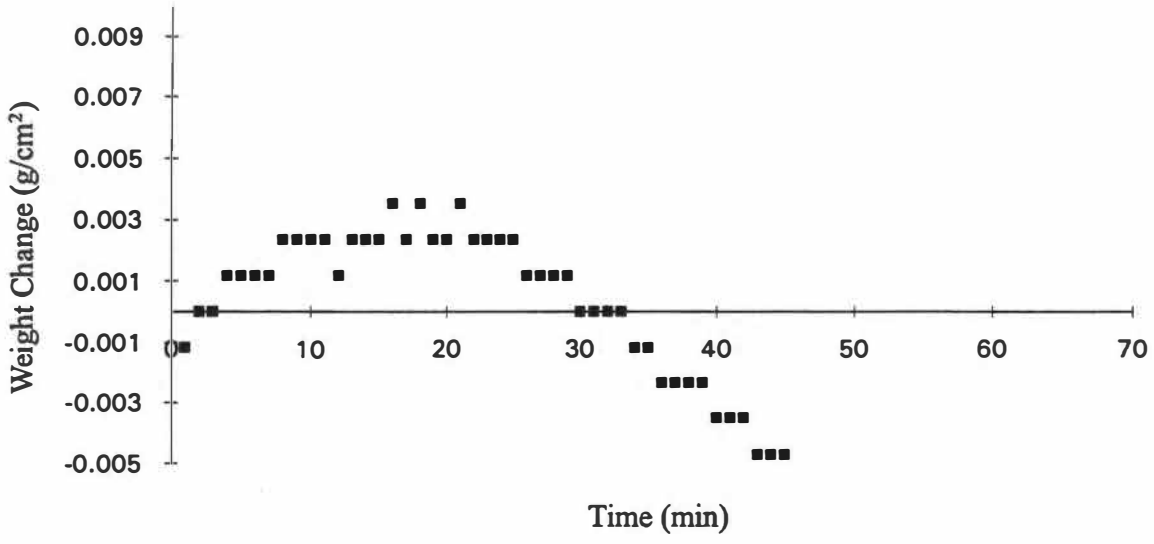

Figure 4.6.7. Thermogram of Run 246, T = 672°C, 4000 ppm HCl.

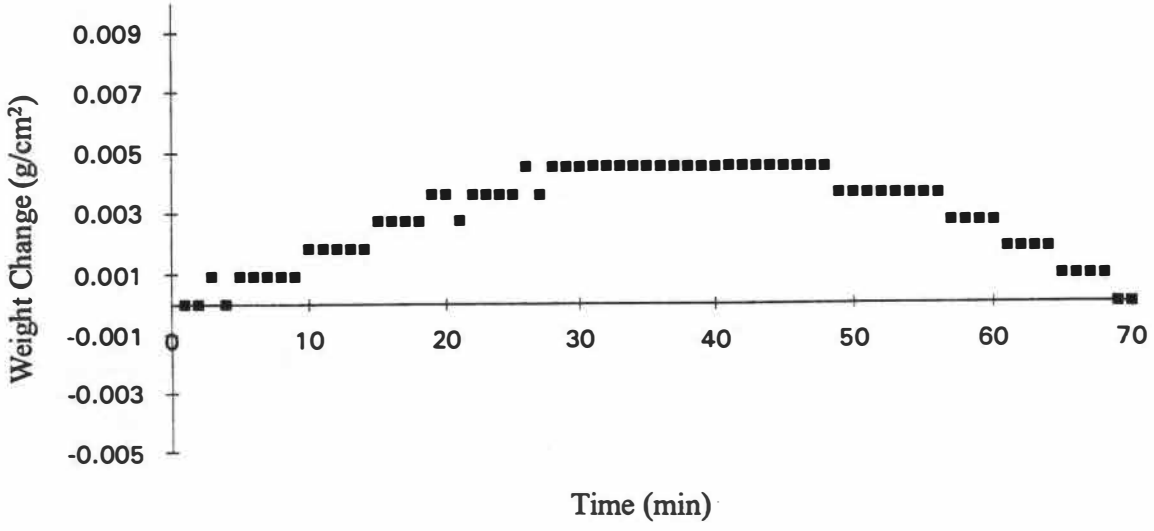

Figure 4.6.8. Thermogram of Run 314, T = 661°C, 2000 ppm HCl.

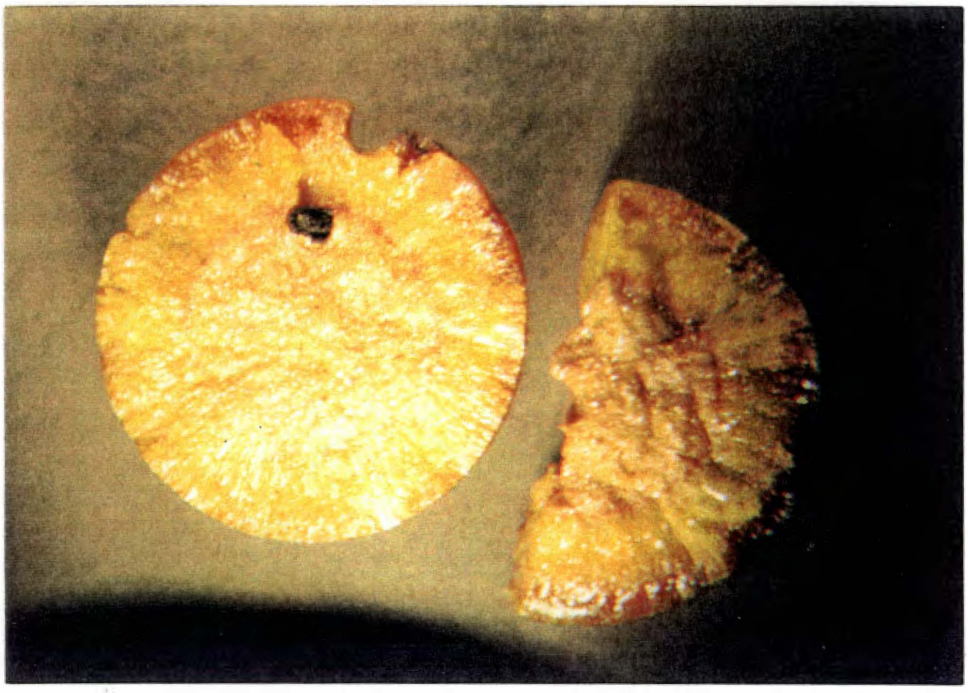

Figure 4.6.9. Unpolished cross section of pellets from Run 313 (left) and Run 314 (right), both prepared at 670°C at comparable reaction times (2 h) at 2000 ppm HCl.

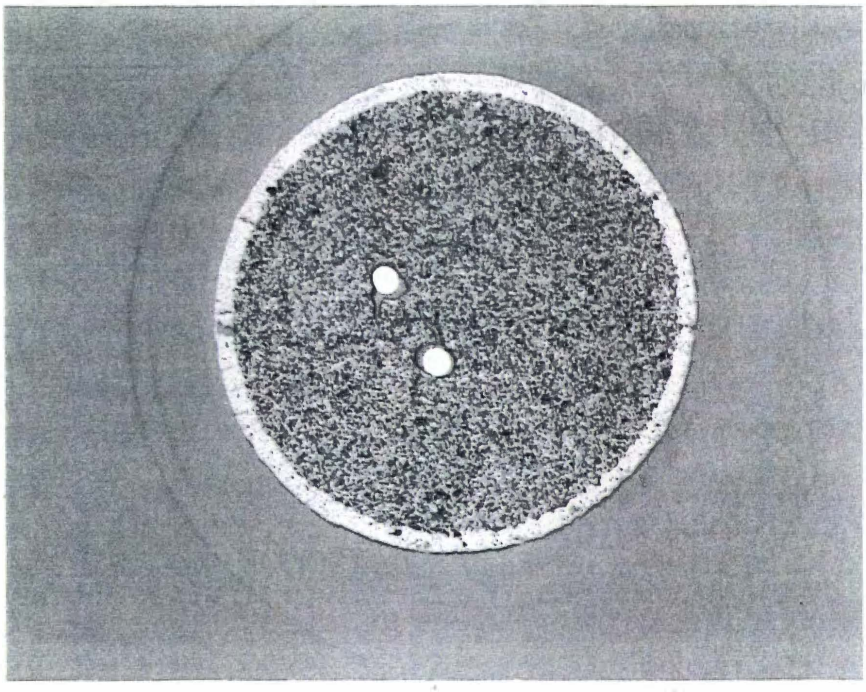

Figure 4.6.10. Polished cross section of pellet from Run 284, prepared at 670°C, 20 min, 2000 ppm HCl.

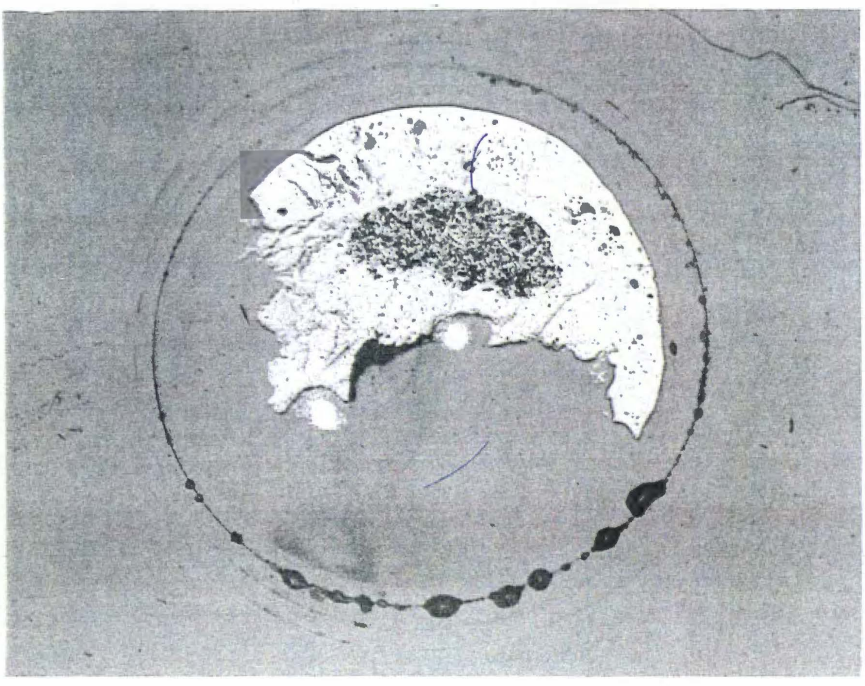

Figure 4.6.11. Polished cross section of pellet from Run 245, prepared at 670°C, 60 min, 2000 ppm HCl.

Here it is very evident that the ash layer is growing rapidly with time and is definitely demarcated with respect to the unreacted core. Figure 4.6.12 is an electron micrograph at 500× of the boundary between the core and ash in Run 245. The ash layer (to the right) is much smoother in texture than the unreacted core, later confirmed to be pure PbO. The dark spots appear to be residual porosity in the sample, and the very light spots may be very shallow holes that are highly reflective or have become charged during the electron bombardment. Figure 4.6.13, of another point in the ash layer of Run 245, now at 1000×, seems to indicate the existence of crystalline facets, alongside features attributable to porosity and cracks. These feature are not believed to result from "pull-out" during the polishing of the sample.

Particulate fume was collected on fabric filters in this regime partly to confirm the strong hypothesis that $PbCl_2$ was actually forming and also to gain information on the nature of the particulate. Although this technique of particle collection results in the formation of agglomerates not necessarily characteristic of the gas phase fume, certain deductions can still be made. The particulate is shown in a electron micrograph (Figure 4.6.14a at 1000× and Figure 4.6.14b at 5000×). Note the apparent existence of fine submicron bead, which seems to have agglomerated. It is believed that the beads were formed

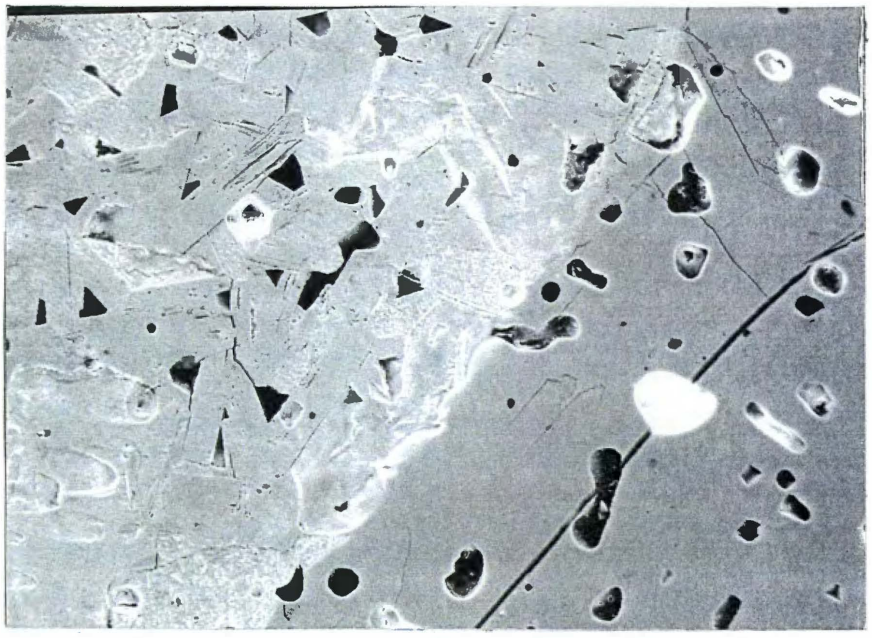

Figure 4.6.12. Electron micrograph at 500× of interface between ash and core of pellet from Run 245, prepared at 670°C, 60 min, 2000 ppm HCl.

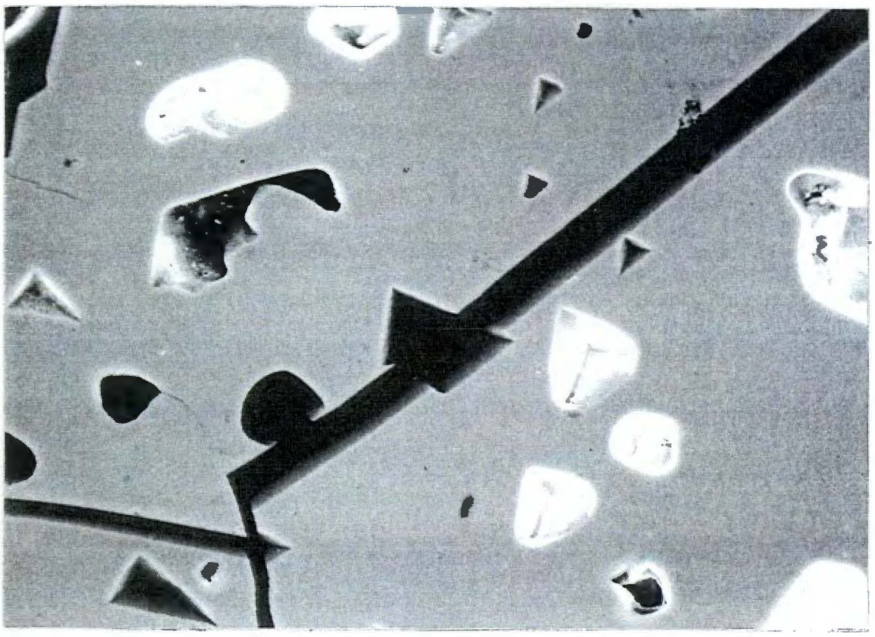

Figure 4.6.13. Electron micrograph at 1000× of middle of ash layer of pellet from Run 245, prepared at 670°C, 60 min, 2000 ppm HCl.

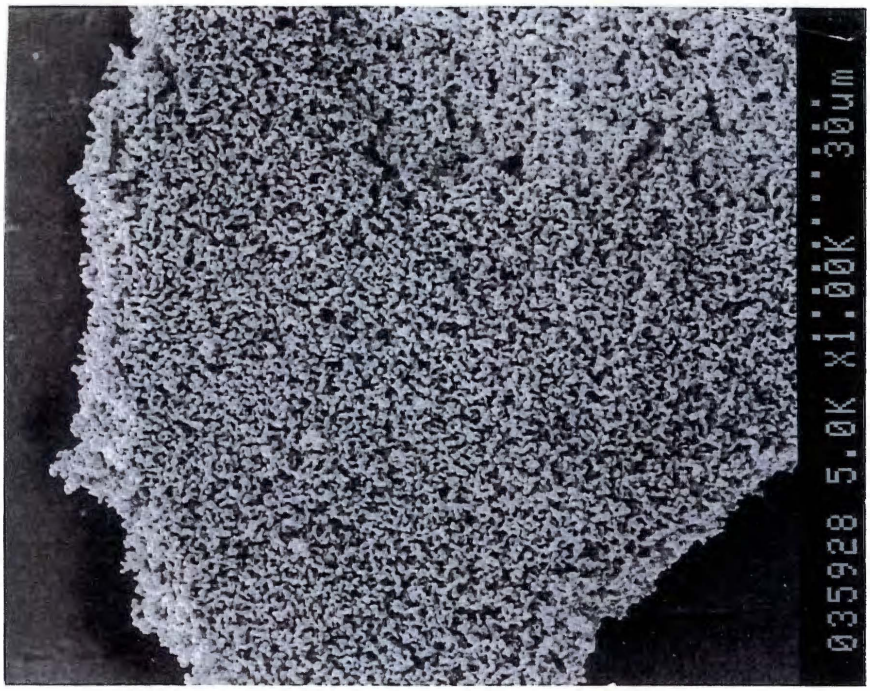

Figure 4.6.14a. Electron micrograph at 1000× of $PbCl_2$ fume formed at 670°C.

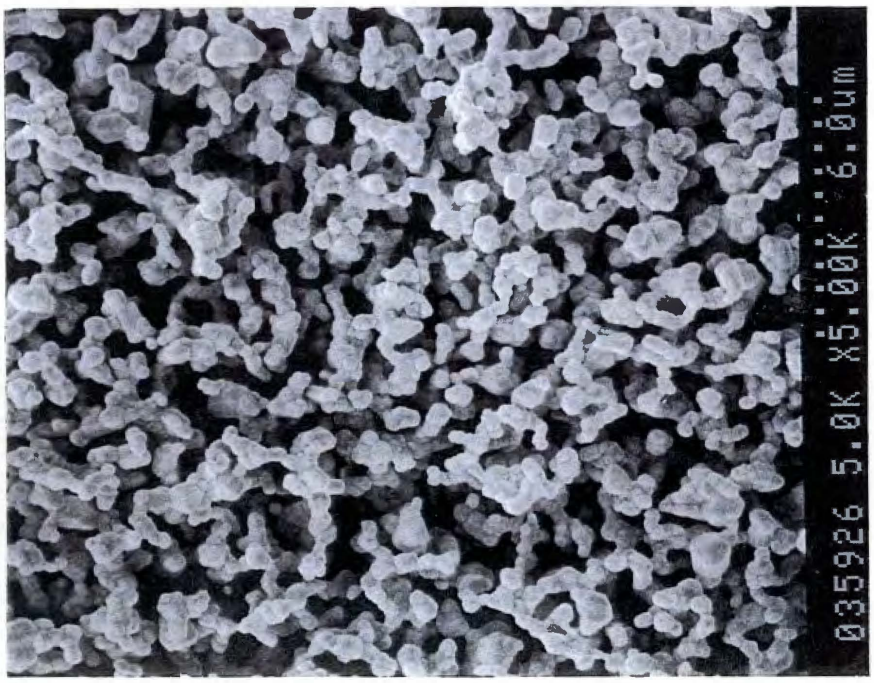

Figure 4.6.14b. Electron micrograph at 5000× of $PbCl_2$ fume formed at 670°C.

early in the condensation process. Figures 4.6.15a and 4.6.15b display the particulate distribution in the submicron range as determined by a TSI model 3030 Electrical Aerosol Analyzer at 550 and 650°C. Each letter refers to a particular batch analysis that was withdrawn at a consecutive 2-min interval from a large flask into the analyzer. The number of particles drops with time because of an exhaustion of the batch supply. Note that the distribution shifts to the right, or to larger particles, at the higher temperatures, which may be an indication of greater agglomeration.

Concentration profiles of the ash layers from Runs 245 and 284 were generated using an expensive wavelength dispersive electron-induced x-ray fluorescence technique. The elemental weight percents as a function of distance in microns from the surface of the particle are shown in Figures 4.6.16 and 4.6.17 for Runs 245 and 284 respectively. The data from Run 284, which had a fairly uniform ash layer, are probably more useful, and these were compared with our model. The data from Run 245, which indicate (at the cross section of polishing) an ash layer of 600 to 700 μm in depth, are probably artifacts. The ash from this sample was not uniform at the outset because the sample had liquified to a point at which it more resembled a droplet than a cylindrical pellet. Secondly, the specimen was polished so deeply that we are partially observing the ash from the

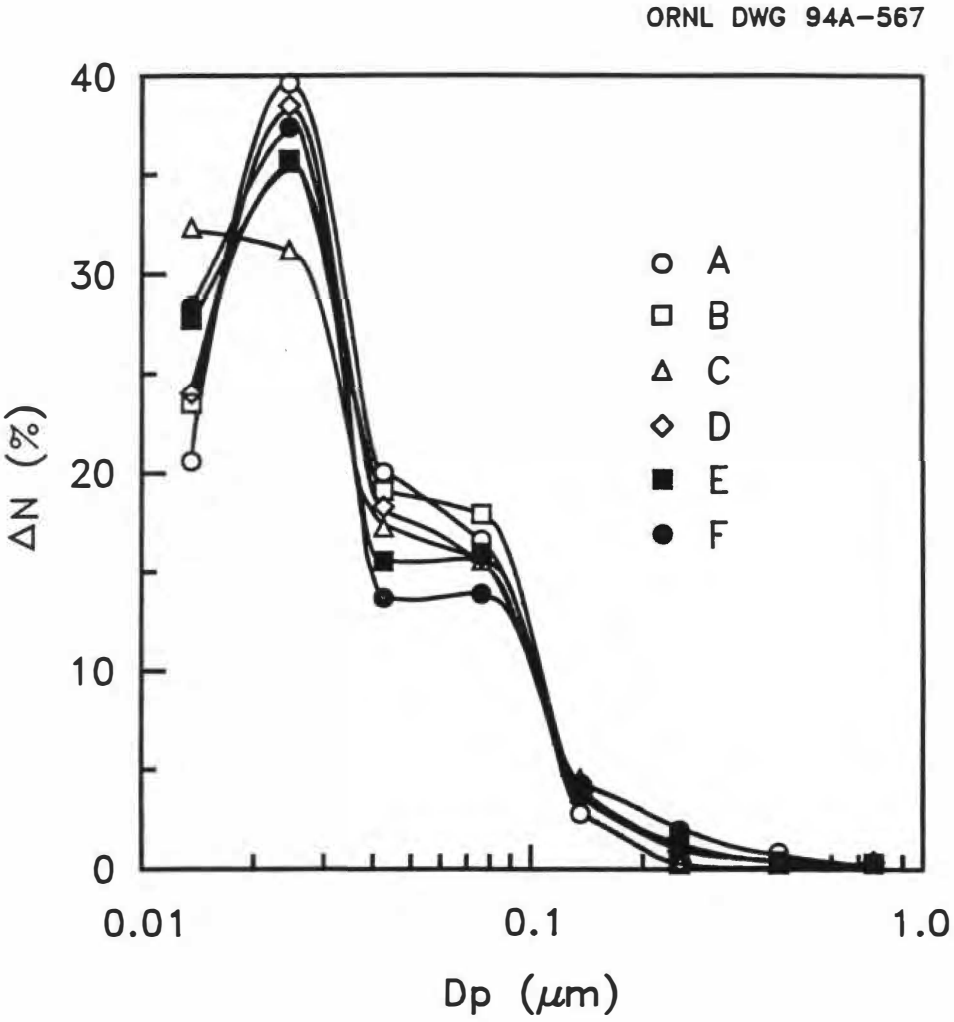

Figure 4.6.15a. $PbCl_2$ particle size distribution as determined by electrical aerosol analyzer at 550°C, number percentage versus particle diameter in microns. (Letters refer to consecutive batch time intervals of 2 min.)

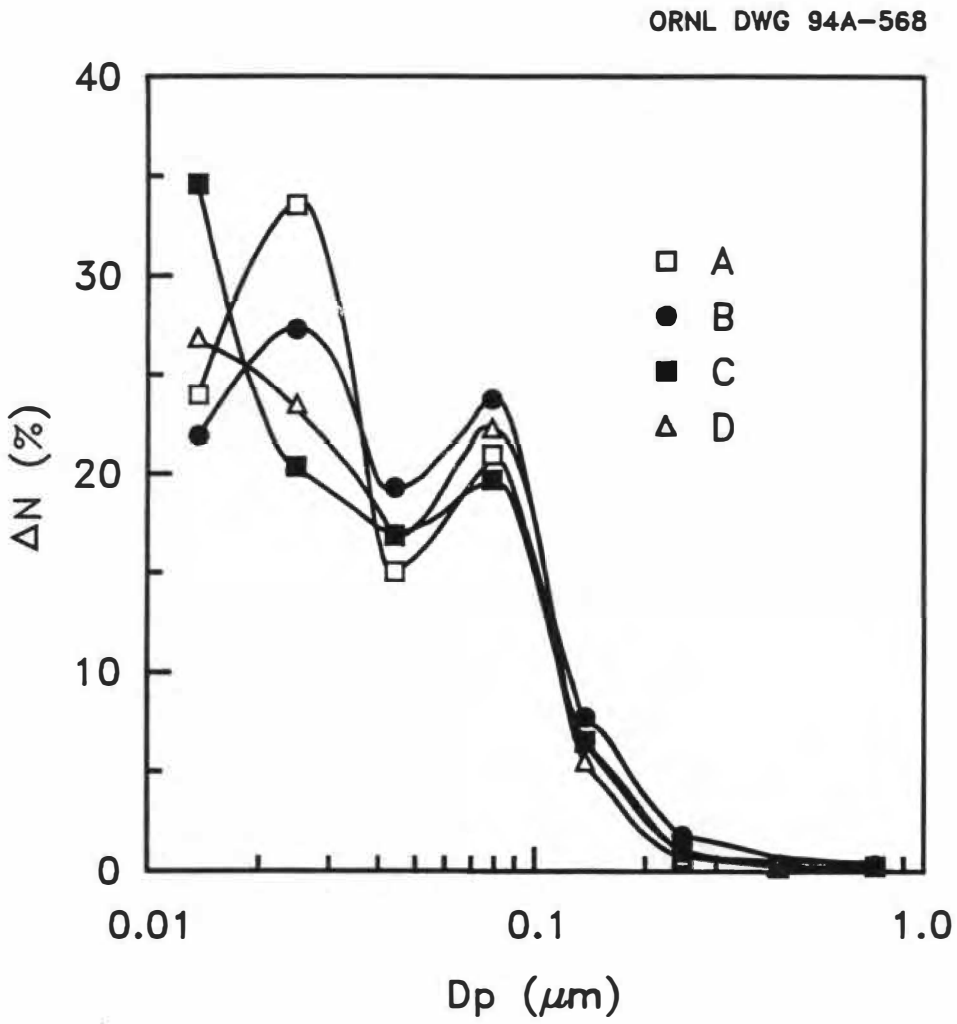

Figure 4.6.15b. $PbCl_2$ particle size distribution as determined by electrical aerosol analyzer at 650°C, number percentage versus particle diameter in microns. (Letters refer to consecutive batch time intervals of 2 min.)

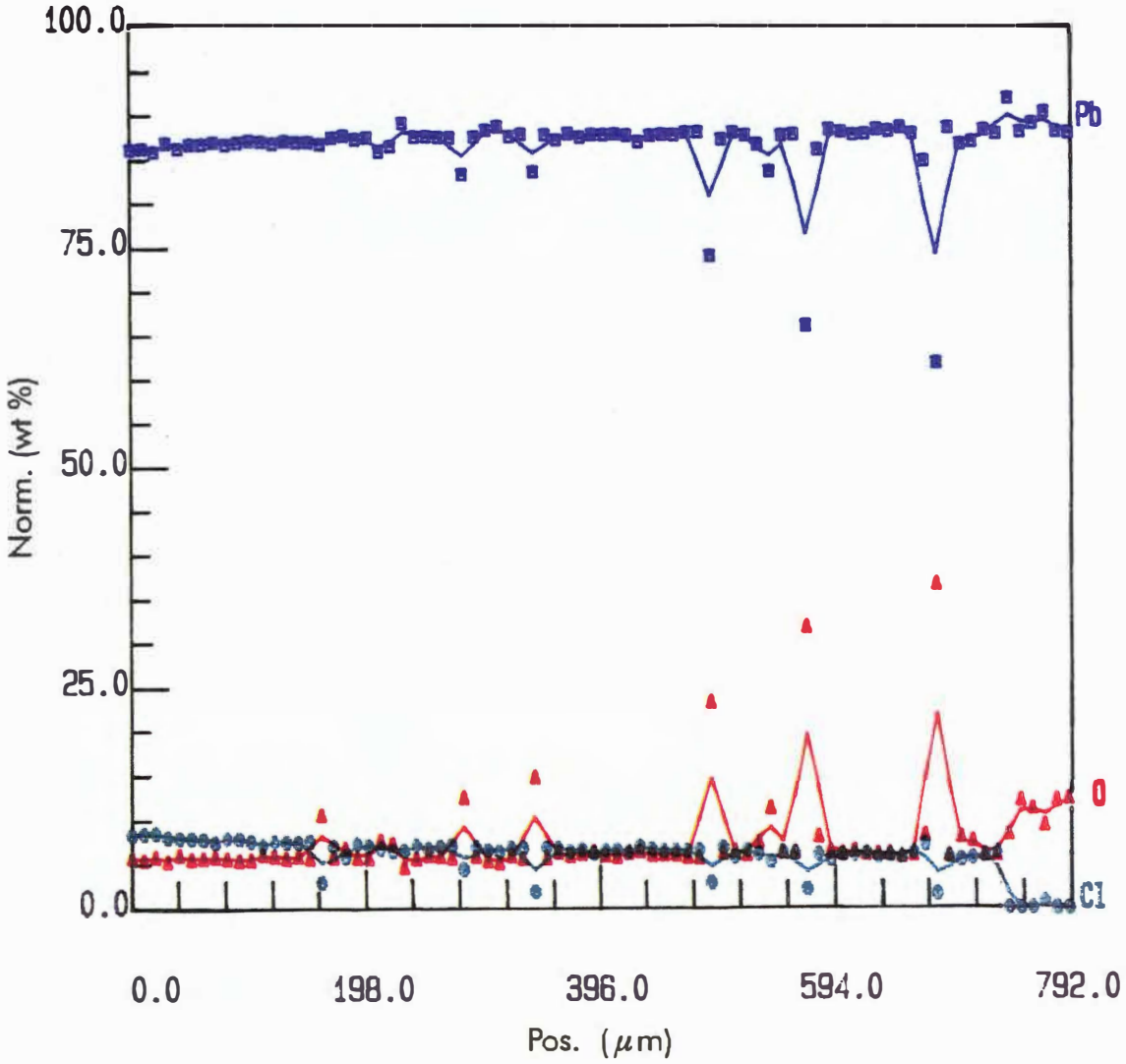

Figure 4.6.16. $PbCl_2$ and chlorine elemental concentration profiles, determined by wavelength dispersive x-ray fluorescence of polished sample, Run 245, T = 670°C, 60 min, 2000 ppm HCl.

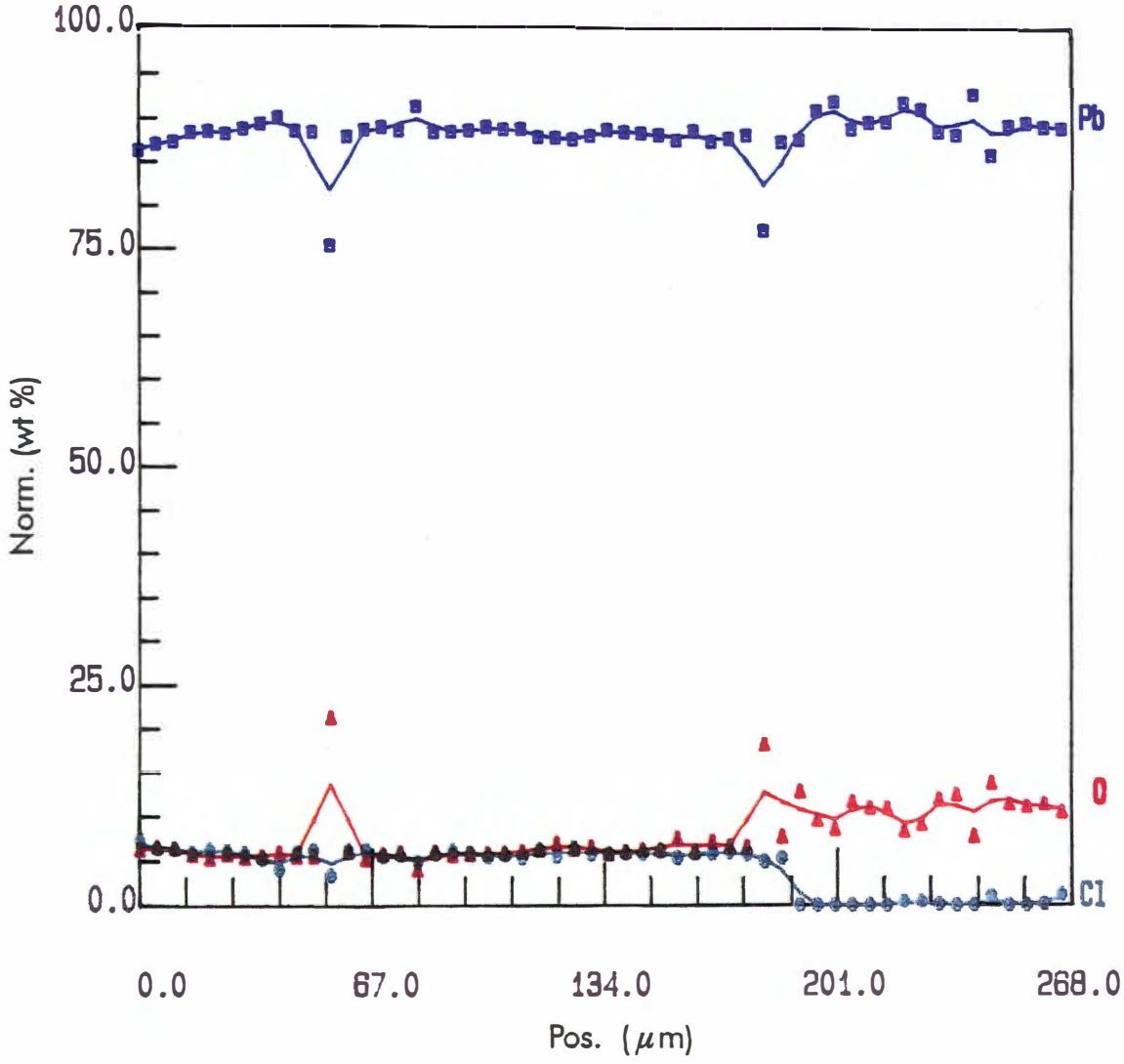

Figure 4.6.17. $PbCl_2$ and chlorine elemental concentration profiles, determined by wavelength dispersive x-ray fluorescence of polished sample, Run 284, T = 674°C, 20 min, 2000 ppm HCl.

bottom surface of the particle rather than at an axial cross section. Both figures are notable for the uniformity of the concentrations of all elements to the point where the chlorine concentration falls to zero. The scatter in the lead and oxygen data observed may be due to surface roughness of the sample, which increases the absorption of x-radiation. Figure 4.6.18 is a schematic of the qualitative predictions of the model. Data are unavailable on the chemical speciation in the ash layer; only the elemental analysis can be obtained. There should be a slight drop in the $PbCl_2$ concentration at the surface of the particle where it is volatilizing and diffusing away.

In a further effort to understand better the nature of the ash layer generated at temperatures in Regime 4, x-ray diffraction patterns were made on pellets from Runs 179 and 206, both generated at about 670°C for 72 and 60 min, respectively, and 2000 ppm HCl. One difficulty was that the entire pellet was ground to a powder and the ash layer of greatest interest then composed a relatively small fraction of the total sample mass. The patterns are shown in Figures D.1 and D.2 in Appendix D. They are fairly reproducible and indicate the possible presence of lead oxychloride species but without a definite match. The figures are placed in Appendix D since it is believed that more recent patterns have superseded them. Patterns of unreacted PbO samples were produced to confirm the existence of PbO, and the

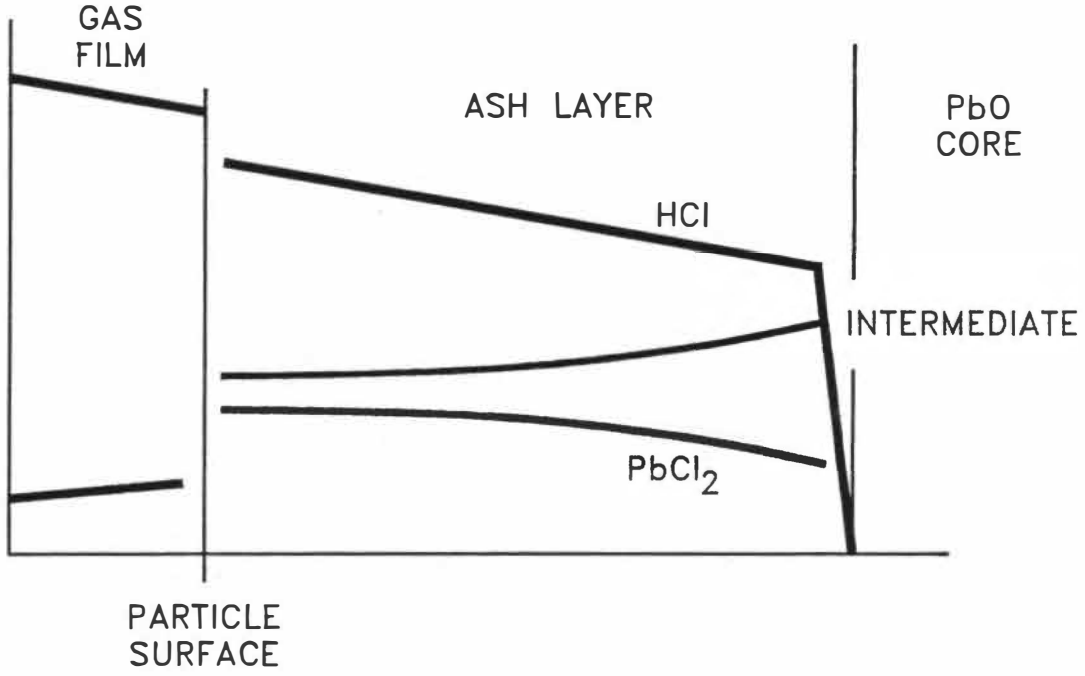

Figure 4.6.18. Schematic of approximate concentration profiles of HCl and $PbCl_2$, Regime 4.

metastable massicot crystalline form was identified, as shown in Figure 4.6.19. The massicot and litharge forms of PbO, orthorhombic and tetragonal, respectively, are readily intraconvertible and difficult to prepare in pure form. A pattern was also prepared of a sample from Run 174, reacted at 670°C, from which the lead chloride had been volatilized. It matched PbO as nearly as could be determined but with one unidentified peak, as seen in Figure 4.6.20. A pattern was made of Run 229, reacted for 90 min at 550°C, but the sample appeared to be poorly crystallized. This particular sample did appear to have been quite fused when it was quenched to room temperature. The standard patterns used to identify compounds are all from the International Center for Diffraction Data database.

A novel x-ray diffraction instrument capable of examining an unpowdered sample was used with interesting results on samples from Run 305, generated at 325°C; Run 311, at 588°C; and Run 316, at 623°C (Figures 4.6.21, 4.6.22, and 4.6.23 respectively). This instrument, the Rigaku RU200H microdiffractometer, uses a rotating anode to dissipate heat generated when the x-ray beam is formed and permits the use of higher-intensity x-rays. It can examine a sample area in the range of microns, through the use of a fiber-optic wave guide, unlike most diffractometers, which require larger samples. The sample is also rotated so as to reduce preferred crystalline orientations. This is partially

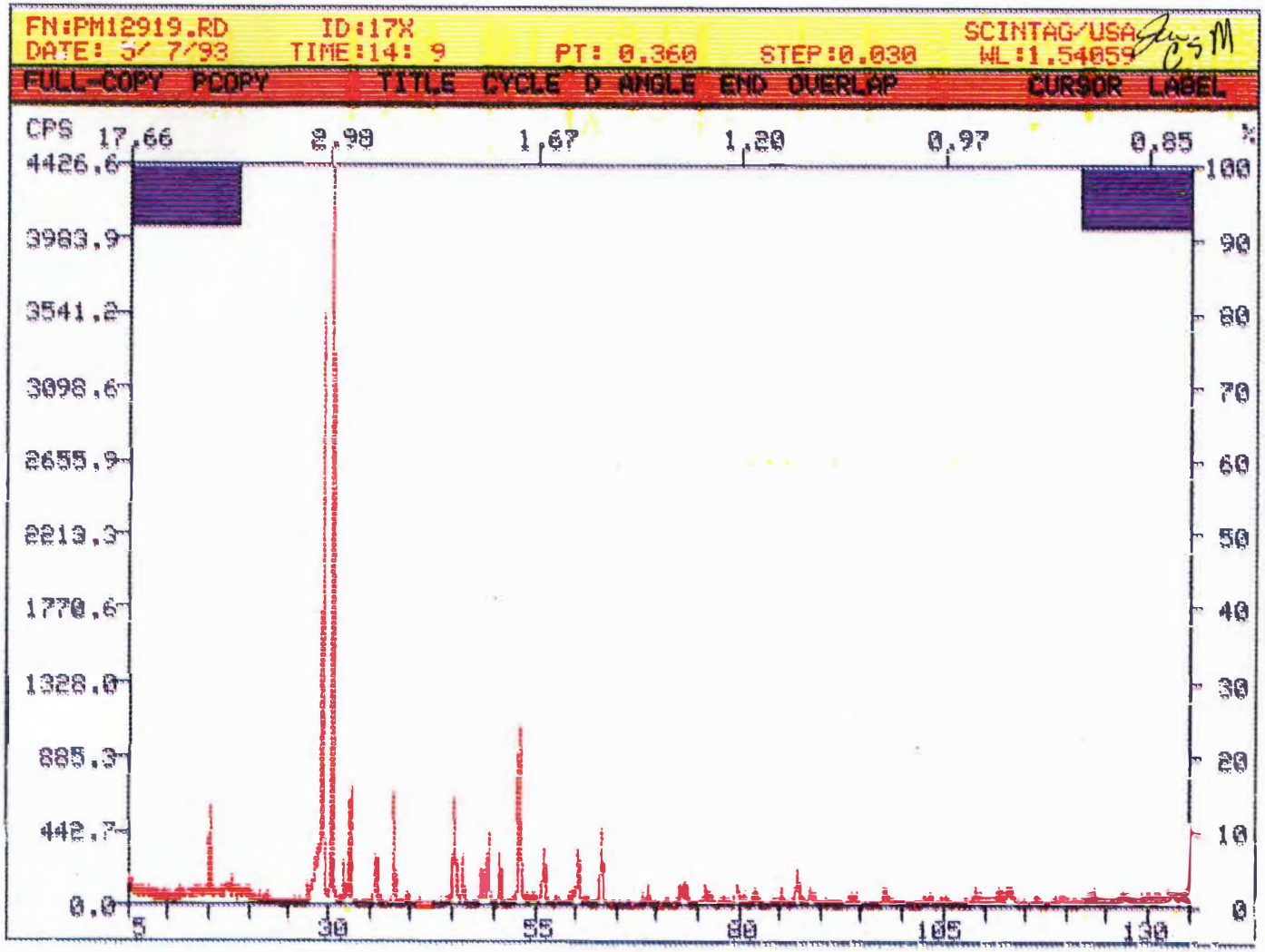

Figure 4.6.19. Powder x-ray diffraction pattern of PbO pellet, heat 17x, unreacted.

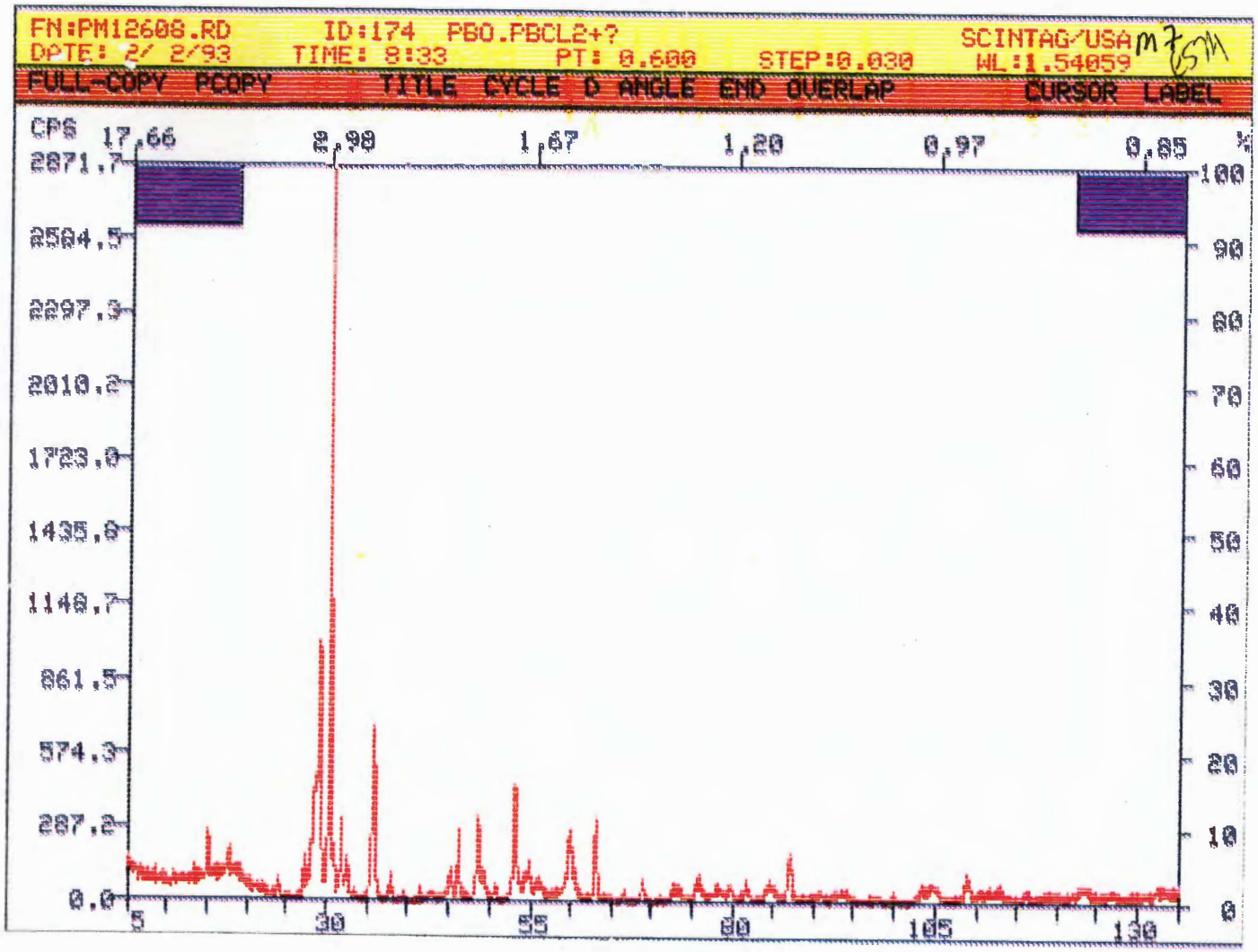

Figure 4.6.20. Powder x-ray diffraction pattern of pellet from Run 174, in which $PbCl_2$ was volatilized following run.

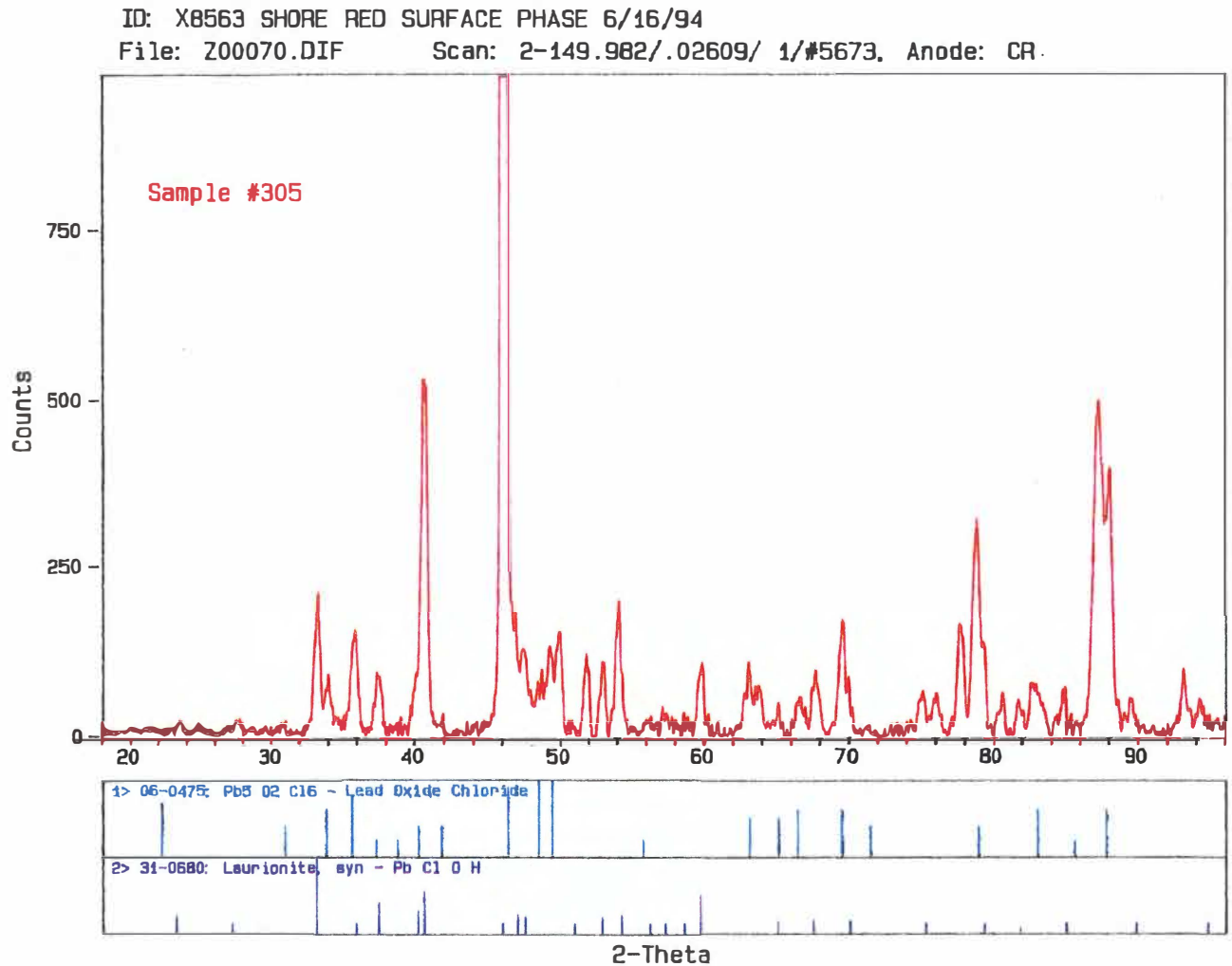

Figure 4.6.21. Powder x-ray microdiffraction pattern of pellet from Run 305, prepared at 325°C, 72 min, 4000 ppm HCl, grey layer, indicating presence of Laurionite.

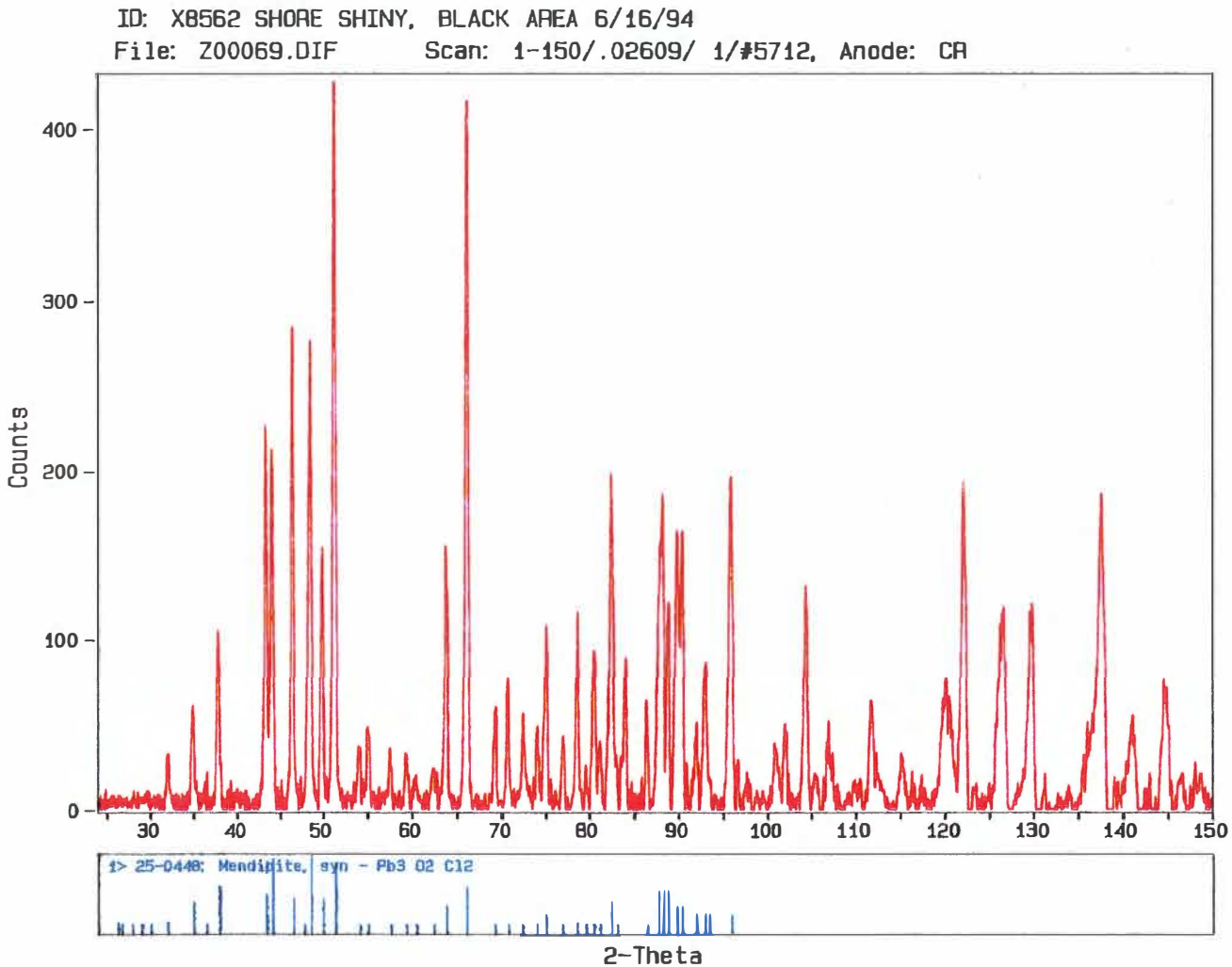

Figure 4.6.22. Powder x-ray microdiffraction pattern of pellet from Run 311, prepared at 588°C, 14 min, 2000 ppm HCl, grey layer, indicating presence of Mendipite.

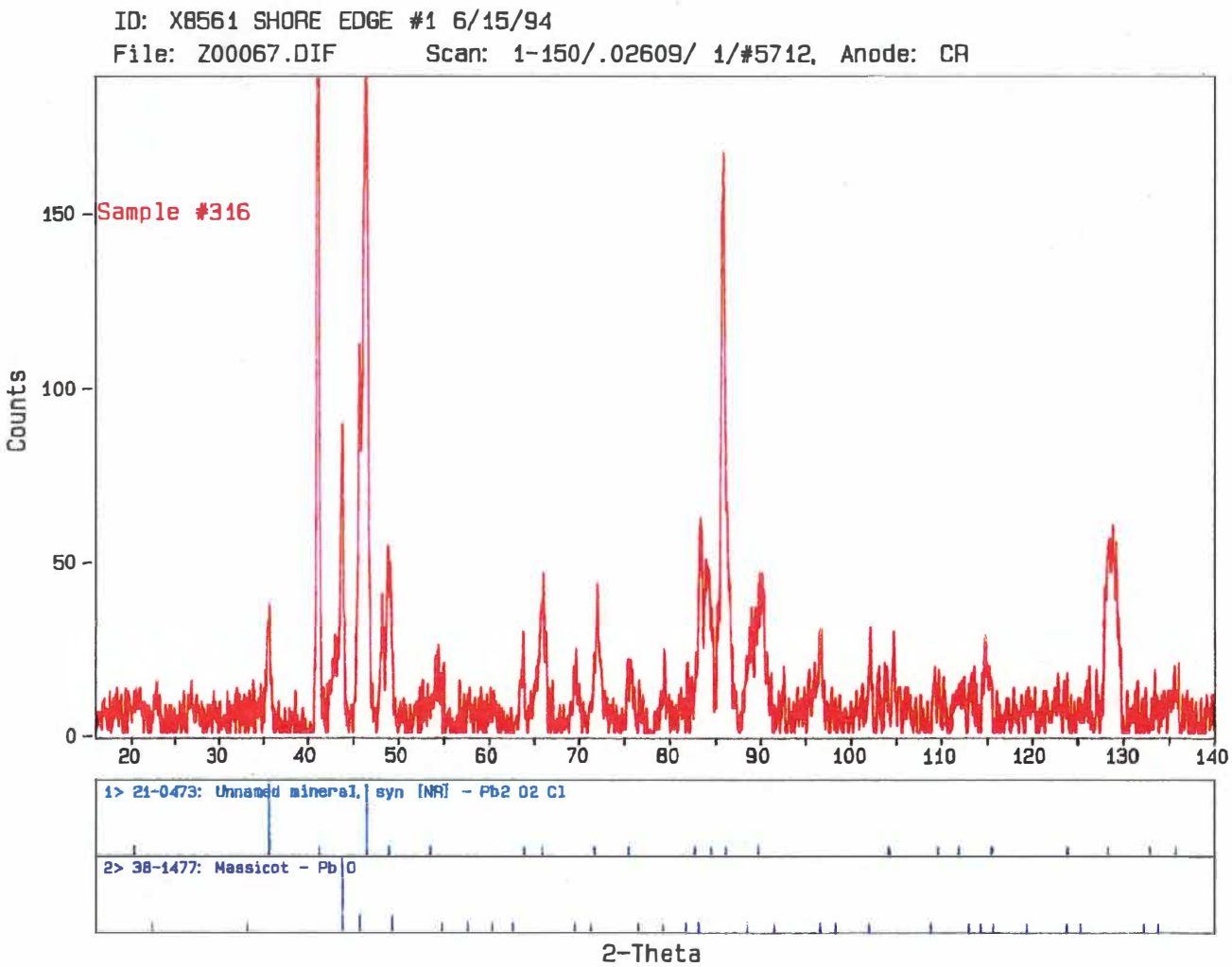

Figure 4.6.23. Powder x-ray microdiffraction pattern of pellet from Run 316, prepared at 623°C, 36 min, 2000 ppm HCl, indicating presence of Pb_2O_2Cl (unnamed compound).

successful; the relative intensities of lines from the experimental samples and the standards differ somewhat. Background or baseline radiation was within normal ranges. Chromium K alpha x-radiation was used. Run 305, whose results were the least reliable and which produced the weakest lines, indicated predominantly the presence of $2PbO{\cdot}Pb_3Cl_6$ or $Pb_5O_5Cl_6$ (which will be labeled T1). This was the underlying grey layer, with the white surface layer scraped away, and it was long suspected to have been an lead oxychloride or hydroxychloride. Another phase appeared to be present but was unidentified. FTIR spectroscopy was also performed on this sample. The spectrum is shown in Figure 4.6.24. At 3500 wave numbers is an indication of an OH stretch, and the presence of a hydroxychloride would be a reasonable hypothesis.

As seen in Figure 4.6.23, the x-ray pattern from Run 316, prepared at 623°C, suggests the presence of Pb_2O_2Cl (T4), with an excellent match of lattice parameters of a tetragonal cell: a=3.8978A and c=13.05A, compared with 3.91A and 13.00A for the standard pattern. A second crystal, $Pb_7O_6Cl_2$ (T5), was also tentatively identified. Variations in the stoichiometry were believed to be present because lines in the standard and the experimental patterns were shifted. The pattern from Run 311 was quite good and revealed only the phase $Pb_3O_2Cl_2$(T2).

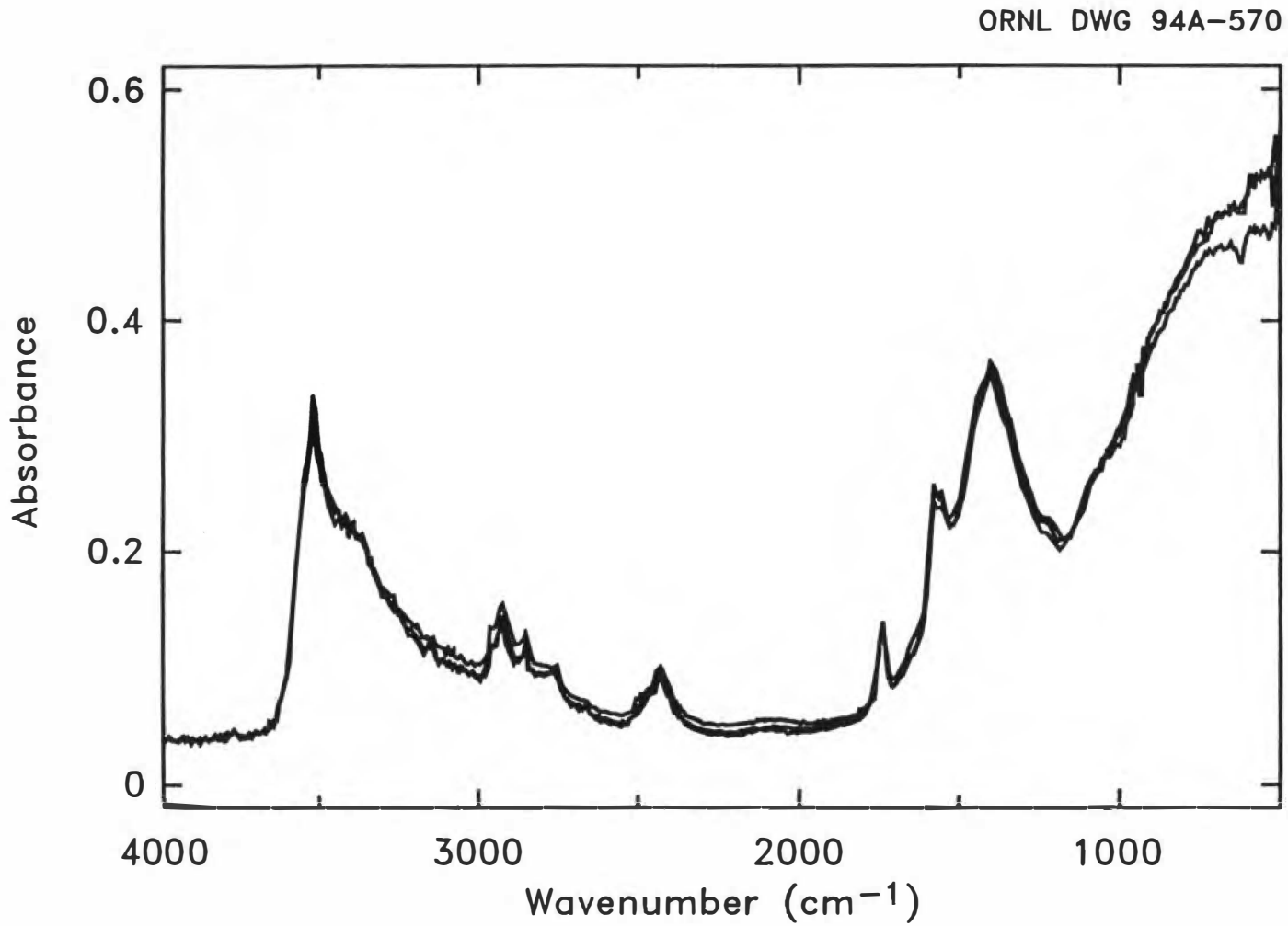

Figure 4.6.24. FTIR spectrum of pellet from Run 305, prepared at 325°C, 52 min, 4000 ppm HCl, indicating presence of OH stretch band.

The most modern phase diagram (Podsiadlo, 1991) indicates the formation of T1 and T2; however, neither T5 nor T4 was found in our studies. T5 was more poorly characterized in the x-ray diffraction pattern database. Another phase Pb_2OCl_2, T3, was identified on the phase diagram but was not found by x-ray diffraction. The phase diagram is shown in Figure 4.6.25 and can be compared with the earlier work of Renaud, shown in Figure 4.5.5. There is no equilibrium explanation of the formation of the distinctly different phases of ash between 580 and 630°C. To be sure, the phases T4 and T5, though mentioned in the literature, are not found on any of the available phase diagrams dating to 1900 (Ruer). According to the phase diagram, T3, also known as Mendipite, decomposes at 525°C. We find that T3 is the predominant phase in samples quenched from 550 to 590°C. Of course, at temperature, we do not know the crystalline composition of any of our samples, even those in which no liquid phase seems to have formed. The morphology could easily alter during quenching. The formation of T3 in the Run 311 sample prepared at 583°C is consistent with indications that the ash from this sample is richer in $PbCl_2$ than that from Run 316.

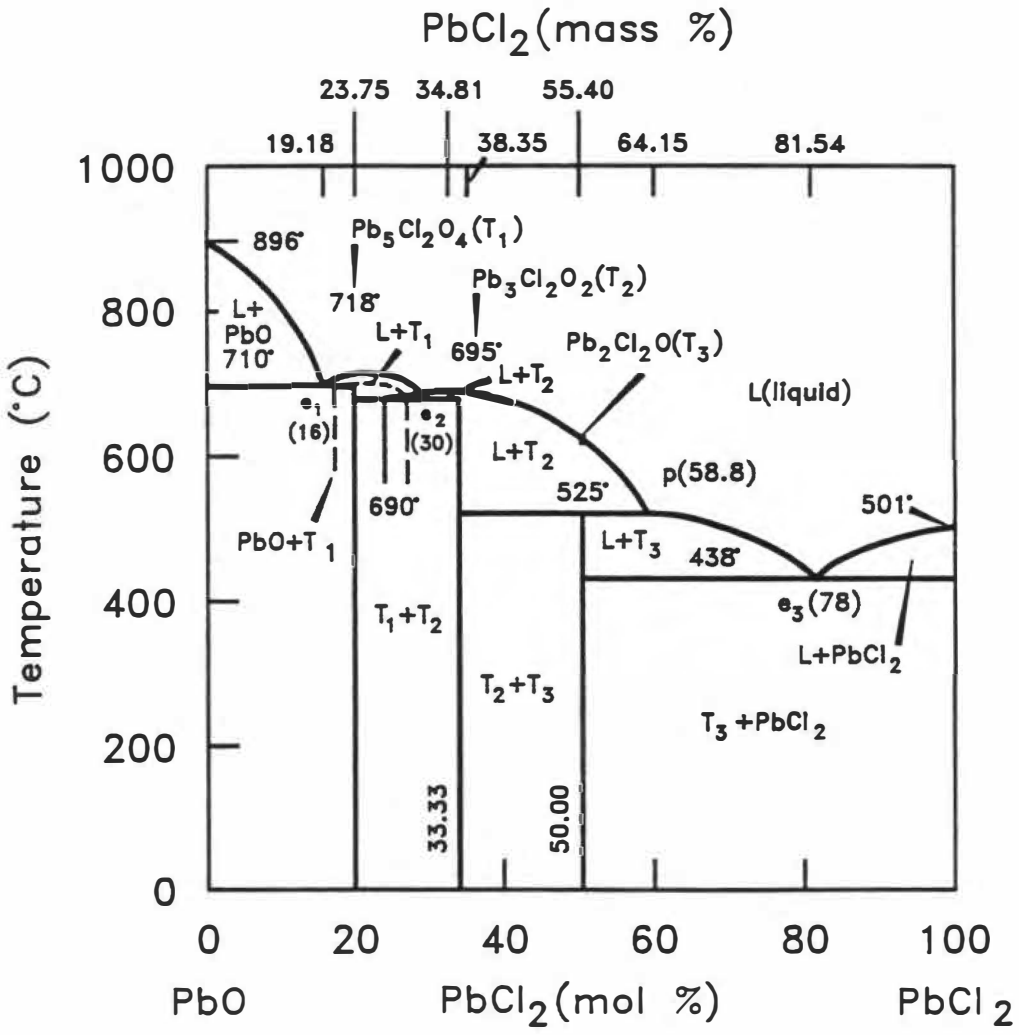

Figure 4.6.25. Recent phase diagram of system PbO-$PbCl_2$ (Podsiadlo, H., *J. Thermal Anal.*, *37*, 1991).

4.6.3 Descriptive Model, Regime 4

As in Regime 3, we apply a shrinking core, moving boundary value model with the formation of a reaction intermediate I2, which is different from the intermediate I1 formed at lower temperature. The model is applied to results at 2000 and 4000 ppm of HCl. Assumptions are as follows. (1) Diffusion of HCl proceeds somewhat more slowly than in Regime 3 because of the formation of a glassy, more viscous ash. (2) HCl reacts homogeneously in the ash layer with the intermediate I2 to form $PbCl_2$. (3) This reaction with I2 is much slower than in Regime 3. (4) No diffusion of I2 occurs because of its comparative massiveness. (5) As in Regime 3, the shrinkage or expansion of the particles is negligible in this regime. (6) Unlike the process observed in Regime 3, diffusion of $PbCl_2$, once formed, is rapid and similar to liquid phase diffusion. We have the following reaction equations:

$$HCl + 2PbO \longrightarrow Pb_2O_2HCl \quad (I2) \qquad (4.6.1)$$

which proceeds very rapidly at the moving boundary and

$$3HCl + I2 \longrightarrow 2PbCl_2 + 2H_2O \qquad (4.6.2)$$

which proceeds homogeneously in the ash layer where intermediate has formed.

We model these reactions and the associated mass transfer with the following three coupled partial differential equations:

$$D_c \partial^2 C/\partial x^2 = \partial C/\partial t + k_2 C I_2 n_c \qquad (4.6.3)$$

$$D_{PbCl_2} \partial^2 [PbCl_2]/\partial x^2 = \partial [PbCl_2]/\partial t - k_2 C I_2 n_{PbCl_2} \qquad (4.6.4)$$

$$\partial I_2/\partial t = -k_2 C I_2 n_{i2} \qquad (4.6.5)$$

The following boundary conditions are applied to the partial differential equation Eq. (4.6.3):

$$D_c \partial C/\partial x|_{x=s} = C dS/dt \qquad (4.6.6)$$

$$N_c|_{x=0} = -D_c \partial C/\partial x|_{x=0} \qquad (4.6.7)$$

$$C|_{t=0} = 0 \qquad (4.6.8)$$

The boundary conditions

$$N_{PbCl2} = [PbCl_2] K_H \gamma_{PbCl_2} \qquad at\ -0 \qquad (4.6.9)$$

$$[PbCl_2] = 0 \quad x > s \qquad (4.6.10)$$

are applied to the partial differential Eq. (4.6.4). Applied to Eq. (4.6.5) are the following boundary conditions

$$I_2 = I_{20} \ at\ x = s \qquad (4.6.12)$$

$$[PbCl_2] = 0 \quad t = 0 \qquad (4.6.11)$$

$$I_2 = 0 \ at\ x > s \qquad (4.6.13)$$

$$I_2 = 0 \ at\ t = 0 \qquad (4.6.14)$$

where I_{2o} is the initial I2 concentration.

A Fortran computer code was written to solve these moving boundary value problems. The most difficult problem from both an algorithmic and stability standpoint is the incorporation of the one moving boundary condition. Actually, there are probably two moving boundaries since the particle surface and the ash phase boundary both move. However, the movement of the particle surface was much less

significant than the progression of the ash layer into the particle in this regime. This effect was neglected in this model.

At first, a technique known as the front tracking method was attempted (Crank, 1984). This is a finite difference technique in which the first and second derivatives of the function, in this case HCl concentration, are evaluated using Lagrangian interpolation formulae at the two grid points nearest the boundary, while the value of HCl concentration at the boundary is by definition zero. The velocity of the boundary, and therefore its progression in distance at each increment in time, can be calculated using Eq. 4.6.6. The position of the boundary will not usually fall on a grid point and should in fact be smaller than one grid spacing. When a new space grid point is reached, the interpolation begins anew, advancing the grid one space. If the velocity is so great that the progress of the boundary is greater than one grid spacing during one time increment, the time increment is reduced. This technique, of course, requires the calculation of very steep derivatives, and although a code incorporating the technique was written, serious stability problems were encountered. Reduction of the time increment and double-precision arithmetic improved the stability slightly, but the range of conditions in which the code would converge was in practice extremely limited.

A second technique, one of a class of "front finding" techniques, was next attempted. In the front finding technique, the particular algorithm used was known as the enthalpy method. This concept was first noted in connection with heat transfer to melting solids, hence the connection with enthalpy. It is perfectly adaptable to reaction kinetic problems. The analogy can be easily understood from a short description.

The grid may now be considered as divided into finite elements. In the boundary element, also known as the "mushy region," during each iteration in time, the quantity of material (in our case, HCl or in the case of heat transfer, enthalpy) flowing into the element is calculated based on the boundary condition equation:

$$-D_c(C_{r,1}-C_r)A-V(C_{t,\delta t}-C_t)/\delta t \qquad (4.6.15)$$

where A is the area of the element and V is its volume. Once the quantity of material has reached a given level, dependent here on the molar density of the ash and its mole fraction of chlorine, the "mushy element" becomes another element in the reacted ash layer, the boundary is advanced one element, and the procedure is repeated. This is analogous to the melting of a solid. In the elements behind the boundary, the reaction of the intermediate and the diffusion of HCl are viewed as proceeding homogeneously. No

diffusion or reaction occurs in elements beyond the boundary element. First- and second-order classic explicit finite difference approximations were used to evaluate first and second derivatives:

$$\partial c/\partial t \approx C_{r+1}-C_r/\delta t \qquad (4.6.16)$$

$$\partial^2 C/\partial x^2 \approx (C_{r+1}-2C_r+C_{r-1})/\delta r^2 \qquad (4.6.17)$$

A listing of the code is given in the Appendix C1. It has the advantage of great stability, provided that the time increment is sufficiently small. A flow diagram is shown in Appendix E, Figure E1.

A plot of the results of the model predictions of sample weight change is shown as a smooth curve in Figure 4.6.26 and compared with the data from Run 245, whose concentration profile was characterized by x-ray fluorescence in Figure 4.6.16. The numerical output of the code is shown in Appendix C2. During the first 30 min, the rate of intermediate (I2) formation predominates, the ash layer thickens, and little intermediate is converted to $PbCl_2$. The conversion of I2 to $PbCl_2$ is modeled as occurring homogeneously in the ash layer behind the boundary. As the ash layer thickens, its rate of growth slows because of the

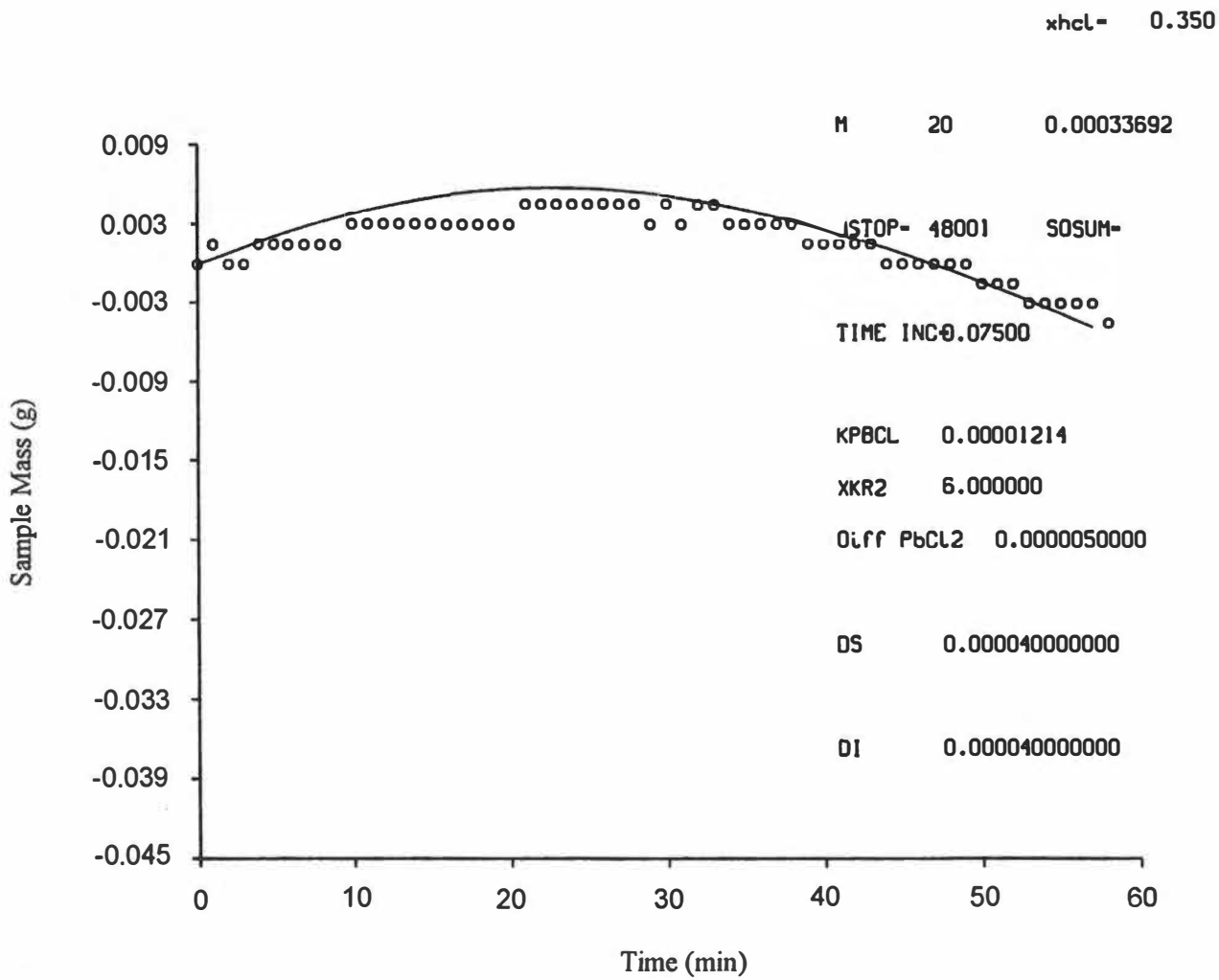

Figure 4.6.26. Thermogram of Run 245, reacted at 670°C with 2000 ppm HCl. Circles represent experimental data; the solid line represents moving boundary model.

greater diffusion distance (similar to the slowing advancement of a thickening ice cap). At a time of approximately 30 min, which varies slightly with the porosity of the particle, the mass rate of volatilization of the $PbCl_2$ formed from the intermediate equals the mass rate of I2 formation. The curve shows a broad, flat peak while this is occurring. The total HCl reaction rate is believed to fall following the plateau period, based on evidence of the declining global reaction rate of samples prepared for increasing time periods as seen in Table 4.6.3. The weight loss curve is generally greater in slope than the weight gain curve observed during the first 20 min of reaction. Figure 4.6.27 is a plot of the model predictions of concentrations of HCl and $PbCl_2$ versus distance from the particle surface with time as a parameter. The advancing curves are depicted at 5-min intervals from 1 to 20 min. Note that as time advances the progress of the front slows. The velocity of the advancing intermediate ash layer is approximately 10 μm/min during the first 20 min of reaction at 2000 ppm of HCl.

Figure 4.6.28 displays the results of the application of the same model to Run 208 generated at 630°C and 2000 ppm HCl. Figures 4.6.29 and 4.6.30 display the results of the model applied to Runs 295 and 259 generated at 630°C and 670°C, respectively, and 4000 ppm HCl. The weight loss increases with increasing time, during which time

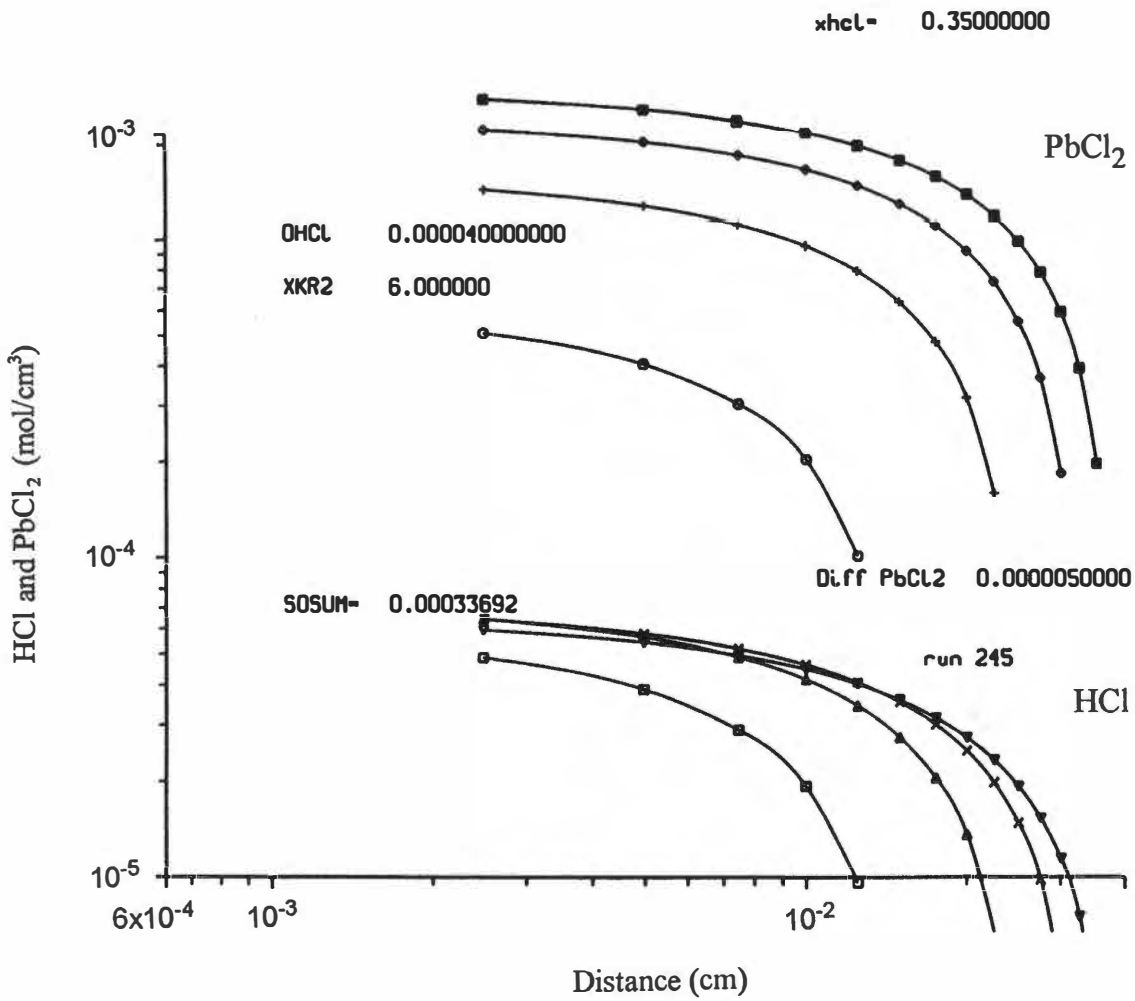

Figure 4.6.27. Concentrations of $PbCl_2$ and HCl versus distance from particle surface, model predictions of Run 245, reacted at 670°C with 2000 ppm HCl. Time is a parameter, each curve within a set representing time advancing by 15 min.

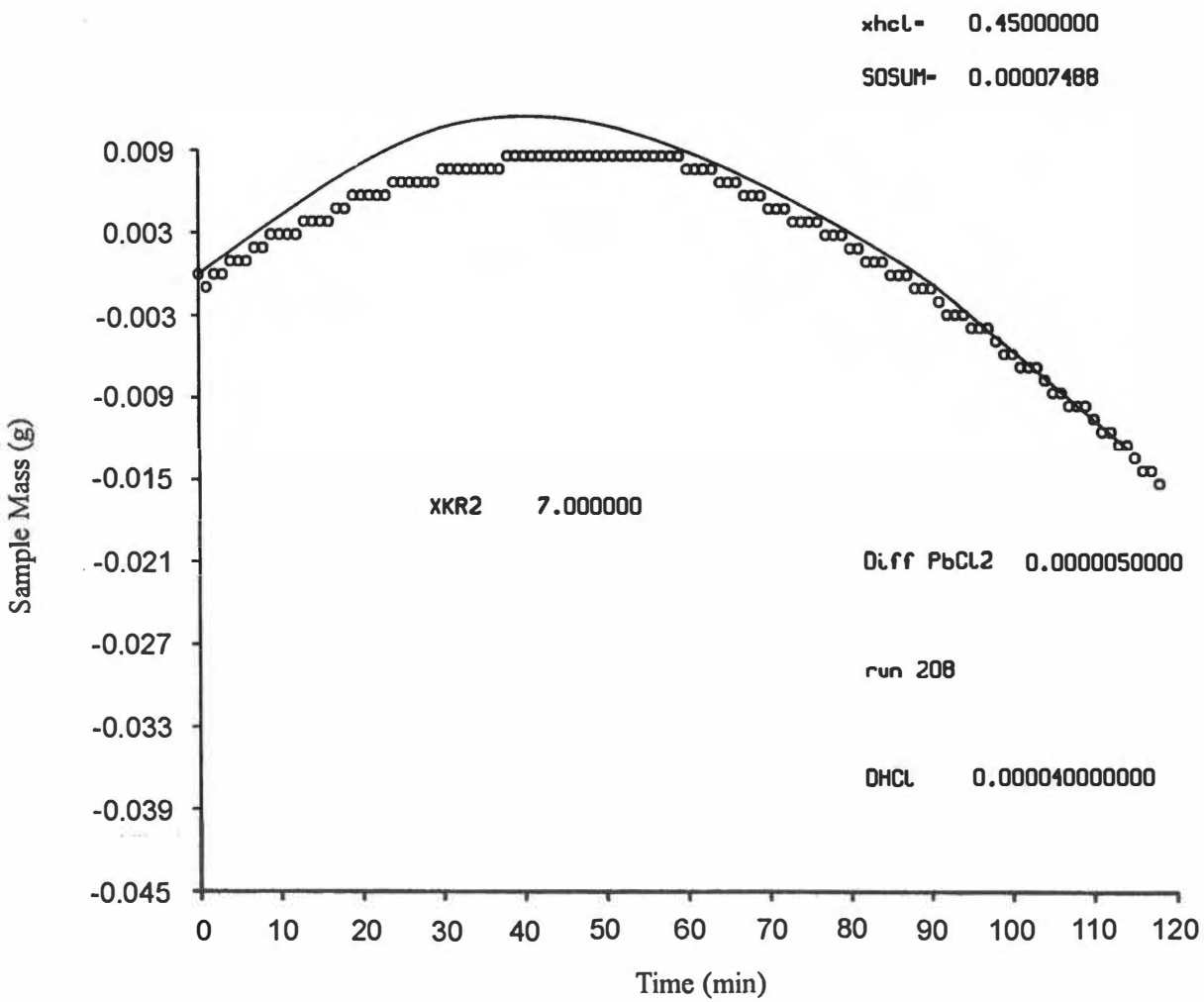

Figure 4.6.28. Thermogram of Run 208, reacted at 630°C with 2000 ppm HCl. Circles represent experimental data; the solid line represents moving boundary model.

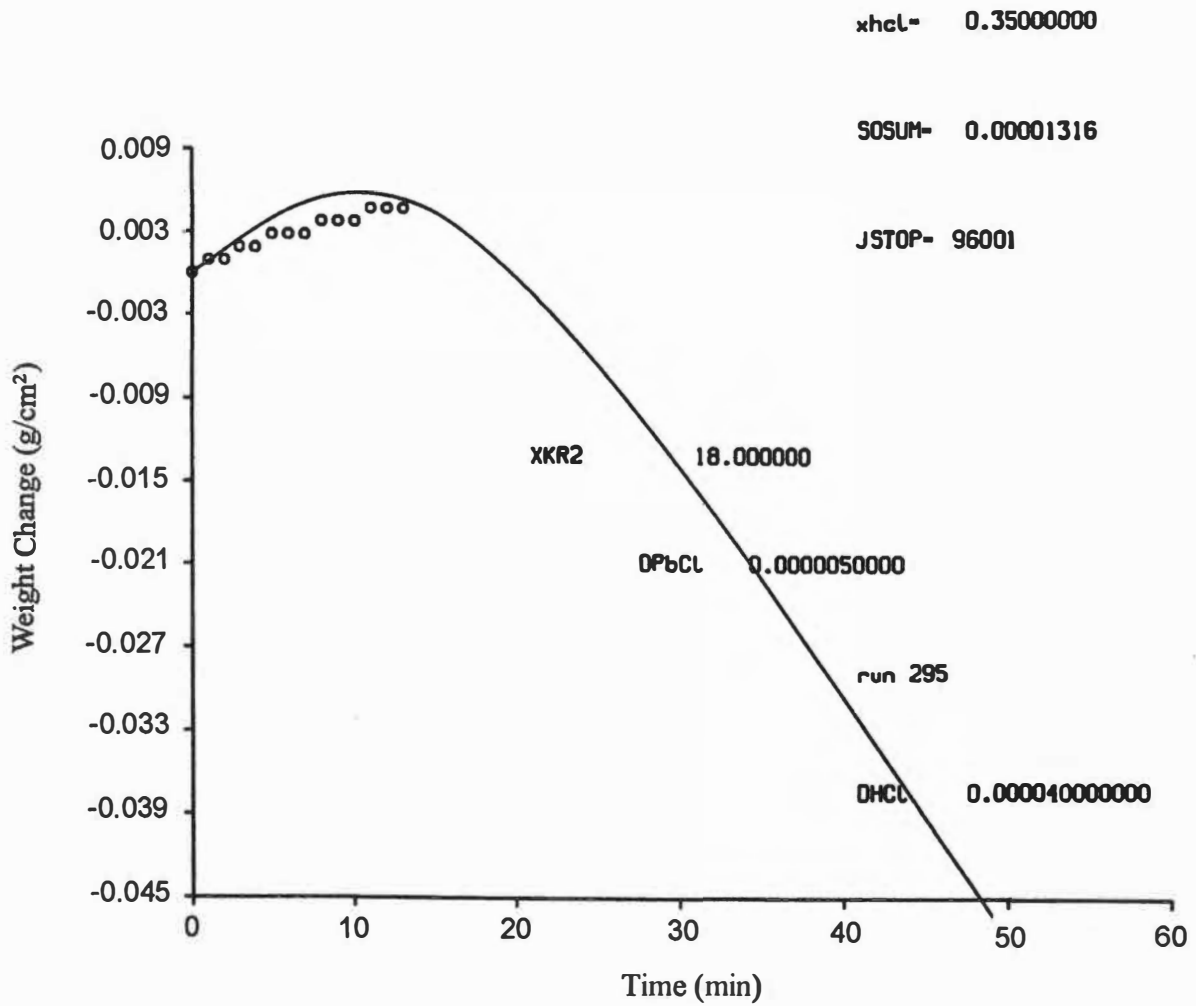

Figure 4.6.29. Thermogram of Run 295, reacted at 630°C with 4000 ppm HCl. Circles represent experimental data; the solid line represents moving boundary model.

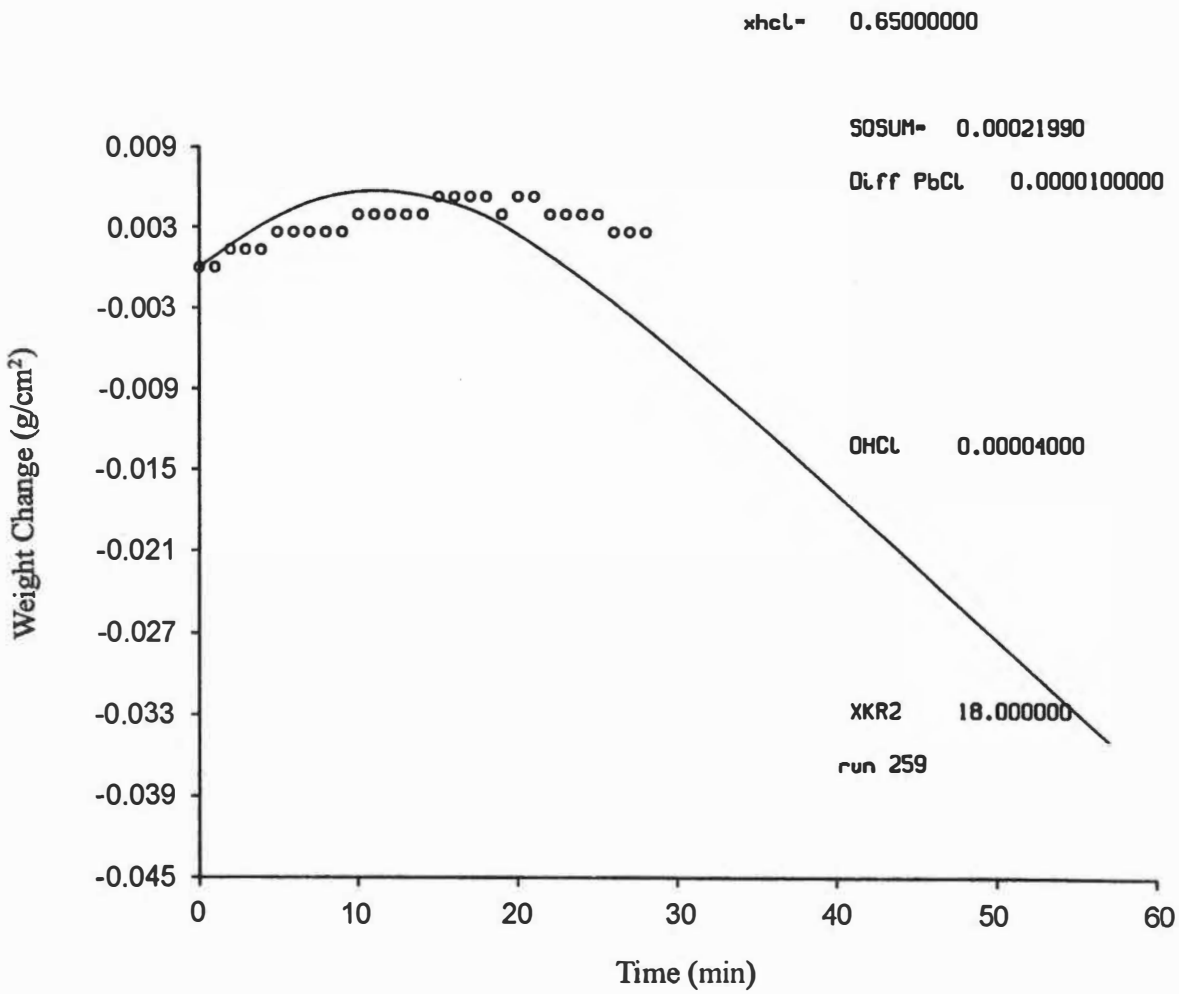

Figure 4.6.30. Thermogram of Run 259, reacted at 670°C with 4000 ppm HCl. Circles represent experimental data; the solid line represents moving boundary model.

the pellets display an increasingly fused appearance. Figure 4.6.10 showing a cross section of Run 284, suggests that the ash layer is still increasing in thickness during this time. Evidently the activity of $PbCl_2$ at the surface of the particle is fairly constant during the weight loss period. The particle diameter does not change appreciably during this period, and the mass transfer coefficient to the gas phase remains fairly constant.

In another view of the model results in this regime, the progress of the moving boundary between ash and unreacted core can be experimentally determined by cross-sectioning pellets reacted for different times at the same temperature. According to this model the distance that the ash layer has grown should be approximately proportional to the square root of the time, and such a fit of the data was made with the model predictions, shown in Figure 4.6.31.

In summary, Regime 4 is characterized by a now rapidly advancing and distinct boundary between the PbO core and a lead oxychloride intermediate but of a different chemical composition than that observed in Regime 3. During the first 30 min of reaction, the boundary advances at an average rate of approximately 10 μm/min and slows with respect to time as expected from the model of a moving boundary value problem. Hydrochloridation rates are initially rapid, approaching 1E-7 mol/($cm^2 \cdot s$) at 2000 ppm HCl, and then fall rapidly because of surface saturation

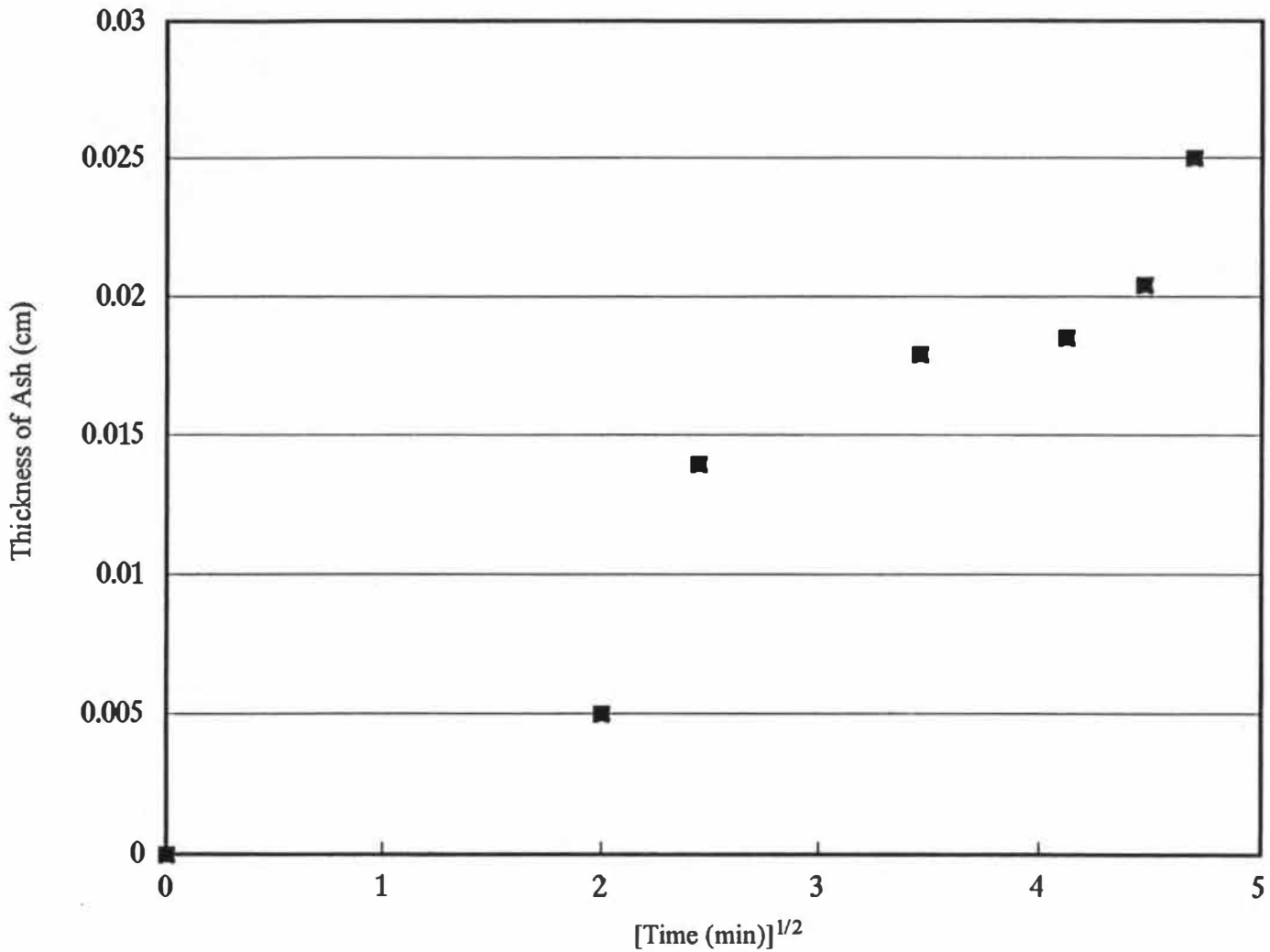

Figure 4.6.31. Thickness of ash layer versus time$^{1/2}$ at different times at 670°C, experimental data.

with HCl. During a period of about 30 min at 630°C, the volatility of the chloride-containing ash is very low and little fume is formed. At higher temperatures (e.g., 670°C), higher HCl concentrations, or lengthening reaction times, the reaction of hydrogen chloride and the ash to produce $PbCl_2$ begins to again dominate as in Regime 3.

4.7. GENERAL OBSERVATIONS ON ALL REGIMES

Three models were applied to describe experimental data based on solutions to partial differential equations: two involving moving boundaries at temperatures from 550 to 690°C and one involving progressive conversion and fixed boundary values at temperatures below 300°C. These three models are all based on basic solutions using finite difference techniques of simultaneous partial differential equations of unsteady state diffusion with chemical reaction. A less fundamental fourth model, based on an empirical equation and a concept of pore plugging, was also tested. The parameters that were developed in applying these models to the experimental data from representative runs are shown in Table 4.7.1. The vapor pressure and activity coefficients of lead dichloride in a lead oxide/chloride melt were adjusted only to reflect changes in the vapor pressure occurring as a result of temperature.

Table 4.7.1. Values of parameters developed from computer models

Run	K_r $(mol/cm^3)^{-1}s^{-1}$	Hk (mol/cc)	D_{HCl} (cm^2/s)	Temp (°C)	HCl (ppm)	Sq Sum Error) $(g/cm^3)^2$	Dpb cm^2/s
			Moving boundary model				
208	7.0	0.45	4E-5	630	2000	7.0E-5	1E-5
245	6.0	0.35	4E-5	670	2000	3.E-4	5E-6
228	500	0.20	2E-4	550	2000	3.E-6	6E-5
310	500	0.20	2E-4	580	2000	1.0E-3	6E-5
259	18.0	0.65	4E-5	670	4000	2.E-4	1E-5
295	18.0	0.35	4E-5	630	4000	1.e-5	1E-5
			Progressive conversion model				
300	0.01	NA*	5E-9	300	2000	4E-4	0.0
			Lee's model				
	R_{po}	Temp	t_p	Sum Sq			
	$(mol/(s \cdot cm^2)$	(°C)	(min)	$(g/cm^{2)2}$			
326	0.0012	260	18	1.3E-6			
328	0.004	280	9.0	5.4E-6			

*Not applicable.

It is interesting to note, though not wholly unexpected, that the least fundamental model, the Lee and Georgakis model, can be adjusted to make the best data fit. It also involves only two parameters.

A progressive conversion model was applied to the low-temperature regime since no distinct phase boundary was observed in pellets from this regime. The results from the progressive conversion model are similar to those of the Lee and Georgakis model since the former also produced a large slowing in the reaction rate after a surface element of ash had formed. Diffusion through this layer was slow and did not permit much additional reaction. The Lee and Georgakis model produced the same effect through pore plugging. An HCl diffusivity characteristic of the solid state, 5E-9 cm^2/s was applied to the progressive conversion model. A small reaction rate was generated in fitting the data, 0.0003 $(mol/cm^3)^{-1}s^{-1}$. The model is sensitive to the assumed surface concentration of Hcl, assumed to be 0.02 moles/cc. The weight gain slows with respect to increasing time.

As noted in Table 4.7.1, adjustments were made in the parameters k_r and H_k in Runs 208, 245, 228, and 310. These adjustments are based on several observations: as noted in Sects. 4.5 and 4.6, the physical appearances of the reacting pellets and the thermograms were greatly different in Regimes 3 and 4. The models assume that two different chemical reactions involving two different intermediate

compounds, I1 and I2, are occurring and that there is a distinct difference in their respective reaction rates. Evidence from the quenched compounds exists to support this hypothesis. Although the forms of the rate equations are similar, both being pseudo first-order reactions, the reaction rates are quite different, 500 versus approximately 14 $(mol/cm)^{-1}$ s^{-1}. The models are sensitive to reaction rate in Regimes 3 and 4 in accord with the hypothesis of the formation of intermediates at different rates. The diffusivity of HCl in the condensed phase is believed to be in the range of liquid diffusivities, perhaps a bit lower at the higher temperatures, since the ash appears to be less liquid at those conditions and less volatile, as noted. The Henry's law constants were heuristically chosen parameters. The physical reasoning is that these values are smaller at the lower temperature range since at these temperatures the surface of the particles consists of a greater concentration of $PbCl_2$ and is therefore less chemisorptive toward HCl than the higher-temperature ash in Regime 4, which is lower in $PbCl_2$ concentration. This hypothesis is consistent with the results from electron microscopy.

The reasons that an ash of distinctly different character forms at a temperature around 600°C are not clear. The ash appears to form rapidly within a limited range of temperatures. This suggests that it is a chemical kinetic phenomenon since chemical reaction rates usually vary

exponentially with temperature while many diffusive phenomena vary with the first or second power of temperature. The second intermediate permits the diffusion of HCl more deeply into the particle, while the first intermediate reacts rapidly with HCl to completion to produce volatile lead dichloride before diffusion can progress to any great distance in the particle. The intermediate I2 may have brought a greater disorder to the lattice, as can occur with certain moving boundary value problems. (Hartley, 1946).

The model at 670°C, Regime 4, also will yield a boundary that has progressed approximately 240 μm within the particle, a distance close to the experimentally determined value of 270 μm. The rates of HCl diffusion into the pellet (labeled XHCl in the printout) are listed in Appendix C2 alongside the rate of diffusion to the pellet surface from the gas (labeled NHCl). It will be noted that initially the two rates are approximately equal and that the rate of gas phase diffusion to the pellet rapidly begins to fall as HCl accumulates at the surface of the particle. The rate of $PbCl_2$ volatilization (labeled XPBCL) gradually rises, producing the plateau region of the many thermograms shown when volatilization of $PbCl_2$ and diffusion of HCl are in a mass balance, and then producing the declining mass curve as XPBCL exceeds XHCl on a mass basis.

Runs 259 and 295 at 4000 ppm HCl required again slight variations in the parameters in order to improve the fit. In particular, in Run 259, the surface of the pellet rapidly became liquified and, after 30 min, quite subject to convection currents, which the model did not take into account. A higher diffusivity of HCl, ~1 × 10^{-4} cm^2/s was applied since the surface appeared to resemble that of Regime 3. A slightly higher reaction rate constant ~18 $(mol/cm^3)^{-1}$ s^{-1}) was applied heuristically in these instances. The reaction may not be linear in HCl concentration as postulated, and the adjustment in reaction is approximately in the range of the increase in HCl concentration.

The results from Run 259 were applied to a finer grid spacing: 40 and 60 elements, as opposed to 20 in most other runs, without a significant change in the sum of the squares of difference between the model prediction and the experimental data. Computer time, however, became very expensive for this expanded grid. Runs 228 and 310 used only 4 to 8 mesh elements, partly in an attempt to conserve computer time, since the elements were much smaller in accordance with the thin, 20 to 40- μm-thick ash layer observed in micrographs of cross-sectioned pellets from this regime. A few computer experiments were conducted in which a large number of elements were applied to Run 228, partly to determine if a fine grid would produce a $PbCl_2$ gradient declining in the direction of the ash surface, as would

occur with volatilization from the surface. Such a gradient was indeed found, which helps validate the code, but the expense in computer time was enormous. The model predictions of the ash depth in Run 228 are somewhat smaller than the actual ash depths, however, and because of convergence problems of the system of nonlinear equations, it was difficult to adjust the parameters to make a much better fit. This discrepancy may arise from convection currents in the liquid ash that result in more rapid mass transfer than predicted on the basis of the molecular liquid phase diffusion coefficient. Runs 228 and 310 are sensitive to the mesh size because the first element in the moving boundary requires a certain time to fill with Hcl, and until that time, $PbCl_2$ is not produced; consequently, the model can indicate a small plateau initially. This plateau could also have been seen in the experimentation if the balance were more sensitive. (Occasionally it was seen.) The fluxes of HCl to the interior of the pellet (XHCL) in the modeled Run 228 are shown in Appendix B2. Unlike in Run 245, shown in Appendix C2, we see that in run 228 the flux of HCl diminishes rapidly reaching a steady state after about 12 min and remains at that rate. Initially the flux is gas phase controlled but quickly shifts to solid phase control as the surface concentration of HCl rises. The flux of $PbCl_2$ (XPBCL) follows a similar trend rising to a steady state that persists during the course of the reaction.

4.8 CONCLUSIONS

Data have been collected on hydrochloridation rates of PbO sintered pellets at simulated hazardous waste incinerator conditions of 2000 and 4000 ppm HCl at temperatures between 260 and 690°C. The data reveal important changes in the mechanisms of lead dichloride formation and volatilization across this range of temperature. (1) Below 310°C, reaction kinetics and solid state diffusion dominate the slow formation of nonvolatile products, lead dichloride and an oxy-chloride or hydroxy-chloride intermediate. This behavior is reasonably described using a model of progressive chemical conversion of a pellet with fixed boundary conditions or a more empirical model of chemical reaction and pore plugging. A hydrochloridation reaction rate of approximately 10^{-7} mol/($cm^2 \cdot s$) at 2000 ppm HCl and an activation energy of 22 kcal/mol were found at 300°C. (2) Between 310 and 450°C, a predominantly lead dichloride powder product is formed, and the hydrochloridation rate, now probably under pore phase diffusional control, increased little. (3) Between 450 and 590°C, a highly volatile lead dichloride and a thin ash layer of reactive lead oxychloride intermediate (I1) are formed but again without a large change in the global reaction rate. A descriptive moving boundary model of a shrinking core with $PbCl_2$ volatilization was applied. A Fortran code was written to solve the coupled partial

differential equations of chemical reaction and diffusion. This model approximated the thermogravimetric data within 7.5% and the movement of the boundary within 50% of experimental results. (4) Between 590 and 690°C, a thick glassy ash layer of a second, more slowly reacting oxychloride intermediate (I2) was found distinct from I1 formed at lower temperature as revealed by x-ray diffraction analysis. Essentially the same model and Fortran code were applied at this higher temperature but with a reaction rate constant two orders of magnitude smaller. At a range of temperatures near 630°C and a concentration of approximately 2000 ppm HCl, a regime exists within which lead dichloride fume formation can be minimized. The model predicted a boundary movement of 240 microns compared with an experimental value of 240 μm during a 20-min reaction. The model will approximate the thermogravimetric data at these temperatures within an average error of 34% and the lead chloride volatilization rates within 16% of experimental results. The model contained two empirical parameters, a reaction rate constant, and a Henry's law constant. Semiempirical values of diffusion coefficients, typical of a viscous liquid phase, were used.

This work includes several important novelties. (1) It is the first instance in which low concentrations of HCl gas were reacted with metal oxides under controlled conditions to simulate an incinerator environment. (2) It is the first

instance in which a volatile lead dichloride species has been detected to form and condense to submicron ash particles in a simulated incinerator environment. Although widely hypothesized to occur in these circumstances, lead dichloride ash has never been chemically identified. (3) It is the first instance in which lead oxychloride intermediate compounds have been found to form under these conditions. (4) It is an early instance of the useful application of an x-ray microdiffraction technique to the identification of thin layers of ash. (5) It is a novel example of the application of moving boundary value techniques to the formation and secondary reaction of solid phase chemical reaction intermediate compounds using the front finding technique. (6) This work has identified possible incinerator operating conditions, subject to pilot scale verification, that may result in reduced lead dichloride fume emissions.

4.9 SIGNIFICANCE TO INCINERATION AND FUTURE WORK

Although it has been found here that conditions exist in the laboratory that can minimize the production of volatile lead chloride compounds and the consequent generation of fine particulate, it remains a reasonable question whether a practical application may be made of these discoveries. The range of temperatures and HCl concentrations at which the volatilization is minimized is

not wide, and incinerators are difficult to control because of variable feed composition, residence time, and bed temperature of the solids. Data are now available from this work on reaction rates in temperature regimes of interest to incinerator kilns. These data could be applied to a model of the particular particle size distribution and other characteristics of the feed to estimate conversions and metal volatilization rates from the kiln.

If data were available on the diffusivity of HCl and Henry's law constants in sintered PbO and the various intermediates, it would be possible to better validate the model. Alternate models may be constructed in which HCl is not the predominant diffusing species but which generate distinct moving boundaries such as were observed here. It is possible, for example, that the chloride ion is diffusing counter to the oxygen ion. A closer examination of the microstructure by high-temperature x-ray diffraction of the intermediates formed near the apparent transition temperature (approximately 590°C) could reveal whether a glass transition or some other phenomenon was occurring. The interesting properties of oxychlorides revealed in this work suggest also the experimentation with other metals, such as chromium, that are perhaps of interest to incineration.

BIBLIOGRAPHY

BIBLIOGRAPHY

Alexiades, V., and A. Solomon 1993. *Mathematical Modeling of Melting and Freezing Processes*, Hemisphere Publishing, Washington, D.C.

Ball, M. C., and M. J. Casson 1978. "Reaction Between Hydrogen Chloride and Lead(II) Salts," *J. Appl. Chem. Biotechnol.* **28**, 765.

Bennett, R. L., and K. T. Knapp 1982. "Characterization of Particulate Emissions from Municipal Wastewater Sludge Incinerators," *Environ. Sci. Technol.* **16**(12), 293.

Bonner, T., et al. 1981. *Hazardous Waste Incineration Engineering*, Noyes Data Corp., Park Ridge, N.J.

Bowen, H. J. M., et al. 1958. *Tables of Interatomic Distances and Configuration in Molecules and Ions*, The Chemical Society, London.

Brunner, C. R. 1989. *Handbook of Hazardous Waste Incineration*, Tab Books, Blue Ridge Summit, Pa., p. 49.

Carroll, G. J., et al. 1990. "Parametric Evaluation of Metal Partitioning at the U.S. EPA Incineration Research Facility," *Proceedings of the Sixteenth Annual Hazardous Waste Research Symposium*, Cincinnati.

Chaleroux, C. 1960. "Contribution a l'Etude de l'Action de L'Acide Chlorhydrique Gazeux sur Certain Oxydes Metalliques," *Ann. Chim. Paris* **5** (Ser. 13), 1069.

Crank, J. 1984. *Free and Moving Boundary Problems*, Clarendon Press, Oxford, p. 163.

Cundy, V. A., et al. 1989. "Rotary Kiln Incineration Combustion Chamber Dynamics," *J. Hazard. Mater.* **22**, 195.

Davison, R. L., et al. 1974. "Trace Elements in Fly Ash, Dependence of Concentration on Particle Size," *Environ. Sci. Technol.* **8**(3), 1107.

Eddings, E., and J. Lighty 1991. "Fundamental Studies of Metal Behavior During Solids Incineration," *Proceedings of the Combustion Institute*, Los Angeles.

Felderhof, B. U., and J. M. Deutch 1976. "Concentration Dependence of the Rate of Diffusion Controlled Reactions," *J. Chem. Phys.* **64**(11), 318.

Hacetoglu, A., and S. N. Flengas 1990. "Thermodynamic Behavior of Molten Metal Oxychlorides. 1. The PbO-$PbCl_2$ System," *Can. J. Chem.* **68**, 236.

Hartley, G. S. 1946. "Diffusion and Swelling of High Polymers," *Trans. Faraday Soc.* **42**, 12.

Heertjes, P. M., and R. M. Jessurun 1973. "Nickel and Cobalt from Iron Laterites," *Trans. Inst. Chem. Eng.* **51**, 293.

Helbe, J. J., and A. Sarofim 1983. *J. Colloid Interface Sci.* **76**, 183.

Ho, T. C., et al. 1992. "Metal Capture During Fluidized Bed Incineration of Wastes Contaminated with Lead Chloride," *Combust. Sci. Technol.* **85**, 101.

Jacobson, N. A., M. J. McNallan, and E. R. Kreidler 1990. "High Temperature Reactions of Ceramics and Metals with Chlorine and Oxygen, *High Temp. Sci.* **27**, 381.

Kaiser, E. R., and J. Tolciss 1963. "Control of Air Pollution from the Burning of Insulated Copper Wire," *J. Air Pollut. Control Assoc.* **13**(1), 5.

Kistler, R. C., and F. Widmer 1987. "Behavior of Chromium, Nickel, Copper, Zinc, Cadmium, Mercury, and Lead During the Pyrolysis of Sewage Sludge," *Environ. Sci. Technol.* **21**(7), 704.

Lapidus, L., and G. Pinder 1982. *Numerical Solutions of Partial Differential Equations in Science and Engineering*, John Wiley and Sons, N.Y.

Lee, D. C., and C. Georgakis 1981. "A Single, Particle-Size Model for Sulfur Retention in Fluidized Bed Coal Combustors," *AIChE J.* **27**(3), 472.

Levenspiel, O. 1972. *Chemical Reaction Engineering*, John Wiley, New York.

McCabe, W. L., et al., *Unit Operations of Chemical Engineering*, McGraw Hill, New York, 1985.

Michell, E. W. 1973. "A Study of the Reaction of Dry Hydrogen Chloride with White Lead Suspended in di-2-Ethyl Hexyl Phthalate at 182°C," *J. Appl. Chem. Biotechnol.* **23**, 273.

Millot, G. 1992. "A New French Plant to Meet the EEC Emission Objectives," *Proceedings of the 1992 Incineration Conference*, Albuquerque, N.M., p. 759.

Mulholland, J. A., and A. F. Sarofim 1991. "The Formation of Inorganic Particles During Suspension Heating of Simulated Aqueous Wastes," *Environ. Sci. Technol.* **25**(2), 268.

Neville, M., and A. F. Sarofim 1982. "The Stratified Composition of Inorganic Submicron Particles Produced During Coal Combustion," *Nineteenth Symposium (International) on Combustion*, The Combustion Institute, p. 1441.

Neville, M., et al. 1981. "Vaporization and Condensation of Mineral Matter During Pulverized Coal Combustion," *Eighteenth International Symposium on Combustion*, The Combustion Institute, p. 1267.

O'Mara, M. M. 1971. "Pyrolysis Gas Chromatographic Analysis of Polyvinyl Chloride. II. In Situ Absorption of HC1 During Pyrolysis and Combustion of PVC," *J. Polym. Sci. Part A-1* **9**, 1401.

Owens, W. D., et al. 1991. "Thermal Analysis of Rotary Kiln Incineration: Comparison of Theory and Experiment," *Combust. Flame* **86**, 101.

Perry, R., and C. Chilton 1973. *Chemical Engineers' Handbook*, 5th ed., McGraw Hill, New York, pp. 20-97.

Podsiadlo, H. 1991. "Phase Equilibria in the Binary System PbO-$PbCl_2$," *J. Therm. Anal.* **37**, 613.

Quann, R. J., and A. F. Sarofim 1982. "Vaporization of Refractory Oxides During Pulverized Coal Combustion," *The Nineteenth International Symposium on Combustion*, The Combustion Institute, p. 1429.

Raask, E., and D. M. Wilkins 1965. "Volatilization of Silica in Gasification and Combustion Processes," *J. Inst. Fuel* **38**, 255.

Smith, R. D., et al. 1974. "Concentration Dependence upon Particle Size of Volatilized Materials in Fly Ash," *Environ. Sci. Technol.* **8**(3), 1107.

Srinivasachar, S., et al. 1992. "Heavy Metal Transformations and Capture During Incineration," *Proceedings of the 85th Annual Meeting of the Air and Waste Management Association*, Kansas City, Mo.

Stull, D. R., and H. Prophet 1971. *JANAF Thermochemical Tables*, 2nd ed., National Bureau of Standards.

Theodore, L., and J. Reynolds 1987. *Introduction to Hazardous Waste Incineration*, Wiley Interscience, New York, p. 34.

Uberoi, M., and F. Shadman 1990. "Sorbents for Removal of Lead Compounds from Hot Fuel Gasses," *AIChE J.* **36**(2), 307.

Waterland, L. R., et al. 1991. "The Fate of Trace-Metals in a Rotary Kiln Incinerator: Tests with Two Different Wet Scrubber Systems," *Proceedings of the Western States Section of the Combustion Institute, 1991 Fall Meeting*, Los Angeles.

Wen, C. Y. 1968. "Noncatalytic Heterogeneous Solid Fluid Reaction Models," *Ind. Eng. Chem.* **60**(9), 34.

Wyslouzil, B., et al. 1992. "Transformation and Capture of Inorganic Lead Compounds During Incineration," presented at the Meeting of the Western States Section of the Combustion Institute, Los Angeles.

Yang, R. T., and M. Steinberg 1977. "A Diffusion Cell Method for Studying Heterogeneous Kinetics in the Chemical Reaction/Diffusion Controlled Region: Kinetics of $C + CO_2 = 2CO$ at 1200-1600°C," *Ind. Eng. Chem. Fundam.* **16**(2), 135.

Zilberman, Y. E., et al. 1969. "The Reaction of Polyvinyl Chloride (PVC) with Basic Lead Sulphates," *Vysokomol. Soyed.* **A11**(7), 1512.

APPENDICES

Appendix A1. COMPUTER PROGRAM REGIME 1

```
C          Finite Difference Solution to Diffusion with Reaction  C
C          Problem
C          This pgm applies to 300C, 60 minutes
C          Run300
C
          Initial and boundary conditions
C           plot is of weight
C
C
C
      DIMENSION ALL(102,62)
      real C(0:102,4),SIG(102),WL(62),rx(62),wt(0:62),data4(0:82)
      real Y(210),ZZ(130),z(130),XHCL(42),MTK,NHCL(42),data2(0:82)
      DIMENSION XF(102),CC(102,62),CIX(102,62)
      real IX(0:130,4), PB(0:130,64),KPBCL,x1(0:130),dif1(82)
     1 ,RGAMMA(22)
      real  XD(0:84),wwl(0:62),wwt(0:62),rx1(62),rrx1(62),X(0:24)
      REAL XNHCL(62)
C      EQUIVALENT (ALL,CC)
      XDIv=2000
      dx=1/xdiv
      MN=20
C INTERMEDIATE IS PBCL2*PBO
      J=1

      in=2
      it=40
C IT=6 IF=1= 20 MIN
C      If=1 CORRESPONDS TO 20 MINUTES
      IF=3
      N=1000*in*if*it

      DIFFI=.5e-8
      DTAU=8./float(in)/10./FLOAT(IT)*3/2
      XKR2=.0003

      IDATA=60
      XKHHCL=0.2
      M=20
      inquire (unit=5)
      open (unit = 5, file= 'data4.dat', status = 'OLD' ,
     1 access= 'sequential ',form='formatted',recordtype='variable')
      do 313 i=1,IDATA
      read  (5,30) data4(i)
      data2(i)=(data4(i)-0.826)/1.2
      xd(i)=float(i)
   30 format(f6.3)
  313 continue
      close (unit=7,status='print')
C
C
C
C     END INPUT VALUES

      FLOATM=M
      DX=1./XDIV*20/FLOAT(M)
      RATION=DTAU/(DX*DX)
      WRITE (6,200) diffs,DTAU,M,KPBCL,diffI,xkr2,n
  200 FORMAT (' DIFS ',G18.8,' DTAU= ',F10.7,' M= ',I4,
     1 ' KPBCL= ', g8.2,/, ' DIFI= ',g8.2,/, ' xkr2= ',g8.2, 'n= ',i9)
      WRITE (6,212) XLIM,xkhhcl
  212 FORMAT( ' XLIM= ',G18.8, ' Hk ',g18.8, ' gamma ')
```

```
      CONST=1-2.*RATION
C     FROSSLING APPROXIMATION



C
C


C        ESTABLISH INITIAL CONDITIONS
C        ESTABLISH BOUNDARY CONDITIONS
      DO 2,I=1,22
      C(I,1)=0
      C(I,2)=0



    2 CONTINUE
C
C
C        COMPUTE CONCENTRATIONS FOR SUCCESSIVE TIME STEPS


C     MAIN INTERATIVE LOOP STARTS
C
      DO 7 IJ=1,N+1
      DO 4 K=1,M-1
      JSTOP=IJ



c      IF (K.NE.2) GO TO 53
      C(1,1)=0.02
      C(1,2)=0.02
   53 CONTINUE
C     THIS SITUATION EXISTS BEHIND THE BOUNDARY ELEMENT
C      CON=CON+1
C      IF (CON.GT.1.) GO TO 800
C      S(K)=FLOAT(K)*1/800*20/FLOAT(M)
C      T(K)=FLOAT(J)*DTAU
C 800  CONTINUE
      J=1
C     BEHIND THE BOUNDARY CALCULATION OF C
C      NHCL(j)=.000098*(.004-XKHHCL*(C(1,2)))
C      WRITE (6,201) NHCL(J),IJ
C 201  FORMAT (G18.8, I6)
C     C(1,j+1)=c(1,j)+nhcl(j)*dtau/dx-diffi*(c(1,j)-c(2,j))/dx*dtau/dx-
C    1 xkr2*c(1,j)*dtau
      c(1,j)=0.02
      IF (K.EQ.1) GO TO 96
C      WRITE (6,298) C(1,1)
  298 FORMAT (' C11= ',G18.8)
      c(1,j)=0.02
      C(K,J+1)=(C(K-1,J)-2*C(K,J)+C(K+1,J))*DIFFI*ration+
     1 C(K,J)+(-XKR2*C(K,J))*DTAU
   96 CONTINUE
C     CALCULATION OF PbO CONCENTRATION
C     ASSUME NO DIFFUSION OF PbO
C
C     CALCULATION OF IX CONCENTRATION
      IX(1,J+1)=IX(1,J)+XKR2*DTAU*C(1,J)*.5
      IX(K,J+1)=IX(K,J)+C(K,J)*XKR2*.5*DTAU
```

```
C       CALCULATION OF PBCL2 CONCENTRATION
        GO TO 4

   67   CONTINUE

C        WRITE (6,16) SIG(K)
   16   FORMAT (' SIGK= ',G16.8)

C
C        write (6,398) SIG(K), c(1,2),K
  398   format(   ' SIGK ', G18.8 , ' c12= ', G18.8, ' K= ',I3)
c        IF (K.GT.2) GO TO 41
c        C(1,2)=0
c    41  CONTINUE
C
C        TERMINATE ITERATIONS FOR THIS TIME INCREMENT IJ

C
     4  CONTINUE
C       SET VALUES

    77  CONTINUE

        DO 76 KA=1,M
        C(KA,1)=C(KA,2)
        IX(KA,1)=IX(KA,2)
C       RESETTING VALUES
    76  CONTINUE

        DO 75, JL=1,MN
        NI=N/MN/if
        IF (IJ.NE.NI*JL*IF) GO TO 75
        XNHCL(JL)=NHCL(1)
        RGAMMA(JL)=GAMMA
        DO 74 JLK=1,M
        CC(JLK,JL)=C(JLK,1)
        CIX(JLK,JL)=IX(JLK,1)
        PB(JLK,JL)=0.036-CIX(JLK,JL)
    74  CONTINUE
    75  CONTINUE

     7  CONTINUE
        DO 71, JL=1,20
        RX(jL)=XNHCL(JL)
        X(JL)=float(if)*FLOAT(JL)
        wWT(jl)=(RX(jl)*27.4)*60.*float(if)+wwt(jl-1)
        Do 68 i=1,20
    68  sumw=(cc(i,jl)+cix(i,jl)*2)*dx*36.4+sumw
        wt(jl)=sumw
        sumw=0
        dif1(jl)=wt(jl)-data2(jl*3)
        sqsum=sqsum +dif1(jl)**2
        wwg=RX(JL)*54.8
        WRITE (6,22) data2(jl*3),WT(jl),RGAMMA(JL)
        RX1(jl)=rx1(jl-1)+rx(jl)
        rrx1(jl)=rx1(jl)/float(jl)
    22  FORMAT(' data ',G18.8,  ' WT = ',E18.8, ' GAMMA ', G18.8
      1 / )
        WRITE (6,26) RrX1(jl)
    26  FORMAT (' RX1= ', G18.8)
    71  continue
        WRITE (6,88) SQSUM
```

```
   88  FORMAT(' SQSUM= ',G18.8)

       DO 25 KI=1,MN
       XHCL(KI)=DIFFI*(CC(1,KI)-CC(2,KI))/DX
c       wt(ki)=xhcl(ki)*180.+wt(k-1)
       WRITE (6,24) wt(ki),XHCL(KI)
   24  FORMAT(' wt=  ',G18.8, ' XHCl= ', G18.8)
       WRITE (6,28) XNHCL(KI)
   28  FORMAT (' NHCL= ',G18.10)
   25  CONTINUE
       MTK=1


   50  DO 5 KK=1,20
       WRITE (6,300) (cC(J,KK),J=1,4,1)
  300  FORMAT (' HCl ',4E17.4)
       WRITE (6,301) (cIX(J,KK),J=1,4)
  301  FORMAT (' IX ',4G17.3)
c       WRITE (6,302) (PB(J,KK),J=1,4)
c  302  FORMAT (' PbCl2 ',4G17.3)

    5  CONTINUE
  750  CONTINUE

       DO 87 K=1,M+1
       X1(K)=((FLOAT(K-1)))/XDIV*20/FLOAT(M)
   87  CONTINUE


  801  CONTINUE
c
c
c
       CALL SYSBUF
       call comprs
       call page (11,9)
       call area2d (9,7)
c       call headin (' CONC VS DISTANCE, TIME AS PARAMETER  ',100,1,3)
c       CALL XNAME ('DISTANCE, CM ',15)
c       CALL YNAME (' CONC, MOLES/CC ',16)
       call xname (' time, min  ',20)
       call yname (' sample mass, g ',22)
       CALL SMOOTH
c       CALL GRAF(0,.005,.025,0,.0002,.0012)
c       CALL LOGLOG (.000625,5,.00001,2)
       XO=FLOAT(IF)*20.
       CALL GRAF (0,10.,60,0.0,.001,.010)

       DO 47 K=1,20
       DO 48 J=1,M
c       Y(J)=CC(J,K)
c       Z(J)=CIX(J,K)

   48   CONTINUE

c       CALL CURVE(X1,Y,M,1)
c       CALL CURVE(X1,Z,M,1)
   47  CONTINUE
       CALL CURVE(X,WT,M,0)
       CALL CURVE(XD,DATA2,idata,-1)
       CALL YTICKS (1)
       call messag ('run 300 ',12,6,7)
```

```
      CALL MESSAG (' DHCl ',12,1,6)

      CALL REALNO (Diffi,14,2,6)
c      CALL MESSAG (' Diff PbCl2 ',15,2,4)
c      CALL REALNO (DIFF2,10,7.3,4)
      CALL MESSAG (' Kr ',6,1,7)
      call realno (xkr2,6,2,7)
c c      CALL MESSAG (' KPBCL= ', 6,6,4)
c c      CALL REALNO (KPBCL,8,7,4)
c       CALL MESSAG (' TIME INC= ',10,6,5)
c       call realno(dtau,5,7,5)
c       CALL INTNO (IT,1,9)
c       CALL MESSAG(' JSTOP= ',10,6,6)
c       CALL INTNO(JSTOP,7,6)
c       CALL MESSAG(' M= ',2,6,7)
c       CALL INTNO(M, 7,7)
      CALL MESSAG(' SQSUM= ',8,6,5)
      call messag (' Hk= ',8,1,4)
      call realno(xkhhcl,8,2,4)
      CALL REALNO(SQSUM,8,7,5)
      CALL ENDPL (0)
      CALL DONEPL
C
  154 CONTINUE
      STOP
      END
```

Appendix A2. COMPUTER OUTPUT REGIME 1

```
DIFS     0.00000000E+00 DTAU=  0.2400000 M=   20 KPBCL= 0.00E+00
DIFI= 0.50E-10  xkr2= 0.10E-03 iterations=15000
XLIM=     0.00000000E+00 Hk     0.12000000E-01

time=3 minutes
WL=      0.00000000E+00 WwT =      0.92811696E-03 GAMMA      0.00000000E+00
RX1=      0.18818267E-06
time=6 minutes
WL=      0.00000000E+00 WwT =      0.14591060E-02 GAMMA      0.00000000E+00
RX1=      0.14792234E-06
time=9 minutes
WL=      0.00000000E+00 WwT =      0.18260505E-02 GAMMA      0.00000000E+00
RX1=      0.12341515E-06

WL=      0.00000000E+00 WwT =      0.21197491E-02 GAMMA      0.00000000E+00
RX1=      0.10744876E-06

WL=      0.00000000E+00 WwT =      0.23766547E-02 GAMMA      0.00000000E+00
RX1=      0.96376915E-07

WL=      0.00000000E+00 WwT =      0.26122001E-02 GAMMA      0.00000000E+00
RX1=      0.88273858E-07

WL=      0.00000000E+00 WwT =      0.28335047E-02 GAMMA      0.00000000E+00
RX1=      0.82073477E-07

WL=      0.00000000E+00 WwT =      0.30442644E-02 GAMMA      0.00000000E+00
RX1=      0.77155931E-07

WL=      0.00000000E+00 WwT =      0.32466622E-02 GAMMA      0.00000000E+00
RX1=      0.73142793E-07

WL=      0.00000000E+00 WwT =      0.34421636E-02 GAMMA      0.00000000E+00
RX1=      0.69792449E-07

WL=      0.00000000E+00 WwT =      0.36318356E-02 GAMMA      0.00000000E+00
RX1=      0.66943812E-07

WL=      0.00000000E+00 WwT =      0.38164898E-02 GAMMA      0.00000000E+00
RX1=      0.64485164E-07

WL=      0.00000000E+00 WwT =      0.39967611E-02 GAMMA      0.00000000E+00
RX1=      0.62336412E-07

WL=      0.00000000E+00 WwT =      0.41732201E-02 GAMMA      0.00000000E+00
RX1=      0.60439412E-07

WL=      0.00000000E+00 WwT =      0.43462641E-02 GAMMA      0.00000000E+00
RX1=      0.58749187E-07

WL=      0.00000000E+00 WwT =      0.45163142E-02 GAMMA      0.00000000E+00
RX1=      0.57232295E-07

WL=      0.00000000E+00 WwT =      0.46836487E-02 GAMMA      0.00000000E+00
RX1=      0.55861477E-07

WL=      0.00000000E+00 WwT =      0.48485310E-02 GAMMA      0.00000000E+00
RX1=      0.54615345E-07

WL=      0.00000000E+00 WwT =      0.50112456E-02 GAMMA      0.00000000E+00
RX1=      0.53477258E-07
```

WL= 0.00000000E+00 WwT = 0.51719509E-02 GAMMA 0.00000000E+00
RX1= 0.52432608E-07
SQSUM= 0.10604977E-03

time=3 minutes
XPBCL= 0.00000000E+00 XHCl= 0.30686405E-07 NHCL=
0.1881826677E-06
time= 6 minutes
XPBCL= 0.00000000E+00 XHCl= 0.39586777E-07 NHCL=
0.1076619967E-06
time= 9 minutes
XPBCL= 0.00000000E+00 XHCl= 0.40816349E-07 NHCL=
0.7440075223E-07

XPBCL= 0.00000000E+00 XHCl= 0.39557584E-07 NHCL=
0.5954958837E-07

XPBCL= 0.00000000E+00 XHCl= 0.37666876E-07 NHCL=
0.5208952913E-07

XPBCL= 0.00000000E+00 XHCl= 0.35774260E-07 NHCL=
0.4775860418E-07

XPBCL= 0.00000000E+00 XHCl= 0.34065938E-07 NHCL=
0.4487117522E-07

XPBCL= 0.00000000E+00 XHCl= 0.32573990E-07 NHCL=
0.4273311660E-07

XPBCL= 0.00000000E+00 XHCl= 0.31281910E-07 NHCL=
0.4103769058E-07

XPBCL= 0.00000000E+00 XHCl= 0.30161061E-07 NHCL=
0.3963934958E-07

XPBCL= 0.00000000E+00 XHCl= 0.29183646E-07 NHCL=
0.3845740792E-07

XPBCL= 0.00000000E+00 XHCl= 0.28326223E-07 NHCL=
0.3744004928E-07

XPBCL= 0.00000000E+00 XHCl= 0.27569746E-07 NHCL=
0.3655138059E-07

XPBCL= 0.00000000E+00 XHCl= 0.26896425E-07 NHCL=
0.3577844154E-07

XPBCL= 0.00000000E+00 XHCl= 0.26296222E-07 NHCL=
0.3508595370E-07

XPBCL= 0.00000000E+00 XHCl= 0.25755527E-07 NHCL=
0.3447896546E-07

XPBCL= 0.00000000E+00 XHCl= 0.25268818E-07 NHCL=
0.3392833747E-07

XPBCL= 0.00000000E+00 XHCl= 0.24827798E-07 NHCL=
0.3343114585E-07

XPBCL= 0.00000000E+00 XHCl= 0.24425004E-07 NHCL=
0.3299163609E-07

XPBCL= 0.00000000E+00 XHCl= 0.24058593E-07 NHCL= 0.3258418602E-07

time =3 minutes

	Element 1	Element 2	Element 3	Element 4
HCl	0.1733E+00	0.1181E-01	0.5234E-03	0.1721E-04
IX	0.900E-03	0.389E-04	0.126E-05	0.326E-07
PbCl2	0.000E+00	0.000E+00	0.000E+00	0.000E+00
time=6 minutes				
HCl	0.2418E+00	0.3343E-01	0.3000E-02	0.1993E-03
IX	0.281E-02	0.240E-03	0.155E-04	0.801E-06
PbCl2	0.000E+00	0.000E+00	0.000E+00	0.000E+00
time=9 minutes				
HCl	0.2701E+00	0.5524E-01	0.7428E-02	0.7416E-03
IX	0.513E-02	0.640E-03	0.611E-04	0.471E-05
PbCl2	0.000E+00	0.000E+00	0.000E+00	0.000E+00
HCl	0.2827E+00	0.7450E-01	0.1320E-01	0.1751E-02
IX	0.763E-02	0.123E-02	0.153E-03	0.155E-04
PbCl2	0.000E+00	0.000E+00	0.000E+00	0.000E+00
HCl	0.2890E+00	0.9079E-01	0.1973E-01	0.3240E-02
IX	0.102E-01	0.197E-02	0.301E-03	0.377E-04
PbCl2	0.000E+00	0.000E+00	0.000E+00	0.000E+00
HCl	0.2927E+00	0.1044E+00	0.2655E-01	0.5166E-02
IX	0.128E-01	0.285E-02	0.509E-03	0.752E-04
PbCl2	000E+00	0.000E+00	0.000E+00	0.000E+00
HCl	0.2952E+00	0.1159E+00	0.3338E-01	0.7454E-02
IX	0.155E-01	0.385E-02	0.779E-03	0.132E-03
PbCl2	0.000E+00	0.000E+00	0.000E+00	0.000E+00
HCl	0.2970E+00	0.1256E+00	0.4001E-01	0.1002E-01
IX	0.181E-01	0.493E-02	0.111E-02	0.210E-03
PbCl2	0.000E+00	0.000E+00	0.000E+00	0.000E+00
HCl	0.2984E+00	0.1338E+00	0.4635E-01	0.1279E-01
IX	0.208E-01	0.610E-02	0.150E-02	0.313E-03
PbCl2	0.000E+00	0.000E+00	0.000E+00	0.000E+00
HCl	0.2996E+00	0.1409E+00	0.5234E-01	0.1569E-01
IX	0.235E-01	0.734E-02	0.194E-02	0.441E-03
PbCl2	0.000E+00	0.000E+00	0.000E+00	0.000E+00
HCl	0.3006E+00	0.1470E+00	0.5795E-01	0.1867E-01
IX	0.262E-01	0.863E-02	0.244E-02	0.595E-03
PbCl2	0.000E+00	0.000E+00	0.000E+00	0.000E+00
HCl	0.3015E+00	0.1524E+00	0.6320E-01	0.2167E-01
IX	0.289E-01	0.998E-02	0.298E-02	0.777E-03
PbCl2	0.000E+00	0.000E+00	0.000E+00	0.000E+00
HCl	0.3023E+00	0.1571E+00	0.6808E-01	0.2466E-01
IX	0.316E-01	0.114E-01	0.358E-02	0.985E-03
PbCl2	0.000E+00	0.000E+00	0.000E+00	0.000E+00
HCl	0.3029E+00	0.1613E+00	0.7262E-01	0.2762E-01
IX	0.344E-01	0.128E-01	0.421E-02	0.122E-02
PbCl2	0.000E+00	0.000E+00	0.000E+00	0.000E+00
HCl	0.3035E+00	0.1651E+00	0.7684E-01	0.3051E-01

IX	0.371E-01	0.143E-01	0.488E-02	0.148E-02
PbCl2	0.000E+00	0.000E+00	0.000E+00	0.000E+00
HCl	0.3040E+00	0.1685E+00	0.8076E-01	0.3333E-01
IX	0.398E-01	0.158E-01	0.559E-02	0.177E-02
PbCl2	0.000E+00	0.000E+00	0.000E+00	0.000E+00
HCl	0.3045E+00	0.1715E+00	0.8441E-01	0.3607E-01
IX	0.426E-01	0.173E-01	0.633E-02	0.208E-02
PbCl2	0.000E+00	0.000E+00	0.000E+00	0.000E+00
HCl	0.3049E+00	0.1742E+00	0.8780E-01	0.3871E-01
IX	0.453E-01	0.189E-01	0.711E-02	0.242E-02
PbCl2	0.000E+00	0.000E+00	0.000E+00	0.000E+00
HCl	0.3053E+00	0.1767E+00	0.9096E-01	0.4126E-01
IX	0.480E-01	0.204E-01	0.791E-02	0.278E-02
PbCl2	0.000E+00	0.000E+00	0.000E+00	0.000E+00
HCl	0.3056E+00	0.1790E+00	0.9391E-01	0.4371E-01
IX	0.508E-01	0.220E-01	0.875E-02	0.316e-02
PbCl2	0.0	0.0	0.0	0.0

Appendix B1. COMPUTER PROGRAM REGIME 3

```
C          THIS IS AT 550C, WT LOSS CURVE RUN 228 MODEL
C            Finite Difference Solution to Diffusion with   C
Reaction Problem

C
C          Initial and boundary conditions
C
C
C
C

       real C(0:102,4),SIG(102),WL(62),rx(62),wt(62),data3(0:82)
       real Y(210),ZZ(130),z(130),XHCL(42),MTK,NHCL(42),data2(0:82)
       REAL XF(102),CC(102,62),CIX(102,62),cpb(102,62),CF,WEI(42)
       real IX(0:130,4), PB(0:130,4),KPBCL,x1(130),dif1(82),RGAMMA(22)
       real  XD(84),ww1(0:62),wwt(0:62),rx1(62),rrx1(62),X(24),XNHCL(62)
       XDIV=1400

       MN=4
       XLIM=.01
C INTERMEDIATE IS PBCL2*PBO

       J=1
       DPB=5.e-7
       in=8
       it=16
C IT=6 IF=1= 20 MIN
C      If=1 CORRESPONDS TO 20 MINUTES
       IF=2
       N=1000*in*if*it
       DIFFI=2.E-4
       DIFFS=2.E-4
       DIX=1.e-6
       DTAU=8./float(in)/10./FLOAT(IT)*3/2/10
       XKR2=80000

C       GAMMA=0.8
C       GAMMA
       IDATA=40
       XKHHCL=4.
       M=MN

C
C
C      END INPUT VALUES

       FLOATM=M

       DX=1./XDIV

       RATION=DTAU/(DX*DX)
       WRITE (6,200) diffs,DTAU,M,KPBCL,diffI,xkr2,n
  200  FORMAT (' DIFS ',G18.8,' DTAU= ',F10.7,' M= ',I4,
     1 ' KPBCL= ', g8.2,/, ' DIFI= ',g8.2,/, ' xkr2= ',g8.2, 'n= ',i9)
       WRITE (6,212) XLIM,xkhhcl
  212  FORMAT( ' XLIM= ',G18.8, ' Hk ',g18.8, ' gamma ')
       CONST=1-2.*RATION
C      FROSSLING APPROXIMATION
C
C
```

```
C          ESTABLISH INITIAL CONDITIONS
C          ESTABLISH BOUNDARY CONDITIONS
        DO 2,I=1,22
        C(I,1)=0
        C(I,2)=0



    2   CONTINUE
C

C
C          COMPUTE CONCENTRATIONS FOR SUCCESSIVE TIME STEPS

        PB(1,1)=0.00001
C       MAIN INTERATIVE LOOP STARTS
C
        DO 7 IJ=1,N+1
        DO 4 K=1,M-1
        JSTOP=IJ



        IF (SIG(K).LT.XLIM) GO TO 67
        IX(K,1)=XLIM/2.0
c        C(1,1)=0
c        C(1,2)=0
   53   CONTINUE
C       THIS SITUATION EXISTS BEHIND THE BOUNDARY ELEMENT
C        CON=CON+1
C        IF (CON.GT.1.) GO TO 800
C        S(K)=FLOAT(K)*1/800*20/FLOAT(M)
C        T(K)=FLOAT(J)*DTAU
C  800   CONTINUE
        J=1
C       BEHIND THE BOUNDARY CALCULATION OF C
        NHCL(j)=.000098*(.002-XKHHCL*(PB(1,1)))
C        WRITE (6,201) NHCL(J),IJ
C  201   FORMAT (G18.8, I6)
        C(1,j+1)=c(1,j)+nhcl(j)*dtau/dx-diffi*(c(1,j)-c(2,j))/dx*dtau/dx-
     1  xkr2*c(1,j)*ix(1,j)*dtau
        IF (K.EQ.1) GO TO 96
C        WRITE (6,298) C(1,1)
  298   FORMAT (' C11= ',G18.8)

        C(K,J+1)=(C(K-1,J)-2*C(K,J)+C(K+1,J))*DIFFI*ration+
     1  C(K,J)+(-XKR2*C(K,J)*IX(K,J))*DTAU
   96   CONTINUE
C       CALCULATION OF PbO CONCENTRATION
C       ASSUME NO DIFFUSION OF PbO
C
C       CALCULATION OF IX CONCENTRATION
        IX(1,J+1)=IX(1,J)-IX(1,J)*XKR2*DTAU*C(1,J)*.5+DIX*(IX(2,J)-
     1  IX(1,J))/DX*DTAU
        IX(K,J+1)=IX(K,J)-IX(K,J)*C(K,J)*XKR2*.5*DTAU+DIX*(IX(K-1,J)-
     1  2*IX(K-1,J)+IX(K+1,J))*RATION

C       CALCULATION OF PBCL2 CONCENTRATION

C       BOUNDARY CONDITION ON PBCL2 AT X=0
C
        CF=1.
```

```
C       CF=STOICHIOMETRIC COEFF
        XPBO=IX(1,J)*.5/(IX(1,J)*.5+PB(1,J))
        IF (XPBO.GE..6) GO TO 213
        GAMMA=1.-1.6*XPBO
        GO TO 214
  213   IF (XPBO.GE.0.8) GO TO 215
        GAMMA=.32-.4*XPBO
        GO TO 214
  215   GAMMA=0
  214   CONTINUE
        GAMMA=1
        KPBCL=GAMMA*2.E-6*2.
        CF=1.
        PB(1,J+1)=PB(1,J)+(XKR2*CF*(C(1,1))*IX(1,J)-KPBCL*PB(1,J)+

      1 Dpb*(IX(2,J)-IX(1,J))/DX)*DTAU
        PB(K,J+1)=(pb(K-1,J)-2*pb(K,J)+pb(K+1,J))*Dpb*RATION+
      1 PB(K,J)+(XKR2*CF*IX(K,J)*(C(K,1)))*DTAU
        EX=PB(1,1)**.5
C
C       BOUNDARY CONDITION AT X=0
C        GO TO 750


C

        GO TO 4
C       CALCULATION FOR MUSHY REGION

    67  CONTINUE

C
        CON=0.0
        D=1./(((XLIM-SIG(K))/XLIM)/DIFFI+(SIG(K)/DIFFS)/XLIM)

C        WRITE (6,16) SIG(K)
    16  FORMAT (' SIGK= ',G16.8)
        IF (K.GE.2) GO TO 40
        NHCL(1)=.000098*(.002-XKHHCL*C(1,1))
        SIG(1)=SIG(1)+nhcl(1)*dtau/dx
        GO TO 77

C       CONSIDER ELEMENTS OTHER THAN INITIAL ONE
40      XC=D*(C(K-1,1)-C(K,1))*DTAU/DX/DX
        SIG(K)=SIG(K)+XC
C        write (6,398) SIG(K), c(1,2),K
  398   format(   ' SIGK ', G18.8 , ' c12= ', G18.8, ' K= ',I3)
c        IF (K.GT.2) GO TO 41
c        C(1,2)=0
c    41  CONTINUE
C
C        TERMINATE ITERATIONS FOR THIS TIME INCREMENT IJ
        GO TO 77

C
     4  CONTINUE
C       SET VALUES

    77  CONTINUE

        DO 76 KA=1,4
        C(KA,1)=C(KA,2)
```

```
      IX(KA,1)=IX(KA,2)
      PB(KA,1)=PB(KA,2)
C     RESETTING VALUES
   76 CONTINUE

      DO 75, JL=1,20
      NI=N/20/if
      IF (IJ.NE.NI*JL*IF) GO TO 75
      XNHCL(JL)=NHCL(1)
      RGAMMA(JL)=GAMMA
      DO 74 JLK=1,4
      CC(JLK,JL)=C(JLK,1)
      CPB(JLK,JL)=PB(JLK,1)
      CIX(JLK,JL)=IX(JLK,1)
   74 CONTINUE
   75 CONTINUE

    7 CONTINUE
      DO 71, JL=1,20
      WL(jl)=CPB(1,JL)*KPBCL
      RX(jl)=DIFFI*(CC(1,JL)-CC(2,JL))/DX/2.
      X(JL)=float(if)*FLOAT(JL)
C      WT(jl)=(RX(jl)*54.8-WL(jl)*278.)*60.*float(if)
      wwl(jl)=wl(jl)*278.*60.*float(if)+WWL(JL-1)
      DO 68 I=1,MN
   68 SUMW=CC(I,JL)*DX*36.4+SUMW
      WT(JL)=SUMW
      dif1(jl)=wt(jl)-data2(jl)
      sqsum=sqsum +dif1(jl)**2
      wwg=RX(JL)*54.8
      WEI(JL)=-WWL(JL)
      WRITE (6,22) WEI(jl),WT(jl),RGAMMA(JL)
      RX1(jl)=rx1(jl-1)+rx(jl)
      rrx1(jl)=rx1(jl)/float(jl)
   22 FORMAT(' WL= ',G18.8,  ' WT CHANGE= ',G18.8, ' GAMMA ', G18.8
     1 / )
      WRITE (6,26) RrX1(jl)
   26 FORMAT (' RX1= ', G18.8)
   71 continue


      DO 25 KI=1,20
      XF(KI)=KPBCL*CPB(1,KI)
      XHCL(KI)=DIFFI*(CC(1,KI)-CC(2,KI))/DX
      WRITE (6,24) XF(KI),XHCL(KI)
   24 FORMAT(' XPBCL= ',G18.8, ' XHCl= ', G18.8)
      WRITE (6,28) XNHCL(KI)
   28 FORMAT (' NHCL= ',G18.10)
   25 CONTINUE
      MTK=1


   50 DO 5 KK=1,20
      WRITE (6,300) (cC(J,KK),J=1,4,1)
  300 FORMAT (' HCl ',4E17.4)
      WRITE (6,301) (cIX(J,KK),J=1,4)
  301 FORMAT (' IX ',4G17.3)
      WRITE (6,302) (cPB(J,KK),J=1,4)
  302 FORMAT (' PbCl2 ',4G17.3)

    5 CONTINUE
  750 CONTINUE
```

```
      DO 87 K=1,M+1
      X1(K)=((FLOAT(K-1)))/XDIV*20/FLOAT(M)
   87 CONTINUE
  801 CONTINUE
      STOP
      END
```

Appendix B2. COMPUTER OUTPUT REGIME 3

```
$run p228
DIFS     0.79999998E-04 DTAU=  0.0000521 M= 8 KPBCL= 0.00E+00
DIFI= 0.80E-04      xkr2=35.    iterations=4608000

XLIM=0.99999998E-02 Hk= 0.15000001

time= 2 min
data2        0.00000000E+00 WT CHANGE=       0.64443587E-03  GAMMA
1.0000000     RX1=     0.19599845E-06
time =4 min
data2        0.00000000E+00 WT CHANGE=       0.10439735E-02  GAMMA
1.0000000     RX1=     0.18035371E-06
time=6 min
data2       -0.55554841E-03 WT CHANGE=       0.81172126E-03  GAMMA
1.0000000    RX1=     0.14823154E-06

data2       -0.55554841E-03 WT CHANGE=       0.23341237E-03  GAMMA
1.0000000    RX1=     0.12111681E-06

data2       -0.11110968E-02 WT CHANGE=      -0.45489147E-03  GAMMA
1.0000000    RX1=     0.10203723E-06

data2       -0.16666453E-02 WT CHANGE=      -0.11750992E-02  GAMMA
1.0000000    RX1=     0.88638139E-07

data2       -0.22222267E-02 WT CHANGE=      -0.18972344E-02  GAMMA
1.0000000    RX1=     0.79032183E-07

data2       -0.27777753E-02 WT CHANGE=      -0.26193697E-02  GAMMA
1.0000000    RX1=     0.71827714E-07

data2       -0.38888720E-02 WT CHANGE=      -0.33415048E-02  GAMMA
1.0000000    RX1=     0.66224239E-07

data2       -0.38888720E-02 WT CHANGE=      -0.40907706E-02  GAMMA
1.0000000    RX1=     0.61394822E-07

data2       -0.50000022E-02 WT CHANGE=      -0.48518367E-02  GAMMA
1.0000000    RX1=     0.57306412E-07

data2       -0.55555506E-02 WT CHANGE=      -0.56129028E-02  GAMMA
1.0000000    RX1=     0.53899409E-07

data2       -0.61110989E-02 WT CHANGE=      -0.63739689E-02  GAMMA
1.0000000    RX1=     0.51016556E-07

data2       -0.66666473E-02 WT CHANGE=      -0.71350350E-02  GAMMA
1.0000000    RX1=     0.48545541E-07

data2       -0.72222287E-02 WT CHANGE=      -0.78961011E-02  GAMMA
1.0000000    RX1=     0.46403997E-07

data2       -0.83333254E-02 WT CHANGE=      -0.86571667E-02  GAMMA
1.0000000    RX1=     0.44530143E-07


data2       -0.88888742E-02 WT CHANGE=      -0.94182324E-02  GAMMA
1.0000000    RX1=     0.42876742E-07

data2       -0.94444221E-02 WT CHANGE=      -0.10179298E-01  GAMMA
1.0000000    RX1=     0.41407056E-07
```

```
data2       -0.10000004E-01  WT  CHANGE=       -0.10940364E-01  GAMMA
1.0000000     RX1=      0.40092072E-07

data2       -0.10555552E-01  WT  CHANGE=       -0.11701429E-01  GAMMA
1.0000000     RX1=      0.38908585E-07


time =2 min
XPBCL=      0.21043348E-12 XHCl=      0.19597985E-06
NHCL=    0.1959984530E-06
time=4 min
XPBCL=      0.42573576E-08 XHCl=      0.16468819E-06
NHCL=    0.1647089647E-06
time= 6 min
XPBCL=      0.15239870E-07 XHCl=      0.83975465E-07
NHCL=    0.8398717455E-07

XPBCL=      0.21255437E-07 XHCl=      0.39764601E-07
NHCL=    0.3977264740E-07

XPBCL=      0.23167496E-07 XHCl=      0.25712426E-07
NHCL=    0.2571893098E-07

XPBCL=      0.23722087E-07 XHCl=      0.21636948E-07
NHCL=    0.2164267165E-07

XPBCL=      0.23755591E-07 XHCl=      0.21390376E-07
NHCL=    0.2139640287E-07

XPBCL=      0.23755591E-07 XHCl=      0.21390369E-07
NHCL=    0.2139640287E-07

XPBCL=      0.23755591E-07 XHCl=      0.21390354E-07
NHCL=    0.2139640287E-07

XPBCL=      0.24227207E-07 XHCl=      0.17923776E-07
NHCL=    0.1793003968E-07

XPBCL=      0.24432333E-07 XHCl=      0.16416120E-07
NHCL=    0.1642235681E-07

XPBCL=      0.24432333E-07 XHCl=      0.16416120E-07
NHCL=    0.1642235681E-07

XPBCL=      0.24432333E-07 XHCl=      0.16416120E-07
NHCL=    0.1642235681E-07

XPBCL=      0.24432333E-07 XHCl=      0.16416120E-07
NHCL=    0.1642235681E-07

XPBCL=      0.24432333E-07 XHCl=      0.16416120E-07
NHCL=    0.1642235681E-07

XPBCL=      0.24432333E-07 XHCl=      0.16416120E-07
NHCL=    0.1642235681E-07

XPBCL=      0.24432333E-07 XHCl=      0.16416115E-07
NHCL=    0.1642235681E-07
```

XPBCL= 0.24432333E-07 XHCl= 0.16416104E-07
NHCL= 0.1642235681E-07

XPBCL= 0.24432333E-07 XHCl= 0.16416099E-07
NHCL= 0.1642235681E-07

HCl	0.5104E-06	0.0000E+00	0.0000E+00	0.0000E+00
IX	0.500E-02	0.000E+00	0.000E+00	0.000E+00
PbCl2	0.105E-06	0.000E+00	0.000E+00	0.000E+00
HCl	0.8577E-06	0.4288E-06	0.0000E+00	0.0000E+00
IX	0.500E-02	0.498E-02	0.000E+00	0.000E+00
PbCl2	0.213E-02	0.284E-03	0.000E+00	0.000E+00
HCl	0.4374E-06	0.2187E-06	0.0000E+00	0.0000E+00
IX	0.500E-02	0.487E-02	0.000E+00	0.000E+00
PbCl2	0.762E-02	0.300E-02	0.000E+00	0.000E+00
HCl	0.3106E-06	0.2071E-06	0.1035E-06	0.0000E+00
IX	0.500E-02	0.485E-02	0.491E-02	0.000E+00
PbCl2	0.106E-01	0.557E-02	0.218E-02	0.000E+00
HCl	0.2009E-06	0.1339E-06	0.6694E-07	0.0000E+00
IX	0.500E-02	0.485E-02	0.480E-02	0.000E+00
PbCl2	0.116E-01	0.711E-02	0.330E-02	0.000E+00
HCl	0.1690E-06	0.1127E-06	0.5633E-07	0.0000E+00
IX	0.500E-02	0.485E-02	0.470E-02	0.000E+00
PbCl2	0.119E-01	0.768E-02	0.375E-02	0.000E+00
HCl	0.1671E-06	0.1114E-06	0.5569E-07	0.0000E+00
IX	0.500E-02	0.485E-02	0.459E-02	0.000E+00
PbCl2	0.119E-01	0.785E-02	0.390E-02	0.000E+00
HCl	0.1671E-06	0.1114E-06	0.5569E-07	0.0000E+00
IX	0.500E-02	0.485E-02	0.448E-02	0.000E+00
PbCl2	0.119E-01	0.785E-02	0.391E-02	0.000E+00
HCl	0.1671E-06	0.1114E-06	0.5569E-07	0.0000E+00
IX	0.500E-02	0.485E-02	0.438E-02	0.000E+00
PbCl2	0.119E-01	0.785E-02	0.391E-02	0.000E+00
HCl	0.1867E-06	0.1400E-06	0.9331E-07	0.4665E-07
IX	0.500E-02	0.485E-02	0.433E-02	0.494E-02
PbCl2	0.121E-01	0.807E-02	0.442E-02	0.164E-02
HCl	0.1709E-06	0.1282E-06	0.8546E-07	0.4273E-07
IX	0.500E-02	0.485E-02	0.433E-02	0.483E-02
PbCl2	0.122E-01	0.861E-02	0.533E-02	0.250E-02
HCl	0.1709E-06	0.1282E-06	0.8546E-07	0.4273E-07
IX	0.500E-02	0.485E-02	0.433E-02	0.473E-02
PbCl2	0.122E-01	0.889E-02	0.575E-02	0.281E-02
HCl	0.1709E-06	0.1282E-06	0.8546E-07	0.4273E-07
IX	0.500E-02	0.485E-02	0.433E-02	0.462E-02
PbCl2	0.122E-01	0.904E-02	0.594E-02	0.293E-02
HCl	0.1709E-06	0.1282E-06	0.8546E-07	0.4273E-07
IX	0.500E-02	0.485E-02	0.433E-02	0.451E-02
PbCl2	0.122E-01	0.908E-02	0.602E-02	0.299E-02

HCl	0.1709E-06	0.1282E-06	0.8546E-07	0.4273E-07
IX	0.500E-02	0.485E-02	0.433E-02	0.440E-02
PbCl2	0.122E-01	0.908E-02	0.602E-02	0.300E-02
HCl	0.1709E-06	0.1282E-06	0.8546E-07	0.4273E-07
IX	0.500E-02	0.485E-02	0.433E-02	0.430E-02
PbCl2	0.122E-01	0.908E-02	0.602E-02	0.300E-02
HCl	0.1709E-06	0.1282E-06	0.8546E-07	0.4273E-07
IX	0.500E-02	0.485E-02	0.433E-02	0.419E-02
PbCl2	0.122E-01	0.908E-02	0.602E-02	0.300E-02
HCl	0.1709E-06	0.1282E-06	0.8546E-07	0.4273E-07
IX	0.500E-02	0.485E-02	0.433E-02	0.408E-02
PbCl2	0.122E-01	0.908E-02	0.602E-02	0.300E-02
HCl	0.1709E-06	0.1282E-06	0.8546E-07	0.4273E-07
IX	0.500E-02	0.485E-02	0.433E-02	0.398E-02
PbCl2	0.122E-01	0.908E-02	0.602E-02	0.300E-02
HCl	0.1709E-06	0.1282E-06	0.8546E-07	0.4273E-07
IX	0.500E-02	0.485E-02	0.433E-02	0.387E-02
PbCl2	0.122E-01	0.908E-02	0.602E-02	0.300E-02

Appendix C1. COMPUTER PROGRAM REGIME 4

```
CCCCCCCCCCCCCCCCCCCCCCCCCCCCCCCCCCCCCCCCCCCCCCCCCCCCCCCCCCCCCCCCCCCCCCCCCCC
C
C          Finite Difference Solution to Diffusion with Reaction Problem
C
C          This pgm applies to 670C, 60 minutes
C
C                                                                      C
C                                                                C
C          plot is of weight                                           C
C                                                                      C
C                                                                      C
C                                                                C
      DIMENSION ALL(102,62)
      real C(0:102,4),SIG(102),WL(62),rx(62),wt(62),data1(0:82)
      real Y(210),ZZ(130),z(130),XHCL(42),MTK,NHCL(42),data2(0:82)
      DIMENSION XF(102),CC(102,62),CIX(102,62),cpb(102,62)
      real IX(0:130,4), PB(0:130,4),KPBCL,x1(0:130),dif1(82),RGAMMA(22)
      real  XD(0:84),wwl(0:62),wwt(0:62),rx1(62),rrx1(62),X(0:64)
      REAL XNHCL(62)
      XDIV=400
      idata=60
      MN=20
      XLIM=.009
C                      INTERMEDIATE IS PBCL*PBO2
      J=1
      open (unit = 5, file= 'data2.dat', status = 'OLD' ,
     1 access= 'sequential ',form='formatted',recordtype='variable')
      do 313 i=1,IDATA
      read  (5,30) data2(i)
      data1(i)=(data2(i)-0.37)/.843/.8
   30 format(f6.3)
  313 continue
      close (unit=7,status='print')

      in=4
      it=4
C IT=6 IF=1= 20 MIN
C      If=1 CORRESPONDS TO 20 MINUTES
      IF=3
      N=1000*in*if*it

      DIFFI=4.e-5
      DIFFS=4.E-5
      DIFF2=4.E-6
      DTAU=8./float(in)/10./FLOAT(IT)*3/2
      XKR2=7.


      IX(1,1)=XLIM/2.
      XKPBCL1=2.E-5
      IDATA=60
      XKHHCL=.45
      M=20

C
C
C     END INPUT VALUES

      FLOATM=M
      DX=1./XDIV*20/FLOAT(M)
      RATION=DTAU/(DX*DX)
      WRITE (6,200) diffs,DTAU,M,KPBCL,diffI,xkr2,n
```

```
  200  FORMAT (' DIFS ',G18.8,' DTAU= ',F10.7,' M= ',I4,
     1 ' KPBCL= ', g8.2,/, ' DIFI= ',g8.2,/, ' xkr2= ',g8.2, 'n= ',i9)
       WRITE (6,212) XLIM,xkhhcl
  212  FORMAT( ' XLIM= ',G18.8, ' Hk ',g18.8, ' gamma ')
       CONST=1-2.*RATION
C      FROSSLING APPROXIMATION
C
C
C
C
C         ESTABLISH INITIAL CONDITIONS
C         ESTABLISH BOUNDARY CONDITIONS

       DO 2,I=1,22
       C(I,1)=0
       C(I,2)=0
    2  CONTINUE
C
C
C         COMPUTE CONCENTRATIONS FOR SUCCESSIVE TIME STEPS


C      MAIN INTERATIVE LOOP STARTS
C
       DO 7 IJ=1,N+1
       DO 4 K=1,M-1
       JSTOP=IJ



       IF (SIG(K).LT.XLIM) GO TO 67
C       IF (K.NE.2) GO TO 53
C       C(1,1)=0
C       C(1,2)=0
   53  CONTINUE
C      THIS SITUATION EXISTS BEHIND THE BOUNDARY ELEMENT
C       CON=CON+1
C       IF (CON.GT.1.) GO TO 800
C       S(K)=FLOAT(K)*1/800*20/FLOAT(M)
C       T(K)=FLOAT(J)*DTAU
C  800  CONTINUE
       J=1
C      BEHIND THE BOUNDARY CALCULATION OF C
       NHCL(j)=.000098*(.002-XKHHCL*(pb(1,1)))
C       WRITE (6,201) NHCL(J),IJ
C  201  FORMAT (G18.8, I6)
       C(1,j+1)=c(1,j)+nhcl(j)*dtau/dx-diffi*(c(1,j)-c(2,j))/dx*dtau/dx-
     1 xkr2*c(1,j)*ix(1,j)*dtau
       IF (K.EQ.1) GO TO 96
C       WRITE (6,298) C(1,1)
  298  FORMAT (' C11= ',G18.8)

       C(K,J+1)=(C(K-1,J)-2*C(K,J)+C(K+1,J))*DIFFI*ration+
     1 C(K,J)+(-XKR2*C(K,J)*IX(K,J))*DTAU
   96  CONTINUE
C      CALCULATION OF PbO CONCENTRATION
C      ASSUME NO DIFFUSION OF PbO
C
C      CALCULATION OF IX CONCENTRATION
       cf=0.5
       IX(1,J+1)=IX(1,J)-IX(1,J)*XKR2*DTAU*C(1,J)*cf
       IX(K,J+1)=IX(K,J)-IX(K,J)*C(K,J)*XKR2*cf*DTAU
```

```
C       CALCULATION OF PBCL2 CONCENTRATION

C       BOUNDARY CONDITION ON PBCL2 AT X=0
C
        CF=1
C       CF=STOICHIOMETRIC COEFF
        XPBO=IX(1,J)*.5/(IX(1,J)*.5+PB(1,J))
        IF (XPBO.GE.0.2) GO TO 218
        GAMMA=1.-XPBO
        GO TO 214
  218   IF (XPBO.GE.0.6) GO TO 213
        GAMMA=1.-1.6*XPBO
        GO TO 214
  213   IF (XPBO.GE.0.8) GO TO 215
        GAMMA=.32-.4*XPBO
        GO TO 214
  215   GAMMA=0
  214   CONTINUE

        KPBCL=GAMMA*XKPBCL1
        cf1=1
        PB(1,J+1)=PB(1,J)+(XKR2*cf1*IX(1,J)*C(1,J)-KPBCL*PB(1,J)+
     1  DIFF2*(PB(2,J)-PB(1,J))/DX)*DTAU
        PB(K,J+1)=(PB(K-1,J)-2*PB(K,J)+PB(K+1,J))*DIFF2*RATION+
     1  PB(K,J)+(XKR2*C(K,J)*cf1*IX(K,J))*DTAU
C
C       BOUNDARY CONDITION AT X=0
C        GO TO 750


C

        GO TO 4
C       CALCULATION FOR MUSHY REGION

    67  CONTINUE
        IF (IX(K,2).NE.0) GO TO 109
        IX(K,2)=xlim/2.
  109   CONTINUE
        CON=0.0
C        D=1./(((XLIM-SIG(K))/XLIM)/DIFFI+(SIG(K)/DIFFS)/XLIM)
        D=diffi
C        WRITE (6,16) SIG(K)
    16  FORMAT (' SIGK= ',G16.8)
        IF (K.GE.2) GO TO 40
        NHCL(1)=.000098*(.002-XKHHCL*Pb(1,1))
        SIG(1)=SIG(1)+nhcl(1)*dtau/dx
        GO TO 77

C
    40  XC=D*(C(K-1,2)-C(K,2))*DTAU/DX/DX
        SIG(K)=SIG(K)+XC
C        write (6,398) SIG(K), c(1,2),K
  398   format(   ' SIGK ', G18.8 , ' c12= ', G18.8, ' K= ',I3)
c        IF (K.GT.2) GO TO 41
c        C(1,2)=0
c    41  CONTINUE
C
C        TERMINATE ITERATIONS FOR THIS TIME INCREMENT IJ
        GO TO 77

C
```

```
    4  CONTINUE
C      SET VALUES

   77  CONTINUE

       DO 76 KA=1,M
       C(KA,1)=C(KA,2)
       IX(KA,1)=IX(KA,2)
       PB(KA,1)=PB(KA,2)
C      RESETTING VALUES
   76  CONTINUE

       DO 75, JL=1,MN
       NI=N/MN/if
       IF (IJ.NE.NI*JL*IF) GO TO 75
       XNHCL(JL)=NHCL(1)
       RGAMMA(JL)=GAMMA
       DO 74 JLK=1,M
       CC(JLK,JL)=C(JLK,1)
       CPB(JLK,JL)=PB(JLK,1)
       CIX(JLK,JL)=IX(JLK,1)
   74  CONTINUE
   75  CONTINUE

    7  CONTINUE
       DO 71, JL=1,20
       WL(jl)=CPB(1,JL)*KPBCL
       RX(jl)=xnhcl(jl)
       X(JL)=float(if)*FLOAT(JL)
       WT(jl)=(RX(jl)*35.4-WL(jl)*278.)*60.*float(if)
       wwl(jl)=wl(jl)*278.*60.+WWL(JL)*278.*60.*float(if)
       wwt(jl)=wwt(jl-1)+wt(jl)
       ii=jl*3
       dif1(jl)=wwt(jl)-data1(ii)
       sqsum=sqsum +dif1(jl)**2
       wwg=RX(JL)*54.8
       WRITE (6,22) dif1(ii),wWT(jl),data1(ii)
       RX1(jl)=rx1(jl-1)+rx(jl)
       rrx1(jl)=rx1(jl)/float(jl)
   22  FORMAT(' dif1 ',G18.8,  ' WT CHANGE= ',G18.8, ' data2 ', G18.8
     1 / )
       WRITE (6,26) RrX1(jl)
   26  FORMAT (' RX1= ', G18.8)
   71  continue
       WRITE (6,88) SQSUM
   88  FORMAT(' SQSUM= ',G18.8)

       DO 25 KI=1,MN
       XF(KI)=KPBCL*CPB(1,KI)
       XHCL(KI)=DIFFI*(CC(1,KI)-CC(2,KI))/DX
       WRITE (6,24) XF(KI),XHCL(KI)
   24  FORMAT(' XPBCL= ',G18.8, ' XHCl= ', G18.8)
       WRITE (6,28) XNHCL(KI)
   28  FORMAT (' NHCL= ',G18.10)
   25  CONTINUE
       MTK=1


   50  DO 5 KK=1,20
       WRITE (6,300) (CC(J,KK),J=1,20,5)
  300  FORMAT (' HCl,1,6, ',4E14.3)
       WRITE (6,301) (CIX(J,KK),J=1,20,5)
```

```
  301  FORMAT (' IX ',4G14.3)
       WRITE (6,302) (CPB(J,KK),J=1,20,5)
  302  FORMAT (' PbCl2 ',4G14.3)

    5  CONTINUE
  750  CONTINUE

       DO 87 K=1,M+1
       X1(K)=((FLOAT(K-1)))/XDIV*20/FLOAT(M)
   87  CONTINUE


  801  CONTINUE
C
C
C



       CALL SYSBUF
       call comprs
       call page (11,9)
       call area2d (9,7)
c       call headin (' CONC VS DISTANCE, TIME AS PARAMETER  ',100,1,3)
c       CALL XNAME ('DISTANCE, CM ',15)
c       CALL YNAME (' CONC, MOLES/CC ',16)
       call xname (' time, min  ',20)
       call yname (' sample mass, g ',22)
       CALL SMOOTH
c       CALL GRAF(0,.005,.025,0,.0002,.0016)
c       CALL LOGLOG (.000625,5,.00001,2)
       XO=FLOAT(IF)*20.
       CALL GRAF (0,10.,XO,-0.045,.006,.010)
       DO 47 K=1,MN,4

       DO 48 J=1,MN
       Y(J)=CC(J,K)
c       Z(J)=CIX(J,K)
       ZZ(J)=CPB(J,K)

   48  CONTINUE

       DO 457 J=1,IDATA
       XD(J)=FLOAT(j-1)
  457  CONTINUE

c       CALL CURVE(X1,Y,M,1)
c       CALL CURVE(X1,Z,M,1)
c       CALL CURVE(X1,ZZ,M,1)
   47  CONTINUE
       CALL CURVE(X,WWT,M,0)
       CALL CURVE(XD,DATA1,idata,-1)
c       CALL YTICKS (1)
       call messag (' run 245 ',12,6,1)
       CALL MESSAG (' DHCl ',12,6,2)
c       CALL REALNO (DiffI,12,7,1)
       CALL REALNO (DiffS,12,7,2)
       CALL MESSAG (' Diff PbCl2 ',15,6,3)
       CALL REALNO (DIFF2,10,7.5,3)
       CALL MESSAG (' XKR2 ',6,6,3.5)
       call realno (xkr2,6,7,3.5)
       CALL MESSAG (' KPBCL= ', 6,6,4)
```

```
      CALL REALNO (KPBCL,8,7,4)
c c     CALL MESSAG (' TIME INC= ',10,6,5)
c c     call realno(dtau,5,7,5)
c      CALL INTNO (IT,1,9)
c      CALL MESSAG(' JSTOP= ',10,6,6)
c      CALL INTNO(JSTOP,7,6)
      CALL MESSAG(' M= ',2,6,7)
      CALL INTNO(M, 7,7)
      CALL MESSAG(' SQSUM= ',8,6,1.5)
      call messag (' xhcl= ',8,6,8)
      call realno(xkhhcl,8,7,8)
      CALL REALNO(SQSUM,8,7,1.5)
      CALL ENDPL (0)
      CALL DONEPL
C
  154 CONTINUE
      STOP
      END
```

Appendix C2. COMPUTER OUTPUT REGIME 4

```
Run 245
DIFS     0.39999999E-04 DTAU=  0.0750000 M=   20 KPBCL= 0.00E+00
DIFI= 0.40E-04  xkr2=  6.0    iterations=48000
XLIM=     0.89999996E-02 Hk     0.34999999

time =3 minutes
dif1         0.00000000E+00  WT  CHANGE=         0.12487425E-02  data2
0.00000000E+00 RX1=      0.19599295E-06
time =6 minutes
dif1         0.00000000E+00  WT  CHANGE=         0.24297019E-02  data2
0.14827804E-02 RX1=      0.19458624E-06
time=9 minutes
dif1         0.00000000E+00  WT  CHANGE=         0.34705854E-02  data2
0.14827804E-02 RX1=      0.19217826E-06

dif1         0.00000000E+00  WT  CHANGE=         0.43361303E-02  data2
0.29656049E-02 RX1=      0.18915379E-06

dif1         0.00000000E+00  WT  CHANGE=         0.49955226E-02  data2
0.29656049E-02 RX1=      0.18562687E-06

dif1         0.00000000E+00  WT  CHANGE=         0.54366072E-02  data2
0.29656049E-02 RX1=      0.18176449E-06

dif1         0.00000000E+00  WT  CHANGE=         0.56578666E-02  data2
0.29656049E-02 RX1=      0.17770139E-06

dif1         0.00000000E+00  WT  CHANGE=         0.56644925E-02  data2
0.44483854E-02 RX1=      0.17353980E-06

dif1         0.00000000E+00  WT  CHANGE=         0.54668481E-02  data2
0.44483854E-02 RX1=      0.16936036E-06

dif1         0.00000000E+00  WT  CHANGE=         0.50785867E-02  data2
0.29656049E-02 RX1=      0.16522515E-06

dif1         0.00000000E+00  WT  CHANGE=         0.45140982E-02  data2
0.44483854E-02 RX1=      0.16117639E-06

dif1         0.00000000E+00  WT  CHANGE=         0.37850428E-02  data2
0.29656049E-02 RX1=      0.15723285E-06

dif1         0.00000000E+00  WT  CHANGE=         0.29080380E-02  data2
0.29656049E-02 RX1=      0.15342334E-06

dif1         0.00000000E+00  WT  CHANGE=         0.18976869E-02  data2
0.14827804E-02 RX1=      0.14976247E-06

dif1         0.00000000E+00  WT  CHANGE=         0.76409499E-03  data2
0.00000000E+00 RX1=      0.14624847E-06

dif1         0.00000000E+00  WT  CHANGE=        -0.47730724E-03  data2
0.00000000E+00 RX1=      0.14289385E-06

dif1          0.00000000E+00  WT  CHANGE=        -0.18195920E-02  data2
-0.14828246E-02 RX1=      0.13968744E-06

dif1          0.00000000E+00  WT  CHANGE=        -0.32490345E-02  data2
-0.29656049E-02 RX1=      0.13663619E-06

dif1          0.00000000E+00  WT  CHANGE=        -0.47601904E-02  data2
-0.29656049E-02 RX1=      0.13372751E-06
```

```
dif1          0.00000000E+00  WT  CHANGE=        -0.63424637E-02  data2
-0.44483854E-02 RX1=      0.13096201E-06

SQSUM=      0.41406034E-04
time=3 minutes
XPBCL=            0.24924236E-11  XHCl=            0.19517152E-06  NHCL=
0.1959929534E-06
time= 6 minutes
XPBCL=            0.99881303E-09  XHCl=            0.19082579E-06  NHCL=
0.1931795026E-06
time=9 minutes
XPBCL=            0.30573326E-08  XHCl=            0.18441922E-06  NHCL=
0.1873622750E-06

XPBCL=            0.56340448E-08  XHCl=            0.17669029E-06  NHCL=
0.1800804199E-06

XPBCL=            0.86636343E-08  XHCl=            0.16730034E-06  NHCL=
0.1715191900E-06

XPBCL=            0.11871760E-07  XHCl=            0.15813553E-06  NHCL=
0.1624525510E-06

XPBCL=            0.15102190E-07  XHCl=            0.14900370E-06  NHCL=
0.1533228300E-06

XPBCL=            0.18256317E-07  XHCl=            0.14015845E-06  NHCL=
0.1444086735E-06

XPBCL=            0.21258149E-07  XHCl=            0.13179134E-06  NHCL=
0.1359248927E-06

XPBCL=            0.24059336E-07  XHCl=            0.12401875E-06  NHCL=
0.1280081250E-06

XPBCL=            0.26649035E-07  XHCl=            0.11654431E-06  NHCL=
0.1206887958E-06

XPBCL=            0.29067404E-07  XHCl=            0.11037721E-06  NHCL=
0.1138539645E-06

XPBCL=            0.31241576E-07  XHCl=            0.10437949E-06  NHCL=
0.1077092833E-06

XPBCL=            0.33201125E-07  XHCl=            0.99120193E-07  NHCL=
0.1021709508E-06

XPBCL=            0.35012196E-07  XHCl=            0.94129703E-07  NHCL=
0.9705247805E-07

XPBCL=            0.36596500E-07  XHCl=            0.89662727E-07  NHCL=
0.9257480826E-07

XPBCL=            0.38078998E-07  XHCl=            0.85794369E-07  NHCL=
0.8838487275E-07

XPBCL=            0.39359804E-07  XHCl=            0.82062328E-07  NHCL=
0.8476492752E-07

XPBCL=            0.40560611E-07  XHCl=            0.79051709E-07  NHCL=
0.8137118357E-07
```

XPBCL= 0.41605691E-07 XHCl= 0.76247787E-07 NHCL= 0.7841743610E-07

time=3 minutes

	element 1	element 6	element 11	element16
HCl	0.122E-04	0.000E+00	0.000E+00	0.000E+00
IX	0.449E-02	0.000E+00	0.000E+00	0.000E+00
PbCl2	0.205E-06	0.000E+00	0.000E+00	0.000E+00

time=6 minutes

HCl	0.355E-04	0.000E+00	0.000E+00	0.000E+00
IX	0.444E-02	0.000E+00	0.000E+00	0.000E+00
PbCl2	0.823E-04	0.000E+00	0.000E+00	0.000E+00

time=9 minutes

HCl	0.455E-04	0.000E+00	0.000E+00	0.000E+00
IX	0.434E-02	0.000E+00	0.000E+00	0.000E+00
PbCl2	0.252E-03	0.000E+00	0.000E+00	0.000E+00
HCl	0.539E-04	0.000E+00	0.000E+00	0.000E+00
IX	0.422E-02	0.450E-02	0.000E+00	0.000E+00
PbCl2	0.464E-03	0.000E+00	0.000E+00	0.000E+00
HCl	0.696E-04	0.193E-04	0.000E+00	0.000E+00
IX	0.408E-02	0.447E-02	0.000E+00	0.000E+00
PbCl2	0.714E-03	0.205E-03	0.000E+00	0.000E+00
HCl	0.741E-04	0.268E-04	0.000E+00	0.000E+00
IX	0.393E-02	0.442E-02	0.000E+00	0.000E+00
PbCl2	0.978E-03	0.368E-03	0.000E+00	0.000E+00
HCl	0.773E-04	0.330E-04	0.000E+00	0.000E+00
IX	0.377E-02	0.435E-02	0.000E+00	0.000E+00
PbCl2	0.124E-02	0.556E-03	0.000E+00	0.000E+00
HCl	0.794E-04	0.379E-04	0.000E+00	0.000E+00
IX	0.362E-02	0.427E-02	0.450E-02	0.000E+00
PbCl	0.150E-02	0.756E-03	0.000E+00	0.000E+00
HCl	0.807E-04	0.418E-04	0.680E-05	0.000E+00
IX	0.346E-02	0.418E-02	0.449E-02	0.000E+00
PbCl2	0.175E-02	0.960E-03	0.160E-03	0.000E+00
HCl	0.813E-04	0.448E-04	0.124E-04	0.000E+00
IX	0.332E-02	0.408E-02	0.447E-02	0.000E+00
PbCl2	0.198E-02	0.116E-02	0.331E-03	0.000E+00
HCl	0.771E-04	0.432E-04	0.151E-04	0.000E+00
IX	0.318E-02	0.399E-02	0.444E-02	0.000E+00
PbCl2	0.220E-02	0.129E-02	0.391E-03	0.000E+00
HCl	0.772E-04	0.447E-04	0.162E-04	0.000E+00
IX	0.305E-02	0.389E-02	0.440E-02	0.000E+00
PbCl2	0.240E-02	0.148E-02	0.558E-03	0.000E+00
HCl	0.771E-04	0.465E-04	0.198E-04	0.000E+00
IX	0.292E-02	0.380E-02	0.436E-02	0.000E+00
PbCl	0.257E-02	0.166E-02	0.742E-03	0.000E+00
HCl	0.735E-04	0.444E-04	0.189E-04	0.000E+00
IX	0.281E-02	0.370E-02	0.432E-02	0.000E+00
PbCl2	0.274E-02	0.177E-02	0.790E-03	0.000E+00

HCl	0.734E-04	0.457E-04	0.218E-04	0.000E+00
IX	0.270E-02	0.361E-02	0.426E-02	0.450E-02
PbCl2	0.288E-02	0.194E-02	0.972E-03	0.000E+00
HCl	0.725E-04	0.462E-04	0.238E-04	0.387E-05
IX	0.259E-02	0.353E-02	0.421E-02	0.450E-02
PbCl2	0.302E-02	0.204E-02	0.108E-02	0.177E-03
HCl	0.702E-04	0.450E-04	0.233E-04	0.379E-05
IX	0.249E-02	0.344E-02	0.416E-02	0.449E-02
PbCl2	0.314E-02	0.217E-02	0.119E-02	0.199E-03
HCl	0.686E-04	0.446E-04	0.244E-04	0.674E-05
IX	0.240E-02	0.336E-02	0.411E-02	0.448E-02
PbCl	0.324E-02	0.225E-02	0.125E-02	0.336E-03
HCl	0.677E-04	0.444E-04	0.245E-04	0.678E-05
IX	0.232E-02	0.328E-02	0.406E-02	0.446E-02
PbCl2	0.334E-02	0.237E-02	0.139E-02	0.399E-03
HCl	0.655E-04	0.431E-04	0.237E-04	0.658E-05
IX	0.223E-02	0.320E-02	0.400E-02	0.445E-02
PbCl2	0.343E-02	0.244E-02	0.143E-02	0.409E-03

END OF DISSPLA

Appendix D. X-RAY DIFFRACTION PATTERNS

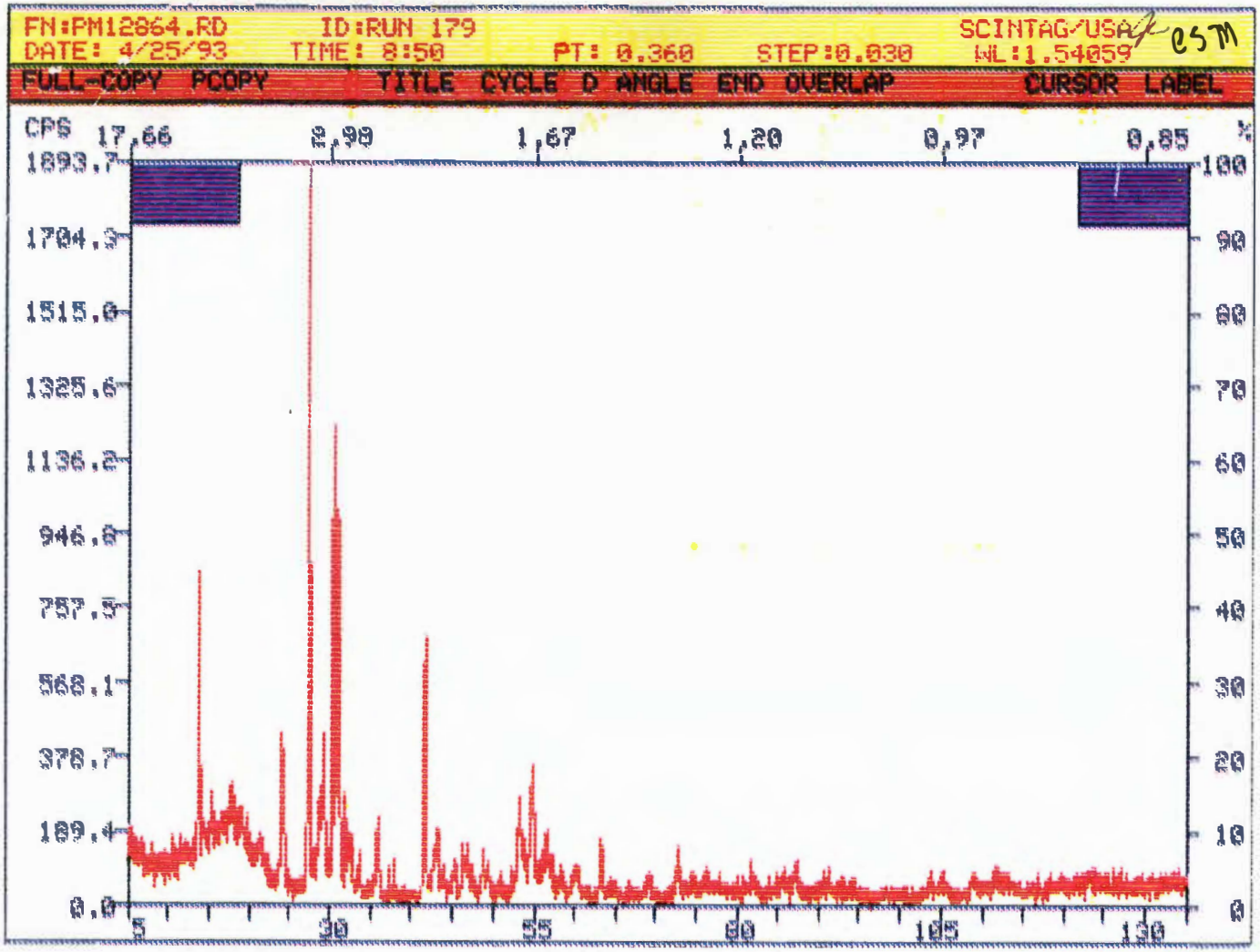

Figure D.1. Powder x-ray diffraction pattern of pellet from Run 174, prepared at 680°C, 62 min, 2000 ppm HCl, without $PbCl_2$ volatilization following run.

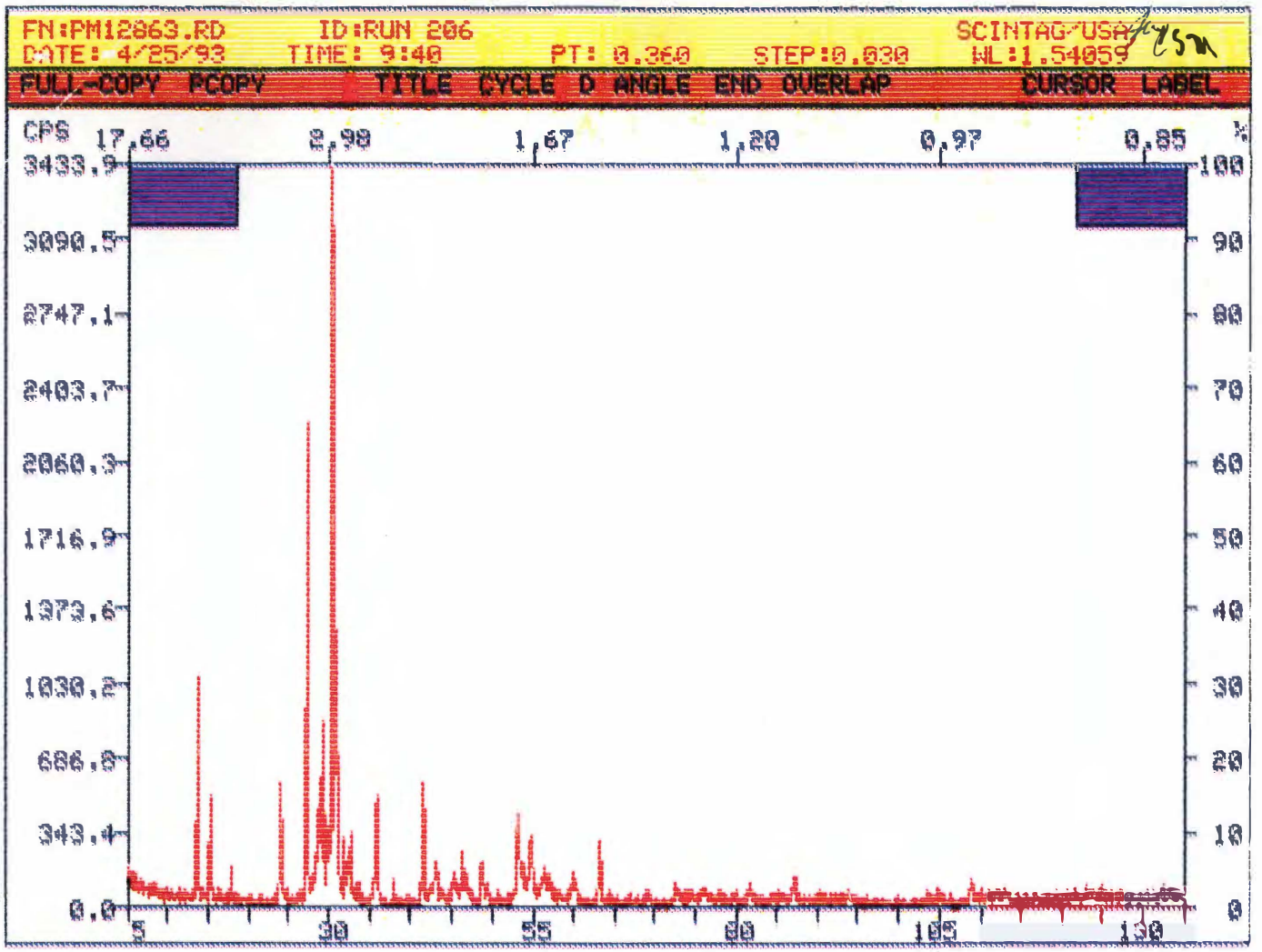

Figure D.2. Powder x-ray diffraction pattern of pellet from Run 206, prepared at 680°C, 60 min, 2000 ppm HCl, without $PbCl_2$ volatilization following run.

APPENDIX E. COMPUTER PROGRAM FLOW DIAGRAM

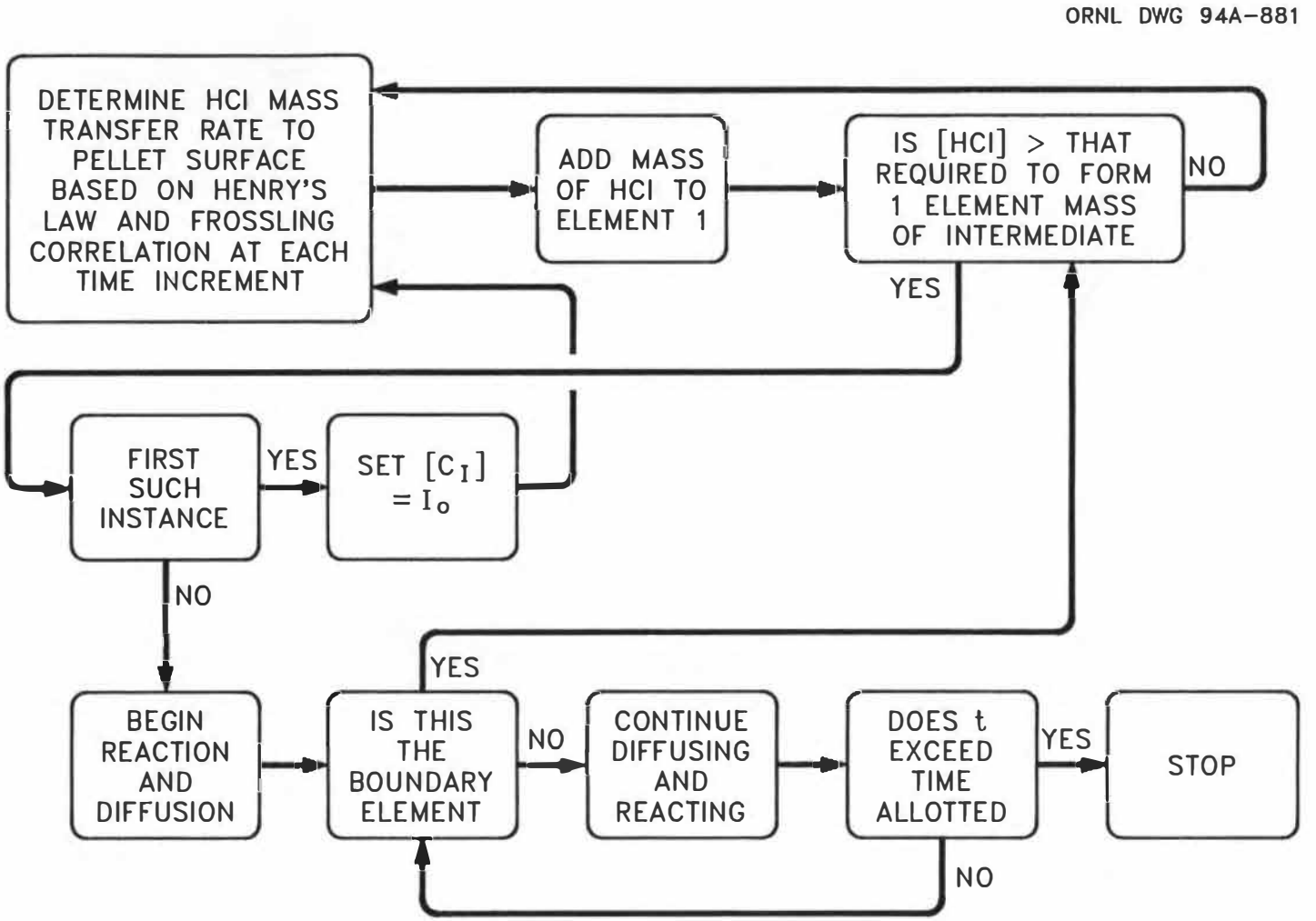

Figure E.1. Flow diagram of moving boundary problem computer code.

VITA

Joel T. Shor was born in Chicago in 1954 and raised in Oak Ridge, Tennessee. He returned to school in Chicago where he obtained a Bachelors of Arts degree in History, 1976. He returned to Tennessee where he obtained his Bachelor of Science in Chemical Engineering in 1979 from the University of Tennessee. He worked one year with Texaco, Inc. at Port Arthur, Texas, and returned to Oak Ridge where he begun work at the Oak Ridge Gaseous Diffusion Plant in the gas centrifuge program. He moved to the Oak Ridge National Laboratory in 1985 where he presently works. He obtained his Master of Science in Chemical Engineering from the University of Tennessee in 1987. He is married to Susan Grodinsky Shor and has one son, Alexander.